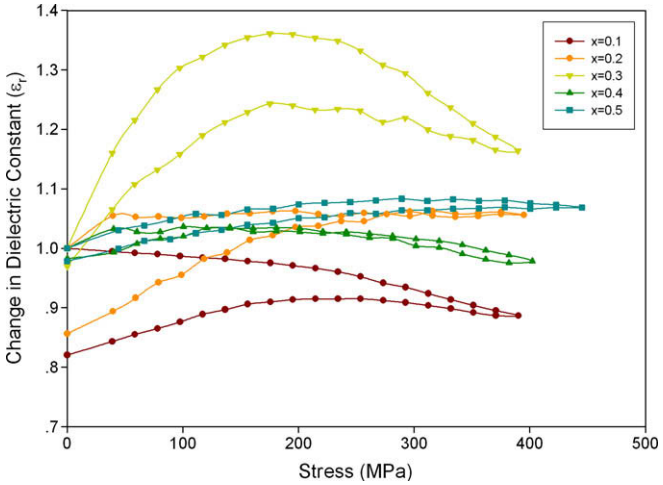

Fig. 1. Relative changes of dielectric constant (ε_r) with compressive stress for $(1-x)$PIN–(x)PT ceramics (measured at 25 °C and 100 kHz).

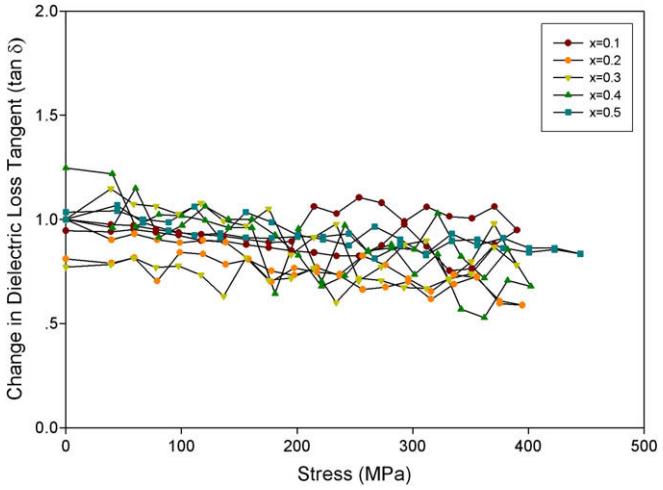

Fig. 2. Relative changes of dielectric loss tangent ($\tan\delta$) with compressive stress for $(1-x)$PIN–(x)PT ceramics (measured at 25 °C and 100 kHz).

decreases with increasing stress. On the other hand, for the tetragonal compositions, with x values of 0.4 and 0.5, the dielectric constant shows very little change with stress. In addition, the compressive stress dependence of the dielectric loss tangent ($\tan\delta$) is observed, as shown in Fig. 2. It can be seen that the dielectric loss tangents during loading and unloading are not significantly different. It is also noticed that the changes in the dielectric properties with the compressive stress obtained in this study are in parts similar to those for PMN–PZT and PMN–PT systems in earlier investigations [10,11].

To understand these experimental results, at least qualitatively, various effects have to be considered. When a compressive stress is applied to the ferroelectric materials in the direction parallel to the poling direction, the domain structure in the material will change to maintain the domain energy at a minimum, because the stress will move some of the polarization away from the poling direction; during this process some of the domains engulf other domains or change shape irreversibly. Under a stress, the domain structure of ferroelectric ceramics may undergo domain switching through non-180° domain walls, de-aging, de poling and clamping of domain walls [10].

The experimental observations, both the drastic change case and the very little change case, can be attributed to competing influences, in an opposite way, of the intrinsic contribution of domains and the extrinsic contribution of re-polarization and growth of micro-polar regions. Under the applied compressive stress, the non-180° domain wall density increases. Hence, the increase of the dielectric constant is observed. The de-aging mechanism, which also increases the dielectric constant [9–11], is also expected to play a role here. Therefore, a combination of the domain switching and the de-aging mechanisms is believed to be a reason for the increase of the dielectric constant during low-stress application, i.e., PIN–PT with $x = 0.2$, 0.3, 0.4 and 0.5. With further increase in the stress, the stress clamping of domain walls, which results in a decrease of domain wall mobility, and the stress induced decrease in switchable part of spontaneous polarization are expected to play a role in the decrease of the dielectric constant [9,10]. In addition, in case of 0.9PIN–0.1PT the continuous decrease in the dielectric constant can be attributed to the switching of 90° domains, which causes the significant decrease in the dielectric constant, as seen in Fig. 1. The cause of the stress dependence of the dielectric loss tangent is a little more straightforward. As depicted in Fig. 2, the clamping of the domain walls under the compressive stress results in a decrease of domain wall mobility and reduces the dielectric loss tangent [25]. This is a reversible effect with the domain wall mobility returning to near the original values, when the applied stress is removed, as seen in Fig. 2 that the dielectric loss tangents return to near their original values after a stress cycle. In addition, a significant decrease in the dielectric constant after a full cycle of stress application has been observed and attributed to the stress induced decrease in switchable part of spontaneous polarization at high stress and the irreversible 90° domain switching [10,25].

4. Conclusions

In this study, the dielectric properties of PIN–PT ceramics with a formula $(1-x)Pb(In_{1/2}Nb_{1/2})O_3$–$(x)PbTiO_3$ (for $x = 0.1$–0.5) prepared by a two stage mixed-oxide method are measured under the compressive stress from 0 to 400 MPa. The results clearly show that the superimposed compression stress has pronounced effects on both the dielectric constant and the dielectric loss tangent of PIN–PT ceramics. The observations are mainly interpreted in terms of competing influences of the intrinsic contribution, and the extrinsic contribution from domain switching through non-180° domain walls, clamping of domain walls, de-aging, and the stress induced decrease in switchable part of spontaneous polarization.

Acknowledgements

This work was supported by the Thailand Research Fund (TRF), Commission on Higher Education (CHE), Development and Promotion of Science and Technology Talents Project (DPST), Faculty of Science and Graduate School of Chiang Mai University.

References

[1] J. Kuwata, K. Uchino, S. Nomura, Jpn. J. Appl. Phys. 21 (1982) 1298.
[2] S. Park, T.R. Shrout, J. Appl. Phys. 82 (4) (1997) 1804.
[3] D. Viehland, J. Powers, Appl. Phys. Lett. 78 (20) (2001) 3112.
[4] L.E. Cross, Ferroelectric 76 (1987) 241.
[5] K. Uchino, Piezoelectric Actuators and Ultrasonic Motors, Kluwer Academic, Boston, 1997.
[6] D. Stansfield, Underwater Electroacoustic Transducers, Bath University Press, Bath, 1991.
[7] R. Yimnirun, S. Ananta, S. Chamunglap, Mater. Chem. Phys. 102 (2007) 165.
[8] R. Yimnirun, S. Ananta, A. Ngamjarurojana, S. Wongsaenmai, Curr. Appl. Phys. 6 (3) (2006) 520.
[9] G. Yang, S.F. Liu, W. Ren, B.K. Mukherjee, Proc. SPIE Sym. Smart Struct. Mater. 3992 (2000) 103.
[10] R. Yimnirun, M. Unruan, Y. Laosiritaworn, S. Ananta, J. Phys. D 39 (2006) 3097.
[11] R. Yimnirun, Int. J. Mod. Phys. B 20 (23) (2006) 3409.
[12] D. Zhou, M. Kamlah, D. Munz, J. Eur. Ceram. Soc. 25 (2005) 425.
[13] S. Wongsaenmai, S. Ananta, E. Meechoowas, R. Yimnirun, J. Phys. D 36 (2003) 1615.
[14] E.F. Alberta, A.S. Bhalla, J. Kor. Phys. Soc. 32 (1998) 1265.
[15] A. Halliyal, U. Kumar, U. Kumar, R.E. Newnham, L.E. Cross, Am. Ceram. Soc. Bull. 66 (4) (1987) 671.
[16] J.R. Belsick, A. Halliyal, U. Kumar, R.E. Newnham, Am. Ceram. Soc. Bull. 66 (4) (1987) 664.
[17] N. Yasuda, M. Fujie, Jpn. J. Appl. Phys. 31 (1992) 3128.
[18] S. Wongsaenmai, O. Khamman, S. Ananta, R. Yimnirun, J. Electroceram., in press. doi: 10.1007/s10832-007-9311-3.
[19] R. Yimnirun, S. Ananta, A. Ngamjarurojana, S. Wongsaenmai, Appl. Phys. A: Mater. Sci. Proc. 81 (2005) 1227.
[20] R. Yimnirun, Y. Laosiritaworn, S. Wongsaenmai, J. Phys. D: Appl. Phys. 39 (2006) 759.
[21] S. Wongsaenmai, A. Bhalla, X. Tan, S. Ananta, R. Yimnirun, Ferroelectr. Lett. 34 (2007) 36.
[22] Wongsaenmai, X. Tan, S. Ananta, R. Yimnirun, J. Alloys Comps. 454 (2008) 331.
[23] N. Vittayakorn, G. Rujijanagul, T. Tunkasiri, X. Tan, D.P. Cann, J. Mater. Res. 18 (2003) 2882.
[24] N. Vittayakorn, G. Rujijanagul, X. Tan, H. He, M.A. Marquardt, D.P. Cann, J. Electroceram. 16 (2006) 141.
[25] Q.M. Zhang, J. Zhao, K. Uchino, J. Zheng, J. Mater. Res. 12 (1997) 226.

International Journal of Modern Physics B
Vol. 23, No. 1 (2009) 105–111

World Scientific
www.worldscientific.com

ELECTRICAL PROPERTIES OF Nb-DOPED $Pb(Zr_{0.52}Ti_{0.48})O_3$ CERAMICS

PIYACHON KETSUWAN, YONGYUT LAOSIRITAWORN,
SUPON ANANTA and RATTIKORN YIMNIRUN*

Department of Physics, Faculty of Science,
Chiang Mai University, Chiang Mai 50200, Thailand
**rattikornyimnirun@yahoo.com*

Received 30 July 2008

The $Pb(Zr_{0.52}Ti_{0.48})O_3$ ceramics with 0.75, 1.0, 1.25 and 1.50%wt of Nb_2O_5 addition were prepared by a conventional mixed oxide technique. It was found that the average grain size of the ceramics decreased from 6 to 1 μm with increasing doping concentration to 1.5%wt. The room temperature dielectric constant and d_{33} reached maximum values of 1050 and 285 pC/N, respectively, at 1%wt Nb-doping. The electrical coercivity (E_c) of Nb-doped PZT decreased, while the polarization values increased, with increasing doping concentration. Most importantly, this study shows that Nb_2O_5-doped PZT ceramics exhibits soft piezoelectric and enhanced ferroelectric behaviors, and the optimum properties can be obtained using suitable doping concentration.

Keywords: Ferroelectric properties; dielectric properties; Nb-doped PZT.

1. Introduction

$Pb(Zr_{0.52}Ti_{0.48})O_3$ is a composition near the morphotropic phase boundary (MPB) of $Pb(Zr,Ti)O_3$ that separates rhombohedral and tetragonal ferroelectric forms with the coexistence of the 14 orientation states: 6-tetragonal and 8-rhombohedral. That is essential to allow the strong polarization for piezoelectricity. As the MPB is nearly vertical on the phase diagram, intrinsic property persists over a wide temperature range.[1] Almost all useful PZT ceramics are doped or modified to improve properties for specific applications.[2] Lead zirconate titanate solid solution modifications are controlled by aliovalent cation additions. The excess charge cation addition is called donor doped or soft PZTs, and the charge deficient cation is acceptor doped or hard PZTs. One approach of modification is off-valent donor doping, such as Nb^{5+} replacing Zr^{4+}. This makes the domain wall move more easily and results in enhanced dielectric constant and coupling factor but reduced electric coercivity.[3]

*Corresponding author.

However, there have only been a few reports on the effect of doping concentration of electrical properties of Nb-doped PZT ceramics prepared with conventional mixed-oxide method.[4–7] This study is therefore aimed at detailed and comprehensive investigation on the effect of doping $Pb(Zr_{0.52}Ti_{0.48})O_3$ with 0.75, 1.0, 1.25 and 1.50%wt of Nb_2O_5 addition on dielectric, piezoelectric and ferroelectric properties.

2. Experimental Method

The $Pb(Zr_{0.52}Ti_{0.48})O_3$ ceramics with addition of 0.75, 1.0, 1.25 and 1.50%wt Nb_2O_5 were prepared by conventional mixed oxide technique from PbO (Fluka 99.0%), ZrO_2 (Fluka 99.0%), TiO_2 (Fluka 99.9%) and Nb_2O_5 (Aldrich 99.9%) powders. After ball milling in ethanol for 24 h, the slurry was dried and calcined at 975°C for 2 h.[8] Then, the calcined powder was pressed into discs (d = 10 mm). The pellets were placed inside a closed alumina crucible covered with lead zirconate ($PbZrO_3$) powder to compensate the PbO volatilization and sintered at 1250°C for 2 h.

The X-ray diffraction (XRD) was used for structure and phase formation analysis. The microstructure was observed by scanning electron microscope (SEM). The bulk densities of sintered discs were measured by the Archimedes method. The dielectric, piezoelectric and ferroelectric properties were determined by automated LCR-meter, d_{33}-meter and a Sawyer-Tower circuit, respectively. The specimens were poled under 20 kV/cm at 120°C for 30 min in silicone oil.[9,10]

3. Results and Discussion

The X-ray diffraction pattern of Nb_2O_5 doped $Pb(Zr_{0.52}Ti_{0.48})O_3$ ceramics with varying concentration is shown in Fig. 1. The peak intensity indicates the formation of perovskite phases, which could be matched with JCPDS file 73-2022 for rhombohedral phase of PZT and JCPDS file 33-0784 for tetragonal phase of PZT. It should be noticed that the coexistence of tetragonal and rhombohedral phase for the undoped and doped PZT at 0.75 and 1.0%wt, which was characterized by (020) and (200) peaks. Finally, the rhombohedral phase became dominant at 1.25 and 1.5%wt.

The densification behavior of the specimens is shown in Fig. 2. The density increases at first with increasing doping concentration from 0.75 to 1.0%wt. Then a drop of the densification is observed when the concentration is further increased. However, the density of doped specimens is smaller than the undoped condition. The surface morphology of sintered ceramics was observed by using scanning electron microscope (SEM), as shown in Fig. 3. The mean grain size of the ceramics was determined by using the line intercept method. The mean grain size tends to decrease with increasing doping concentration. Similar observations have been reported in other systems.[4,6,7] This observation indicates that Nb_2O_5 addition had inhibited grain growth during the solid-solution process, as also reported earlier.[11,12]

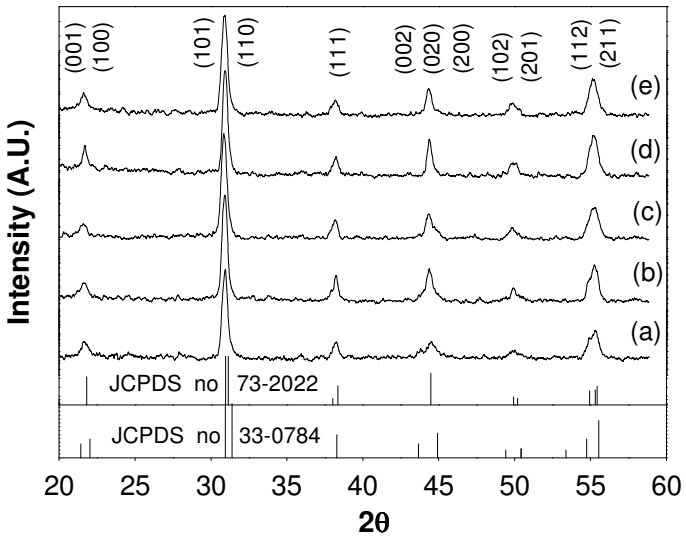

Fig. 1. XRD pattern of Nb_2O_5-doped $Pb(Zr_{0.52}Ti_{0.48})O_3$ ceramics sintered at 1250°C for 2 h with varying concentration (a) 0%wt, (b) 0.75%wt, (c) 1.0%wt, (d) 1.25%wt and (e) 1.5%wt.

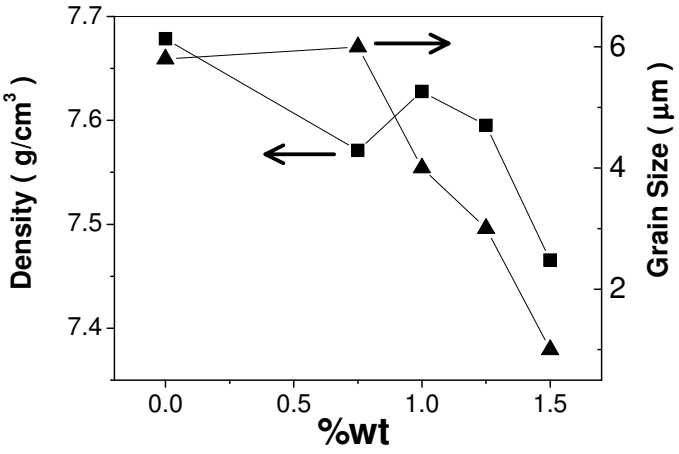

Fig. 2. Dependence of density and grain size of Nb_2O_5-doped $Pb(Zr_{0.52}Ti_{0.48})O_3$ ceramics on the doping concentration.

The room temperature dielectric constant and piezoelectric d_{33}-constant show a similar trend that is observed on densification behavior. The ε_r and d_{33}-constants increase with increasing doping from 0.75 to 1.0%wt. Then a drop of the ε_r and d_{33} is observed when the concentration is further increased, as shown in Fig. 4. In addition, both values of Nb_2O_5 doped samples are better than those of the undoped sample. This trend is also observed in $Pb(Zr_{0.51}Ti_{0.49})O_3$ ceramics doped with 5.5 mol% Nb_2O_5 as reported by Chu *et al.*[7]

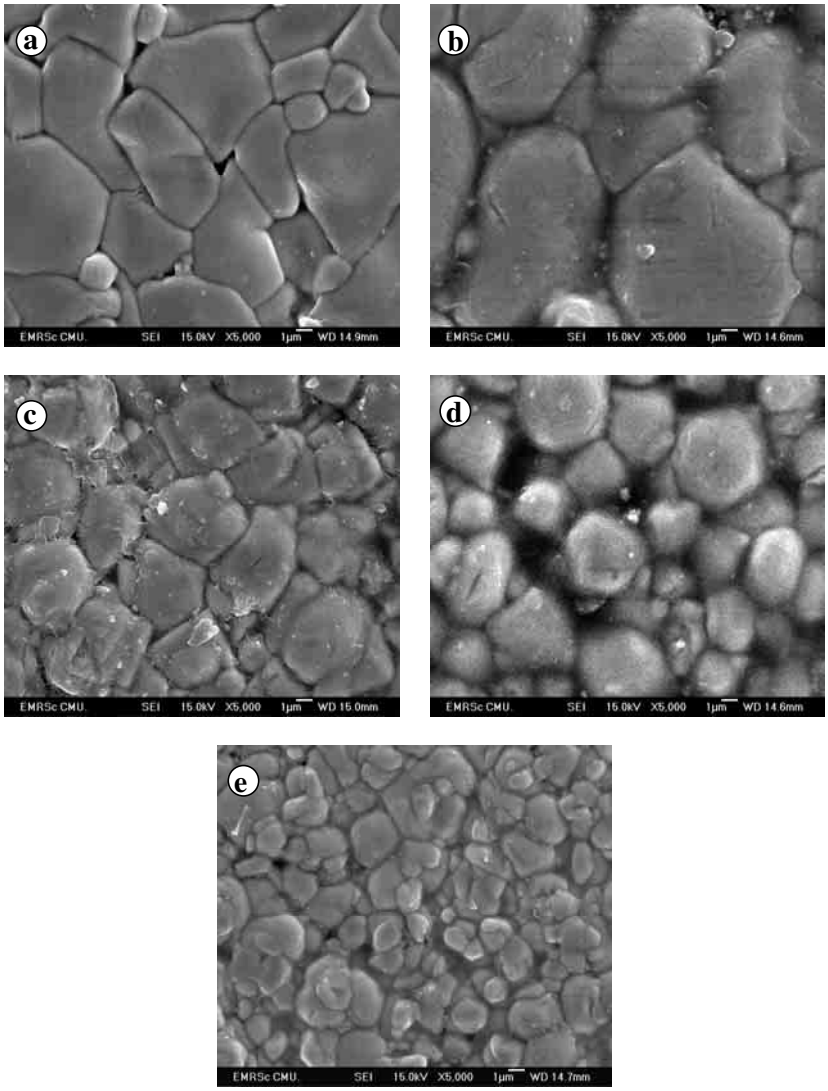

Fig. 3. SEM micrographs of Nb_2O_5-doped $Pb(Zr_{0.52}Ti_{0.48})O_3$ ceramics with doping concentration (a) 0%wt, (b) 0.75%wt, (c) 1.0%wt, (d) 1.25%wt and (e) 1.5%wt.

The ferroelectric hysteresis behavior of $Pb(Zr_{0.52}Ti_{0.48})O_3$ with addition of 0.75, 1.0, 1.25 and 1.50%wt Nb_2O_5 is shown in Fig. 5. The electrical coercivity (E_c) is seen to decrease, while the polarization values increase with increasing doping concentration. These observations clearly indicate the soft piezoelectric behavior of Nb-doped PZT, as expected.

It should also be noted that earlier investigations[11,13,14] observed enhanced electrical properties, particularly dielectric properties, with decreasing grain size in

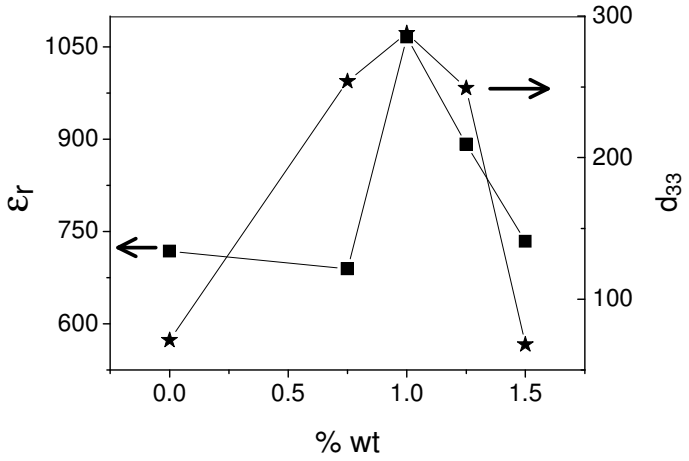

Fig. 4. The room temperature dielectric constant measured at 1 kHz and piezoelectric d_{33}-constant as a function of doping concentration of Nb_2O_5-doped $Pb(Zr_{0.52}Ti_{0.48})O_3$ ceramics.

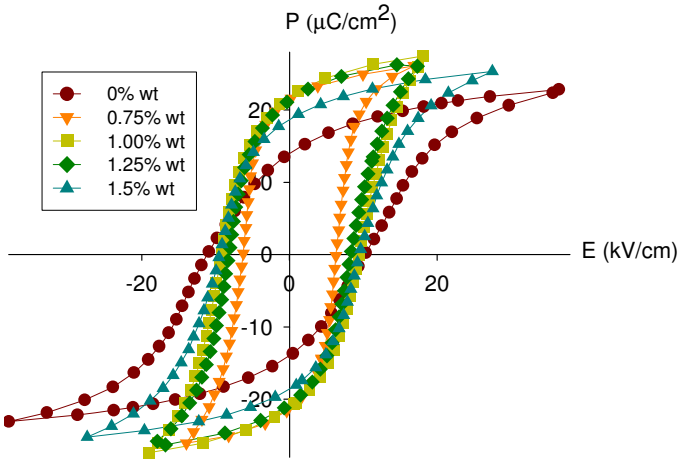

Fig. 5. P-E hysteresis loops of Nb_2O_5-doped $Pb(Zr_{0.52}Ti_{0.48})O_3$ ceramics.

perovskite ferroelectrics, such as PZT-based and BT-based ceramics. Therefore, one could state that the enhanced electrical properties observed in this study are partly due to decreasing grain size, as observed in Fig. 3. However, it should also be pointed out that there is a competing influence of the decreased density, which generally deteriorates electrical properties. These two competing microstructural features result in nearly constant dielectric constant (ε_r) in undoped and 0.75%wt Nb_2O_5 doped PZT ceramics, as shown in Fig. 4. However, with further increase in Nb_2O_5 concentration to 1.0%wt, the significant increase of ε_r is observed, possibly due to increased density and decreased grain size simultaneously. Although the grain

size continues to decrease with higher Nb_2O_5 concentration, the dielectric constant decreases significantly, likely due to a strong decrease in the density. Another possible reason for the decrease in the dielectric constant, as well as the d_{33} constant, beyond 1.0%wt Nb_2O_5 addition is a phase transition from mixed tetragonal and rhombohedral to mainly rhombohedral, as described earlier and shown in Fig. 1.

In addition to the relationship between the phase and microstructural features, and the electrical properties as described above, enhanced electrical properties can also be attributed to the softening effect with addition of Nb_2O_5 into PZT ceramics. As is well-known, a soft doping ion may soften the properties of piezoelectric ceramics, i.e., dielectric constant (ε_r) and piezoelectric d_{33} constant are enhanced, while the coercivity is reduced, as observed in Figs. 4 and 5. When ions with small ionic radius like Nb^{5+} enter into the perovskite lattice of PZT, they occupy the B-sites to replace Zr^{4+}/Ti^{4+} ions. Since the doping ions have higher valence than +4, extra positive charges entering the lattice and Pb vacancies have to be created to ensure electroneutrality. In a lattice having Pb vacancies, transfer of atoms is easier than in a perfect lattice; thus domain motions can be caused by a smaller electric field.[13,15] Therefore, the coercivity of Nb_2O_5 doped PZT ceramics is reduced, as compared to undoped PZT, as seen in Fig. 5. In addition, Pb-vacancies are negatively charged, and these can be paired with Nb^{5+} ions to form defect dipoles, which can be aligned when there is a spontaneous polarization or when there is an applied electric field. This will create a larger polarization, and hence explain why the doped PZT has larger polarization values than the undoped PZT, as seen in Fig. 5. The decrease in the d_{33} constant and the polarization values for PZT ceramics containing more than 1.0%wt Nb_2O_5 is likely due to the significant decrease in the density and the phase transition from mixed tetragonal and rhombohedral to mainly rhombohedral, as described earlier.

4. Conclusion

The effects of doping on the electrical properties of $Pb(Zr_{0.52}Ti_{0.48})O_3$ ceramics with addition of 0.75, 1.0, 1.25 and 1.50%wt Nb_2O_5 were investigated. The density increases at first with increasing doping concentration from 0.75 to 1.0%wt. Then a drop of the densification is observed when the concentration is further increased. It was found that the average grain size of the ceramics decreased from 6 to 1 μm with increasing Nb_2O_5 doping concentration to 1.5%wt. The room temperature dielectric constant and d_{33} reached maximum values of 1050 and 285 pC/N, respectively, at 1%wt Nb-doping. The electrical coercivity decreases, while the polarization values increase, with increasing doping concentration.

Acknowledgments

This work was supported by the Thailand Research Fund (TRF), Commission on Higher Education (CHE), Graduate School and Faculty of Science, Chiang Mai University.

References

1. L. E. Cross, *Mater. Chem. Phys.* **43**, 108 (1996).
2. G. H. Haertling, *J. Amer. Ceram. Soc.* **82**(4), 797 (1999).
3. K. Okazaki and K. Nagata, *J. Amer. Ceram. Soc.* **56**, 82 (1973).
4. M. Takahashi and S. Takahashi, *Jpn. J. Appl. Phys.* **9**, 1009 (1970).
5. M. D. Durruthy, *J. Mater. Sci.* **34**, 2311 (1999).
6. C. L. Huang, B. H. Chen and L. Wu, *Solid State Commun.* **130**, 19 (2004).
7. S. Y. Chu, T. Y. Chen, I. T. Tsai and W. Water, *Sensor and Actuators A* **113**, 198 (2004).
8. W. Chaisan, R. Yimnirun, S. Ananta and D. P. Cann, *Mater. Lett.* **59**(28), 3732 (2005).
9. R. Yimnirun, S. Ananta and P. Laoratanakul, *J. Eur. Ceram. Soc.* **25**(13), 3225 (2005).
10. R. Yimnirun, *Ferroelectrics* **331**, 9 (2006).
11. V. Singh, H. H. Kumar, D. K. Kharat, S. Hait and M. P. Kulkarni, *Mater. Lett.* **60**, 2964 (2006).
12. D. M. Hammer and M. J. Hoffmann, *J. Am. Ceram. Soc.* **81**, 3277 (1998).
13. R. F. Zhang, H. P. Zhang, J. Ma, Y. Z. Chen and T. S. Zhang, *Solid State Ionics* **166**, 219 (2004).
14. R. Yimnirun, R. Tipakorntitikul and S. Ananta, *Int. J. Mod. Phys. B* **20**(17), 2415 (2006).
15. W. Qiu and H. H. Hng, *Mater. Chem. Phys.* **75**, 151 (2002).

International Journal of Modern Physics B
Vol. 23, No. 3 (2009) 403–410

World Scientific
www.worldscientific.com

DIELECTRIC PROPERTIES OF LEAD MAGNESIUM NIOBATE-LEAD TITANATE CERAMICS PREPARED BY MIXED-OXIDE METHOD

RATTIKORN YIMNIRUN

Department of Physics, Faculty of Science, Chiang Mai University, Chiang Mai 50200 Thailand
rattikornyimnirun@yahoo.com

Received 9 September 2006

In this study, the $(1-x)\mathrm{Pb}(\mathrm{Mg}_{1/3}\mathrm{Nb}_{2/3})\mathrm{O}_{3-x}\mathrm{PbTiO}_3$ (when $x = 0.1$, 0.3 and 0.5) ceramics were prepared from PMN and PT powders by a mixed-oxide method. The dielectric properties of the ceramics were measured as functions of both temperature (-150–400°C) and frequency (100 Hz–1 MHz). The results indicated that the dielectric properties of pseudo-cubic phase 0.9PMN-0.1PT and tetragonal phase 0.5PMN-0.5PT ceramics followed that of relaxor and normal ferroelectric behaviors, respectively, while the dielectric behaviors of a near MPB phase 0.7PMN-0.3PT ceramic showed a mixture of normal and relaxor ferroelectric behaviors. In addition, the Curie temperature (T_C) increased with increasing PT contents, while the diffusivity decreased. This confirmed a gradual transition from a relaxor ferroelectric behavior in 0.9PMN-0.1PT to a normal ferroelectric behavior in 0.5PMN-0.5PT. The difference in dielectric behaviors was attributed to the structural symmetry of the ceramics.

Keywords: PMN-PT; dielectric properties.

1. Introduction

Ceramics are one of the many classes of electronic materials. The electronic industries are demanding smaller, higher packing density and higher frequency electronic devices.[1] Among those features, volume efficiency can be easily improved by reduction of the dimensions of devices and by increasing the dielectric constant of the materials used. This is particular in the case for capacitor industry, in which uses of high dielectric constant ceramics are of great success. A family of materials which dominates the industry is lead-based ferroelectrics, especially lead magnesium niobate, $\mathrm{Pb}(\mathrm{Mg}_{1/3}\mathrm{Nb}_{2/3})\mathrm{O}_3$ or PMN, and its solid solution with lead titanate, PbTiO_3 or PT, the so-called PMN-PT compounds, which show dielectric constant in excess of 20,000, making them candidate materials for capacitors.[2] In addition, they exhibit electrostrictive behavior at temperatures above their transition temperatures. This particular feature leads to their uses in transducers and actuators.[3,4]

Lead magnesium niobate (PMN) is generally established as a representative of relaxor ferroelectrics. Although the Curie temperature of PMN is well below room temperature,[5] it can be easily shifted upward with PT addition, a normal ferroelectric compound which has a transition at 490°C. A spontaneous phase transition is indicated in the solid solution PMN-PT as a result of a change in the degree of ordering induced by substitution of cationic sites. An addition of ∼28% PT causes the material to revert to a normal ferroelectric tetragonal phase with $T_C \sim 130$°C. The $(1-x)$PMN-(x)PT system also shows a morphotropic phase boundary (MPB) near $x \sim 0.4$, separating pseudo-cubic phase and tetragonal phases. As observed in other systems such as PZN-PT and PZT, anomalously large dielectric and piezoelectric properties are observed for compositions lying near the MPB.[6] This study is aimed at investigating the dielectric properties, as functions of both temperature and frequency, of ceramics in PMN-PT system. In particular, three compositions, 0.9PMN-0.1PT, 0.7PMN-0.3PT and 0.5PMN-0.5PT representing pseudo-cubic, near MPB and tetragonal phases, respectively, are chosen for the study to examine the roles of MPB, as well as to establish the structure-property relations for the PMN-PT system.

2. Materials and Methods

The $Pb(Mg_{1/3}Nb_{2/3})O_3$–$PbTiO_3$ ceramics were prepared from PMN and PT powders by a mixed-oxide method. Perovskite-phase PMN powders were obtained via a well-known columbite method,[7] while PT powders were prepared by a more conventional mixed-oxide method. For PMN powders, the magnesium niobate ($MgNb_2O_6$) powders were first prepared by mixing starting MgO (>98%) (Fluka, Switzerland) and Nb_2O_5 (99.9%) (Aldrich, Germany) powders and then calcining the mixed powders at 1100°C for 3 hours with the heating/cooling rates of 20°C/min. This yielded a so-called columbite powder ($MgNb_2O_6$). The columbite powders were subsequently ball-milled with PbO (99%) for 24 hours. The mixed powders were calcined at 800°C for 1 hour with the heating/cooling rates of 20°C/min. X-ray diffraction analysis was employed to confirm the formation of perovskite-phase PMN. PT powders were prepared from reagent-grade PbO (99%) and TiO_2 (98.5%) starting powders (Fluka, Switzerland). These powders were ball-milled for 24 hours and then calcined at 600°C for 1 hour with the heating/cooling rates of 20°C/min. The $(1-x)Pb(Mg_{1/3}Nb_{2/3})O_{3-x}PbTiO_3$ powders (when $x = 0.1$, 0.3 and 0.5) were subsequently prepared from the precursor PMN and PT powders by a mixed-oxide technique. Initially, PMN and PT powders for a given composition were weighed and then ball-milled in ethanol for 24 hours. The mixed powders were calcined for 2 hours at 900, 800 and 750°C for compositions with $x = 0.1$, 0.3 and 0.5, respectively, with the heating/cooling rates of 20°C/min. To fabricate PMN-PT ceramics, the calcined powders were pressed hydraulically to form disc-shaped pellets 15 mm in diameter and 2 mm thick, with 5 wt.% polyvinyl alcohol (PVA) as a binder. The pellets were stacked in a covered alumina crucible. Finally, the sintering was

carried out at a sintering temperature for 2 hours with 15 min/°C heating and cooling rates. The sintering temperature was optimized at 1240°C for compositions with $x = 0.1$ and 0.3, and at 1220°C for composition with $x = 0.5$. More details of the powder and ceramic preparation studies were described thoroughly in previous publication[8] and will not be included in this present context, which is focused on the dielectric properties of the successfully prepared ceramics.

The dielectric properties of the sintered ceramics were studied as functions of both temperature and frequency with an automated dielectric measurement system. The computer-controlled dielectric measurement system consisted of an LCR-meter (Hewlett–Packard Precision LCR-Meter HP 4284A), a temperature chamber (Delta Design 9023) and a computer system. The detailed description of this system was explained elsewhere.[9] For dielectric property characterizations, the sintered samples were lapped to obtain parallel faces, and the faces were then coated with silver paint as electrodes. The samples were heat-treated at 750°C for 12 min to ensure the contact between the electrodes and the ceramic surfaces. The capacitance and the dielectric loss tangent were determined over the temperature of −150 and 400°C with the frequency ranging from 100 Hz to 1 MHz. The measurements were carried out on cooling continuously. Before each cooling run, the samples were first heated up to 400°C and then cooling run was performed at the rate of 4°C/min. The dielectric constant was then calculated from $\varepsilon_r = Cd/\varepsilon_0 A$, where C is the capacitance of the sample, d and A are the thickness and the area of the electrode, respectively and ε_0 is the dielectric permittivity of vacuum ($8.854 \times 10^{-12} F/m$).

3. Results and Discussion

The experimental results on physical properties, the phase formation behavior and microstructure features of all the sintered ceramics are presented and discussed thoroughly elsewhere.[10] Hence, these results will not be shown here. However, it should be stated here that the sintered ceramics are in perovskite phase with a pseudo-cubic crystal structure for 0.9PMN-0.1PT, and with a tetragonal crystal structure for 0.5PMN-0.5PT. It is of interest to see that 0.7PMN-0.3PT composition shows a mixed pseudo-cubic and tetragonal symmetry, which confirms that the MPB of the PMN-PT system lies between $x = 0.3$ and 0.4.[6] Table 1 includes the density and grain-size range for all ceramic compositions. It should be noted that

Table 1. Physical and dielectric properties of PMN-PT ceramics (at 1 kHz).

Ceramic	Density (g/cm^3)	Grain size (μm)	T_C (°C)	Maximum properties		Room temp. properties		Diffusivity (γ)
				ε_r	$\tan\delta$	ε_r	$\tan\delta$	
0.9PMN-0.1PT	7.98	0.42 – 3.66	38	25400	0.049	19400	0.087	1.96
0.7PMN-0.3PT	7.86	0.41 – 2.80	197	23500	0.011	2320	0.022	1.63
0.5PMN-0.5PT	7.78	0.48 – 3.76	250	23200	0.085	1010	0.025	1.14

a variation in these physical features could impose significant effects on dielectric properties. However, as seen in Table 1, the density and the grain size range are not significantly different, and are not expected to show marked effects on the dielectric properties of the ceramics. Therefore, in this case, it is reasonable to assume that the dielectric properties of the ceramics are mainly influenced by their structural symmetry, as will be discussed in the following context.

The dielectric properties, e.g., dielectric constant (ε_r) and $\tan\delta$, are measured as functions of both temperature and frequency, as shown in Figs. 1(a)–1(c). As listed in Table 1, the Curie temperature (T_C) (determined at measuring frequency of 1 kHz) increases from 38°C in 0.9PMN-0.1PT to 250°C in 0.5PMN-0.5PT. This is a direct result of PT addition to PMN ($T_C \sim -8$°C) since PT itself has a Curie temperature of 490°C.[11] The maximum dielectric constant for all the ceramics studied is in excess of 20,000. This is clearly a reason for their potential applications in capacitors.[1–4] As shown in Fig. 1(a), for 0.9PMN-0.1PT ceramic, both dielectric constant (ε_r) and dielectric loss tangent ($\tan\delta$) exhibit strong temperature-frequency dependence below the transition temperature. This is a typical dielectric behavior of relaxor ferroelectrics,[3] in which a strong temperature-frequency dependence is observed and the temperatures of maximum dielectric constant and dielectric loss tangent are shifted to higher temperature with increasing frequency. The maximum value of the dielectric constant decreases with increasing frequency, while that of the dielectric loss tangent increases. The dielectric properties then become frequency independent above the transition temperature.[12–14] PMN is a well-known relaxor ferroelectric material with diffused phase transition (DPT) as a result of a short-range ordered structure with a nanometer scale heterogeneity in composition.[12] Small addition of PT to PMN causes an increase in T_C, but the strong relaxor behavior still exists. In addition, since 0.9PMN-0.1PT ceramic has a pseudo-cubic symmetry, it is therefore intrinsically electrostrictive (i.e., its electrically-induced strain is quadratically proportional to the applied electric field and is nonhysteretic).[4] With its enhanced dielectric properties at room temperature, as listed in Table 1, it is widely employed in transducers and actuators.[2–4]

Further increase in PT contents leads to more observable normal ferroelectric behavior because PT is intrinsically a normal ferroelectric.[3,4] The dielectric properties of 0.7PMN-0.3PT ceramic, as plotted in Fig. 1(b), exhibit a mixture of both normal and relaxor characteristics, in which the transition temperature is not shifted as much as for relaxor 0.9PMN-0.1PT ceramic. Similar tendency has also been observed in several prior investigations.[12–14] It should be noted that 0.7PMN-0.3PT ceramic composition is close to MPB of the PMN-PT system. Therefore, its structural symmetry is a mixture of pseudo-cubic and tetragonal, which in turn causes a mixture of normal and relaxor characteristics observed for dielectric properties. With a tetragonal symmetry, the 0.5PMN-0.5PT ceramic, on the other hand, exhibits a normal ferroelectric behavior with a very sharp phase transition. As plotted in Fig. 1(c), the dielectric properties of 0.5PMN-0.5PT ceramic change significantly with temperature, but are nearly independent of frequency, except in the vicinity

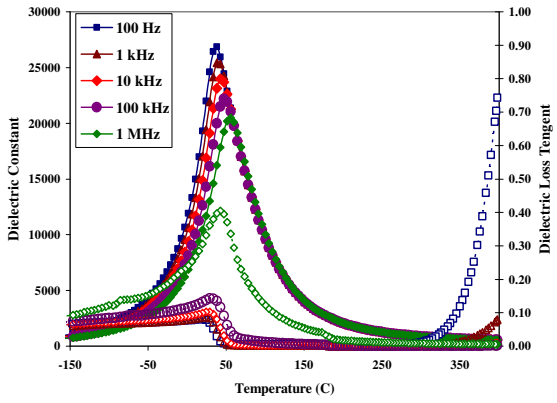

(a)

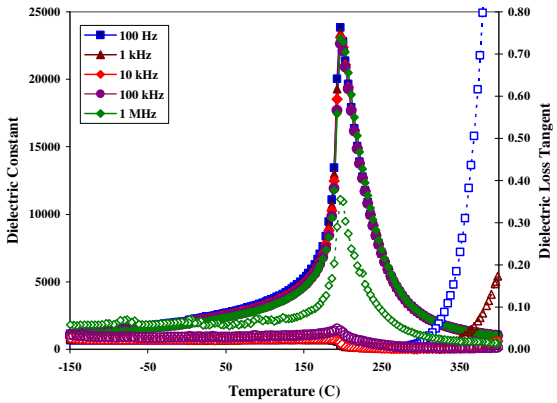

(b)

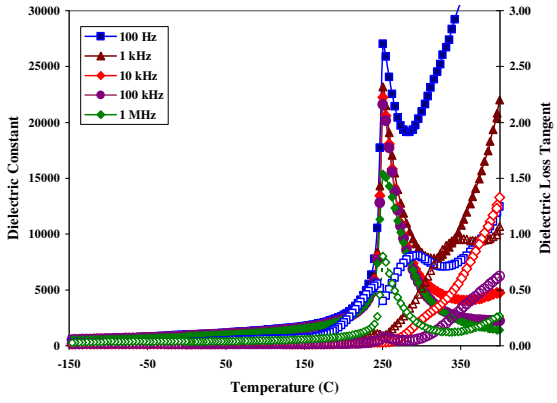

(c)

Fig. 1. (Color on line) Temperature and frequency dependences of dielectric properties of (a) 0.9PMN-0.1PT ceramic, (b) 0.7PMN-0.3PT ceramic and (c) 0.5PMN-0.5PT ceramic (open markers with dotted lines indicate data for the dielectric loss tangent ($\tan\delta$) at the same frequency).

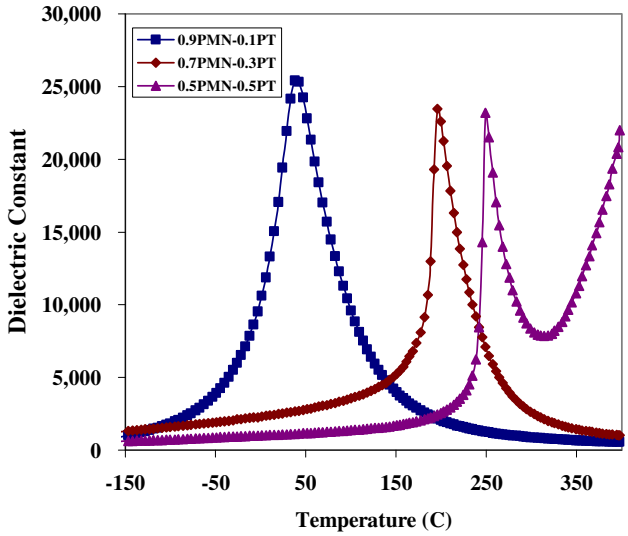

Fig. 2. (Color on line) Temperature dependence of dielectric constant of PMN-PT ceramics (measured at 1 kHz).

of the phase transformation temperature. This is a typical characteristic of normal ferroelectric ceramics with a long-range ordered structure.[3,12] It should also be noted here that the dielectric properties in all ceramics increase significantly at high temperature as a result of thermally activated space charge conduction.[13,14]

When PT is added to form the binary system with PMN, the T_C increases monotonically, as shown in Table 1 and Fig. 2, and the dielectric behavior is shifted from relaxor ferroelectric towards normal ferroelectric. The degree of broadening or diffuseness is used to assess such behavior in the observed dielectric variation. This could be estimated with the diffusivity (γ) using the expression $\ln(1/\varepsilon_r - 1/\varepsilon_{\max})$ versus $(T - T_{\max})^{\gamma}$. The value of γ can vary from 1, for normal ferroelectrics with a normal Curie–Weiss behavior, to 2, for completely disordered relaxor ferroelectrics.[13–16] The plots in Fig. 3 show that the variation is very linear. The mean value of the diffusivity (γ) is extracted from these plots by fitting a linear equation. The values of γ listed in Table 1 vary between 1.14 for 0.5PMN-0.5PT and 1.96 for 0.9PMN-0.1PT. These results confirm that diffuse phase transition occur in 0.9PMN-0.1PT ceramic ($\gamma = 1.96$) with a nearly complete disorder characteristic, while a strong normal ferroelectric behavior is observed for 0.5PMN-0.5PT ceramic with $\gamma = 1.14$. With the γ value of 1.63, 0.7PMN-0.3PT ceramic is expected to possess a mixed behavior, as is confirmed by the dielectric data plotted in Fig. 1(b). In addition, it should also be noted that even if it is established that the diffuseness could be caused by the decrease of grain size in a perovskite ferroelectric material,[12] the observed difference of the degree of the diffuseness in this study is not a result of the grain size variation because of the uniformity of the grain size range of the ceramics studied.

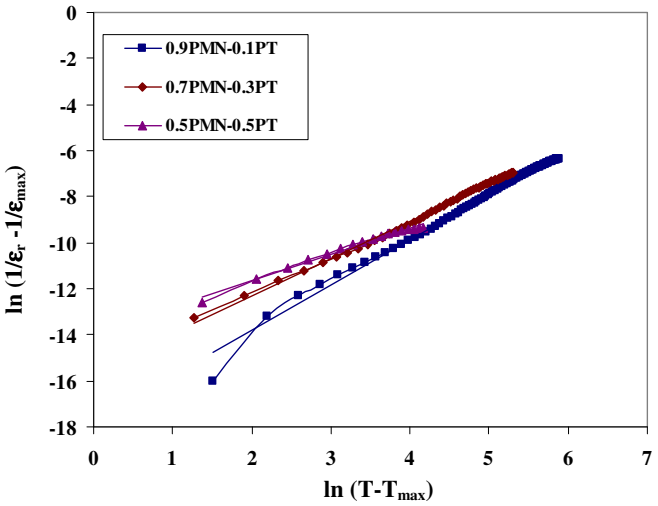

Fig. 3. (Color on line) Variation of $\ln(1/\varepsilon_r - 1/\varepsilon_{\max})$ versus $\ln(T - T_{\max})$ of PMN-PT ceramics in the paraelectric region at 1 kHz.

4. Conclusion

The $(1-x)\mathrm{Pb}(\mathrm{Mg}_{1/3}\mathrm{Nb}_{2/3})\mathrm{O}_{3-x}\mathrm{PbTiO}_3$ (when $x = 0.1$, 0.3 and 0.5) ceramics are prepared from PMN and PT powders by a mixed-oxide method. The dielectric properties of the ceramics are determined as functions of both temperature and frequency with an automated dielectric measurement system. The measurement takes place over the temperature range of -150°C and 400°C with measuring frequency between 100 Hz and 1 MHz. The results indicate that the dielectric properties of pseudo-cubic phase 0.9PMN-0.1PT and tetragonal phase 0.5PMN-0.5PT ceramics follow that of relaxor and normal ferroelectric behaviors, respectively, while the dielectric behaviors of a near MPB phase 0.7PMN-0.3PT ceramic show a mixture of normal and relaxor ferroelectric behavior. In contrast to an increase in T_C with increasing PT contents, the degree of broadening or diffuseness shows a decrease, which confirms a transition from a relaxor ferroelectric behavior in 0.9PMN-0.1PT to a normal ferroelectric behavior in 0.5PMN-0.5PT. The difference in dielectric behaviors is attributed to the structural symmetry of the ceramics.

Acknowledgments

The author expresses his gratitude for financial support from the Thailand Research Fund (TRF). Help with the sample preparation by Dr. A. Udomporn and with the dielectric measurements by Dr. Y. Somiya are gratefully acknowledged.

References

1. A. J. Moulson and J. M. Herbert, *Electroceramics: Materials, Properties, Applications*, 2nd edn. (John Wiley & Sons Ltd, New York, 2003).

2. G. H. Haertling, *J. Am. Ceram. Soc.* **82**(4), 797 (1999).
3. L. E. Cross, *Mater. Chem. Phys.* **43**, 108 (1996).
4. S. E. Park and T. R. Shrout, *Mater. Res. Innov.* **1**, 20 (1997).
5. G. A. Smolenskii and A. I. Agranovskaya, *Sov. Phys.-Solid State* **1**, 1429 (1960).
6. S. W. Choi, J. M. Tang and A. S. Bhalla, *Ferroelectrics* **189**, 27 (1996).
7. S. L. Swartz and T. R. Shrout, *Mater. Res. Bull.* **17**, 1245 (1982).
8. A. Udomporn and S. Ananta, *Mater. Lett.* **58**, 1154 (2004).
9. Q. Jiang, Electrically induced fatigue effects and reliability in piezoelectric and electrostrictive ceramics, Ph.D. thesis, The Pennsylvania State University, University Park (1992).
10. A. Udomporn, Preparation and structural characterization of lead magnesium niobate-lead titanate ceramics, Ph.D. thesis, Chiang Mai University, Chiang Mai (2004).
11. B. Jaffe, W. R. Cook and H. Jeffe, *Piezoelectric Ceramics* (Academic Press, New York, 1997).
12. V. Koval, C. Alemany, J. Briancin, H. Brunckova and K. Saksl, *J. Eur. Ceram. Soc.* **23**, 1157 (2003).
13. R. Yimnirun, S. Ananta and P. Laoratanakul, *Mater. Sci. Eng. B* **112**, 79 (2004).
14. R. Yimnirun, S. Ananta and P. Laoratanakul, *J. Eur. Ceram. Soc.* **25**, 3225 (2005).
15. E. F. Alberta and A. S. Bhalla, *J. Phys. Chem. Solids* **63**, 1759 (2002).
16. W. Chaisan, R. Yimnirun, S. Ananta and D. P. Cann, *Mater. Lett.* **59**, 3732 (2005).

Materials Chemistry and Physics 114 (2009) 569–575

Contents lists available at ScienceDirect

Materials Chemistry and Physics

journal homepage: www.elsevier.com/locate/matchemphys

Effect of two-stage sintering on phase formation, microstructure and dielectric properties of perovskite PMN ceramics derived from a corundum $Mg_4Nb_2O_9$ precursor

R. Wongmaneerung[a], R. Yimnirun[b], S. Ananta[b,*]

[a] Department of Physics, Faculty of Science, Maejo University, Chiang Mai 50290, Thailand
[b] Department of Physics, Faculty of Science, Chiang Mai University, Chiang Mai 50200, Thailand

ARTICLE INFO

Article history:
Received 31 January 2008
Received in revised form
16 September 2008
Accepted 2 October 2008

Keywords:
Lead magnesium niobate
Perovskite
Sintering
Dielectric properties

ABSTRACT

Pure and dense relaxor perovskite ceramics of lead magnesium niobate (PMN) have been successfully fabricated by using a combination between a corundum $Mg_4Nb_2O_9$ *B*-site precursor and a two-stage sintering techniques. Effect of doubly sintering on phase formation, microstructure and dielectric properties of the PMN ceramics was determined via XRD, SEM and dielectric measurement. It has been found that under suitable two-stage sintering schemes, dense and pure perovskite PMN ceramics derived from a corundum *B*-site precursor route can be successfully achieved with better dielectric properties than those of ceramics from either a conventional or a two-stage sintered columbite *B*-site precursor methods.

1. Introduction

Relaxor perovskite ferroelectric lead magnesium niobate, $Pb(Mg_{1/3}Nb_{2/3})O_3$ (PMN), -based-ceramics are widely employed for electronic applications such as multilayer capacitors, electrostrictive actuators and components working by induced piezoelectric effect [1,2]. Principal role in the properties of the niobates plays intrinsic cationic substitution which form additional anharmonic electron–phonon interaction [3] determining the principal electronic and optical properties. However, the main hindrance to the utilization of these PMN-based materials in electronic device applications has been the lack of simple, reproducible fabrication technique for dense and pure perovskite phase [4–6]. Moreover, it would also be highly desirable for these materials to be fired at relatively low temperatures, permitting the use of low-cost electrode materials, e.g. copper or nickel [1,2]. It is well-known that the fabrication of PMN via a solid-state reaction method is complicated by the formation of an undesired lead-niobate-based pyrochlore phases during the final stage of reaction between mixed oxides and the high volatility of lead oxide [5–8]. Several approaches have been introduced to minimize the pyrochlore phases and improve the reproducibility of their dielectric properties [9–12]. These involve modification of solid-state or wet chemical methods, but most of them leave 3–5 wt% pyrochlore phase in the sintered products [7,8]. In connection with this, a "columbite" method [8] where $MgNb_2O_6$ is formed first, followed by its reaction with PbO to form the perovskite PMN, has become one of the most effective solid-state reaction method which has been widely employed to produce PMN since 1982 [8]. Alternatively, different kinds of precursor such as $Pb_3Nb_2O_8$ [13] or "corundum" $Mg_4Nb_2O_9$ [14] have been introduced instead of $MgNb_2O_6$. Amongst all the approaches reported so far, most attention has been concentrated on the powder processing, whereas investigation of modified sintering techniques for the production of PMN ceramics has not been widely carried out [15]. In practice, sintering is a crucial stage which can significantly affect the densification and the dielectric properties of the PMN ceramics more strongly than the choice of reaction precursors.

In our previous work [15], a combination between the columbite *B*-site precursor and the two-stage sintering techniques has been proposed to achieve the densification of PMN ceramic bodies without significant grain growth. However, so far, no work has been done on the investigation of the two-stage sintering PMN ceramics derived from a corundum *B*-site precursor route. Therefore, in this work, an attempt has been made to fabricate and characterize the relaxor perovskite PMN ceramics by employing a combination of the corundum precursor and the two-stage sintering methods. The influence of doubly sintering condition on phase formation,

* Corresponding author. Tel.: +66 53 943376; fax: +66 53 943445.
E-mail address: suponananta@yahoo.com (S. Ananta).

0254-0584/$ – see front matter © 2008 Elsevier B.V. All rights reserved.
doi:10.1016/j.matchemphys.2008.10.003

microstructure and dielectric properties of the PMN ceramics is investigated.

2. Materials and methods

The starting materials were commercially available oxide powders of PbO, MgO and Nb_2O_5 (Aldrich, 99% purity) with an average particle size of 3–5 μm. A corundum *B*-site precursor route [16] employing intermediate phase of $Mg_4Nb_2O_9$ was adopted for the preparation of PMN powders. In this method, MgO and Nb_2O_5 were reacted at 1050 °C for 4 h with heating/cooling rates of 10 °C min^{-1} to form $Mg_4Nb_2O_9$ [17,18], prior to reaction with PbO at 950 °C for 1 h with heating/cooling rates of 30 °C min^{-1} [16]. All powders were prepared by using a simple mixed oxide method via a rapid-vibro milling technique for 30 min with corundum media in isopropyl alcohol, as detail described in our previous works [17–19]. Ceramic fabrication was achieved by adding 3 wt% polyvinyl alcohol (PVA) binder, prior to pressing as pellets in a pseudo-uniaxial die press. Each pellet was placed in an alumina crucible together with an atmosphere powder of identical chemical composition. After the binder burn out at 500 °C for 1 h, sintering was carried out with a dwell time of 1 h at each step, with constant heating/cooling rates of 20 °C min^{-1} applied. Three sets of the first sintering temperature (T_1) were designed for the two-stage sintering case: 1025, 1050 and 1075 °C. Variation of the second sintering temperature (T_2) between 950 and 1025 °C was carried out for each case.

Densities of the final sintered products were measured by using the Archimedes principle. Sintered ceramics were examined by room-temperature X-ray diffraction (Siemen D-500 diffractometer) using Cu Kα radiation to identify the phase formed. The microstructural development was characterized using a scanning electron microscopy (JEOL JSM-840A). Mean grain size of the sintered ceramics was subsequently estimated by employing the linear intercept method [20]. In order to evaluate the dielectric properties, dense ceramics were polished to form flat, parallel faces and then coated with gold electrodes. The dielectric properties were measured at various frequencies using a LCR meter (HIOKI 3532-50), on cooling through the transition range (−50 to 100 °C) with a rate of 3 °C min^{-1}.

3. Results and discussion

X-ray diffraction patterns of the PMN ceramics doubly sintered at various conditions are displayed in Fig. 1, indicating the formation of both perovskite and impurity phases in each case. The results indicated that a single phase of perovskite PMN (yield of 100% within the limitations of the XRD technique) is found at only three sets of sintering conditions: i.e. at 1025/1000 °C, 1050/1025 °C and 1075/1025 °C. The strongest reflections in the majority of all XRD traces indicate the formation of the $Pb(Mg_{1/3}Nb_{2/3})O_3$ perovskite phase, which could be matched with JCPDS file no. 81-861, in agreement with other works [21,22]. To a first approximation, this major phase has a cubic phase in space group *Pm*3*m* (no. 221) with cell parameter *a* = 404.41 pm [23]. For other doubly sintering conditions, additional weak reflections of the pyrochlore-type phase previously observed in normal sintered PMN case [20] are found to co-exist along with the perovskite PMN. It should be attributed to many factors, including the poor mixing of the employed powders derived from the mechanical milling technique and the PbO evaporation [21,22]. Whilst it is possible to obtain better mixing through planetary- or jet-milling method [1], these mechanical millings can lead to seriously higher contaminations (which in turn lead to another problem of getting rid of all of them). Hence, one has to balance between these two factors in each case. In addition, as suggested in the literature [24], the PbO evaporation could also be determined by measuring weigh loss by assuming that the PbO is the only evaporating component in the system, which in most case is still incorrect.

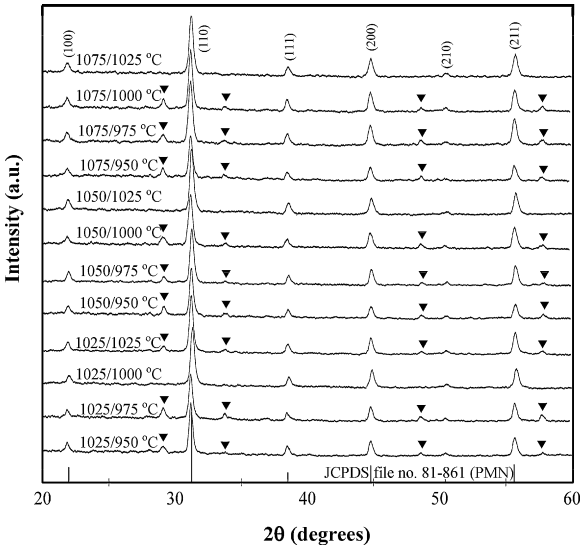

Fig. 1. XRD patterns of PMN ceramics doubly sintered at various conditions.

Nonetheless, this minor phase could be correlated with pyrochlore phase of composition $Pb_{1.86}(Mg_{0.24}Nb_{1.76})O_{6.5}$ (marked by ▼), and could be matched with JCPDS file no. 82-388 [25]. This phase has a pyrochlore-type structure with a cubic unit cell *a* = 10.60 Å, space group *Fd*3*m* (no. 227). Moreover, no evidence of other pyrochlore phases such as $Pb_2Nb_2O_7$, $Pb_3Nb_4O_{13}$, and $Pb_{1.83}Nb_{1.71}Mg_{0.29}O_{6.39}$ has been observed here whereas these phases were found in other works [5,8,15]. By comparison with other processing routes, it is found that only one set of double-sintering condition was found to produce a single phase perovskite PMN (at 1025/1100 °C) in the two-stage sintered columbite-route PMN [15] whilst a minimum temperature of up to 1225 °C is required for the normal sintered columbite-route PMN ceramics [21]. This observation indicates that the $Mg_4Nb_2O_9$ precursor is a better precursor to get rid of the unwanted pyrochlore phase, probably due to the better chemical reactivity between PbO and $Mg_4Nb_2O_9$.

In order to evaluate the relative amounts of perovskite and pyrochlore phases in each doubly sintering condition, the following approximation was employed, as in the earlier PMN and PFN studies [15]:

$$\text{perovskite phase(wt\%)} = \frac{I_p}{I_p + I_m} \times 100$$

Here I_p and I_m refer to the intensities of the (1 1 0) perovskite and (2 2 2) minor phase peaks, respectively, these being the most intense reflections in the XRD patterns of both phases. For the purposes of estimating the concentration of minor phase present, Eq. (1) has been applied to the diffraction patterns obtained (Table 1). Table 1 also presents the relative density and grain size data of the two-stage sintered PMN samples compared with conventional case [21]. Generally, it is evident that as the sintering temperature increases, the density of almost all the samples increases. The two-stage sintered corundum-route PMN ceramics reaches a maximum density of ~97% at 1075/1025 °C, each for 1 h (normal sintered columbite-route PMN samples exhibit equivalent densification after sintered at 1275 °C for 2 h [21]). On the other hand, two-stage sintered columbite-route PMN ceramics exhibit less densification and a sintering scheme of 1125/1100 °C, each for 2 h, is required to reach a densification level of ~91% [15]. Moreover, it can be seen that the relative density of the two-stage sintered corundum-route PMN ceramics increases from 85 to 97% with increasing sintering temperature, whilst grain size changes only slightly (about 2.1–2.9 μm). This is probably because the two stage sintering proceeds in a "frozen" microstructure and has the effect on grain growth. Hence, the kinetics are sufficient for reaching fairly high density, whilst providing the benefit of suppression grain growth [26,27]. The physical characteristics of various two-stage sintered PMN samples obtained by different *B*-site precursors are also compared in Table 1. Apart from employing shorter dwell time and faster heating/cooling rates, it can be noticed that

Table 1
Physical properties of PMN ceramics doubly sintered at various conditions.

T_1 (°C)	T_2 (°C)	Perovskite phase[a] (wt%)	Relative density[b] (%)	Grain size range (mean)[c] (μm)
1025	950	83.5	90	1.1–2.9 (2.0)
1025	975	92.0	91	1.1–3.0 (2.0)
1025	1000	100	94	1.2–3.0 (2.1)
1025	1025	96.4	96	1.0–2.9 (1.9)
1050	950	87.1	85	1.2–2.8 (2.0)
1050	975	89.1	93	1.3–3.0 (2.2)
1050	1000	92.4	94	1.3–3.0 (2.2)
1050	1025	100	96	1.4–3.2 (2.3)
1075	950	84.3	93	1.5–3.4 (2.5)
1075	975	88.6	94	1.5–3.8 (2.7)
1075	1000	92.0	95	1.6–4.0 (2.8)
1075	1025	100	97	1.6–4.2 (2.9)
1025	1100	100	91	2.0–7.0 (4.5) (Ref. [14])
1275	–	100	96	3.2–15.6 (9.4) (Ref. [20])

[a] The estimated precision of the perovskite phases is ±1%.
[b] The estimated precision of the density is ±1%.
[c] The estimated precision of the grain size is ±10%.

optimized sintering temperature and/or dwell time of the two-stage sintered corundum-route PMN ceramics in this work is lower than the normal sintering [21] and equivalent to the two-stage sintered columbite-route PMN ceramics [15]. This observation could be attributed mainly to the effectiveness of a combination between the two-stage sintering and the corundum *B*-site precursor methods.

As-fired and fracture surface SEM micrographs of corundum-route PMN samples doubly sintered with different schemes are shown in Fig. 2(i) and (ii), respectively. Clearly, the free surface microstructure of the two-stage sintered corundum-route PMN ceramics is significantly different from those of the normal and the two-stage sintered columbite-route PMN sample [15,21] which exhibits highly dense microstructure with abnormal grains of size around ~3–4 μm due to the recrystallization during firing and variation of stoichiometric compositions [28]. Their grain sizes are in the range of 1–4 μm which is significantly lower than those observed in the normal and the two-stage sintered columbite-route PMN ceramics (Table 1) [15,21]. Moreover, with careful observation (Fig. 2(i)), it can be found that PMN grains in two-stage sintered sample also exhibit whisker-like shape, similar to the results observed by Chaisan et al. [29]. With sizes of ~300–500 nm in length and ~60–100 nm in width, these whiskers are seen to distribute and coat on the grains (only at the surfaces). By using an energy dispersive X-ray (EDX) analysis, the chemical composition of these whiskers is identified as $Pb(Mg_{0.33}Nb_{0.67})O_3$. Even though exact mechanism of the microstructure observed here is not well established, but it should be noted that the various features of microstructure in PMN ceramics depend on the grain growth rate in the different planes [30]. However, the sintered process and growth environment also play an important role in the formation of microstructures [31]. In this work, the occurrence of a typical abnormal grain growth commonly found in the PMN-based systems [32–35] is observed and is likely to be caused by atom attachment to surface or boundary steps either produced by two-dimensional nucleation and lateral growth mechanism or existing at screw dislocations or the coalescence of grains and the consequent formation of grain boundaries with re-entrant edges [34,35]. MgO inclusion may act as a sintering inhibitor because of grain size. Therefore, grain growth is suppressed during the sintering process. It is possible that small amount of MgO are dissolved in the PbO-rich liquid or PMN at high firing temperatures, and its segregation at the grain–liquid interface and grain boundary may have made their step energies finite and hence made them sufficiently singular to cause these abnormal grain growth, as found in the PMN-PT system [32,33]. However, in this work grain boundaries inside these abnormal grains were not clearly observed by SEM. To answer this question, the crystallographic orientation of the grains should be examined further by using other techniques such as TEM or electron backscattered diffraction.

In general, SEM micrographs of fracture surfaces (Fig. 2(ii)) shows highly dense microstructures consisting of equiaxed grains, in agreement with other workers [6,15,21]. The grains are similar in shape, with significant variation in size (0.2–3.5 μm). Moreover, micrograph shows a few pores at triple points. Minor phases can be found in these micrographs, in particular at the grain boundaries and at the triple point junctions. These phases could be clearly distinguished from the microstructure features of the perovskite parent phase, in term of brightness (too bright and too dark). EDX analysis (Table 2) shows the chemical composition of the minor phases, neighbouring the parent PMN phase (marked as "1"), to be $Pb(Mg_{0.6}Nb_{1.9})O_{6.35}$ (bright area; marked as "2") in contrast to the XRD result (Fig. 1), and MgO (dark area; marked as "3"), although the concentration is too low for detection by X-ray, in consistent with earlier work [16]. In addition, it is seen that the PMN samples also have an intergranular fracture mechanism, indicating that the grain boundaries are mechanically weaker than the grains [31], similar to the results previously observed in the two-stage sintered columbite-route PMN ceramics [15].

The dielectric properties of PMN ceramics doubly sintered at various conditions were measured at frequencies between 100 Hz and 100 kHz in the temperature range from −120 to +100 °C as shown in Fig. 3. In general, the typical relaxor behavior [1,2] with the characteristic dispersive frequency dependence of the dielectric maxima has been observed in all samples. Fig. 4(a) and (b) shows a comparison of the dielectric properties at 1 kHz of PMN ceramics doubly sintered at various conditions. It is clear that the maxima in the dielectric constant versus temperature plots increase noticeably with increase in the sintering temperature. Similar trend is also observed for $T(\varepsilon_{r,max})$ and $\tan\delta_{max}$. The dielectric properties

Table 2
Dielectric properties (at 1 kHz) of PMN ceramics doubly sintered at various conditions.

EDX positions	Composition (at%)			Possible phase
	Pb (M)	Mg (K)	Nb (L)	
1	50.83	17.05	32.12	$Pb(Mg_{0.33}Nb_{0.67})O_3$
2	28.21	16.97	54.82	$Pb(Mg_{0.6}Nb_{1.9})O_{6.35}$
3	–	100	–	MgO

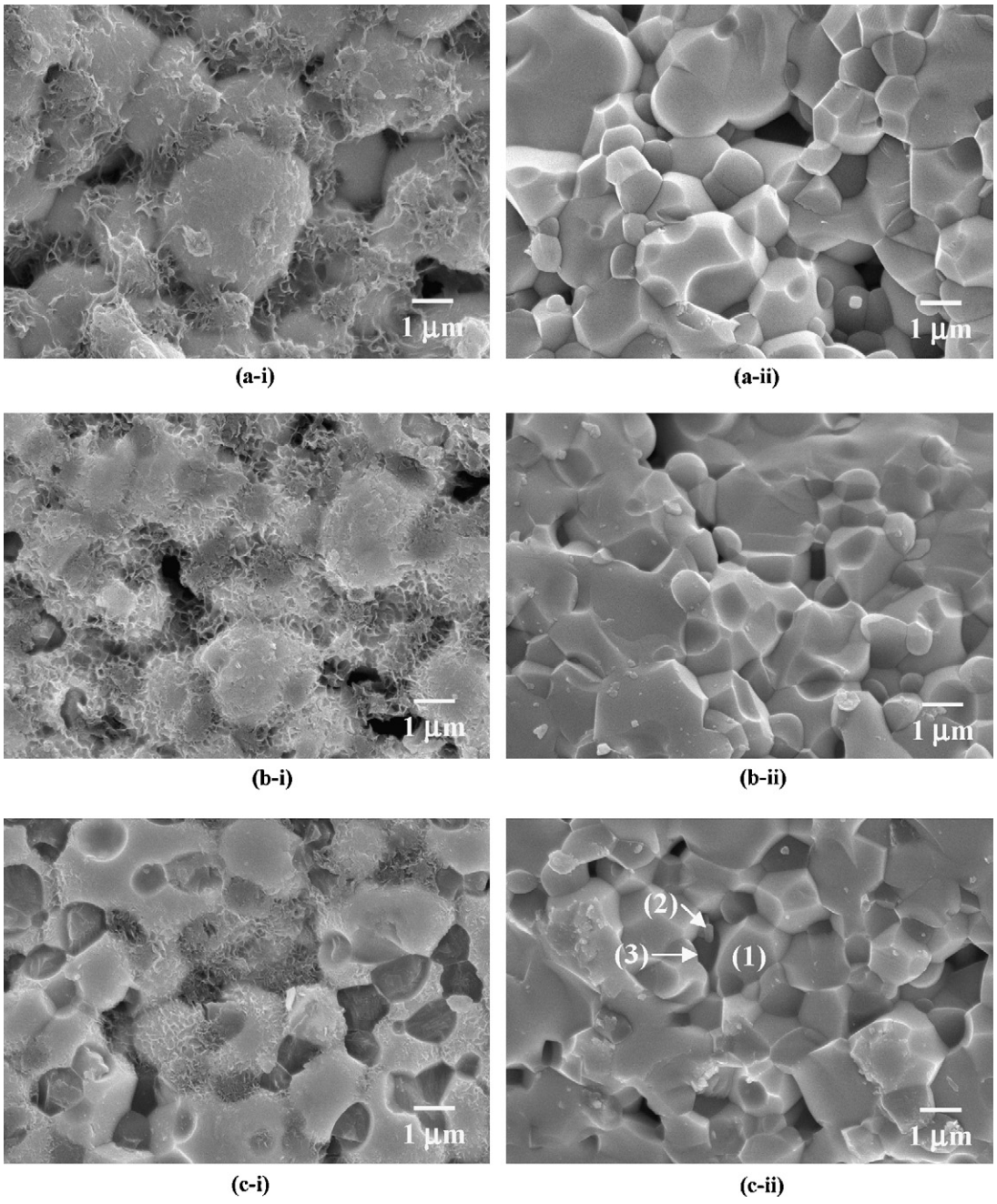

Fig. 2. SEM micrographs of as-fired (i) and fracture surfaces (ii) of PMN ceramics doubly sintered at (a) 1025/1000 °C, (b) 1050/1025 °C and (c) 1075/1025 °C, for constant dwell time of 1 h at each stage.

at room temperature also show the same dependency on sintering temperature, i.e. both $\varepsilon_{r,25\,^\circ C}$ and $\tan\delta_{25\,^\circ C}$ increase. Hence, it can be stated that the magnitude of both dielectric constant and dielectric loss in PMN ceramics depend considerably upon the heat treatment conditions. As also listed in Table 3, all doubly sintered PMN samples exhibit the maximum dielectric constant of about 20,708–24,291 at 1 kHz with temperature of maximum dielectric constant, $T(\varepsilon_{r,max})$, of about −15 to −18 °C, in good agreement with other researchers [5–10]. As listed in Table 2, it can be noticed that the presence of MgO phase may slightly shift the temperature of $\varepsilon_{r,max}$. In addition, since the grain size of all the doubly sintered corundum-route PMN ceramics are not significantly different (ranging from 2.1 to 2.9 μm, as listed in Table 1), the difference in dielectric properties should be attributed to the difference in density, which increases from 94 to 97% with increasing sintering temperature (as listed in Table 1). The statement that the density plays a crucial role in controlling the dielectric properties is further supported when comparing the dielectric properties of the doubly sintered corundum-route PMN ceramics with those of the normal sintered and doubly sintered columbite-route PMN ceramics, as listed in Table 3. Here, one can clearly see that the dielectric constant values (both $\varepsilon_{r,25\,^\circ C}$ and $\varepsilon_{r,max}$) in doubly sintered corundum-route PMN ceramics are very close to those observed in the normal sintered PMN [36]. It should be noted that these ceramics have very different grain size (2.9 and 9.4 μm, respectively, as listed in Table 1), but similar density values, i.e. 96–97%. On the other hand, as listed in Tables 1 and 3, the dielectric constants of the doubly sintered columbite-route and corundum-route PMN

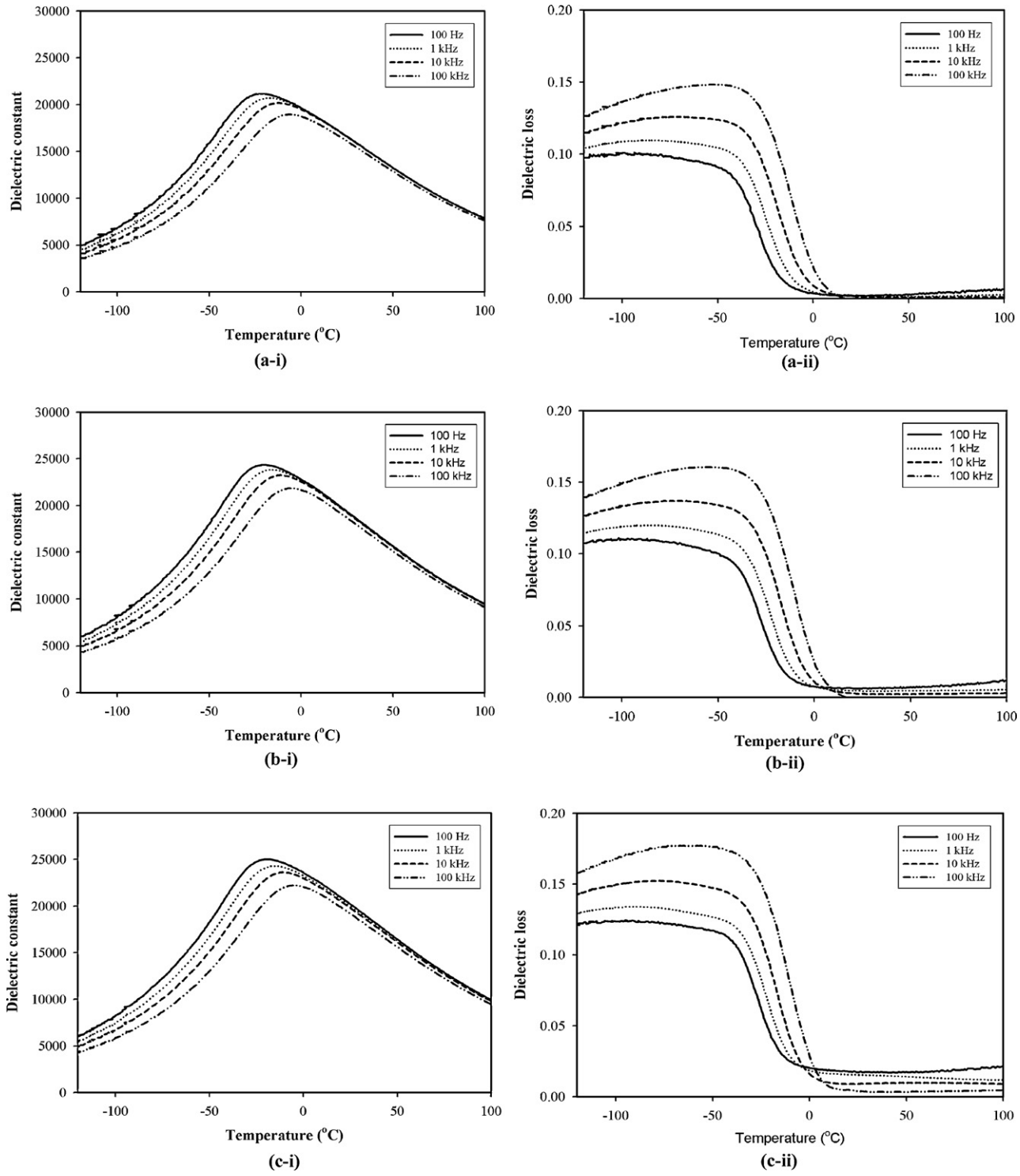

Fig. 3. Variation with temperature of: (i) dielectric constant (ε_r) and (ii) dielectric loss ($\tan\delta$) for PMN ceramics doubly sintered at: (a) 1025/1000 °C, (b) 1050/1025 °C and (c) 1075/1025 °C, for constant dwell time of 1 h at each stage.

ceramics with very different density (91 and 97%, respectively) are significantly different, even though they have similar average grain size. This clearly indicates that density, not the average grain size, could be the controlling factor for such observation [37]. It should be noted that the presence of MgO results in an enhancement of the dielectric constant of PMN ceramics, as also observed by Lu and Lee [38]. This was originally attributed to the elimination of the pyrochlore phase, consistent with the XRD results.

The degree of broadening or diffuseness in the observed dielectric variation could be estimated with the diffusivity (γ) using the expression $(\varepsilon_{r,max}/\varepsilon_r) - 1$ versus $(T - T_{max})^2$. The value of γ can vary from 1 to 2, for completely disordered relaxor ferroelectrics [39,40]. The plots in Fig. 5 show that the variation is very linear. The mean value of γ is extracted from those plots by fitting a linear equation. The values of γ for all doubly sintered corundum-route PMN samples are generally very similar (varying between 1.66 and 1.79),

Table 3
EDX analysis on doubly sintered PMN ceramics derived from a corundum *B*-site precursor route.

Dielectric properties (1 kHz)	Sintering temperatures (T_1/T_2) (°C) and dwell time of each step (h)				
	Columbite-route		Corundum-route		
	1275, 2 (Ref. [20])	1025/1100, 2 (Ref. [14])	1025/1000, 1	1050/1025, 1 (this work)	1075/1025, 1
$\varepsilon_{r,25\,°C}$	18,268	9,500	15,372	18,313	19,023
Tan $\delta_{25\,°C}$	0.01	0.001	0.001	0.004	0.009
$T_{\varepsilon r,max}$	−9	−10	−17.5	−16.3	−15
$\varepsilon_{r,max}$	24,003	13,910	20,708	23,823	24,291
tan δ_{max}	0.20	0.12	0.11	0.12	0.14
Diffusivity (γ)	–	–	1.79	1.66	1.67

indication of close to completely disordered relaxor behavior in the ceramics sintered by this route.

Here, the effect of two-stage sintering on phase formation, microstructure and dielectric properties of the PMN ceramics derived from a corundum *B*-site precursor route was investigated and compared with both the normal and the two-stage sintered columbite-routes. The different microstructural characteristics, density and amount of secondary phase present in sintered PMN ceramics strongly influence the dielectric properties of these materials, leading to superior electrical behavior in two-stage sintered corundum-route PMN sample. In comparison to the normal sintering method, although a disadvantage of the proposed two-stage sintering method is a greater time requirement, the significant reduction in firing temperature is a possible development, particularly with regard to the drive towards electrodes of lower cost for electronic products [1,2,26]. In general, these PMN ceramics exhibit complex microstructures which are a result of variation

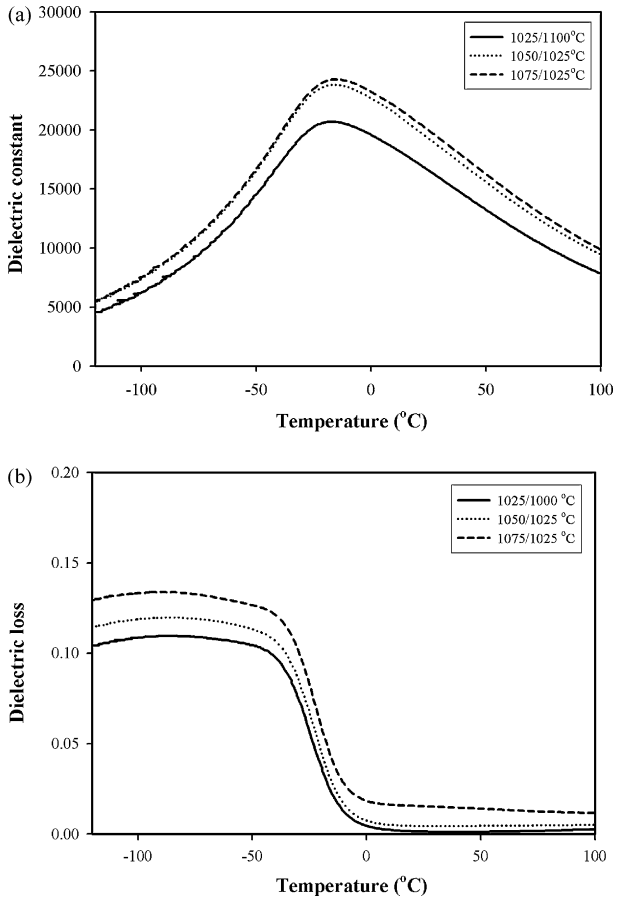

Fig. 4. Variation with temperature of: (a) dielectric constant and (b) dielectric loss at 1 kHz for PMN ceramics doubly sintered at various conditions.

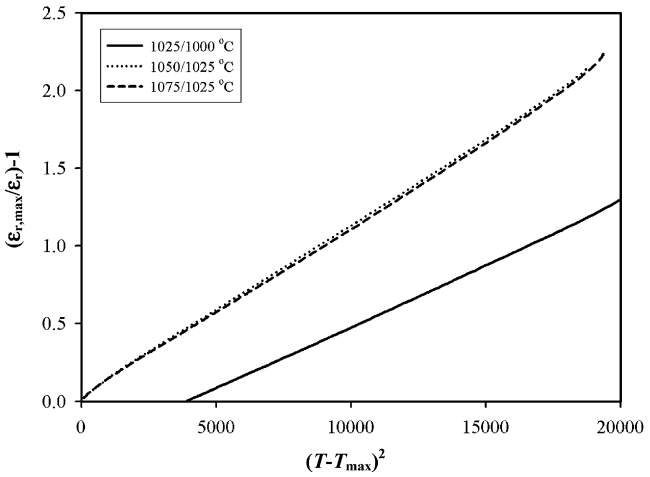

Fig. 5. Dependence of $(\varepsilon_{r,max}/\varepsilon_r) - 1$ with $(T - T_{max})^2$ for PMN ceramics doubly sintered at various conditions.

in grain size, shape and orientation, variation in chemical homogeneity and densification, and the presence of additional minor phase, pores and (micro) cracks. These factors, which are strongly influence by the sintering conditions, have an important effect on the dielectric properties. Furthermore, the PMN ceramics showed a comparable perovskite yield, maximum density, and dielectric properties to those obtained by the partial oxalate [36], or even better than those fabricated by the sol–gel [11], the freeze-drying [41], and the citrate-gel [42] methods.

4. Conclusion

This work demonstrated that, under suitable processing conditions, the properties of the PMN ceramics derived from a combination between the corundum *B*-site precursor and the two-stage sintering methods are equivalent to (or even better than) those obtained from a well-known columbite route (either a normal or a two-stage sinterings). It has been found that the two-stage sintering can effectively suppress the grain growth in perovskite PMN.

Acknowledgements

This work was supported by the Thailand Research Fund (TRF) and the Commission on Higher Education (CHE).

References

[1] A.J. Moulson, J.M. Herbert, Electroceramics, 2nd ed., Wiley, Chichester, 2003.
[2] G.H. Haertling, J. Am. Ceram. Soc. 82 (1999) 797.
[3] I.V. Kityk, M. Makowska-Janusik, M.D. Fontana, M. Aillerie, A. Fahmi, Cryst. Res. Technol. 36 (2001) 577.
[4] S.J. Jang, L.E. Cross, K. Uchino, J. Am. Ceram. Soc. 64 (1981) 209.

[5] M. Lejeune, J.P. Boilot, Ceram. Int. 8 (1982) 99.
[6] S.L. Swartz, T.R. Shrout, W.A. Schulze, L.E. Cross, J. Am. Ceram. Soc. 67 (1984) 311.
[7] J. Chen, A. Gorton, H.M. Chen, M. Harmer, J. Am. Ceram. Soc. 69 (1986) C303.
[8] S.L. Swartz, T.R. Shrout, Mater. Res. Bull. 17 (1982) 1245.
[9] M. Lejeune, J.P. Boilot, Am. Ceram. Soc. Bull. 64 (1984) 679.
[10] J.P. Guha, H.U. Anderson, J. Am. Ceram. Soc. 69 (1986) C287.
[11] F. Chaput, J.P. Boilot, M. Lejeune, R. Papiernik, L.G. Pfaizgrag, J. Am. Ceram. Soc. 72 (1989) 1355.
[12] Y.C. Liou, J.H. Chen, Ceram. Int. 30 (2004) 17.
[13] K. Sreedhar, A. Mitra, Mater. Res. Bull. 32 (1997) 1643.
[14] P.A. Joy, K. Sreedhar, J. Am. Ceram. Soc. 80 (1997) 770.
[15] S. Ananta, N.W. Thomas, J. Eur. Ceram. Soc. 19 (1999 2917).
[16] R. Wongmaneerung, T. Sarakonsri, R. Yimnirun, S. Ananta, Mater. Sci. Eng. B 132 (2006) 292.
[17] R. Wongmaneerung, T. Sarakonsri, R. Yimnirun, S. Ananta, Mater. Sci. Eng. B 130 (2006) 246.
[18] S. Ananta, Mater. Lett. 58 (2004) 2530.
[19] S. Ananta, Mater. Lett. 58 (2004) 2834.
[20] R.L. Fullman, Trans. AIME 197 (1953) 447.
[21] S. Ananta, N.W. Thomas, J. Eur. Ceram. Soc. 19 (1999) 629.
[22] S. Ananta, N.W. Thomas, J. Eur. Ceram. Soc. 19 (1999) 155.
[23] Powder Diffraction File No. 81-861, International Centre for Diffraction Data, Newton Square, PA, 2000.
[24] H.C. Ling, A.M. Jackson, M.F. Yan, W.W. Rhodes, J. Mater. Res. 5 (1990) 629.
[25] Powder Diffraction File No. 82-338, International Centre for Diffraction Data, Newton Square, PA, 2000.
[26] P. Lucas, W.T. Petuskey, J. Am. Ceram. Soc. 84 (2001) 2150.
[27] H.T. Kim, Y.H. Han, Ceram. Int. 30 (2004) 1719.
[28] S.H. Hur, J.K. Lee, K.W. Park, H.S. Hong, S.J. Park, Mater. Lett. 35 (1998) 78.
[29] W. Chaisan, R. Yimnirun, S. Ananta, Ferroelectrics 346 (2007) 84.
[30] M.H. Lin, J.F. Chou, H.Y. Lu, J. Eur. Ceram. Soc. 20 (2000) 517.
[31] O. Guillon, F. Thiebaud, D. Perreux, C. Courtoris, P. Champagne, A. Leriche, J. Crampon, J. Eur. Ceram. Soc. 25 (2005) 2421.
[32] C.E. Seo, D.Y. Yoon, J. Am. Ceram. Soc. 88 (2005) 963.
[33] U.J. Chung, J.k. Park, N.M. Hwang, H.Y. Lee, D.Y. Kim, J. Am. Ceram. Soc. 85 (2002) 965.
[34] S.B. Lee, N.M. Hwang, D.Y. Yoon, M.F. Henry, Metal. Mater. Trans. A 31 (2000) 985.
[35] H.K. Lee, J.S. Kim, N.M. Hwang, D.Y. Kim, J. Eur. Ceram. Soc. 20 (2000) 731.
[36] S.M. Gupta, C.S. Harendranath, A.R. Kulkarni, Ceram. Int. 23 (1997) 191.
[37] R. Wongmaneerung, R. Yimnirun, S. Ananta, Appl. Phys. A 86 (2007) 249.
[38] C.H. Lu, J.T. Lee, J. Ceram. Soc. Jpn. 103 (1995) 1122.
[39] R. Rai, S. Sharma, Solid State Commun. 129 (2004) 305.
[40] E.F. Alberta, A.S. Bhalla, J. Phys. Chem. Sol. 63 (2002) 1759.
[41] W.B. Ng, J. Wang, S.C. Ng, L.M. Gan, J. Mater. Chem. 8 (1998) 2239.
[42] Y.S. Hang, H.B. Park, S.J. Kim, J. Eur. Ceram. Soc. 18 (1998) 613.

Dynamic ferroelectric hysteresis scaling of $BaTiO_3$ single crystals

N. Wongdamnern,[1] A. Ngamjarurojana,[1] Y. Laosiritaworn,[1,2] S. Ananta,[1] and R. Yimnirun[1,2,a)]
[1]*Department of Physics, Faculty of Science, Chiang Mai University, Chiang Mai 50200, Thailand*
[2]*Research Center in Theoretical and Computational Physics, Thailand Center of Excellence in Physics, Chiang Mai 50200, Thailand*

(Received 27 September 2008; accepted 17 January 2009; published online 25 February 2009)

The scaling behavior of the dynamic hysteresis of ferroelectric $BaTiO_3$ single crystals was investigated. Two sets of the scaling relation of hysteresis area $\langle A \rangle$ against frequency f and field amplitude E_0 were clearly established. Above the coercive field, the scaling took a form of $\langle A \rangle \propto f^{-0.195} E_0^{0.950}$. On the other hand, the scaling in the form of $\langle A \rangle \propto f^{1.667E_0-2.804} E_0^{4.157}$ was obtained under subcoercive field condition. While these scaling relations were generally comparable to previously reported ones, it was found that the f and E_0 exponents depended on E_0 and f, respectively, which was in contrast to the prior theoretical prediction and experimental investigations. © *2009 American Institute of Physics*. [DOI: 10.1063/1.3086317]

I. INTRODUCTION

The dynamic hysteresis, i.e., hysteresis area $\langle A \rangle$ as a function of the field amplitude E_0 and frequency f has become important consideration in many applications, whose performance is related to the signal amplitude and frequency, as well as in more recently developed ferroelectric random access memories (Fe-RAMs).[1–4] Therefore, it is technologically helpful to understand the scaling behavior so that the ultrahigh frequency hysteresis can be predicted in devices. Hence, there have been reports on the scaling behavior of the dynamic hysteresis in ferromagnetic and ferroelectric thin films, with some discrepancies between theoretical and experimental results.[5–14] Many theoretical studies have been focused on the power-law scaling,

$$\langle A \rangle \propto f^{\alpha} E_0^{\beta}, \tag{1}$$

(where α and β are exponents that depend on the dimensionality and symmetry of the system) of hysteresis curves in polarization systems.[5–9]

Earlier investigations[5,6,8,14–16] have reported the scaling relations in thin films of some ferroelectric materials, such as $Pb(Zr,Ti)O_3$ (or PZT), $Bi_4Ti_3O_{12}$, and $SrBi_2Ta_9O_4$, as summarized in Table I. We also reported the scaling relations for soft and hard PZT bulk ceramics.[17–20] Most recently the scaling behavior of a ferroelectric liquid crystal was also reported.[21] As listed in Table I, it is interesting to observe that scaling behaviors of different materials derived from theoretical models, thin-film, and bulk ceramics are generally comparable (only slight difference in exponents m and n), suggesting that materials with similar domain structures should have very comparable dynamic hysteresis and scaling behavior, as previously proposed in our recent investigations.[17,19,22] It could be stated that the dynamic hysteresis (hence the scaling behavior) is mainly controlled by available domain states and polarization switching mechanism. Our previous investigations in soft and hard PZT bulk ceramics have shown indirect evidence of the influence of the different domain states on the dynamic hysteresis behavior.

However, giving the complexity of the dopant types and concentrations in the commercial ceramics investigated, it was too complicated to directly evaluate the domain state contribution to dynamic behavior in the ceramics. It is thus

TABLE I. Dynamic scaling exponents for different systems [refer to Eq. (1)].

System	α	β	Refs.
$(\Phi^2)^2$ and $(\Phi^2)^3$ models	−1	2	5 and 6
Q-state Potts model			
Saturated Loops		1	14
Minor Loops		4	14
	−0.66	2	15
Nd-doped $Bi_4Ti_3O_{12}$ thin-Film	−0.33	2	16
$SrBi_2Ta_9O_4$ thin-film	−0.33	3	14
$Pb(Zr,Ti)O_3$ thin-films	−0.33	1	41
$PbTiO_3$/polymer Composite	−1	2	42
Soft PZT bulk ceramic			
Saturated Loops	−0.25	1	17
Minor Loops	−0.33	3	17
Hard PZT bulk ceramic			
Saturated Loops	−0.28	0.89	19
Minor Loops	−0.43	3.19	19
PZT-PZN bulk ceramic			
Minor Loops	−0.42	3.65	22
$Na_{0.5}Bi_{0.5}TiO_3$ ceramic			
Minor Loops	−0.39	2.63	43
{001}-$BaTiO_3$ single crystals			
Saturated Loops	-0.195 ± 0.016	0.950 ± 0.056	This work
Minor Loops	$(1.667)E_0 - 2.804$	4.157 ± 0.092	This work

a)Author to whom correspondence should be addressed. E-mail: rattikornyimnirun@yahoo.com.

more suitable to study such influence in material with more distinct domain structures, particularly single crystals of simple ferroelectric materials, of which the scaling behavior has surprisingly yet to be reported. Thus, we present the results on the scaling behaviors of the dynamic hysteresis of tetragonal $BaTiO_3$ single crystals. As will be seen, the dynamic hysteresis and scaling behaviors of the $BaTiO_3$ single crystal are comparatively very similar to those of the other more complex materials previously reported. More interestingly, it is found that an intercorrelation of f and E_0 exponents is obtained, which is in contrast to the prior theoretical prediction and experimental investigations.

II. EXPERIMENTAL

The dynamic hysteresis (P-E) loops of tetragonal {001}-$BaTiO_3$ single crystals grown by the Remeika process[23,24] containing a-c domains[25,26](triangular-shaped plates with 5 mm edge length and thickness of 0.5 mm) were characterized at room temperature (25 °C) by using a modified Sawyer-Tower circuit with f covering from 1 to 300 Hz and E_0 from 0 to 6.6 kV/cm. Measurements were parallel to the tetragonal (001) direction. The electric field was applied to a sample by a high voltage ac amplifier (Trek 610D) with the input sinusoidal signal from a function generator (HP 3310A). The P-E loops were recorded by a digital oscilloscope (HP 54645A, 100 MHz). Each loop was obtained after 20 sampling cycle to average out the noise deformation.

III. RESULTS AND DISCUSSION

The hysteresis loops at different E_0 but fixed f (100 Hz), and at different f but fixed E_0 (6.0 kV/cm) are shown in Fig. 1. As shown in Fig. 1(a), for applied fields lower than the coercive field, the loop does not saturate. With further increase in E_0 beyond E_c, the loop area $\langle A\rangle$, remanent polarization (P_r), and coercive field (E_c) increase until well saturated loop is achieved. Similar observations have been reported in ferroelectric thin films and bulk ceramics.[8,10,14,17,19,22] The $\langle A\rangle$, P_r, and E_c decrease with an increase in frequency, as shown in Fig. 1(b). As already established in our previous investigations,[17,19,22] the scaling behavior can be divided into two distinct regimes; that for the saturated loops ($E_0 > E_c$) and the other for the minor loops ($E_0 < E_c$). The same can be applied for the case of the $BaTiO_3$ single crystals, as seen in an inset of Fig. 1(a) that the change in $\langle A\rangle$ with E_0 follows two distinctly different trends with the applied field amplitude $E_0 = E_c$ (1.7 kV/cm)[25,27] being a critical turning point. It should be noted that the E_c is generally frequency dependent [$E_c(f)$], but in this case the measuring frequency range is not too extensive to cause large variation in E_c, as seen in an inset of Fig. 1(a). Thus, the fixed E_c of 1.7 kV/cm can be used effectively.

Thus, to obtain the scaling relations for the $BaTiO_3$ single crystals, one can fit the data with Eq. (1) where exponents α and β are determined directly from the experimental data. By plotting $\langle A\rangle$ against f at fixed E_0, one obtains the exponent α. On the other hand, the exponent β can be obtained from plotting $\langle A\rangle$ against E_0 at fixed f. In conjunction with the least square-fitting method, the methodology outlined above is applied to obtain the exponents α and β from the saturated loop ($E_0 > E_c$) and the minor loop data ($E_0 < E_c$). Figures 2(a) and 2(b) show a variation in exponent α with E_0 and a variation in exponent β with f, respectively. Evidently, the two exponents depend slightly on the frequency f and significantly on the field amplitude E_0, with $E_0 = E_c$ being the critical turning point. The variations in both exponents obtained here are in strong contrast to most of the previous investigations,[5–9,11,14–22] in which the scaling exponents are normally treated as constant and depend only on the dimensionality and symmetry of the system, not the frequency f and field amplitude E_0, as stated previously in Eq. (1).

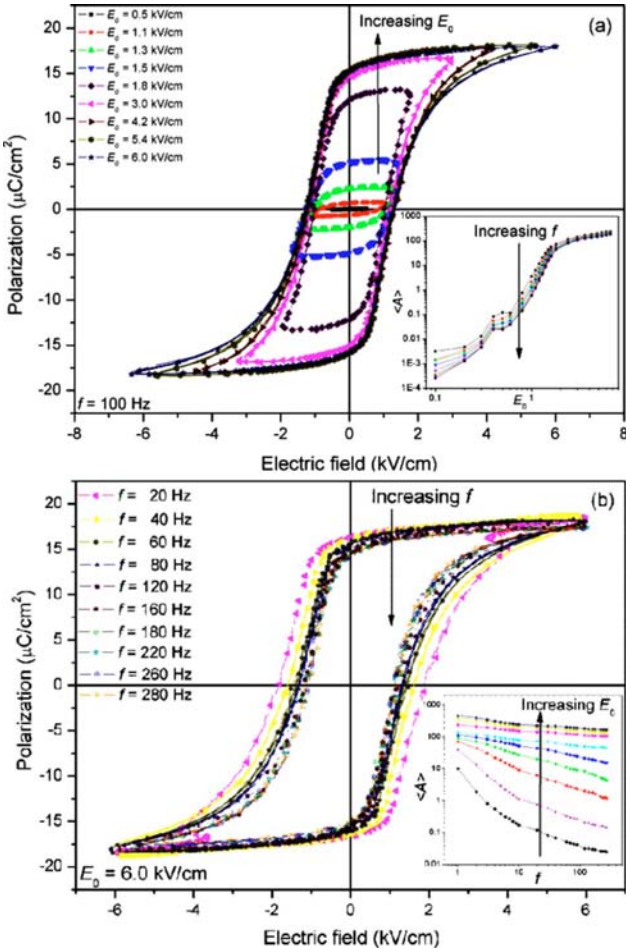

FIG. 1. (Color online) Hysteresis loops for {001}-$BaTiO_3$ single crystals (a) at various E_0 and f=100 Hz and (b) at various f and E_0=6.0 kV/cm. Shown in insets are changes in $\langle A\rangle$ with f and E_0 at some measuring conditions.

From Fig. 2(a), two linear relations can be obtained for the variation in f-exponent α with E_0. With $E_0 < E_c$, a strong field-dependent relation $\alpha = (1.667)E_0 - 2.804$ (with $R^2 \sim 0.97$) is obtained, while a much weaker field-dependent relation $\alpha = -(8.07 \times 10^{-3})E_0 - 0.163$ (with $R^2 \sim 0.93$) is attained at $E_0 > E_c$. Furthermore, as displayed in Fig. 2(b), two very weak frequency-dependent relations are obtained for the variation in E_0-exponent β with f, e.g., $\beta = (6.105 \times 10^{-4})f + 4.065$ (with $R^2 \sim 0.94$) and $\beta = (3.730 \times 10^{-4})f + 0.894$ (with $R^2 \sim 0.95$) for $E_0 < E_c$ and $E_0 > E_c$, respectively. It is impor-

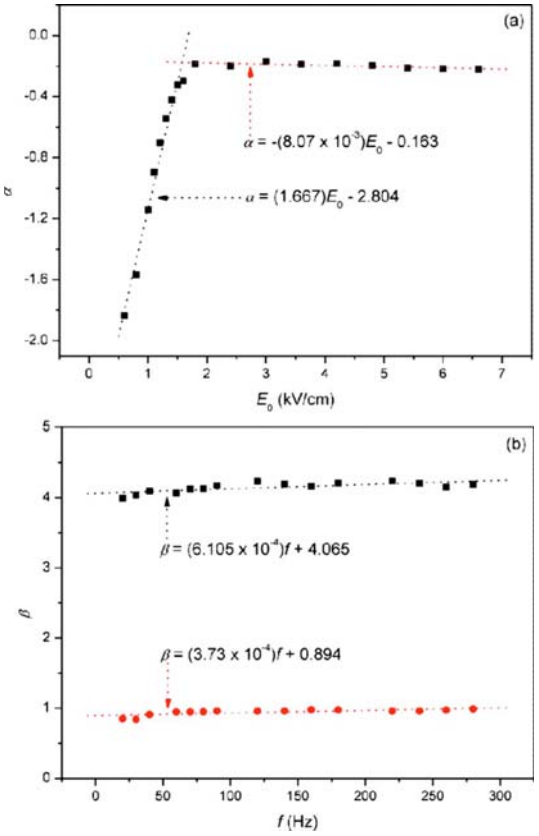

FIG. 2. (Color online) (a) Variation in exponent α with E_0 and (b) variation in exponent β with f in subcoercive field ($0.1 \leq E_0 \leq 1.6$ kV/cm) (black square markers) and beyond coercive field ($1.8 \leq E_0 \leq 6.6$ kV/cm) (red circle markers) conditions. Dotted lines indicate linear relations fitted to data in each regime.

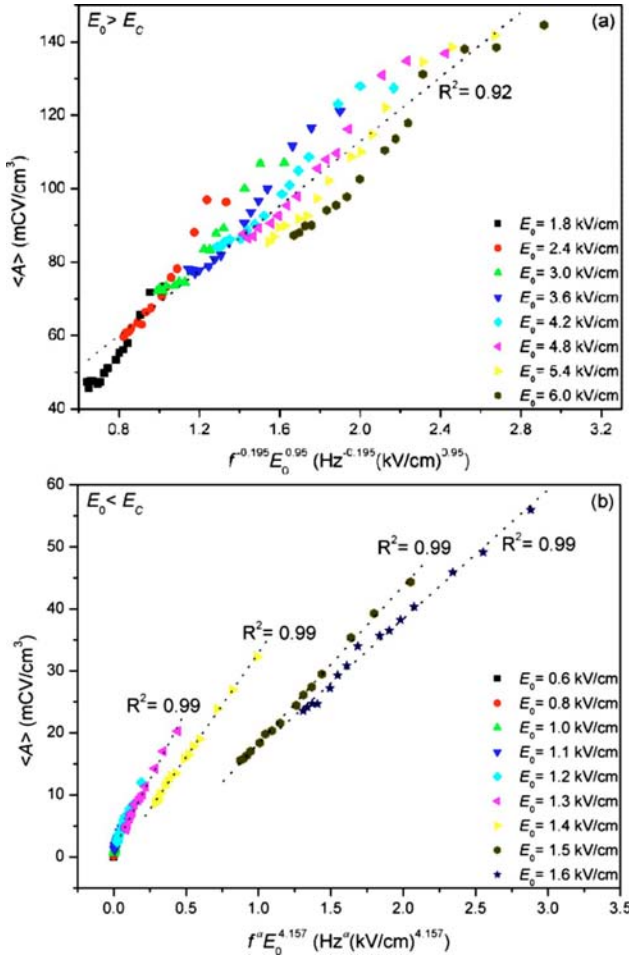

FIG. 3. (Color online) Scaling of hysteresis for {001}-$BaTiO_3$ single crystals (a) area $\langle A \rangle$ against $f^{-0.195}E_0^{0.95}$ and for the saturated loops ($E_0 > E_c$) (b) area $\langle A \rangle$ against $f^{\alpha}E_0^{4.157}$ for the minor loops ($E_0 < E_c$). The dotted lines represent the fitting.

tant to point out that not only the complex scaling behaviors of a ferroelectric prototype $BaTiO_3$ single crystal are revealed but the relations expressed above also provide useful and critical information in understanding the scaling behaviors in other ferroelectric materials previously reported, as listed in Table I, and will be discussed later.

Obviously, with very small coefficients to E_0 and f terms (for the whole range of E_0 and f used in this study), one can estimate the exponents $\alpha = -0.195 \pm 0.016$ and $\beta = 0.950 \pm 0.056$ when $E_0 > E_c$. As plotted in Fig. 3(a), it is revealed that the saturated loop data can be fitted reasonably well ($R^2 \sim 0.92$), within the measured uncertainty, by

$$\langle A \rangle \propto f^{-0.195} E_0^{0.950}. \tag{2}$$

On the other hand, for the case of $E_0 < E_c$ only the exponent $\beta = 4.157 \pm 0.092$ can be estimated, while the relation $\alpha = (1.667)E_0 - 2.804$ has to be used due to its strong field-dependent nature. Therefore, the scaling relation for the minor loops of the $BaTiO_3$ single crystals takes the form of

$$\langle A \rangle \propto f^{1.667E_0 - 2.804} E_0^{4.157}, \tag{3}$$

which fitted very well ($R^2 \sim 0.99$) with the minor loop data at each E_0, as plotted in Fig. 3(b).

The scaling relation obtained in Eq. (2) for the saturated loops of $BaTiO_3$ single crystals indicates that $\langle A \rangle$ decays more slowly with f and grows more slowly with E_0 than the theoretical prediction from $(\Phi^2)^2$ and $(\Phi^2)^3$ models, as well as most of the other ferroelectric materials in both thin-film and bulk forms, as compared in Table I. In the saturated loop case, when comparing the E_0-exponent β listed in Table I, it is very interesting to observe that the β value (approximately 1) in our present study on $BaTiO_3$ single crystal is similar to those obtained earlier for the bulk ceramics and that directly estimated from Monte Carlo method based on Q-state planar Potts model,[14] while it is much lower than those derived from $(\Phi^2)^2$ and $(\Phi^2)^3$ models and ferroelectric thin films ($\beta \sim 2-3$). A qualitative explanation for the difference may come from the polarization-interaction terms as considered in the $(\Phi^2)^2$ and $(\Phi^2)^3$ models, in which the polarization flip just has one contribution, i.e., polarization reversal.[5,6] Similarly, as explained thoroughly in our previous reports,[17,20] main polarization switching contribution in thin films would also be from the 180° domain reversal. Hence, a similar polarization switching kinetics is expected in the two cases. On the other hand, in the single crystals and bulk ceramics, there are influences of many depolarizing effects[17] arisen from domain walls, boundaries, space charges, immobile defects, etc., which may retard the external field. Consequently, the energy barrier is very much higher, which leads to slower

polarization-flip kinetics. Therefore, a lower exponent for the E_0 term is expected in these types of materials.

A more quantitative approach to explain a near linear dependence of hysteresis area with electric field amplitude E_0 can be drawn upon the domain reversal nature through the nucleation and growth concept,[28] which was theoretically established very nicely for $BaTiO_3$ materials.[7,8] Here the domain reversal can be characterized by an effective characteristic time [combining simultaneous contributions from both the new domain nucleation rate ($\tau_n \propto E_0^{-2/3}$) and the domain boundary motion velocity ($\tau_v \propto E_0^{-4/3}$)] $\tau' = \sqrt{\tau_n \tau_v} \propto E_0^{-1}$.[16,29] If this effective characteristic time represents the response of the domain reversal to the varying external field at a given frequency, it should be inversely proportional to the hysteresis area $\langle A \rangle$. Therefore, it can be assumed that $\langle A \rangle \propto E_0$, which is in very good agreement with the present study.

Furthermore, in the case of saturated loops, the f-exponent α of $BaTiO_3$ single crystal is smallest in absolute value among those listed in Table I. In our previous reports, the depolarizing effects, acting as a buffer to polarization-reversal mechanism, were already discussed as the reason of a relatively weaker dependence on f in bulk ceramics than that observed in thin films and predicted from theoretical models.[17,19] As for the smallest response to f in the single crystals, an explanation may simply be a result of a near saturation of polarization in the single crystals under the applied field beyond its coercive field, as shown in Fig. 1(a), under which the crystal is nearly in a single-domain-like state, unlike in thin films and bulk ceramics with multidomain states.[1,30,31] This has resulted in a relatively weaker dependence on f than those observed in most of the other ferroelectric thin films and bulk ceramics. It should also be noted here that a deviation of the experimentally obtained scaling relations from the theoretical prediction may be due to the fact that the models[5,6] is relevant to the insulating defect-free single domain samples with very low dielectric anisotropy and low electroelastic coupling, which clearly is not the case for the $BaTiO_3$ single crystals with a well-known large dielectric anisotropy.[1,25,30,31]

For the minor loop scaling relation in Eq. (3) and as listed in Table I, the E_0-exponent β ($\sim$4.157) in the $BaTiO_3$ single crystals is approximately in the same order (3–4) as to that in PZT thin film,[8,14] as well as those in minor loops of PZT and PZN-modified PZT bulk ceramics.[17,19,22] As explained in our previous investigations,[17,19] this is attributed to the fact that the main polarization orientation mechanism in thin films and in subcoercive field condition for single crystals and bulk ceramics is likely from the reversible 180° domain rotation (which also occurs at much faster rate than the irreversible process), as the irreversible non-180° domain switching is normally accompanied with mechanical strain, it occurs at higher E-field than 180° domain rotation does. Therefore, under low E-fields, one would expect the 180° domain rotation to occur first.[32–37] This explains why the scaling behavior of the single crystals and bulk ceramics at low E fields is similar to that of thin films and why the response to E_0 at subcoercive field occurs at much faster response ($\beta \sim 2-4$) than that at higher field amplitude ($\beta \sim 1$). It should also be noticed that the β=4.157 obtained experimentally in this study agrees very well with the β value of 4 obtained from the previous simulation study using Monte Carlo method based on Q-state planar Potts model.[14]

Another important implication of this study is the fact that the f-exponent α is strongly field dependent in subcoercive field condition, as seen in Fig. 2(a). This may provide a hint to explain such variation in the α value, as listed in Table I, which may be caused from an experimental limitation to fully achieve the saturation state in most of the previous high-field dynamic hysteresis studies available in literature. In fact, the α value for all previous investigations falls between -0.195 (that of saturated loop of $BaTiO_3$ obtained here, believed to be the upper limit of the f exponent) and -1 [theoretically obtained from $(\Phi^2)^2$ and $(\Phi^2)^3$ models for non-saturated loops]. The upper limit of the α value is believed to be related to available domain states in the material, previously proposed in our investigations,[19,22] or growth dimension in growth kinetics model proposed by Ishibashi and Orihara[38,39] based on Kolmogorov-Avrami model. Nonetheless, more investigations are clearly required to support this hypothesis.

It should also be noticed that the scaling relations obtained in this current study is only applicable to high frequency limit. This is because at lower frequency range (<1 Hz) another set of scaling relations must be formulated, as seen in both previous theoretical and experimental works that $\langle A \rangle$ is rapidly increasing, then turning to zero at much lower frequency. In addition, the high frequency limit in prior investigations in thin films is usually in the range of 1–100 kHz, the maximum frequency of 300 Hz used in this study may not be viewed as a high frequency limit as compared to those cases. The range of excitation parameters in this study is limited by equipments used. The field amplitude used here is reasonable as saturated P-E loops are already obtained. Therefore, while the higher field amplitude could be obtained, no new information is revealed. The major limitation in this current study is probably the frequency range of 1–300 Hz, which seems rather narrow, as compared to previous investigations in thin films. However, this can be explained very easily. All of the previous investigations on scaling behavior of ferroelectric materials are on thin films. Therefore, it is much easier to apply only 1–10 V to obtain saturated P-E loops and most of the function generators can provide this voltage in very wide frequency range (0.0001 Hz to >1 MHz). As a result, most of the previous investigations were carried out in boarder range, as compared to current study in much thicker samples. Since this work was carried out on single crystal plates with nearly 1 mm thick, the amplifier can only provide high electric field (6 kV/cm) up to 300 Hz.

Based on the arguments mentioned, the scaling relations are considered applicable within the range of the experimental conditions. Nevertheless, it is interesting to point out that, through extrapolation of the scaling relations presented in Fig. 2 for exponents α and β to the range of field amplitude of 10–50 kV/cm and frequency of 1–10 kHz used in the case of many previous thin-film studies, one could easily obtain the exponents α and β close to those previously reported as listed in Table I. For instance, with E_0 of 25 kV/cm and f of

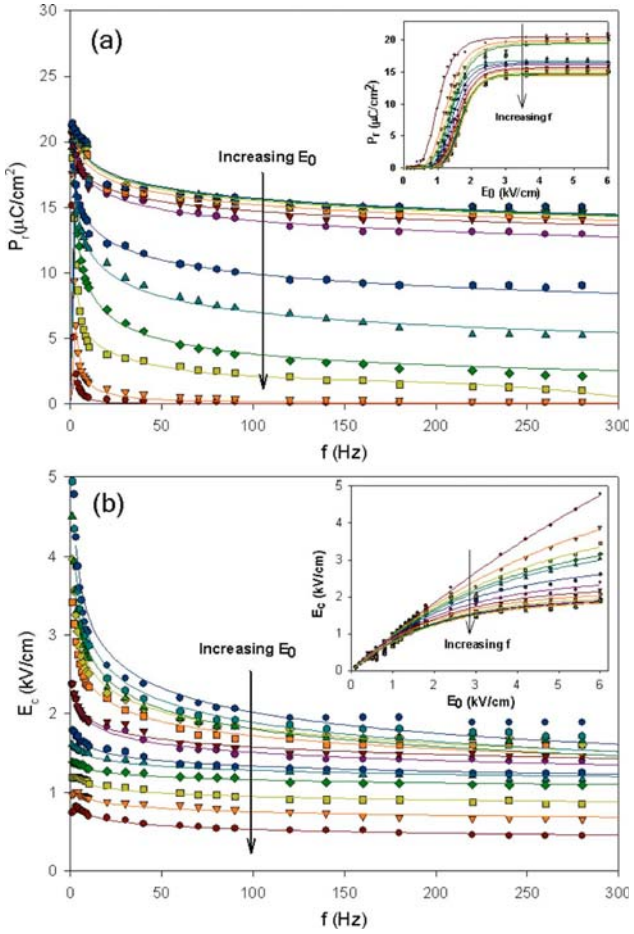

FIG. 4. (Color online) Linear plots between (a) P_r and f for various E_0 and (b) E_c and f for various E_0. Solid lines indicate power-law fitting to the data. Also shown in insets of respective figure are linear plots of P_r and E_c with E_0 for various f.

5 kHz, the exponents α and β of -0.365 and 2.759 (as compared to -0.33 and 2–3 for thin films) can be obtained. More importantly, it should still be emphasized that the scaling relations obtained in this study is mostly applicable within the range of excitation parameters mentioned above.

Finally, we look at the measured P_r and E_c as functions of f and E_0, as plotted in Fig. 4. One can observe decaying of both P_r and E_c with f, while both parameters increase to saturation with E_0, as seen in insets of Fig. 4. As the frequency of the applied field increases, it is expected for P_r to decrease because some of the domains cannot follow the applied field. Hence, it takes lower electric field to force the polarizations to become zero, hence lower coercive field is observed. It is important to note that both P_r and E_c will not increase indefinitely as $f \rightarrow 0$. As reported in many previous investigations,[7,8,11,14–16,39] the two parameters reach maxima at certain f, then begin to decrease to finite values (usually called static P_r and E_c) as $f \rightarrow 0$. However, due to an equipment limitation such very low f range could not be performed in this study. Nonetheless, the measured P_r and E_c as functions of f seen in Fig. 4 imply power-law relations between the two parameters and f, as also widely reported in literature.[2,4,38,39] On the other hand, as seen from insets of Fig. 4 rather complex relations with E_0 are obtained, hence will not be discussed here. Therefore, with least-square fitting method with $R^2 > 0.95$ (with some variation), the power-law scaling of $P_r(f)$ and $E_c(f)$ for saturated loop data ($E_0 > 1.7$ kV/cm) takes the forms of

$$P_r \propto f^{-0.079}, \tag{4}$$

$$E_c \propto f^{-0.164}. \tag{5}$$

Since approaching saturation the hysteresis area can be roughly estimated with $(2P_r)(2E_c)$,[20,40] so an empirical relation $\langle A \rangle \propto f^{-0.243}$ is available from Eqs. (4) and (5). Although at fixed E_0 this relation is not too far from Eq. (2) with $\langle A \rangle \propto f^{-0.195}$, the difference in the f-exponent could arrive from the complex relations between P_r, E_c, and E_0, as displayed in insets of Fig. 4 and discussed above. Nonetheless, these two scaling methods seem to agree reasonably well.[41–43] So once the scaling of area to the frequency is found, it is possible to guess how the E_c would scale with f if the scaling relation between P_r and f is known or vice versa. Similarly, scaling of area to frequency and to temperature has also been reported in previous investigations.[20,39]

IV. CONCLUSIONS

Two sets of the scaling relation for $BaTiO_3$ single crystals are established based upon the coercive field. The scaling in the form of $\langle A \rangle \propto f^{-0.195} E_0^{0.950}$ is obtained when $E_0 > E_C$, while the scaling takes the form of $\langle A \rangle \propto f^{1.667E_0 - 2.804} E_0^{4.157}$ when $E_0 < E_C$. Although, these scaling relations that are comparable to those of the other more complex materials, the intercorrelation between the f and E_0 exponents is obtained, which is in contrast to the prior theoretical prediction and experimental investigations.

ACKNOWLEDGMENTS

This work was financially supported by the Thailand Center of Excellence in Physics (through the Research Center in Theoretical and Computational Physics). Partial supports for N.W., A.N., and S.A. from the Thailand Research Fund (TRF), Commission on Higher Education (CHE), Graduate School and Faculty of Science, Chiang Mai University are also acknowledged. Thanks are also due to Edward M. Sabolsky of Penn State University for providing the single crystals.

[1] B. Jaffe, W. R. Cook, and H. Jaffe, *Piezoelectric Ceramics* (Academic, New York, 1971).
[2] J. F. Scott, Ferroelectr. Rev. **21**, 1 (1998).
[3] K. Uchino, *Ferroelectric Devices* (Marcel Dekker, New York, 2000).
[4] R. Waser, U. Böttger, and M. Grossmann, in *Ferroelectric Random Access Memories*, edited by H. Ishiwara, M. Okuyama, and Y. Arimoto (Springer-Verlag, Berlin, Heidelberg, 2004).
[5] M. Rao, H. R. Krishnamurthy, and R. Pandit, Phys. Rev. B **42**, 856 (1990).
[6] M. Acharyya and B. K. Chakrabarti, Phys. Rev. B **52**, 6550 (1995).
[7] J.-M. Liu, H. L. W. Chan, C. L. Choy, and C. K. Ong, Phys. Rev. B **65**, 014416 (2001).
[8] J.-M. Liu, H. L. W. Chan, C. L. Choy, Y. Y. Zhu, S. N. Zhu, Z. G. Liu, and N. B. Ming, Appl. Phys. Lett. **79**, 236 (2001).
[9] M. Rao and R. Pandit, Phys. Rev. B **43**, 3373 (1991).
[10] Q. Jiang, H. N. Yang, and G. C. Wang, Phys. Rev. B **52**, 14911 (1995).
[11] B. Pan, H. Yu, D. Wu, X. H. Zhou, and J.-M. Liu, Appl. Phys. Lett. **83**, 1406 (2003).
[12] Y.-H. Kim and J.-J. Kim, Phys. Rev. B **55**, R11933 (1997).

[13]J.-H. Park, C.-S. Kim, B.-C. Choi, B. K. Moon, J. H. Jeong, and I. W. Kim, Appl. Phys. Lett. **83**, 536 (2003).
[14]J.-M. Liu, H. L. W. Chan, and C. L. Choy, Mater. Lett. **52**, 213 (2002).
[15]J.-M. Liu, B. Pan, H. Yu, and S. T. Zhang, J. Phys.: Condens. Matter **16**, 1189 (2004).
[16]J.-M. Liu, B. Pan, K. F. Wang, and H. Yu, Ceram. Int. **30**, 1471 (2004).
[17]R. Yimnirun, Y. Laosiritaworn, S. Wongsaenmai, and S. Ananta, Appl. Phys. Lett. **89**, 162901 (2006).
[18]R. Yimnirun, S. Wongsaenmai, S. Ananta, and Y. Laosiritaworn, Appl. Phys. Lett. **89**, 242901 (2006).
[19]R. Yimnirun, R. Wongmaneerung, S. Wongsaenmai, A. Ngamjarurojana, S. Ananta, and Y. Laosiritaworn, Appl. Phys. Lett. **90**, 112908 (2007).
[20]R. Yimnirun, R. Wongmaneerung, S. Wongsaenmai, A. Ngamjarurojana, S. Ananta, and Y. Laosiritaworn, Appl. Phys. Lett. **90**, 112906 (2007).
[21]S. S. Bhattacharyya, M. Rahman, A. Mukherjee, B. K. Chaudhuri, and A. Yoshizawa, Appl. Phys. Lett. **92**, 122909 (2008).
[22]R. Yimnirun, N. Wongdamnern, N. Triamnak, M. Unruan, A. Ngamjarurojana, S. Ananta, and Y. Laosiritaworn, J. Appl. Phys. **103**, 086105 (2008).
[23]E. M. Sabolsky, A. R. James, S. Kwon, S. Trolier-Mckinstry, and G. L. Messing, Appl. Phys. Lett. **78**, 2551 (2001).
[24]E. M. Sabolsky, S. Trolier-Mckinstry, and G. L. Messing, J. Appl. Phys. **93**, 4072 (2003).
[25]F. Jona and G. Shirane, *Ferroelectric Crystals* (Dover, New York, 1993).
[26]B. Jiang, Y. Bai, J. L. Cao, Y. Su, S. Q. Shi, W. Chu, and L. Qiao, J. Appl. Phys. **103**, 116102 (2008).
[27]W. J. Merz, Phys. Rev. **91**, 513 (1953).
[28]J. D. Gunton, M. San Miguel, and P. S. Sahmi, in *Phase Transitions and Critical Phenomena*, edited by C. Domb and J. L. Lebowitz (Academic, London, 1983), Vol. 8, p. 267.
[29]H. L. Stadler and P. L. Zacumanids, J. Appl. Phys. **34**, 3255 (1963).
[30]M. E. Caspari and W. J. Merz, Phys. Rev. **80**, 1082 (1950).
[31]M. E. Lines and A. M. Glass, *Principles and Applications of Ferroelectrics and Related Materials* (Oxford University Press, Oxford, 1977).
[32]N. Uchida and T. Ikeda, Jpn. J. Appl. Phys. **4**, 867 (1965).
[33]A. Gruverman, O. Auciello, and H. Tokumoto, Annu. Rev. Mater. Sci. **28**, 101 (1998).
[34]D. Bolten, U. Böttger, and R. Waser, Appl. Phys. Lett. **84**, 2379 (2004).
[35]T. Tsurumi, T. Sasaki, H. Kakemoto, T. Harigai, and S. Wada, Jpn. J. Appl. Phys. **43**, 7618 (2004).
[36]S. Trolier-McKinstry, N. B. Gharb, and D. Damjanovic, Appl. Phys. Lett. **88**, 202901 (2006).
[37]K. Lee and S. Baik, Annu. Rev. Mater. Res. **36**, 81 (2006).
[38]Y. Ishibashi and N. Orihara, Integr. Ferroelectr. **9**, 57 (1995).
[39]J. M. Liu, W. M. Wang, Z. G. Liu, H. L. Chan, and C. L. Choy, Appl. Phys. (Berlin) **A75**, 507 (2002).
[40]G. L. Yuan, J.-M. Liu, S. T. Zhang, D. Wu, Y. P. Wang, Z. G. Liu, H. L. W. Chan, and C. L. Choy, Appl. Phys. Lett. **84**, 954 (2004).
[41]J.-M. Liu, H. P. Li, C. K. Ong, and L. C. Lim, J. Appl. Phys. **86**, 5198 (1999).
[42]B. Pan, Y. Yang, L. C. Yu, J. M. Liu, K. Li, Z. G. Liu, and H. L. W. Chan, Mater. Sci. Eng., B **99**, 179 (2003).
[43]N. Wongdamnern, T. Sareein, and R. Yimnirun (to be published).

Journal of Alloys and Compounds 475 (2009) 473–478

Contents lists available at ScienceDirect

Journal of Alloys and Compounds

journal homepage: www.elsevier.com/locate/jallcom

Fabrication and dielectric properties of lead titanate nanocomposites

R. Wongmaneerung[a], A. Rujiwatra[b], R. Yimnirun[c], S. Ananta[c,*]

[a] Department of Physics, Faculty of Science, Maejo University, Chiang Mai 50290, Thailand
[b] Department of Chemistry, Faculty of Science, Chiang Mai University, Chiang Mai 50200, Thailand
[c] Department of Physics, Faculty of Science, Chiang Mai University, Chiang Mai 50200, Thailand

ARTICLE INFO

Article history:
Received 14 January 2008
Received in revised form 8 July 2008
Accepted 13 July 2008
Available online 6 September 2008

Keywords:
Lead titanate
Perovskite
Composites
Microstructure
Dielectric properties

ABSTRACT

A simple powder mixing and pressure-less sintering process for fabrication of $PbTiO_3$ (PT) nanocomposites (micron-sized PT matrix reinforced with either PT nanoparticles or nanofibers) has been developed to enhance both densification and dielectric properties. The potentiality of a ceramic-nanocomposite technique as a low-cost and simple ceramic fabrication to obtain highly dense and pure PT/PT composites was demonstrated. It has been found that both densification and dielectric properties of the composites fabricated in this work were significantly enhanced, as compared to the two-stage sintering and the conventional PT ceramics.

1. Introduction

Pure and dense lead titanate ($PbTiO_3$ or PT) ceramic, which is of interest as a component in commercial electroceramic materials, is regarded to be one of the most difficult lead-based perovskite ferroelectric ceramics to produce [1–3]. The most important properties of PT ceramics are high Curie temperature (~490 °C), large mechanical-quality factor and pyroelectric coefficient [4,5]. Moreover, PT when combined with other oxides can form a series of ferroelectric materials that exhibit many of the most desirable dielectric, piezoelectric and pyroelectric properties for use in electronic and electro-optic devices at high frequency and high temperature, such as infrared sensors, actuators and hydrophones [1–3]. However, PT ceramic is mechanically weak due to large distortion of the tetragonal phase at room temperature which is characterized by the ratio between the lattice parameters (c/a, hereafter called tetragonality, ~1.06 [6,7]). Apart from general problems of PbO volatilization and associated high porosity, the stress induced by cooling through the phase transition can create cracking in bulk ceramics.

To overcome these problems, several techniques have been introduced, such as utilizing nanopowders, using additives, employing spark-plasma sintering and carrying out appropriated milling and sintering conditions [8–13]. All these techniques are aimed at reducing the lattice tetragonality of bulk ceramics, even though they inevitably affect the phase formation, structure and electrical properties of materials in different ways. Amongst all the issues reported so far, most attention has been concentrated on the use of additives and chemically derived powder processing, whereas investigations on modified particle packing or composite techniques have not been widely carried out [14,15].

Recently, ceramic-nanocomposites in which nanosized phases were dispersed within the matrix grains and/or at the grain boundaries have emerged as a novel approach of improving materials properties [16]. The mechanical properties of ceramics are known to be improved significantly by dispersing ceramic-nanoparticles into the ceramic-matrix grains or grain boundaries. However, the degree of improvement in their properties is dependent on the type of composite system involved [16]. Few studies have reported on ferroelectric matrix/metal nanodispersoid [17] and ferroelectric matrix/non-ferroelectric nanodispersoid [18] composite systems, and it is not yet clear how these dispersoids affect the properties of nanocomposites. Moreover, the problem of property trade-off, i.e., a deterioration of electrical properties still remains unsolved. In other words, the improvement of mechanical property can only be realized only by sacrificing electrical properties. So far, a little has been reported on the fabrication of ferroelectric matrix/ferroelectric nanodispersoid composite systems [19]. However, no work on the perovskite PT ceramic-nanocomposites has been reported yet.

Therefore, in this work, ferroelectric matrix/ferroelectric nanodispersoid PT composite has been developed to resolve these problems. With this new scheme, instead of using only micron-

* Corresponding author. Tel.: +66 53 943367; fax: +66 53 943445.
E-mail address: suponananta@yahoo.com (S. Ananta).

0925-8388/$ – see front matter © 2008 Elsevier B.V. All rights reserved.
doi:10.1016/j.jallcom.2008.07.074

sized PT powders as reported in our previous works [13,20], two different types of PT nanodispersoid (nanoparticles and nanofibers) were adopted as starting materials. The influence of both PT nanodispersoids on densification, microstructure and dielectric properties of the composites will be discussed and compared with the conventional method.

2. Experimental procedure

The starting PT materials for the fabrication of self-reinforced PT matrix/PT nanodispersoid composites were micron-sized PT powders, nanopowders, and nanofibers (Fig. 1), which were synthesized via ball-milling, vibro-milling, and hydrothermal techniques, respectively. The characteristics of each starting PT materials and their processing details are described in our previous works [21–23]. The powder mixtures (matrix:dispersoid ratio of 1:1) were formed into pellets by adding 3 wt.% polyvinyl alcohol (PVA) binder, prior to pressing in a pseudo-uniaxial die press at 100 MPa. It should be noted here that preliminary study of other matrix:dispersoid ratios, e.g. 0.7:0.3 and 0.6:0.4 was carried out and the complete solid-solution microstructure type commonly observed in the conventional PT processing was observed in all cases, indicating the solubility effect of the perovskite PT/PT (although their morphologies are different) limiting the possibility of composite formation. Each pellet was placed in an alumina crucible together with an atmosphere powder of identical chemical composition [20]. Such a composite cannot be fabricated by hot-pressing in the reduced atmosphere because the Pb-based perovskite is easily decomposed in the atmosphere. In this work, the composites were prepared by using simple pressure-less sintering method. Sintering was carried out at various temperatures (1000–1225 °C), for 1 h with heating/cooling rates of 1 °C/min [13,20] applied. These firing conditions were advocated from our previous work on PT ceramics with experimental details presented in Refs. [13,20].

Densities of the sintered products were determined by using the Archimedes principle. X-ray diffraction (XRD; Siemens-D500 diffractometer) was carried out at room temperature using Cu Kα radiation to identify the phase formed. The lattice parameters and tetragonality factor (c/a) of the sintered ceramics were calculated from the XRD patterns [24]. The microstructural development was characterized using a scanning electron microscopy (SEM; JEOL JSM-840A), equipped with an energy dispersive X-ray (EDX) analyzer. Mean grain sizes of the sintered ceramics were subsequently estimated by employing the linear intercept method [25]. In order to evaluate the dielectric properties, densified ceramics were polished to form flat and parallel faces. The samples were coated with silver-paste electrodes which were fired on both sides of the samples at 700 °C for 1 h. The dielectric properties were measured using a HIOKI 3532-50 LCR meter, on cooling through the transition range (550–25 °C) with a rate of 5 °C/min at high frequencies ranging from 1 to 5 MHz. Values of the dielectric constant were corrected for porosity by using the relationship $\varepsilon_r = \varepsilon_{r(measured)} \times$ theoretical density/sintered density [26].

3. Results and discussion

X-ray diffraction patterns of the PT composites reinforced with various PT dispersoids and sintered at various temperatures are displayed in Fig. 2, indicating the formation of single phase perovskite in all cases. The strongest reflections in the majority of all XRD traces indicate the formation of the PT perovskite phase of lead titanate which could be matched with JCPDS file no. 6-452, in agreement with other works [10–13]. To a first approximation, this phase has a tetragonal perovskite-type structure in space group $P4/mmm$ with cell parameters $a = 389.93$ pm and $c = 415.32$ pm [27]. All the peaks were assigned to PT, and no reaction phase between different PT starting materials was detected. Moreover, there is no significant difference between the PT nanocomposites reinforced with either PT nanopowders or nanofibers, after sintered at temperatures ranging from 1150 to 1200 °C. This observation could be attributed mainly to the high purity of the employed starting materials together with the optimized firing conditions. The samples sintered with temperature below 1150 °C were broken into pieces after sintering process, whilst the samples sintered at 1225 °C exhibited severe melted areas. Thus, no further characterization can be performed on these samples.

It should be noted that a single phase of perovskite is found in all PT composites similar with the two-stage sintering samples [20], in contrast to the observations for the conventional case [13] (Table 1). No evidence of pyrochlore phase of $PbTi_3O_7$ composition

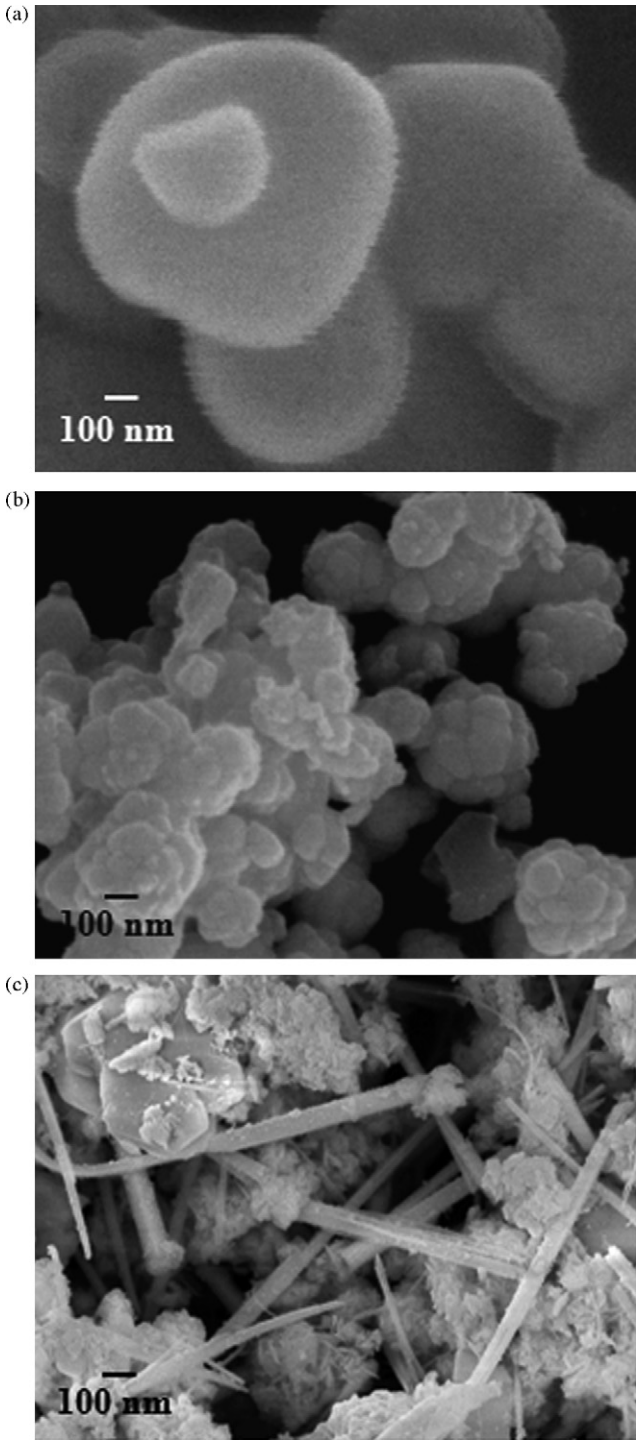

Fig. 1. SEM micrographs of the starting PT dispersoids: (a) micron-sized powders, (b) nanopowders, and (c) nanofibers.

reported earlier by other workers [21,28] was found, nor was any evidence of other second phases [29] being present. This could be due to the lower firing temperature of the nanocomposite samples as compared to the conventional PT ceramics, leading to a smaller degree of lead losses and consequently avoiding the pyrochlore formation, in consistent with other works [30,31], whilst a sufficient arrangement of grain-packing required for ceramic densification still be reached. However, many other factors come into play, e.g. homogeneity of materials, reactivity of starting powders, and pro-

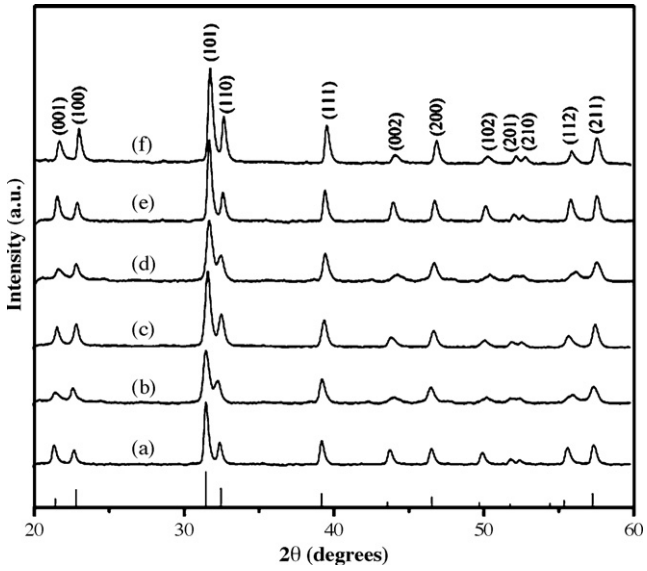

Fig. 2. XRD patterns of PT composites reinforced with PT nanopowders after sintered at (a) 1150 °C, (b) 1175 °C and (c) 1200 °C, and reinforced with PT nanofibers after sintered at (d) 1150 °C, (e) 1175 °C and (f) 1200 °C, for 2 h.

cessing variables. These XRD results clearly show that, in general, the different processing methods used for preparing PT ceramics gave rise to a different phase formation in the sintered materials. The absence of minor phase in composite samples was related to the more reactive process used.

Table 1 also shows tetragonality factor (c/a), relative density and average grain size of each nanocomposite sample, comparing with the conventional and the two-stage sintered samples, respectively. Generally, it is evident that as the sintering temperature increases, the density of almost all the samples increases. However, it can be seen that the sintering behavior of PT ceramics derived from different processing techniques were dissimilar. Two-stage sintering PT ceramics reached a maximum density of ~97% at 900/1200 °C [20]. Whilst conventional PT samples exhibit reduced densification, and a temperature of 1225 °C was required to reach a densification level of ~94% [13]. On the other hand, both types of PT nanocomposites sintered at 1200 °C exhibit the highest relative density of about 98% with a smallest average grain size of less than 1.0 μm. By comparison with conventional PT ceramics, lower values of tetragonality (c/a) are found in all nanocomposite cases, equivalent to those observed in the two-stage sintering case, indicating lower internal stress in these nanocomposites. More interestingly, all nanocomposite samples do not suffer from severe stresses as a result of the high c/a ratio so they have not broken into pieces after experienced the sintering process or once subjected to a cycle of high temperature measurement of dielectric properties, as reported previously for the conventional and two-stage sintering PT cases [13,20].

Microstructural features (free and fracture surfaces) of both PT nanocomposites sintered at different temperatures for 2 h are shown in Figs. 3 and 4. It was found that average grain sizes increase with the sintering temperature (Fig. 3). The PT nanodispersoids were found to locate both within the matrix and at the grain boundaries (see enlarged insertion in Fig. 3(d)). The microstructure of the composites is that of the nanocomposites classified as "nanomicro" and "nanofiber" types [16].

Representative fracture surfaces for both types of PT nanocomposites are given in Fig. 4. It is seen that a uniform grain shape of typical perovskite ceramics [9,30,31] is observed, with sizes in the range of 0.2–2.8 μm. It should be noted that the average grain size of both PT nanocomposites is <1.7 μm, which is less than the critical value of 3 μm [11,32,33] and gives rise to a volumetric percentage enough to buffer the anisotropic stress caused by the phase transition [32]. Here, it is believed that PT nanodispersoids with random orientations result in lower internal stress in composite samples because they compensate the anisotropy of thermal expansion coefficients.

By comparison with conventional PT ceramics [13], almost clean microstructures with highly uniform, denser angular grain-packing and more homogeneous are generally observed in both types of self-reinforced PT nanocomposites. These microstructures are typical of a solid-state sintering mechanism. In the present study (Figs. 3 and 4), the microstructural features of both types of PT nanocomposites with various sintering temperatures ranging from 1150 to 1200 °C are not significantly different. However, it should be noted that higher angularly grains were evidenced for higher sintering temperature. The observation that the sintering temperature effect may also play an important role in obtaining a high angularity grains of perovskite ceramics is also consistent with other similar systems [30,31]. Moreover, abnormal grain growth probably due to the inhibition of grain growth mechanism during doubly sintering process [20,34] was also found in some samples, as shown in Figs. 3(c and d) and 4(f). It is also of interest to point out that evidence of intergranular fracture has been found for the existence of microcracks (arrowed) along the grain boundaries of the composite samples self-reinforced with PT nanoparticles (Fig. 4(a–c)). The different microstructure evolution of PT nanocomposites confirms the importance of the processing method including the morphological characteristics of the dispersed phase, consistent with other works [32,35]. Whilst the grain size of both nanocomposites is approximately the same, the density and microstructure of PT samples sintered at higher temperatures indicated that the composite

Table 1
Sintering behavior of PT ceramics derived from different fabrication techniques

Processing [Ref.]	Sintering temperature (°C)	Perovskite phase[a] (%)	Relative density[b] (%)	Tetragonality factor (c/a)	Grain size[c] (μm)	Average grain size (μm)
Normal sintering [13]	1225	89.20	93.00	1.063	41.0–83.0	62.0
Two-stage sintering [20]	900/1200	100.00	97.02	1.061	1.0–2.2	1.6
Composite reinforced with nanopowders	1150	100.00	96.33	1.059	0.2–0.6	0.40
	1175	100.00	97.02	1.053	0.3–1.0	0.65
	1200	100.00	97.85	1.061	0.6–2.0	1.30
Composite reinforced with nanofibers	1150	100.00	95.68	1.053	0.3–1.3	0.80
	1175	100.00	96.76	1.058	0.4–1.3	0.85
	1200	100.00	97.45	1.061	0.5–2.8	1.65

[a] The estimated precision of the perovskite phase is ±0.1%.
[b] The estimated precision of the density is ±0.1%.
[c] The estimated precision of the grain size is ±10%.

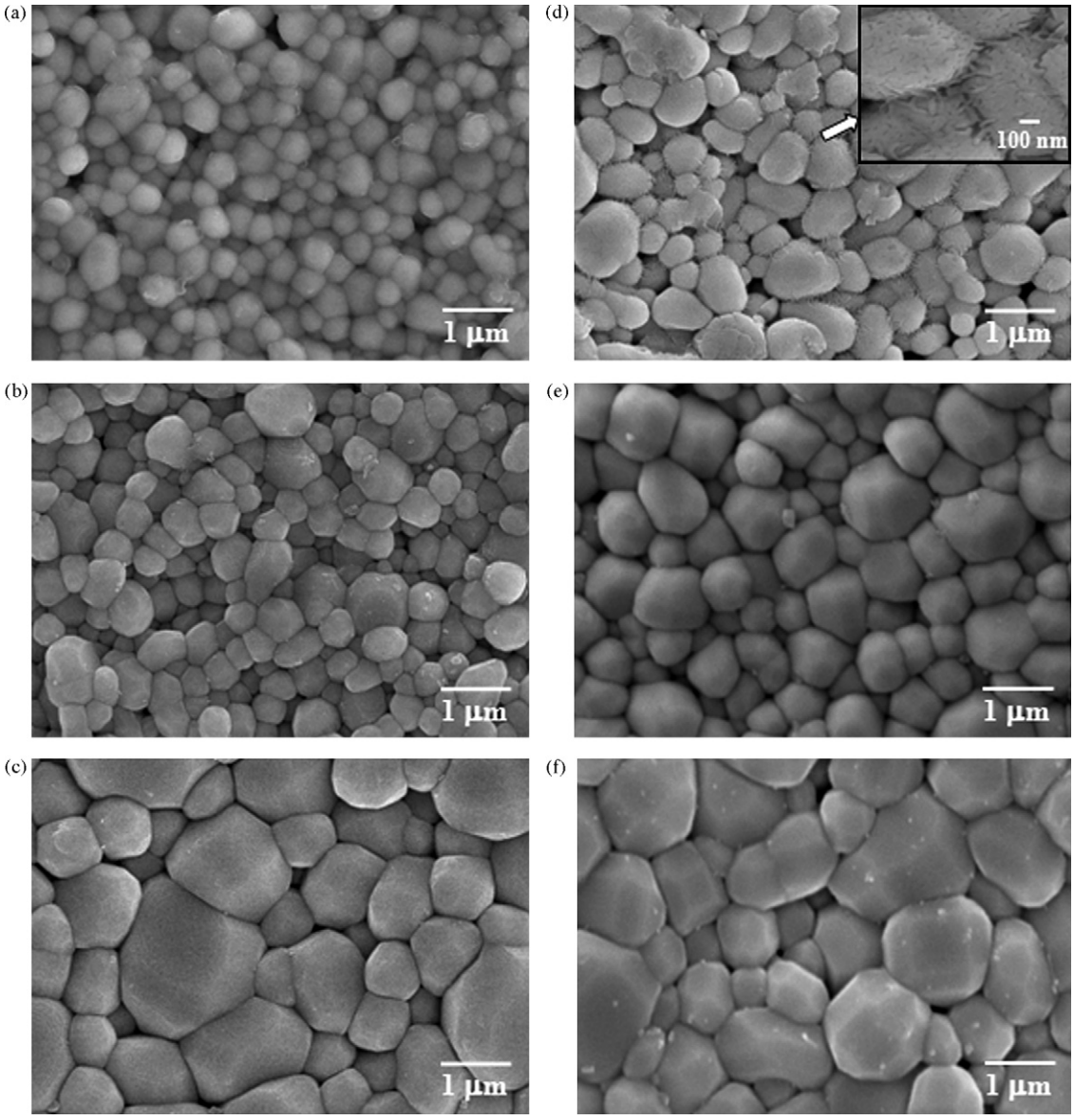

Fig. 3. Free surface of PT composites reinforced with PT nanopowders after sintered at (a) 1150 °C, (b) 1175 °C and (c) 1200 °C, and reinforced with PT nanofibers after sintered at (d) 1150 °C, (e) 1175 °C and (f) 1200 °C, for 2 h.

method of PT matrix reinforced with PT nanofibers was preferable for obtaining dense PT ceramics.

Interestingly, all the nanocomposite samples sintered at 1150–1200 °C remained unbroken. It may be assumed that the nanocomposites consisting of very fine dispersoids suffer less deformation, caused by the high value of c/a ratio, than the ceramics with significantly large grains (Table 1). Consequently, the experimental work carried out here suggests that the optimum conditions for forming the highly dense PT samples in this work are both types of PT/PT nanocomposites sintered at 1200 °C, 2 h dwell time, and 1 °C/min heating/cooling rates.

The dielectric properties of PT samples fabricated with different techniques are also compared in Table 2. In general, they all behave as typical normal ferroelectric materials [3]. The Curie temperatures are about the same for all samples measured whilst the variation of dielectric constant and dielectric loss of both types of PT nanocomposites seems to be somewhat related to the sintering temperatures. This observation indicates that densification and the presence of the second phases accompanied with porosities are the key factors responsible for the dielectric response of the products. Moreover, this study demonstrated that the dielectric properties of PT ceramics are also influenced by microstructural features and arrangement especially the microcracks and final density rather than by only grain size itself.

Table 2
Dielectric properties of PT ceramics derived from different fabrication techniques

Processing [Ref.]	Frequency (MHz)	T_C (°C)	$\varepsilon_{25°}$	$\varepsilon_{r,max}$	$\tan\delta_{max}$
Normal sintering [13]	1	482	243	7680	1.07
Two-stage sintering [20]	1	484	209	8198	0.95
Composite reinforced with nanopowders	1	486	244	8523	1.09
	3	486	245	7517	0.91
	5	487	247	7144	0.76
Composite reinforced with nanofibers	1	488	248	9104	0.81
	3	489	246	7110	0.57
	5	489	242	6801	0.45

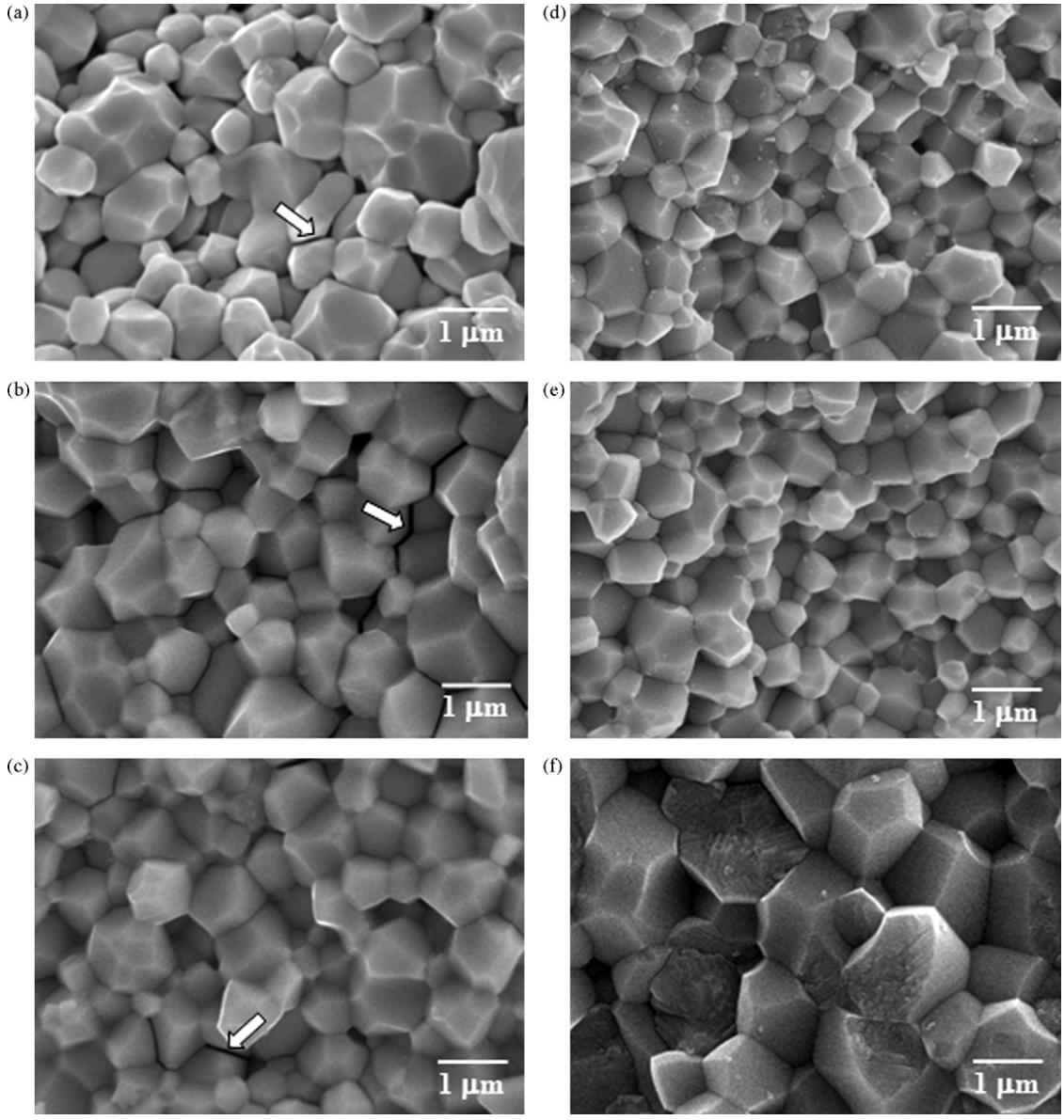

Fig. 4. Fracture surface of PT composites reinforced with PT nanopowders after sintered at (a) 1150 °C, (b) 1175 °C and (c) 1200 °C, and reinforced with PT nanofibers after sintered at (d) 1150 °C, (e) 1175 °C and (f) 1200 °C, for 2 h.

The different microstructure and the different amount of secondary phases present in the sintered PT ceramics strongly influence the dielectric properties of these materials, leading to relatively superior dielectric behavior in PT/PT nanocomposites. The secondary phases in conventional PT sample are interconnected at grain boundaries and, as suggested by Wang and Schulze [31], exert more influence on the dielectric properties than when they are isolated. The influence of densification and microcracks on dielectric properties of these PT composites can be clearly observed in Fig. 5, where the dielectric constant and dissipation factor as a function of temperature are shown, respectively.

The maximum dielectric constant values at 1 MHz in both PT nanocomposites were 2–5% higher than in two-stage sintering and conventional PT samples (Table 2). As mentioned earlier, the reason for this is the high amount of secondary phase present in conventional PT ceramics and the presence of a PbO-rich secondary phase, with low dielectric constant, which could form a continuous layer between grains, decreasing the dielectric constant of the two-stage sintering samples [13,36].

The results obtained in this work suggest that, in general, these PT/PT nanocomposites exhibit complex microstructures which are inherently heterogeneous. The heterogeneity is a result of variation in grain size and orientation; variation in chemical homogeneity; and the presence and distribution of additional minor phase, pores and (micro) cracks. These factors, which are strongly influenced by the sintering conditions, have an important effect on the dielectric properties of the materials and their reproducibility. However, these results suggest that better densification can be introduced into piezoceramics by fabricating ceramic-nanocomposites reinforced with piezoelectric nanodispersoids. Two aspects of this study are significant: (i) reductions in the maximum required sintering temperature (or the required prolong firing time) are possible as compared to the conventional (or the two-stage sintering) method and (ii) a framework has been established for developing self-reinforced piezoceramic-nanocomposite technique for better

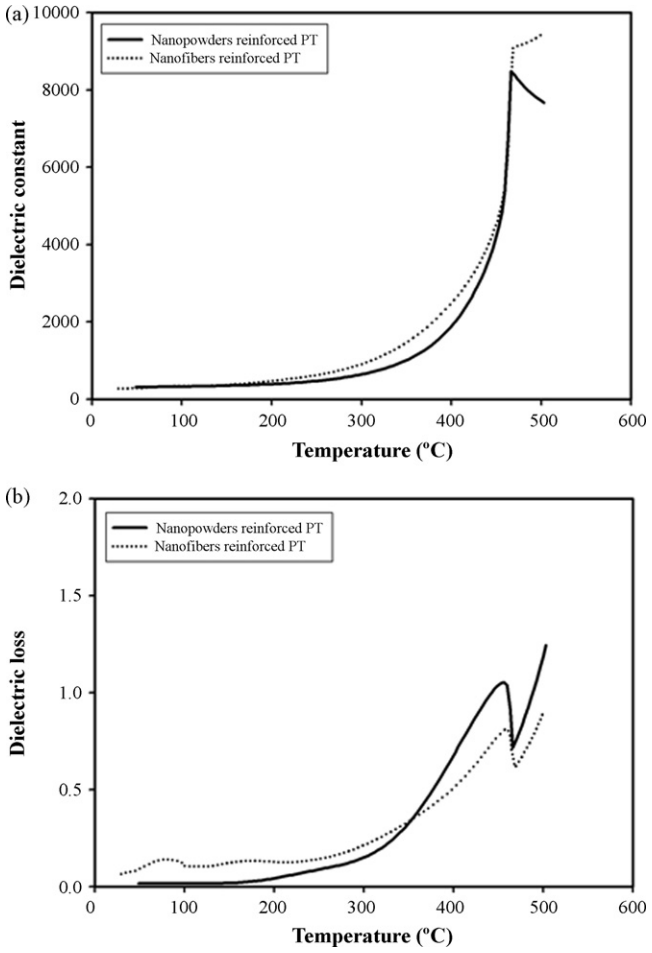

Fig. 5. Variation with temperature of (a) dielectric constant (ε_r) and (b) dielectric loss ($\tan\delta$) at 1 MHz for PT composites reinforced with PT nanopowders compared with those reinforced with PT nanofibers.

densification with retainable electrical properties of other piezoelectric materials, particularly those containing low melting point constituents.

For better understanding and verifying the attractiveness of the nanocomposite technique further, a systematic study on the effect of another piezoelectric nanodispersoids such as $BaTiO_3$ or PZT on the phase formation, densification, microstructure and electrical properties of the piezoelectric-based ceramic-nanocomposites is required.

4. Conclusions

The potentiality of a ceramic-nanocomposite technique as a low-cost and simple ceramic fabrication to obtain highly dense and pure PT/PT composites was demonstrated. It has been found that both densification and dielectric properties of the composites fabricated in this work were significantly enhanced, as compared to the two-stage sintering and the conventional PT ceramics, which is likely due to the fine-grain and reduced tetragonality as well as anisotropies of stress and domain motion in the composites.

Acknowledgements

We thank the Thailand Research Fund (TRF), the Commission on Higher Education (CHE) and the National Nanotechnology Center (NANOTEC), NSTDA, for all support.

References

[1] B. Jaffe, W.R. Cook, H. Jaffe, Piezoelectric Ceramics, Academic Press, New York, 1971.
[2] G.H. Haertling, J. Am. Ceram. Soc. 82 (1999) 797–818.
[3] A.J. Moulson, J.M. Herbert, Electroceramics, 2nd ed., Wiley, Chichester, 2003.
[4] T. Takahashi, Am. Ceram. Soc. Bull. 69 (1990) 691–695.
[5] L.E. Cross, Mater. Chem. Phys. 43 (1996) 108–115.
[6] G. Shirane, S. Hoshino, J. Phys. Soc. Jpn. 6 (1951) 265–270.
[7] G. Shirane, R. Pepinsky, B.C. Frazer, Acta Crystallogr. 9 (1956) 131–140.
[8] H. Takeuchi, S. Jyomura, E. Yamamoto, Y. Ito, J. Acoust. Soc. Am. 72 (1982) 1114–1120.
[9] L.B. Kong, W. Zhu, O.K. Tan, J. Mater. Sci. Lett. 19 (2000) 1963–1966.
[10] T. Suwannasiri, A. Safari, J. Am. Ceram. Soc. 76 (1993) 3155–3158.
[11] T. Takeuchi, M. Tabuchi, I. Kondoh, N. Tamari, H. Kageyama, J. Am. Ceram. Soc. 83 (2000) 541–544.
[12] J.S. Forrester, J.S. Zobec, D. Phelan, E.H. Kisi, J. Solid State Chem. 177 (2004) 3553–3559.
[13] A. Udomporn, K. Pengpat, S. Ananta, J. Eur. Ceram. Soc. 24 (2004) 185–188.
[14] F. Ye, L. Liu, J. Zhang, M. Iwasa, C.L. Su, Compos. Sci. Technol. 65 (2005) 2233–2239.
[15] R. Gadow, F. Kern, A. Killinger, Mater. Sci. Eng. B 148 (2008) 58–64.
[16] T. Ohji, Y.K. Jeong, Y.H. Choa, K. Niihara, J. Am. Ceram. Soc. 81 (1998) 1453–1460.
[17] H.T. Chung, D.S. Cheong, C.S. Kim, Mater. Lett. 59 (2005) 920–924.
[18] S. Jiansirisomboon, A. Watcharapasorn, Curr. Appl. Phys. 8 (2008) 48–52.
[19] H. Beltran, N. Maso, E. Cordoncillo, A.R. West, J. Electroceram. 18 (2007) 277–282.
[20] R. Wongmaneerung, R. Yimnirun, S. Ananta, Appl. Phys. A 86 (2007) 249–255.
[21] A. Udomporn, S. Ananta, Mater. Lett. 58 (2004) 1154–1159.
[22] R. Wongmaneerung, R. Yimnirun, S. Ananta, Mater. Lett. 60 (2006) 2666–2671.
[23] A. Rujiwatra, N. Thammajak, T. Sarakonsri, R. Wongmaneerung, S. Ananta, J. Crystal Growth 289 (2006) 224–230.
[24] H. Klug, L. Alexander, X-ray Diffraction Procedures for Polycrystalline and Amorphous Materials, 2nd ed., Wiley, New York, 1974.
[25] R.L. Fullman, Trans. AIME 197 (1953) 447–452.
[26] S.L. Swartz, T.R. Shrout, W.A. Schulze, L.E. Cross, J. Am. Ceram. Soc. 67 (1984) 311–315.
[27] JCPDS-ICDD Card no. 6-452, International Centre for Diffraction Data, Newtown Square, PA, 2000.
[28] J. Tartaj, C. Moure, L. Lascano, P. Durán, Mater. Res. Bull. 36 (2001) 2301–2310.
[29] M.L. Calzada, M. Alguero, L. Pardo, J. Sol–Gel Sci. Technol. 13 (1998) 837.
[30] S. Ananta, N.W. Thomas, J. Eur. Ceram. Soc. 19 (1999) 1873–1881.
[31] H.C. Wang, W.A. Schulze, J. Am. Ceram. Soc. 73 (1990) 825–832.
[32] Y. Matsuo, H. Sasaki, J. Am. Ceram. Soc. 49 (1966) 229–230.
[33] S.R. Dhage, Y.B. Khollam, H.S. Potdar, S.B. Deshpande, B.D. Sarwade, D.K. Date, Mater. Lett. 56 (2002) 564–570.
[34] S. Ananta, N.W. Thomas, J. Eur. Ceram. Soc. 19 (1999) 2917–2930.
[35] S. Chattopadhyay, P. Ayyub, V.R. Palkar, M. Multani, Phys. Rev. B 52 (1995) 13177–13179.
[36] M. Villegas, A.C. Caballero, M. Kosec, C. Moure, P. Duran, J.F. Fernandez, J. Mater. Res. 14 (1999) 891–897.

Journal of Alloys and Compounds 474 (2009) 241–245

Contents lists available at ScienceDirect

Journal of Alloys and Compounds

journal homepage: www.elsevier.com/locate/jallcom

Effects of addition of BT on structural phase formation and electrical properties of relaxor ferroelectric $Pb(In_{0.5}Nb_{0.5})_{(1-x)}Ti_{(x)}O_3$ ceramics

S. Wongsaenmai [a,*], S. Ananta [b], R. Yimnirun [b]

[a] Department of Physics, Faculty of Science, Maejo University, Chiang Mai 50290, Thailand
[b] Department of Physics, Faculty of Science, Chiang Mai University, Chiang Mai 50200, Thailand

ARTICLE INFO

Article history:
Received 18 January 2008
Received in revised form 11 June 2008
Accepted 15 June 2008
Available online 13 August 2008

Keywords:
Relaxor ferroelectric
Wolframite precursor method
Vibro-milling technique
PBINT

ABSTRACT

In this study, the solid solution of $Pb(In_{0.5}Nb_{0.5})_{(1-x)}Ti_{(x)}O_3$ with 20 mol% of BT (where $x = 0.0$, 0.1, 0.2 and 0.3) ceramics was prepared by the wolframite precursor method via a vibro-milling technique. The concentration of 20 mol% of BT was the lowest amount of BT to help stabilize the perovskite phase formation of PIN ceramics in this study. The variation of x between 0.0 and 0.3 ($0.0 \leq x \leq 0.3$; $\Delta x = 0.1$) was chosen based on the non-MPB composition of this PINT system to focus on the compositions with relaxor behavior. The phase formation of the ceramics was investigated as a function of compositions. The XRD patterns investigation showed that the ceramics gradually changed from the pseudo-cubic to tetragonal phase between the compositions $x = 0.2$ and 0.3, indicating a shift in the MPB of the PINT system with BT addition. Correspondingly, large dielectric constant maximum (ε_m) was observed over the same compositions. The remanent polarization (P_r) was also maximized at this composition, which indicated enhanced electrical properties near the MPB of this PBINT system. These results clearly indicated that the addition of BT had strong influence on phase formation and the electrical properties of the PINT system.

1. Introduction

The relaxor ferroelectric ceramics, which have the $Pb(B'B'')O_3$ complex perovskite structure, show broad dielectric transition maxima, high dielectric constant over a wide temperature range and frequency dispersion of dielectric properties and high electrostrictive strains [1,2]. These owning excellent properties attract for application as multilayer capacitor, piezoelectric transducer and electrostrictive actuator [2,3]. It is known that the main problem of these materials is the difficult to obtain the single-phase perovskite because of its inherently small electronegativity difference and low tolerance factor [4]. It has reported that the addition of the largest electronegativity difference and tolerance factor such as BT to PZN- and PMN-based system helps to stabilize the perovskite phase formation [5,6]. Lead indium niobate (PIN) is of interest for its chemical ordering study. It is a member of relaxor family with a 1:1 stoichiometric of B-site ordering which can be brought from disordered state into ordered state by thermal treatment [7]. The disordered state of PIN exhibits relaxor behavior which shows broad dielectric maximum near 66 °C [8,9]. In contrast, the ordered state shows antiferroelectric behavior with a sharp peak in dielectric constant vs. temperature curve observed at 168 °C [8,10]. However, the most interesting in this material is the solid solution with PT normal ferroelectric, because of their T_c higher than 250 °C near the MPB for the single crystal [11]. It is difficult to eliminate the pyrochlore phase in preparation, even though the wolframite precursor method was used. Interestingly, the addition of BT to help elimination the pyrochlore phase was reported in other systems of PZN-PT–BT and PMN-PT–BT [12,13]. In this present work, the addition of BT to PINT system was obtained by the wolframite precursor method to obtain the pure phase perovskite via vibro-milling technique. The phase formation and transition were investigated from the XRD patterns and the lattice parameters. The possible MPB of this PBINT system was examined with XRD patterns and electrical properties.

2. Experimental

The powders of $Pb(In_{0.5}Nb_{0.5})_{(1-x)}Ti_{(x)}O_3$ with 20 mol% of BT (where $x = 0.0$, 0.1, 0.2, and 0.3, abbreviated as PBINT) were synthesized by the wolframite precursor method via a vibro-milling technique. The concentration of 20 mol% of BT was lowest amount of BT to help stabilize the perovskite phase formation of PIN ceramics in this study. The secondary phase was found in the compositions lower than that of 20 mol% of BT (results are not shown). The wolframite ($InNbO_4$) was first prepared by mixing starting indium oxide (In_2O_3) and niobium oxide (Nb_2O_5) (Aldrich, 99.9% purity). Mixed powders were milled by a vibratory laboratory mill (McCrone micronizing mill) for 0.5 h and calcined at optimized calcination temperature of 900 °C for 4 h to obtain the intermediate precursor $InNbO_4$ [14,15]. The wolframite precursor powders were subsequently mixed with lead oxide (PbO) (Fluka, 99%

* Corresponding author. Tel.: +66 53 873525; fax: +66 53 872206.
E-mail address: wongsaenmai@yahoo.com (S. Wongsaenmai).

0925-8388/$ – see front matter © 2008 Elsevier B.V. All rights reserved.
doi:10.1016/j.jallcom.2008.06.112

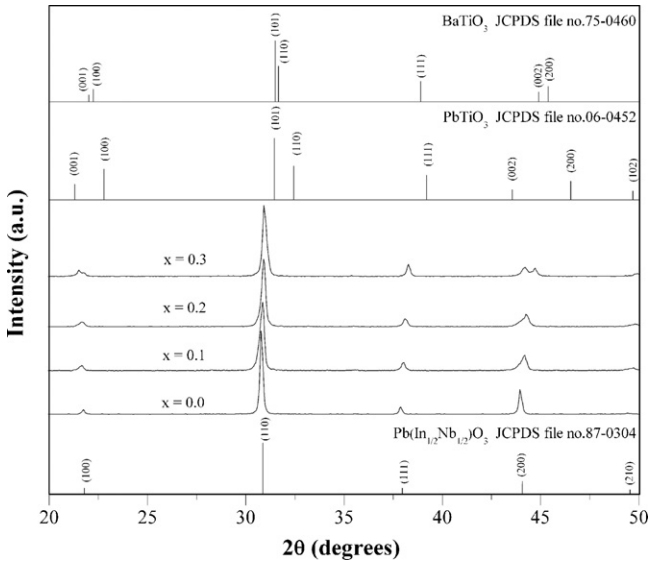

Fig. 1. XRD patterns of PBINT ceramics obtained at optimum sintering temperature.

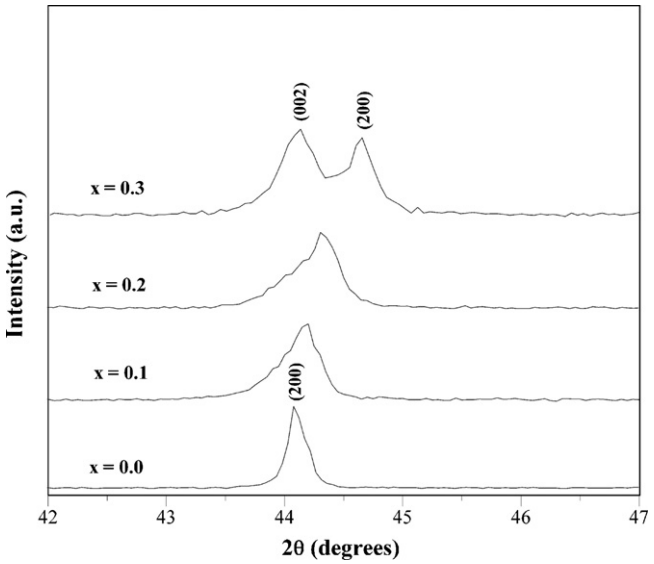

Fig. 2. Selected region XRD patterns of PBINT ceramics.

purity), $BaCO_3$ (Fluka, 99% purity) and titanium oxide (TiO_2) (Riedel-de Haën, 99% purity) according to the compositions of $Pb(In_{0.5}Nb_{0.5})_{(1-x)}Ti_{(x)}O_3$ with 20 mol% of BT where $x = 0.0$, 0.1, 0.2, and 0.3 and re-milled for 0.5 h. Excess amount of PbO (2 mol%) and In_2O_3 (2 mol%) were added in this stage. After drying at 120 °C for 2 h, the mixtures were calcined at temperature between 1050 and 1150 °C for 2 h with heating/cooling rate of 5 °C/min to determine optimum firing condition for every composition, in closed alumina crucible. After that, the calcined powders were pressed hydraulically to form disc-shaped pellets 10 mm in diameter and 2 mm thick, using 3 wt.% polyvinyl alcohol as binder. The pellets with composition between $x = 0.0$ and 0.3 were sintered in a closed alumina crucible at temperature between 1250 and 1300 °C for 2 h with heating/cooling rate of 10 °C/min. To prevent PbO evaporation, the pellets were placed on the same powder.

The phase formation of the sintered ceramics was analyzed by X-ray diffraction (XRD), using Cu Kα radiation to determine the phases formed and optimum firing temperatures for the formation of desired phase. The relative amount of the perovskite phase was determined from the relative intensities of the major XRD peaks of perovskite (1 1 0) and pyrochlore (2 2 2) ($I_{perov(1\,1\,0)}/I_{perov(1\,1\,0)} + I_{pyro(2\,2\,2)}$) [16]. Lattice parameters of the perovskite phases were determined by Cohen's method in conjunction with the least squares method [17]. The microstructure was investigated by scanning electron microscopy (SEM, JEOL Model JSM 840A). For the evaluation of electrical properties, gold electrodes were sputtered on both sides of the samples. The dielectric properties were measured with an LCR meter (HP-4284A, Hewlett-Packard, Santa Clara, CA) in conjunction with an environmental chamber (9023, Delta Design, Poway, CA). A heating rate of 2 °C/min and frequency of 1 kHz were used during measurement. Ferroelectric hysteresis loops were evaluated at various temperatures (25, −20, −50 and −80 °C) with a standardized ferroelectric test system (RT-66A, Radiant Technologies, Albuquerque, NM). A peak electric field of 30 kV/cm was applied.

3. Results and discussion

The XRD patterns of the dense PBINT ceramics as function of PT concentration at room temperature are shown in Fig. 1. It is evident that a complete crystalline solid solution of pure perovskite phase occurs throughout the studied compositional range of the PBINT system. The main difference of these XRD patterns can be observed on the peak of (2 0 0) reflection near $2\theta \sim 44–45°$, because the single (2 0 0) reflection peak indicates the pseudo-cubic phase, whereas the splitting in two peaks of (2 0 0)/(2 0 0) shows the tetragonal phase. For better viewing, the selected region of the (2 0 0) reflections near $2\theta \sim 44–45°$ are shown in Fig. 2, which exhibits the phase transformation from the pseudo-cubic to the tetragonal phase near the compositions of $x = 0.2$ and 0.3. Therefore, it can be expected that the MPB of this system lies between the compositions $x = 0.2$ and 0.3.

It is also supported by the lattice parameters, as listed in Table 1, that the region near same the compositions between $x = 0.2$ and 0.3 shows rapid increase in the tetragonality factor of c/a to 1.01. It is also seen that the addition of PT leads to shrinking of the a-axis while the c-axis expands, resulting in the average lattice parameter decrease. In comparison to the PINT system, the average lattice parameter of composition $x = 0.0$ (as $a = 0.4127$ nm) is larger than that of the PIN ceramics (as $a = 0.4117$ nm) [18]. However, the average lattice parameter decreases with increasing PT concentration for both of PINT and PBINT ceramic systems. It is expected that diffusion of the smaller Ti cation into B-site results in a decrease in lattice constant and the partial substitution of the larger Ba cation into A-site causes an increase in the average lattice parameters [19–21]. From the results of the XRD patterns and the lattice parameters, it is believed that the MPB of the PBINT system lies between the compositions $x = 0.2$ and 0.3. Additionally, it is also indicated that the addition of BT induces a shift of the MPB in the PINT system. Similar shift of the MPB has been reported in other systems such as PMN-PT and PZN-PT [13,22,23].

Fig. 3 shows the SEM micrographs of the PBINT ceramics. The grain size was estimated from the SEM observation, as listed in Table 1, together with the density. In general, the irregular grains

Table 1
Physical properties and the lattice parameters of PBINT ceramics

Composition (x)	Calcination temperature (°C)	Sintering temperature (°C)	Lattice constant (nm)				Bulk density (g/cm^3)	Percentage of theoretical density (%)	Grain size (μm)
			a	c	c/a	$(a^2c)^{1/3}$			
0.0	1150	1300	0.4126	–	1	0.4127	7.89	93.2	1.90
0.1	1000	1250	0.4100	–	1	0.4100	7.78	90.1	2.13
0.2	1050	1250	0.4096	–	1	0.4096	7.84	92.6	2.26
0.3	1050	1250	0.4052	0.4109	1.01	0.4067	7.86	97.1	2.58

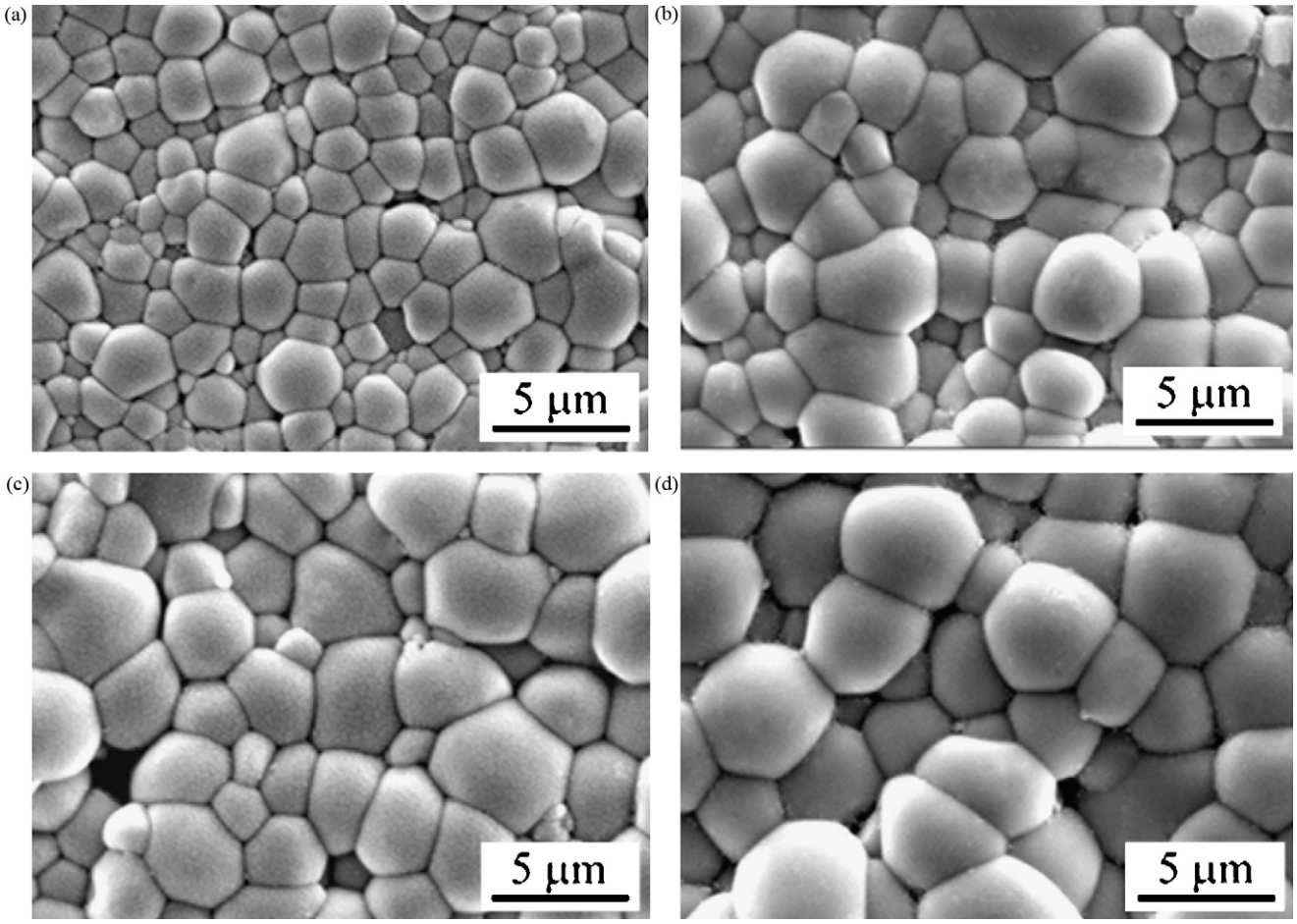

Fig. 3. SEM micrographs of PBINT with various compositions: (a) $x = 0.0$, (b) $x = 0.1$, (c) $x = 0.2$ and (d) $x = 0.3$.

and porosities can be observed, while the pyrochlore phase could not be found in the microstructure, good agreement with the XRD investigation. Clearly, the addition of PT and BT helps to stabilize the perovskite phase, a result of their difference in electronegativity and tolerance factor [5]. Additionally, the relative densities in the range of 90–97% theoretical density are obtained. These densities strongly influence the electrical properties, which will be presented in the following part. Moreover, the average grain size is in the range of 1–3 μm, indicating the fine grain size for this system [24]. The average grain size increased from 1.90 μm for the composition of $x = 0.0$–approximately 2.58 μm for the composition of $x = 0.3$. However, it should be noticed that the microstructure of all the compositions also represents two distinct grain sizes, i.e. large grains (~5 μm) and submicron grains. It is clearly evident that the addition of PT noticeably enhances grain growth.

The temperature dependence of the dielectric constant (at 1 kHz) as a function of composition is displayed in Fig. 4. All compositions show broad maximum of the dielectric constant. More details of the dielectric properties underlying frequency and their relaxor behavior have been reported in our previous work [25]. The dielectric constant maxima (ε_m) slightly increase with the composition of $x = 0.1$ and then drastically increase with more PT concentrations.

As listed in Table 2, large dielectric constant maxima are obtained at the composition of $x = 0.2$ ($\varepsilon_m = 17{,}366$ at 1 kHz) and $x = 0.3$ ($\varepsilon_m = 18{,}541$ at 1 kHz). It is known that the solid solution of lead-based relaxor and normal ferroelectric (PT) shows extra high dielectric constant maximum near the MPB [26]. Based on the XRD patterns and the lattice parameters, the maximization of the dielectric properties near the MPB has also been correlated with the reduction of the lattice distortion, as previously reported in the PZT system [27]. The temperatures of dielectric constant maximum (T_m) are also summarized in Table 2. It can be seen that increasing PT concentration leads to a shift of T_m to a higher temperature,

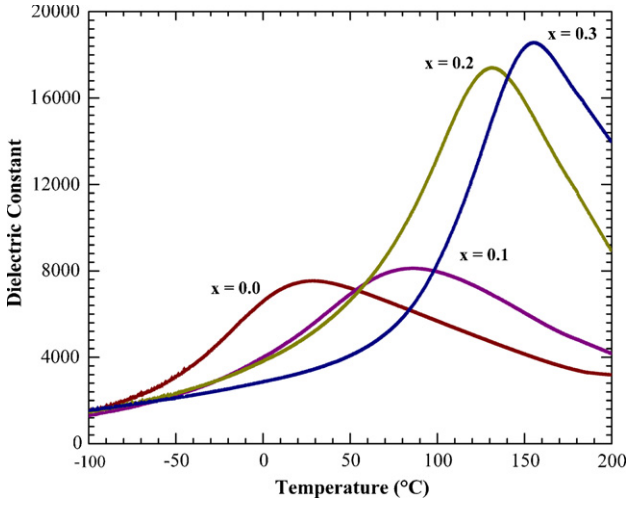

Fig. 4. Temperature dependence of the dielectric constant at 1 kHz for PBINT ceramics.

Table 2
Dielectric properties of PBINT ceramics at 1 kHz

Composition (x)	T_m (°C)	Dielectric properties			
		25 °C		At T_m	
		ε_r	tan δ	ε_m	tan δ
0.0	26	7500	0.030	7591	0.029
0.1	85	5326	0.076	8093	0.027
0.2	130	4953	0.068	17,366	0.038
0.3	155	3339	0.039	18,541	0.047

as expected since the transition temperature of PT is very high (~490 °C) [28]. However, it should be noticed that the T_m in PBINT is lower than that in the PINT system even at the same composition, as reported in our previous work [29]. The T_m is shifted to lower temperature by the addition of BT, with similar results observed in PMN-PT–BT and PZN-PT–BT systems [12,13]. This is probably related to BT-based solid solutions tend to posses pinched-type phase transition due to the lack of lone-pair electron associated with lead ions [26,30].

Fig. 5 illustrates a series of the polarization (P–E) hysteresis loops at various temperatures (25, −20, −50 and −80 °C) with a driving electric field of 30 kV/cm for PBINT ceramics. All ceramics show well-developed hysteresis loops with decreasing temperature. The composition x = 0.0 shows the slim-type hysteresis loop at room temperature, and the loop opens up with decreasing temperatures, indicating the development in the volume fraction of local polar regions with decreasing temperature [31]. It is also observed that the hysteresis loops differ in shapes depending on the composition. The typical "slim" hysteresis loops is found at the composition x = 0.0, then the loop shape gradually changes to the typical "square" hysteresis loops with increasing PT concentration. The square type loops are due to abruptly switching of a domain structure with an electric field, which is typical for a phase of strong normal ferroelectric PT that contains long-range corporations between dipoles in the ferroelectric micro-domain [27]. On the other hand, the slim-type loop is owing to more sluggish reversal, typical of a phase with a suppressed long-range of interaction micro-domain. The value of the polarization parameters such as the remanent polarization (P_r), the saturated polarization (P_s) and the coercive fields (E_c) evaluated from the hysteresis loop are also listed in Table 3. The E_c is seen to be strongly depending on temperature for all compositions, while the P_r changes only slightly.

The variations of the values of hysteresis loops parameters; i.e. the remanent polarization (P_r) and the coercive fields (E_c), evaluated from the hysteresis loops are shown in Fig. 6. The maximum of the P_r is observed near the compositions x = 0.2 and 0.3, indication of the MPB region of this PBINT system. It is generally accepted that the domain wall can easily move around the MPB because of the coexistence of the pseudo-cubic and tetragonal phases in ferro-

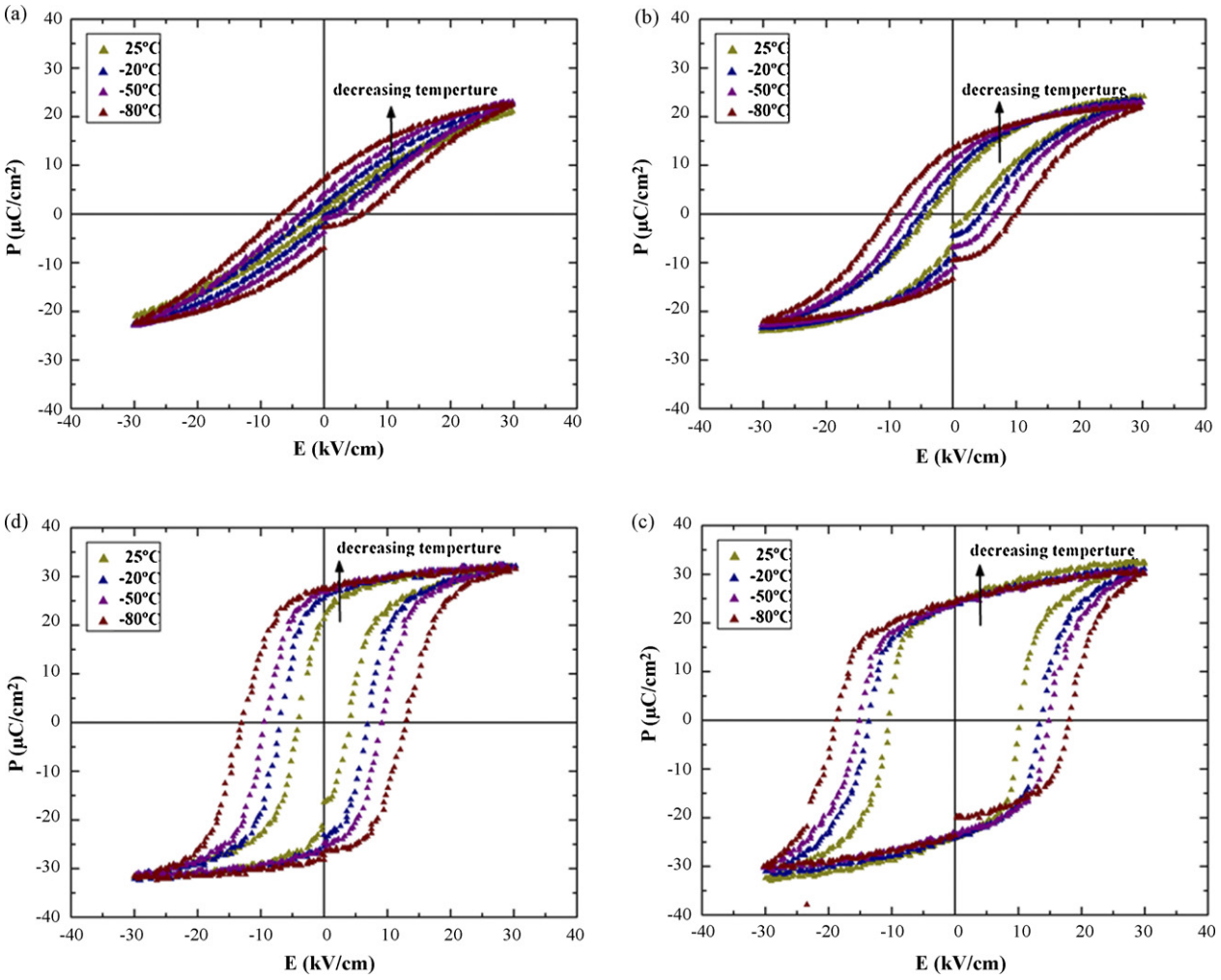

Fig. 5. Hysteresis loops of PBINT as a function of temperature 25, −20, −50 and −80 °C for various compositions (a) x = 0.1, (b) x = 0.2 (c) x = 0.3 and (d) x = 0.4.

Table 3
Ferroelectric properties of PBINT ceramics

Composition (x)	Ferroelectric properties							
	At 25 °C				At −80 °C			
	P_r (μm/cm^2)	P_s (μm/cm^2)	E_c (kV/cm)	R_{sq}[a]	P_r (μm/cm^2)	P_s (μm/cm^2)	E_c (kV/cm)	R_{sq}[a]
0.0	1.09	20.22	0.29	0.84	7.08	22.43	6.02	0.41
0.1	6.67	24.12	2.67	0.42	14.70	24.24	9.78	0.74
0.2	22.48	31.84	4.24	0.94	28.40	32.79	13.04	1.12
0.3	24.60	31.44	10.08	1.11	25.75	32.47	18.08	1.25

[a] Hysteresis loop squareness.

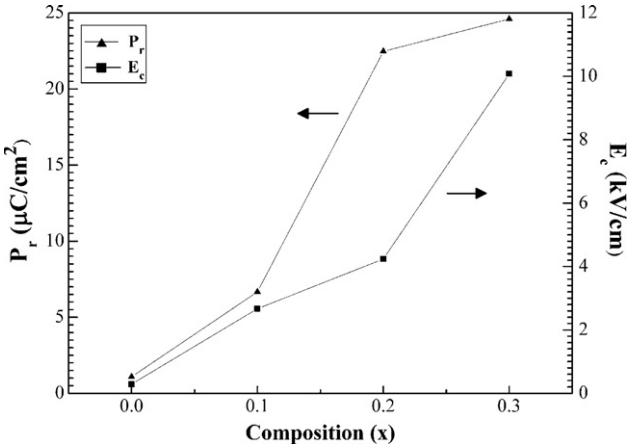

Fig. 6. Composition dependence of the P_r and E_c of PBINT ceramics at room temperature.

electric materials, which induces the high P_r [32]. In addition, the linear increase of the E_c indicates the increasing in the extent of the tetragonal phase with increasing PT concentration, which makes domain switching more difficult [33].

Finally, the ferroelectric characteristic of the ceramics can also be assessed with the hystersis loop squareness (R_{sq}), which is typically understood to be ratio of P_r/P_s, where P_r is the remanent polarization at zero electric field and P_s is the saturated polarization obtained at some finite field strength below the dielectric breakdown. One can also use the loop squareness to measure not only the deviation in the polarization axis but also that in the electric field axis with the empirical expression, $R_{sq} = (P_r/P_s) + (P_{1.1E_c}/P_r)$ where $P_{1.1E_c}$ is the polarization at the field equal to $1.1E_c$. For the ideal square loop, R_{sq} is equal to 2.00. The R_{sq} parameter, listed in Table 3 for all compositions at 25 and −80 °C, clearly shows more loop squareness with increasing PT concentration.

From the results of this study, it believed that the MPB of the PBINT system lies between the compositions $x = 0.2$ and 0.3. This is confirmed by the phase transformation observed in the XRD patterns, and the examined lattice parameters. The electrical properties; i.e. dielectric constant and the P–E hysteresis loops also exhibit excellent values near these compositions. These results clearly indicate that the addition of BT has strong effect on phase formation, microstructure and the electrical properties of the PINT system. In comparison with the PINT system, the addition of BT leads to a shift of the MPB region, increases the grain size, and enhances the electrical properties.

4. Conclusion

The pure phase of solid solution of $Pb(In_{0.5}Nb_{0.5})_{(1-x)}Ti_{(x)}O_3$ with 20 mol% of BT (where $x = 0.0$, 0.1, 0.2 and 0.3) ceramics was obtained by the wolframite precursor method via a vibro-milling technique. The XRD investigation showed that the ceramics gradually changed from the pseudo-cubic to tetragonal phase between the compositions $x = 0.2$ and 0.3. Correspondingly, large dielectric constant maximum (ε_m) were also obtained at the same compositions. The remanent polarization (P_r) also maximized near these compositions, which indicated enhanced electrical properties near the MPB composition. These results clearly indicated that the addition of BT had strong effect on phase formation, microstructure and the electrical properties of the PINT system.

Acknowledgements

This work was supported by the Thailand Research Fund (TRF), Commission on Higher Education (CHE), and Ministry of University Affairs in Thailand.

References

[1] R.E. Newnham, S. Trolier-Mckinstry, Ceram. Trans. 32 (1993) 1–18.
[2] T.R. Shrout, A. Halliyal, Am. Ceram. Soc. Bull. 66 (1987) 704–711.
[3] L.E. Cross, Mater. Chem. Phys. 43 (1996) 108–115.
[4] C.A. Randall, A.S. Bhalla, T.R. Shrout, L.E. Cross, J. Mater. Res. 5 (1990) 829–834.
[5] A. Halliyal, U. Kumar, R.E. Newnham, L.E. Cross, Am. Ceram. Soc. Bull. 66 (1987) 671–676.
[6] D.H. Kang, K.H. Yoon, J. Mater. Sci. 26 (1991) 56–60.
[7] C.A. Randall, A.S. Bhalla, Jpn. J. Appl. Phys. 29 (1990) 327–333.
[8] E.F. Alberta, A.S. Bhalla, J. Phys. Chem. Solids 63 (2002) 1759–1769.
[9] J. Wang, K.Z. Baba-Kishi, H.L.W. Chan, C.L. Choy, C.W. Tai, A.S. Bhalla, Ferroelectrics 272 (2002) 267–272.
[10] M. Iwata, S. Katagiri, H. Orihara, M. Maeda, I. Suzuki, H. Ohwa, N. Yasuda, Y. Ishibashi, Ferroelectrics 301 (2004) 179–183.
[11] N. Yasuda, H. Ohwa, M. Kume, K. Hayashi, Y. Hosono, Y. Yamashita, J. Cryst. Growth 229 (2001) 299–304.
[12] U. Kumar, L.E. Cross, A. Halliyal, J. Am. Ceram. Soc. 75 (1992) 2155–2164.
[13] L. Ruan, L. Li, Z. Gui, J. Mater. Sci. Lett. 16 (1997) 1020–1022.
[14] S. Wongsaenmai, S. Ananta, R. Yimnirun, Mater. Lett. 61 (2007) 2426–2429.
[15] S. Wongsaenmai, S. Ananta, R. Yimnirun, J. Mater. Sci. 42 (2007) 3754–3760.
[16] S.L. Swartz, T.R. Shrout, Mater. Res. Bull. 17 (1982) 1245–1250.
[17] B.D. Cullity, Elements of X-ray Diffraction, Addison–Wesley, New York, 1978.
[18] S. Wongsaenmai, X. Tan, S. Ananta, R. Yimnirun, Appl. Phys. A 88 (2007) 323–328.
[19] R.D. Shannon, Acta Crystallogr. A 32 (1976) 751–767.
[20] B.A. Malkov, Yu.N. Venevtsev, Inorg. Mater. (Transl. of Neorg. Mater.) 13 (1977) 1182–1192.
[21] S. Nomura, H. Arima, Jpn. J. Appl. Phys. 11 (1972) 358–364.
[22] W. Zhu, A.L. Andrei, P.Q. Mantas, J.L. Baptista, J. Am. Ceram. Soc. 84 (2001) 1740–1744.
[23] J.C. Bruno, T.C. Boni, C. Cavalheiro, M.A. Zaghete, Mater. Res. Bull. 43 (2008) 297–304.
[24] M. Pham-Thi, C. Augier, H. Dammak, P. Gaucher, Ultrasonics 44 (2006) e627–e631.
[25] S. Wongsaenmai, S. Ananta, R. Yimnirun, R. Guo, A.S. Bhalla, Ferroelectr. Lett. Sect. 34 (2007) 36–45.
[26] B. Jaffe, W.R. Cook, H. Haffe, Piezoelectric Ceramics, Academi Press, New York, 1971.
[27] M.R. Soares, A.M.R. Senos, P.Q. Mantes, J. Eur. Ceram. Soc. 19 (1999) 1865–1871.
[28] R. Wongmaneerung, R. Yimnirun, S. Ananta, Appl. Phys. A 86 (2007) 249–255.
[29] S. Wongsaenmai, S. Ananta, R. Yimnirun, Mater. Sci. Eng., submitted for publication.
[30] R.E. Newham, J. Mater. Educ. 5 (1983) 947–982.
[31] C.H. Wang, J. Eur. Ceram. Soc. 22 (2002) 2033–2038.
[32] V. Sundar, R.E. Newnham, Ferroelectrics 135 (1992) 431–446.
[33] J.T. Zeng, K.W. Kwok, H.L.W. Chan, J. Am. Ceram. Soc. 89 (2006) 2828–2832.

Journal of Alloys and Compounds 475 (2009) 456–462

Contents lists available at ScienceDirect

Journal of Alloys and Compounds

journal homepage: www.elsevier.com/locate/jallcom

Effects of SiC nanofibers addition on microstructure and dielectric properties of lead titanate ceramics

R. Wongmaneerung[a,*], P. Singjai[b], R. Yimnirun[b], S. Ananta[b]

[a] Department of Physics, Faculty of Science, Maejo University, Chiang Mai 50290, Thailand
[b] Department of Physics, Faculty of Science, Chiang Mai University, Chiang Mai 50200, Thailand

ARTICLE INFO

Article history:
Received 31 May 2008
Received in revised form 8 July 2008
Accepted 10 July 2008
Available online 23 August 2008

Keywords:
Lead titanate
Perovskite
Composite
Dielectric properties

ABSTRACT

Dense perovskite ferroelectric $PbTiO_3$ (or PT) ceramics reinforced with SiC nanofibers have been successfully fabricated by a simple solid-state mixed oxide and conventional sintering method. Phase formation, densification, microstructure and dielectric properties of the composites were investigated as a function of SiC content. Addition of SiC nanofibers to a PT matrix did not result in unexpected reaction phase. Microstructural observations revealed that some SiC nanofibers were heterogeneously dispersed in PT matrix and at the matrix boundaries. The grain size was decreased significantly with addition of SiC nanofiber. Though the densification and mechanical strength were improved, the dielectric properties of PT/SiC composites were degraded dramatically.

1. Introduction

Perovskite ferroelectric lead titanate ($PbTiO_3$ or PT) based ceramics which exhibit excellent dielectric, piezoelectric and pyroelectric properties have been widely employed in sensor, transducer and actuator applications, especially for devices working at high-temperature and high-frequency conditions [1–3]. However, pure and dense PT ceramic is regarded to be one of the most difficult lead-based perovskite ferroelectrics to produce especially via a simple solid-state reaction method [2,3]. It suffers from low mechanical properties and the resulting poor electrical reliability mainly due to large distortion of the tetragonal phase at room temperature [3]. This phase transformation causes a complicated stress system in the ferroelectric material, and then results in the generation of internal stress and mechanically twined microstructure at room temperature. For further high-power applications used under severe circumstances, its poor mechanical and electrical reliability become a critical limitation on the application of this material. Especially in multilayer piezoelectric actuators, the high electric driving field needed to produce a large displacement may cause mechanical and electrical degradation [2,3]. Therefore, improving mechanical properties of PT-based materials is worthwhile.

To overcome such problems, several techniques have been introduced [4–9]. Amongst all the issues reported so far, most attention has been concentrated on the use of additives and chemically derived powder processing, whereas investigations on modified particle packing or composite techniques have not been widely carried out [10,11]. Recently, Niihara [12] had reported that small amount of submicro- or nano-scale second phase could largely improve the mechanical properties of ceramic matrix. In the past few years, this composite idea has been applied to some perovskite ferroelectric ceramics such as $BaTiO_3$/SiC [13], PZT/SiC [14] and PZT/Ag [15] systems. However, to our knowledge, the fabrication of PT composites reinforced with SiC nanofibers has not been reported so far.

Therefore, in this work, small amount SiC nanofibers (0.1–5.0 wt%) reinforced PT ceramics are fabricated by conventional sintering method. The effect of SiC additions on densification, microstructure and dielectric properties of the composites have been discussed and compared with the monolithic PT ceramics.

2. Experimental procedure

Monolithic $PbTiO_3$ (PT) ceramics and PT/SiC composites were prepared using a conventional ceramic fabrication method. The starting materials were $PbTiO_3$ powders (average particle size ~1–5 μm) and β-SiC nanofibers (average diameter ~80–100 and ~15–100 μm in length), as shown in Fig. 1. Characteristic properties of starting materials and detail of their fabrication procedures were already described elsewhere [16,17]. Briefly, different amounts (0.1–5.0 wt% or 0.03–1.55 vol%) of SiC nanofibers were ultrasonically dispersed in ethanol for 10 min before mechanically vibro-mixing [16] with the PT powders and 1 wt% of PVA binder for 30 min. The slurry was dried at 120 °C and sieved into a fine powder. The mixed powders of each composition were pressed into green pellet under a uniaxial press at 100 MPa, placed on high purity alumina spacer inside a closed alumina crucible. The PVA binder was

* Corresponding author.
E-mail address: re_nok@yahoo.com (R. Wongmaneerung).

0925-8388/$ – see front matter © 2008 Elsevier B.V. All rights reserved.
doi:10.1016/j.jallcom.2008.07.051

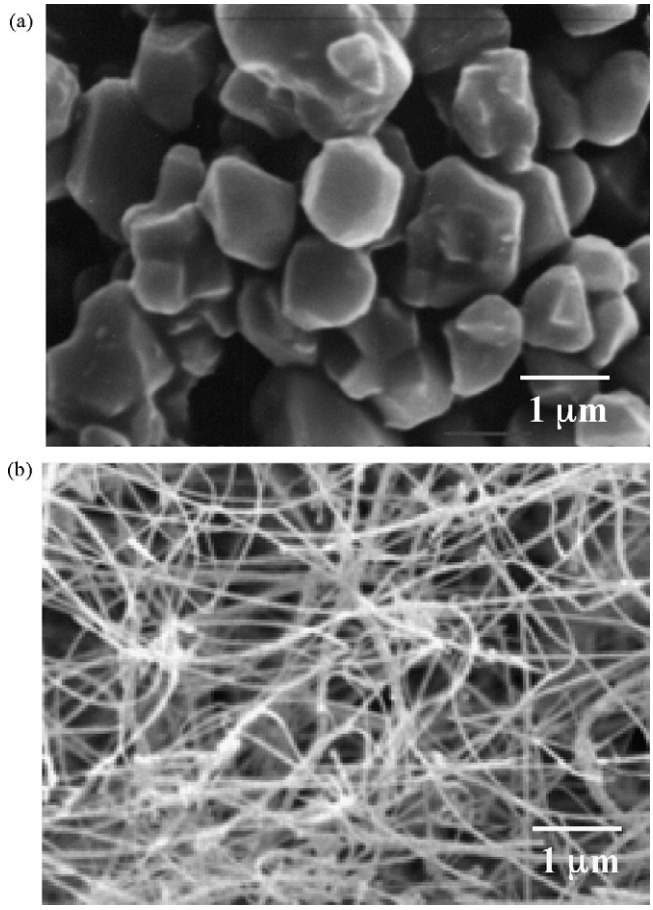

Fig. 1. SEM micrographs of the fabricated (a) PT powders and (b) SiC nanofibers.

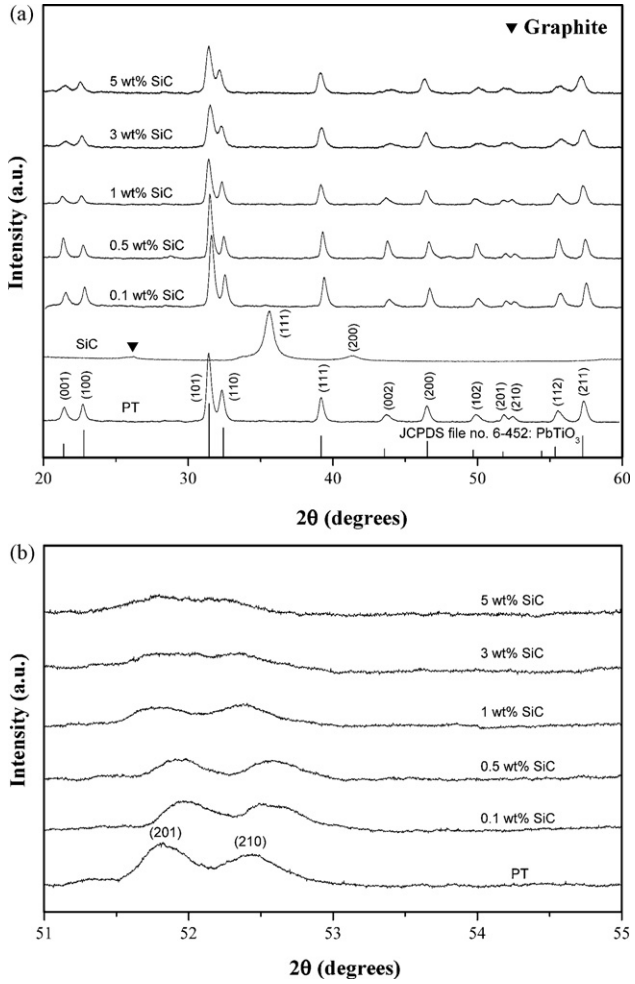

Fig. 2. XRD patterns of monolithic PT ceramics and PT/SiC composites after sintered at 1200 °C for 1 h with heating/cooling rates of 1 °C/min.

burnt out at 550 °C with heating/cooling rates of 10 °C/min and sintered at 1200 °C for 1 h with slow heating/cooling rates of 1 °C/min (in order to avoid the sample damage after sintering [9,18]). A PbO atmosphere was also maintained during sintering using PT powders with identical chemical composition in order to minimize the lead loss due to evaporation [9,18].

Phase identification of the sintered samples was characterized by using room temperature X-ray diffraction technique (XRD; Siemens-D500 diffractometer) with Cu $K_{\alpha 1}$ radiation. The lattice parameters and tetragonality factor (c/a) of the sintered samples were calculated from the XRD patterns [18,19]. The bulk density was determined by using the Archimedes principle in distilled water, and the relative density calculated using the theoretical density of PT [1]. Microstructure and fracture surface of the samples were examined with a scanning electron microscopy (SEM; JEOL JSM-840A). The average grain size of each composition was determined by linear intercept method using SEM photograph [9]. For electrical measurement, silver paste was fired on both sides of the polished samples at 600 °C as electrode. The dielectric properties were studied as a function of temperature. The capacitance was measured with a HP4284A LCR meter in connection with a Delta Design 9023 temperature chamber and a chamber holder capable of high temperature measurement, on cooling through the transition range (550–25 °C) with a rate of 5 °C/min at high frequencies range from 1 to 5 MHz.

3. Results and discussion

X-ray diffraction patterns of the monolithic PT and PT/SiC composites sintered at 1200 °C for 1 h are shown in Fig. 2(a), indicating the formation of only single phase perovskite in all cases. All the peaks were identified as tetragonal $PbTiO_3$, which could be matched with JCPDS file no. 6-452 [20], in agreement with other works [4–9]. No reaction phases between the PT matrix and SiC addition were observed in these XRD patterns. Moreover, there is no trace of the SiC phase was detected in all composites. The amount of SiC remaining in the composite may have been too small to be detected by XRD, and peak broadening due to particle size effects may have also been a factor [19]. It should be noted that the XRD patterns show some sign of peak splitting, e.g. (2 0 1)/(2 1 0) peaks which is an indication of tetragonal PT phase [16,20] however, the splitting was less well defined in the higher amount of SiC-containing samples, as shown in Fig. 2(b).

Table 1 also shows tetragonality factor (c/a), relative density and grain sizes of all compositions. The values of c/a for all PT/SiC composites are significantly lower than that of monolithic PT ceramics, indicating lower internal stress in these PT/SiC composites. With increasing SiC content, the c/a value, the density and the average grain size was decreased, in consistent with other similar perovskite-based systems [13,14]. More interestingly, all composite

Table 1
Physical properties of PT/SiC composites after sintered at 1200 °C for 1 h with heating/cooling rates of 1 °C/min

SiC nanofiber (wt%)	Tetragonality (c/a)	Relative density (%)	Grain size[a] (mean) (μm)
0.0	1.063	94	20.0–65.0 (36)
0.1	1.061	95	0.5–2.2 (0.8)
0.5	1.061	91	0.5–2.6 (0.7)
1.0	1.060	90	0.2–1.6 (0.6)
3.0	1.057	84	0.1–0.9 (0.4)
5.0	1.057	72	0.1–0.7 (0.3)

[a] The estimated precision of the grain size is ±10%.

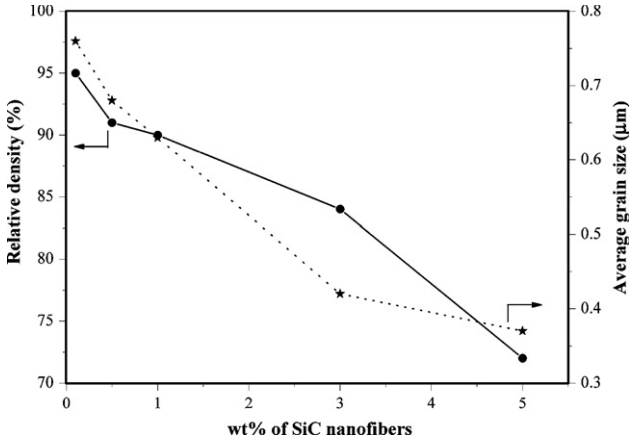

Fig. 3. Variation of relative density and average grain size of PT/SiC composites with SiC content.

samples do not suffer from severe stresses as a result of the high c/a ratio so they have not broken into pieces after experienced the sintering process or once subjected to a cycle of high temperature measurement of dielectric properties, as reported previously for the conventional and two-stage sintering PT cases [9,18]. Arlt et al. [21] have shown that for the grain size of less than 1 μm, the lower value of c/a ratio was found with the reduction of grain size. In the present study, the average grain size of all PT/SiC composites is obviously smaller than 1 μm (Table 1 and Fig. 3). Thus, it is believed that the major factor to reduce the tetragonality factor is mainly attributed to the grain growth suppression effect of SiC addition [13,14].

However, there is little change in the tetragonality factor of PT composites when the content of SiC is higher than 3.0 wt%. Furthermore, there is no SiC phase appearing in any PT/SiC composites. Thus, it can be estimated that the solubility of SiC in PT matrix is higher than 5 wt% (or 1.55 vol%) [22]. It is well known that PT system has an ABO_3-type perovskite structure. The A-sites are occupied by Pb^{2+} ions and the B-sites by Ti^{4+} ions. Although a dopant can go either to the A- or B-site, its distribution on the two sites being a function of the valence and ionic radius of the dopants [1,3]. However, in this study, the possibility of a Si^{4+} ion substitution which will create an oxygen vacancy to compensate charge neutrality and the distortion of oxygen octahedron structure [3] resulting in the variation of tetragonality (c/a) should not be the case since no sufficient ionization or diffusion can be expected for SiC at 1200 °C.

The influence of SiC additions on the relative density of PT composites sintered at 1200 °C for 1 h in air is also shown in Table 1 and Fig. 3. Generally, it is evident that the monolithic PT ceramics and PT/SiC composites (with less than 1 wt% SiC) could be sintered to above 90% of the theoretical density even at a temperature as low as 1200 °C. As the SiC content increases (especially at 0.5 wt% SiC), the relative density of the samples decrease in good agreement with those found for the PZT/SiC [20], PZT/Al_2O_3 [23], $BaTiO_3$/Al_2O_3 [24] and $BaTiO_3$/NiO [25] composites. In the case of $BaTiO_3$/Al_2O_3 and $BaTiO_3$/NiO systems [24,25], it was also shown that addition of secondary phase caused enlargement of particle size in green body, resulting in low density observed in sintered samples. In this work, the addition of SiC nanofibers into PT matrix had the same effect as those of Al_2O_3 and NiO. The inhibition of densification was evidenced from the large fraction of opened pores in 1.0 and 5.0 wt% SiC/PT samples (Figs. 4c(ii) and d(ii)) compared to the monolithic PT (Fig. 4a(i)). It should be noted that remarkable change of average grain size was observed on addition of a non-perovskite SiC phase, and the small quantity added had quite significant effect on the sinterability of PT ceramics by suppressing the liquid-phase (PbO-rich phases) sintering mechanism commonly found for typical monolithic PT [9,18]. This sintering behavior can be associated with the grain growth suppression of SiC nanofibers inside the PT matrix. In this system, the formation of oxygen vacancies due to Si^{4+} ion substitution in the perovskite structure is not considered to be another reason responsible for the sintering behaviour of PZT/SiC composites. Thus, the assumption of oxygen vacancies accelerate mass transfer and densification, which result in high relative density observed in other system [15,26] is not valid in this study.

A distribution of SiC fibers in a matrix may decrease the sintering rate by inducing tensile mean stress in the matrix [27,28]. The effects are less pronounced for a PT matrix, wherein the tensile mean stress approaches the sintering potential, resulting in substantial retardation of sintering, as observed experimentally. However, the SiC nanofiber has a diminished retardation effect in a lower strength ferroelectric typed of PT matrix, because the stresses are more readily relaxed. The specific source of this difference is not yet understood. Several researchers [27–29] have found that application of an initial gap between the fiber and matrix to delay stress development, are shown to be crucial requirements for densification of ceramic matrix materials.

Microstructural features, free (i) and fracture (ii) surfaces, of the monolithic PT ceramics and PT/SiC composites sintered at 1200 °C for 1 h are displayed in Fig. 4. The grain structure of both monolithic PT ceramics and PT/SiC composites were more or less equiaxed. Growth of the matrix grains in the PT/SiC composites is thought to be inhibited by reaction between the matrix and SiC phases [28,30]. In general, the small grain size results in high mechanical properties. Because of the relatively low reactivity between PT and SiC [28], SiC has significant effect on overall microstructural arrangement and therefore also the mechanical properties [3,12]. Observation of the microstructure by SEM showed that the SiC phase was randomly dispersed in the PT matrix. The average grain size of PT matrix (determined by a linear intercept as shown in Table 1) is also given as a function of SiC content in Fig. 3. The average grain sizes were found to decrease with the addition of SiC, indicating that SiC inhibited grain growth as earlier proposed by other workers [13,14]. The SiC nanofibers were found to locate both within the matrix and at the grain boundaries (see enlarged insertion in Fig. 4e(i)). The overall microstructural arrangement of the PT/SiC composites found in this study can be roughly classified as “nanofiber” types according to the model advocated by Kuntz et al. [30].

As mentioned previously, a small quantity of dispersed fiber is enough to control the grain growth mechanism and as a consequence to effectively reinforce the PT matrix. It seems that the grain boundary movement is depressed by the SiC fibers, as can be seen in Fig. 4(c). This may be caused by the grain boundary pinning force of SiC, which depressed the migration of PT grain boundaries during the sintering process [31], pointed out by other researchers [23,24]. In general, spontaneous cracking of polycrystalline ceramics results from the internal stresses between grains, owing to incompatible strains from either thermal expansion anisotropy or phase transformation [2,3,32]. The spontaneous cracking observed in the present study must be caused by the paraelectric to ferroelectric phase transformation.

Generally, the fracture mode of pure perovskite PT ceramics is known to be an intergranular [9,18]. In the present study, the fracture mode of 0.1 wt% SiC composite (Fig. 4b(ii)) is predominantly intergranular-type as well as that of monolithic PT ceramic (Fig. 4a(ii)), because the clear grain boundary can be observed. In general, the samples with intergranular fracture include the pores and impurities in the grain boundaries are weaker compared to those of the other part. In comparison with the typical monolithic PT ceramics [5,9], almost clean microstructures with highly uniform, denser angular grain-packing and more homogeneous are

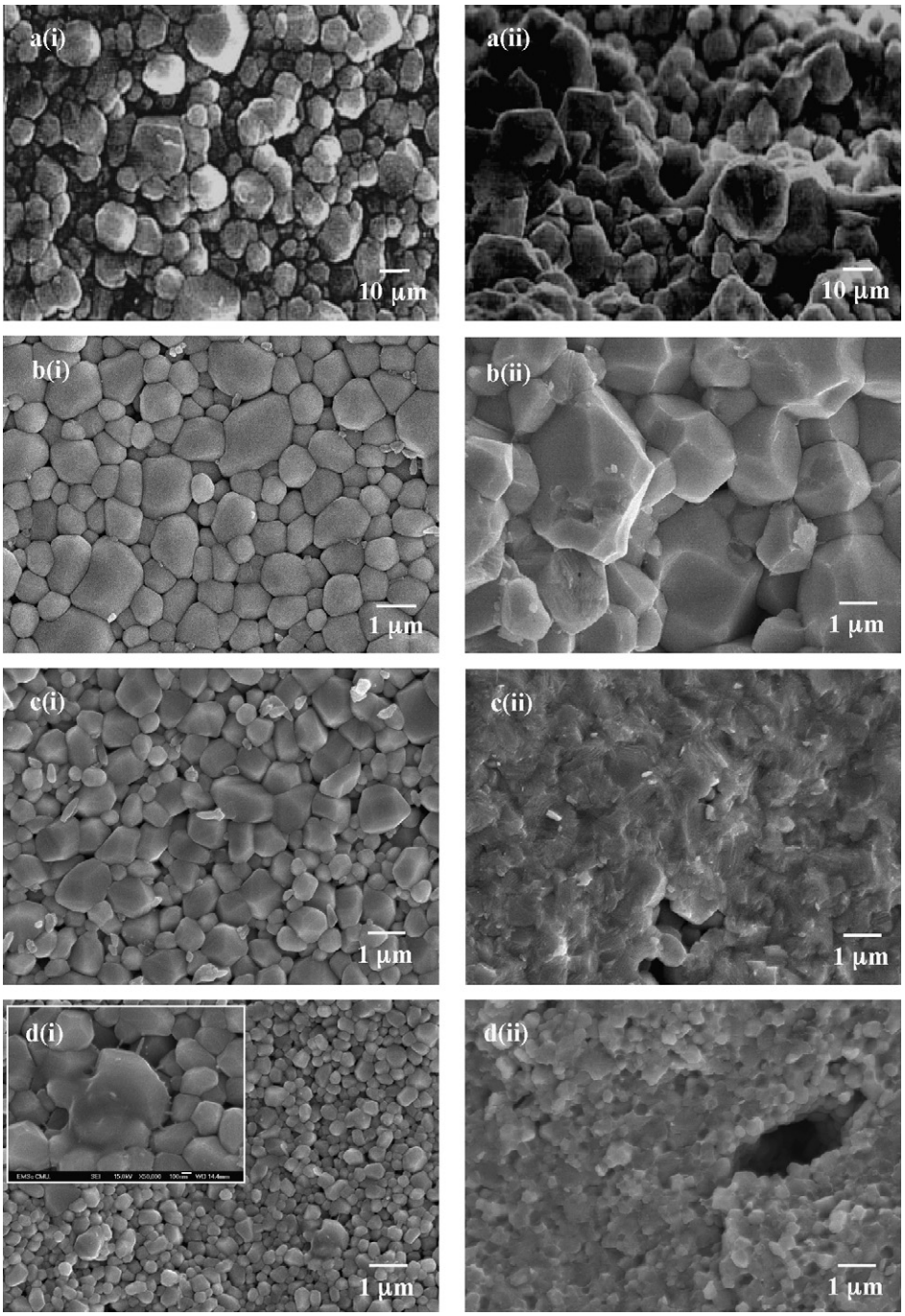

Fig. 4. Free (i) and fracture (ii) surfaces of (a) monolithic PT ceramics and PT/SiC composites with (b) 0.1 wt%, (c) 1 wt% and (d) 5 wt% of SiC content.

generally observed in PT/SiC composites. Interestingly, all samples remained unbroken. On the other hand, with increasing SiC content, the grain boundary in the fracture surface became obscure as shown in Fig. 4c(ii) and d(ii), and the fracture changed from intergranular to transgranular surface. This kind of characteristic was also found for the PZT/SiC composites earlier reported by Chen et al. [33]. Furthermore, it should be noted that the average grain size of both PT nanocomposites is <1.5 μm, which is less than the critical value of 3 μm [9,28] and gives rise to a volumetric percentage enough to buffer the anisotropic stress caused by the phase transition [3,28]. The reduced grain size of the composites is considered to be responsible for the improvement of their mechanical properties [5,6,18].

The influence of SiC content upon the dielectric-temperature characteristics of PT/SiC nanocomposite ceramics at various high frequencies over the temperature range of 25–550 °C is illustrated in Fig. 5, owing to the fact that the most desirable dielectric properties of PT ceramics for use in electronic devices are at high frequency range (MHz–GHz) and not much work has been reported on the electrical properties at frequency higher than 100 kHz. Thus, the high frequency range available from the dielectric equipment testing of 1–5 MHz has been performed in this study. The dielectric constant (ε_r) and dielectric loss ($\tan\delta$) values at room temperature and a ferroelectric–paraelectric phase transition temperature (T_C) are also listed in Table 2. Generally, they all behave as typical normal ferroelectric materials [1–3]. Moreover, it can be seen that except

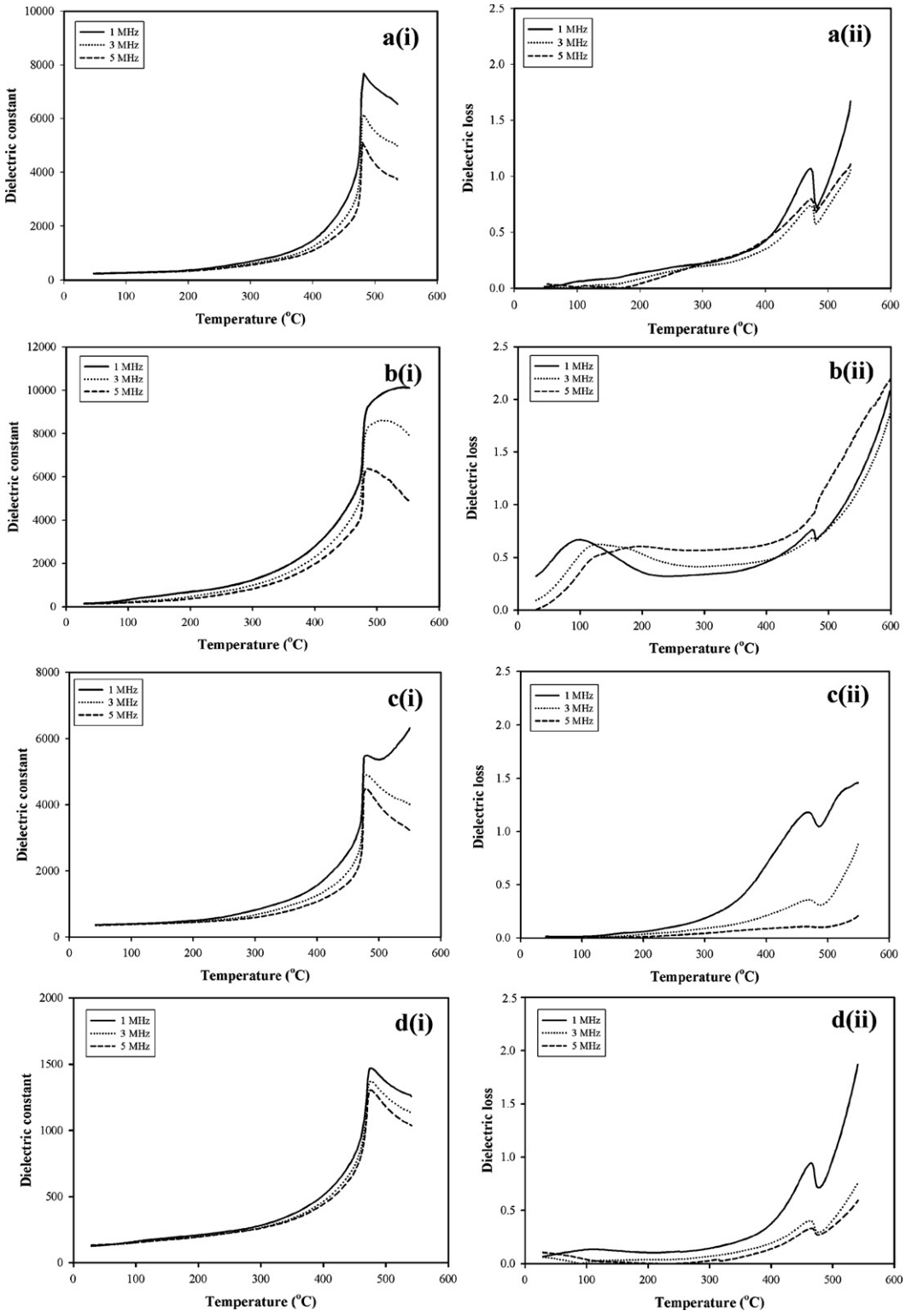

Fig. 5. Variation with temperature of dielectric constant (ε_r) and dielectric loss ($\tan\delta$) at 1 MHZ for (a) monolithic PT ceramics and PT/SiC composites with (b) 0.1 wt%, (c) 1 wt% and (d) 5 wt% of SiC content.

at 0.1 wt% SiC, increasing the SiC content caused a reduction in the dielectric constant (and increase in dielectric loss for PT/SiC composites with SiC > 0.1 wt%). Similar trend in dielectric values at T_C was also observed. The reduction in ε_r and also the increase in $\tan\delta$ with the content of SiC additive could be attributed mainly to an increase in porosity, as can be seen in Fig. 4. It can be said that the SiC nanofibers did not so much react with PT matrix. Other reason which is possible is that the presence of more non-ferroelectric SiC phase. The SiC fiber seems to be acting in the same way as porosity because the SiC is nonpiezoelectric material. Domain wall motion clamping due to the reduced grain size [34] is also considered to be another possible reason responsible for the low dielectric con-

Table 2
Dielectric properties of PT/SiC composites measured at 1 MHz

SiC nanofiber (wt%)	T_C (°C)	$\varepsilon_{25°C}$	$\tan\delta_{25°C}$	$\varepsilon_{r,max}$	$\tan\delta_{max}$
0.0	482	243	0.02	7680	1.07
0.1	485	149	0.32	9337	0.76
1.0	482	268	0.08	5493	1.18
5.0	475	128	0.02	1470	0.95

stant of SiC/PT composites. The results on dielectric measurement were also in agreement with a previous report in the perovskite-based PZT/SiC and $BaTiO_3$/SiC systems [13,14,33]. In those cases, the domain clamping due to oxygen vacancies and reduction in grain size was thought to cause the decrease in dielectric constant. In this work, the grain size of these composites was rather small therefore domain clamping due to grain size was probably one of the main factors. Furthermore, this work demonstrated that the dielectric properties of PT/SiC nanocomposite ceramics are also influenced by microstructural features and arrangement especially the microcracks and final density. It is seen that with the increase of SiC content, the peak of T_C kept a clear shape and shifted towards lower temperatures (Table 2 and Fig. 6). The shift of the phase transformation temperature in these PT/SiC composites might be due to a relaxation of transformation-induced internal stress by the SiC fiber dispersed in the PT matrix. Similar effect was also found in the MgO/$BaTiO_3$ nanocomposites where T_C of the $BaTiO_3$ dispersoids shifted to lower temperatures upon the incorporation of Mg ion [35].

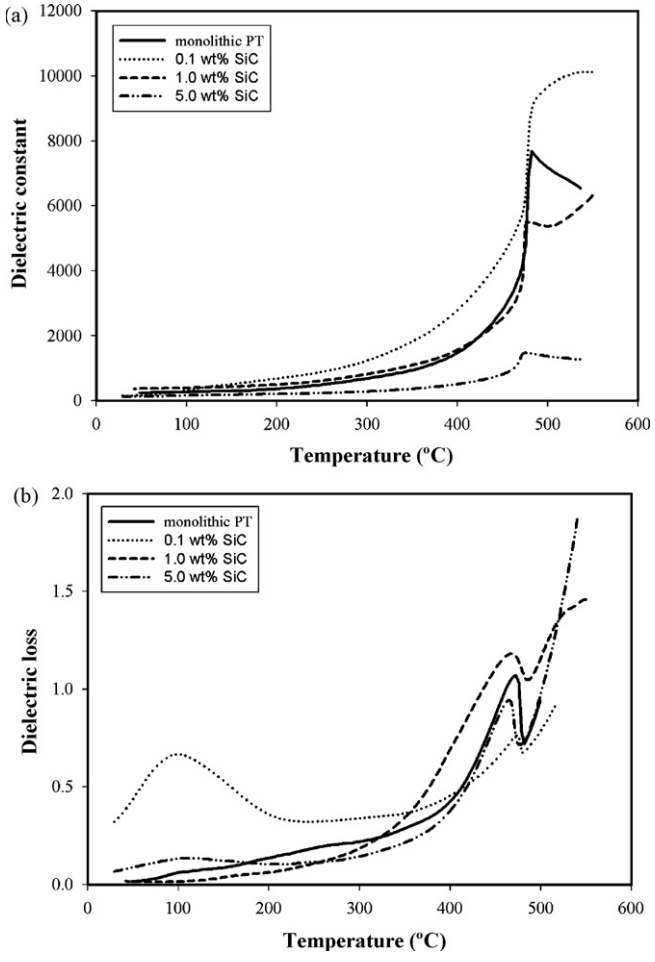

Fig. 6. Variation with temperature of (a) dielectric constant and (b) dielectric loss at 1 MHz of PT/SiC composites as a function of SiC content.

The results obtained in this work suggest that these composites exhibit complex microstructures which are inherently heterogeneous. The heterogeneity is a result of variation in grain size, fiber length and orientation, variation in chemical homogeneity; and the presence and distribution of additional phases and pores. These factors have an important effect on the dielectric properties of the materials. Although improving mechanical properties of PT-based ceramics is worthwhile, the problem of dielectric properties trade-off especially a deterioration of dielectric constant still remains unsolved. Further work on the PT ceramics reinforced with the piezoelectric nanomaterials, e.g. PZT, $BaTiO_3$ or ZnO nanofibers should be very helpful for gaining better understanding of these piezoceramic nanocomposite systems.

4. Conclusions

The influence of SiC nanofiber addition on phase formation, microstructure and dielectric properties of perovskite PT ceramics fabricated by a simple, inexpensive solid-state reaction method has been examined and reported for the first time. If small amount of 0.1 wt% SiC nanofibers was added into perovskite PT matrix, dense PT/SiC composites with good mechanical and dielectric properties could be successfully produced by a simple mixed oxide and conventional sintering method. Addition of SiC nanofibers was found to inhibit densification and suppress grain growth, in agreement with results from other ferroelectric nanocomposite systems. The dielectric properties were also influenced by SiC addition in analogous with the porosity.

Acknowledgements

This work was supported by the Thailand Research Fund (TRF), the Commission on Higher Education (CHE), the National Nanotechnology Center (NANOTEC) and the Faculty of Science, Chiang Mai University and Maejo University.

References

[1] B. Jaffe, W.R. Cook, H. Jaffe, Piezoelectric Ceramics, Academic Press, New York, 1971.
[2] G.H. Haertling, J. Am. Ceram. Soc. 82 (1999) 797–818.
[3] A.J. Moulson, J.M. Herbert, Electroceramics, 2nd ed., Wiley, Chichester, 2003.
[4] H. Takeuchi, S. Jyomura, E. Yamamoto, Y. Ito, J. Acoust. Soc. Am. 72 (1982) 1114–1120.
[5] L.B. Kong, W. Zhu, O.K. Tan, J. Mater. Sci. Lett. 19 (2000) 1963–1966.
[6] T. Suwannasiri, A. Safari, J. Am. Ceram. Soc. 76 (1993) 3155–3158.
[7] T. Takeuchi, M. Tabuchi, I. Kondoh, N. Tamari, H. Kageyama, J. Am. Ceram. Soc. 83 (2000) 541–544.
[8] J.S. Forrester, J.S. Zobec, D. Phelan, E.H. Kisi, J. Solid State Chem. 177 (2004) 3553–3559.
[9] A. Udomporn, K. Pengpat, S. Ananta, J. Eur. Ceram. Soc. 24 (2004) 185–188.
[10] J.S. Reed, Principles of Ceramic Processing, 2nd ed., Wiley, New York, 1995.
[11] T. Nagai, H.J. Hwang, M. Yasuoka, M. Sando, K. Niihara, J. Am. Ceram. Soc. 81 (1998) 425–453.
[12] K. Niihara, J. Ceram. Soc. Jpn. 99 (1991) 974–982.
[13] H.J. Hwang, K. Niihara, J. Mater. Sci. 33 (1998) 549–558.
[14] T. Yamamoto, H. Igarashi, K. Okazaki, Ferroelectrics 63 (1985) 281–288.
[15] H.J. Hwang, M. Yasuoka, M. Sando, M. Toriyama, J. Am. Ceram. Soc. 82 (1999) 2417–2422.
[16] R. Wongmaneerung, R. Yimnirun, S. Ananta, Mater. Lett. 60 (2006) 1447–1452.
[17] T. Jintakosol, P. Singjai, Key Eng. Mater. 353–358 (2007) 2171–2174.
[18] R. Wongmaneerung, R. Yimnirun, S. Ananta, Appl. Phys. A 86 (2007) 249–255.
[19] H. Klug, L. Alexander, X-ray Diffraction Procedures for Polycrystalline and Amorphous Materials, 2nd ed., Wiley, New York, 1974.
[20] JCPDS-ICDD Card no. 6-452. International Centre for Diffraction Data. Newtown Square, PA, 2000.
[21] G. Arlt, D. Hennings, G. de With, J. Appl. Phys. 58 (1985) 1619–1625.
[22] R.B. Atkin, R.M. Fulrath, J. Am. Ceram. Soc. 53 (1970) 51–52.
[23] K. Tajima, H.J. Hwang, M. Sando, K. Niihara, Key Eng. Mater. 161–163 (1999) 505.
[24] S. Jiansirisomboon, A. Watcharapasorn, Cur. Appl. Phys. 8 (2008) 48–52.
[25] W.H. Tzing, W.H. Tuan, Ceram. Int. 25 (1999) 69–75.
[26] P.H. Xiang, X.L. Dong, C.D. Feng, N. Zhong, J.K. Guo, Ceram. Int. 30 (2004) 765–772.

[27] Y. Matsuo, H. Sasaki, J. Am. Ceram. Soc. 49 (1966) 229–230.
[28] Y. Xu, A. Zangvil, A. Kerber, J. Eur. Ceram. Soc. 17 (1997) 921–928.
[29] C.H. Hsueh, J. Am. Ceram. Soc. 71 (1988) C442–C444.
[30] J.D. Kuntz, G.D. Zhan, A.K. Mukherjee, MRS Bull. 1 (2004) 22–27.
[31] M. Hillert, Acta Metall. 36 (1988) 3177–3181.
[32] R.C. Pohanka, S.W. Freiman, B.A. Bender, J. Am. Ceram. Soc. 61 (1978) 72–75.
[33] H. Chen, H. Yang, X. Dong, Y. Wang, Phys. Stat. Sol. (a) 203 (2006) R61–R63.
[34] T. Yamamoto, K. Yamamoto, R. Tanaka, K. Okazaki, T. Ueyama, Jpn. J. Appl. Phys. 28 (1989) 63–66.
[35] T. Nagai, H.J. Hwang, M. Yasuoka, M. Sando, K. Niihara, Ceram. Trans. 85 (1997) 369–378.

Current Applied Physics 9 (2009) 802–806

Contents lists available at ScienceDirect

Current Applied Physics

journal homepage: www.elsevier.com/locate/cap

Effects of Zr/Ti ratio on dielectric and ferroelectric properties of $0.8Pb(Zr_xTi_{1-x})O_3$–$0.2Pb(Co_{1/3}Nb_{2/3})O_3$ ceramics

Anurak Prasatkhetragarn [a,*], Muangjai Unruan [a], Athipong Ngamjarurojana [a], Yongyut Laosiritaworn [a], Supon Ananta [a], Rattikorn Yimnirun [a], David P. Cann [b]

[a] Department of Physics, Faculty of Science, Chiang Mai University, 239 Huay Kaew Road, Chiang Mai 50200, Thailand
[b] Materials Science, School of Mechanical, Industrial and Manufacturing Engineering, Oregon State University, Corvallis, OR 97331, United States

ARTICLE INFO

Article history:
Received 9 July 2008
Accepted 23 July 2008
Available online 14 August 2008

PACS:
85.50.–n
77.22.–d
77.22.Ch
77.80.Bh

Keywords:
PZT–PCN
MPB
Zr/Ti ratio
Dielectric properties
Ferroelectric properties

ABSTRACT

The influences of Zr/Ti ratio on electrical properties of the $0.8Pb(Zr_xTi_{1-x})O_3$–$0.2Pb(Co_{1/3}Nb_{2/3})O_3$ ceramics prepared by a mixed-oxide method (with $x = 0.46$, 0.48, 0.50, 0.52, and 0.54) have been investigated in order to identify the morphotropic phase boundary composition in this system. With XRD analysis, the crystal structure of dense specimens appeared to change gradually from tetragonal to rhombohedral with increasing Zr content. The dielectric properties measurements showed a maximum dielectric constant at $x = 0.50$, while the transition temperature decreased with increasing Zr content in the system. Moreover, all ceramics showed diffused phase transition behaviors with a minimum diffusivity at $x = 0.50$. In addition, the Polarization–Electric field (P–E) hysteresis loops of the ceramic systems also changed significantly with the Zr content. Interestingly, the loop squareness parameter reached maximum around $x = 0.50$. Other ferroelectric hysteresis parameters showed noticeable change at $x = 0.50$. These results clearly showed the significance of Zr/Ti ratio in controlling the electrical properties of the PZT–PCN ceramic systems.

1. Introduction

Lead-based perovskite-type solid solutions consisting of relaxor and normal ferroelectrics have attracted great interest at the compositions close to the morphotropic phase boundary (MPB) because of their excellent dielectric, piezoelectric, and electrostrictive properties, which are useful in actuating and sensing applications [1]. Lead zirconate titanate, $Pb(Zr_xTi_{1-x})O_3$ or PZT ceramics have been investigated from both fundamental and applied viewpoints [1,2]. The MPB of PZT is located at a $PbTiO_3$:$PbZrO_3$ of 0.52:0.48 and separates the Ti-rich tetragonal phase from the Zr-rich rhombohedral phase [3]. Furthermore, the MPB composition has a high T_c of 390 °C, which allows piezoelectric devices to be operated at relatively high temperatures. Most commercial PZT ceramics are designed in the vicinity of the MPB with various doping methods in order to achieve high properties [2,4–7]. Recently, many piezoelectric ceramic materials have been developed from binary systems containing a combination of relaxor and normal ferroelectric materials [2] that yield high dielectric permittivities (e.g., $Pb(Zr_{1/2}Ti_{1/2})O_3$–$Pb(Ni_{1/3}Nb_{2/3})O_3$ (PZT–PNN) [4], and $Pb(Zr_{1/2}Ti_{1/2})O_3$–$Pb(Mg_{1/3}Nb_{2/3})O_3$ (PZT–PMN) [5]), excellent piezoelectric coefficients (e.g., $Pb(Zr_{1/2}Ti_{1/2})O_3$–$Pb(Zn_{1/3}Nb_{2/3})O_3$ (PZT–PZN) [6]), and high pyroelectric coefficients (e.g., $Pb(Ni_{1/3}Nb_{2/3})O_3$–$PbTiO_3$–$PbZrO_3$ (PNN–PT–PZ) [7]).

Lead cobalt niobate, $Pb(Co_{1/3}Nb_{2/3})O_3$ or PCN, which exhibits a perovskite structure and a Curie temperature of ≈−30 °C, is a relaxor ferroelectric material with a high dielectric constant [8,9]. On the basis of the above mentioned approach, solid solutions of PZT and PCN are expected to synergistically combine the properties of both the normal ferroelectric PZT and relaxor ferroelectric PCN, which could exhibit electrical properties that are better than those of the single-phase PZT and PCN [8–11]. Our previous investigation on $(1-x)$PZT–(x)PCN ceramic systems has already shown excellent electrical properties with the MPB at $x = 0.2$. Previously, the influences of Zr/Ti ratio on electrical properties have been extensively investigated in PZT [12–15], PZT–PZN [16], PZT–PMMN [17], and PZT–SiO_2 [18]. However, there have been no systematic studies on the relationship between Zr/Ti ratio, physical and electrical properties of ceramics within specific morphotropic phase boundary compositions of PZT and PCN.

* Corresponding author. Tel.: +66 53 941921x443; fax: +66 53 943445.
E-mail address: Prasatkhetragarn@yahoo.com (A. Prasatkhetragarn).

1567-1739/$ - see front matter © 2008 Elsevier B.V. All rights reserved.
doi:10.1016/j.cap.2008.07.019

Therefore, the overall purpose of this study is to determine the influence of Zr/Ti ratio on phase formation, microstructure, dielectric and ferroelectric properties of $0.8Pb(Zr_xTi_{1-x})O_3$–$0.2Pb(Co_{1/3}Nb_{2/3})O_3$ where $x = 0.46$, 0.48, 0.50, 0.52, and 0.54) ceramic systems.

2. Experimental procedure

The specimens studied were fabricated according to the formula: $0.8Pb(Zr_xTi_{1-x})O_3$–$0.2Pb(Co_{1/3}Nb_{2/3})O_3$, where $x = 0.46$, 0.48, 0.50, 0.52, and 0.54. Raw materials of PbO, ZrO_2, TiO_2, CoO, and Nb_2O_5 with >99% purity were used to prepare samples. The columbite $CoNb_2O_6$ precursor was weighed and introduced into the batch calculations. The $CoNb_2O_6$ powder was prepared at calcination temperature of 1100 °C for 2 h [8]. In the present work, the $0.8Pb(Zr_xTi_{1-x})O_3$–$0.2Pb(Co_{1/3}Nb_{2/3})O_3$ samples were prepared from PbO, ZrO_2, TiO_2, and $CoNb_2O_6$ powders using the solid-state reaction of these raw materials. The powders were mixed by a vibratory-milling technique in ethanol for 6 h. After drying, the product was calcined in an alumina crucible at a temperature of 950 °C [19]. The calcined powders were uniaxially cold-pressed at 5000 psi into disc-shaped pellets with a diameter of 12.7 mm and a thickness of 1 mm, with 3 wt% poly vinyl alcohol (PVA) added as a binder. Following binder burnout at 500 °C, the pellets were sintered at 1200 °C for 2 h at a heating/cooling rate of 5 °C/min [19].

The phase structure of the powders was analyzed via X-ray diffraction (XRD; Bruker-AXS D8). The microstructures of the sintered samples were examined using scanning electron microscopy (SEM; JEOL JSM-840A). The dielectric properties of the samples were measured using an automated measurement system. An Agilent 4284A LCR meter was used to measure the dielectric properties over a wide temperature range using a NorECS ProboStat high temperature measurement cell. The room temperature ferroelectric properties were examined using a simple Sawyer–Tower circuit at fixed measuring frequency of 50 Hz.

3. Results and discussion

Perovskite phase formation and crystal structure were determined by XRD at room temperature. The XRD patterns of $0.8Pb(Zr_xTi_{1-x})O_3$–$0.2Pb(Co_{1/3}Nb_{2/3})O_3$, where $x = 0.46$, 0.48, 0.50, 0.52 and 0.54 are correlated with JCPDS file number 70-4057, as shown in Fig. 1, showing a perovskite structure for all compositions. The pyrochlore phase is not observed in this system. In the XRD patterns, the crystal structure of the specimens appears to change gradually from tetragonal to rhombohedral with increasing Zr content, as presented in Fig. 1(a). There also appears an MPB between tetragonal and rhombohedral phases around Zr/Ti = 50/50. As shown in Fig. 1(b), XRD peak profiles of the (200) and (002) peaks at $x = 0.46$ and 0.48 indicate the tetragonal phase. At the $x = 0.50$ composition, (020) peak is observed, indicating the coexistence of the tetragonal and rhombohedral phases, as shown in Fig. 1(c). The (020) peak in compositions $x = 0.52$ and 0.54 has indicated that the crystal has transformed into rhombohedral phase. Previously, a similar behavior was also observed with increasing Zr content in PZT, PZT–PZN, PZT–PMMN, and PZT–SiO_2 based ceramics [13–18].

Effects of Zr/Ti ratio on the microstructure of the $0.8Pb(Zr_xTi_{1-x})O_3$–$0.2Pb(Co_{1/3}Nb_{2/3})O_3$ ceramics are displayed in Fig. 2. The grain size of the ceramics varies considerably from 1.00 to 11.31 μm, as listed in Table 1. However, the average grain size only slightly increases with increasing Zr content. Since the grain size of PZT-based materials strongly depends on the composition ratio, nucleation energy, and growth energy, the compositions with lower Zr content need higher growth energy. This trend is similar to those reported in the literature [14,20]. Since the microstructure of all compositions does not differ significantly, it should not play an important role in controlling electrical properties of this ceramic system.

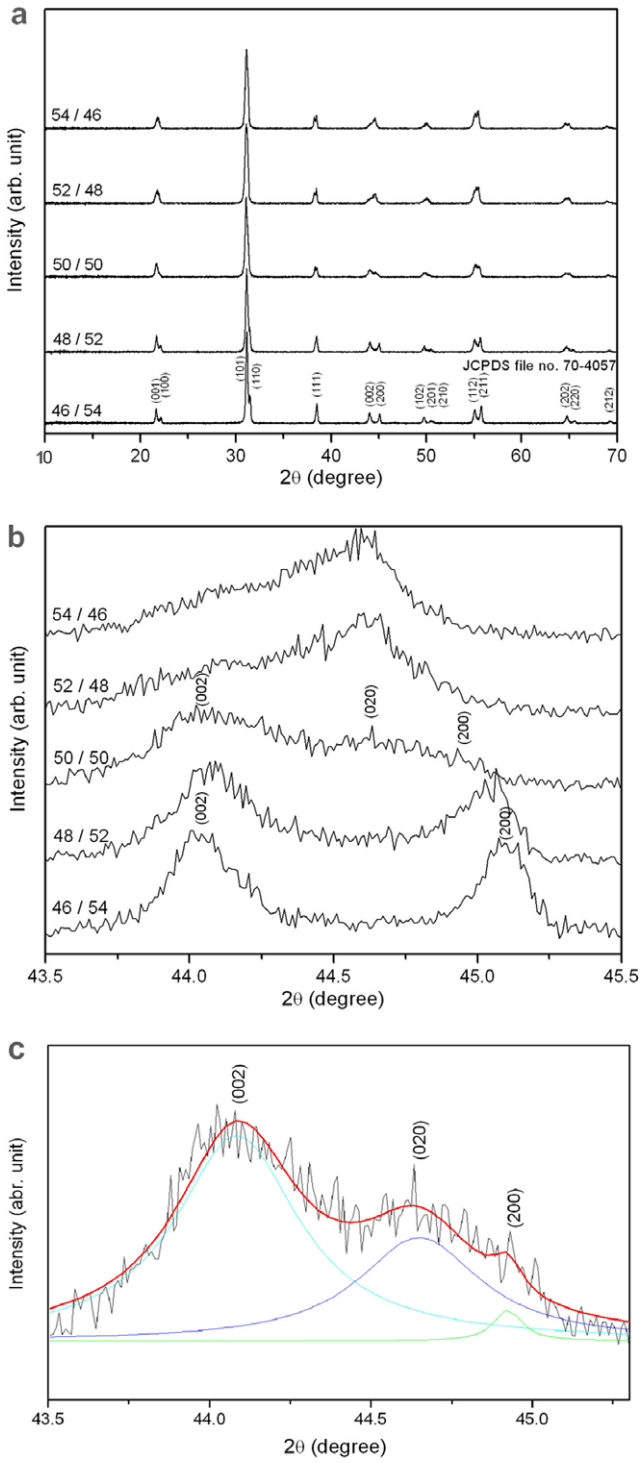

Fig. 1. XRD patterns of $0.8Pb(Zr_xTi_{1-x})O_3$–$0.2Pb(Co_{1/3}Nb_{2/3})O_3$ ceramics; (a) with $x = 0.46$, 0.48, 0.50, 0.52 and 0.54, (b) the (200) and (002) peaks profile at various Zr/Ti ratios and (c) coexistence of tetragonal/rhombohedral phases at $x = 0.50$ composition.

Temperature dependences of the dielectric constant (ε_r) and dielectric loss tangent ($\tan\delta$) of the $0.8Pb(Zr_xTi_{1-x})O_3$–$0.2Pb(Co_{1/3}Nb_{2/3})O_3$ ceramics are displayed in Fig. 3. At room temperature

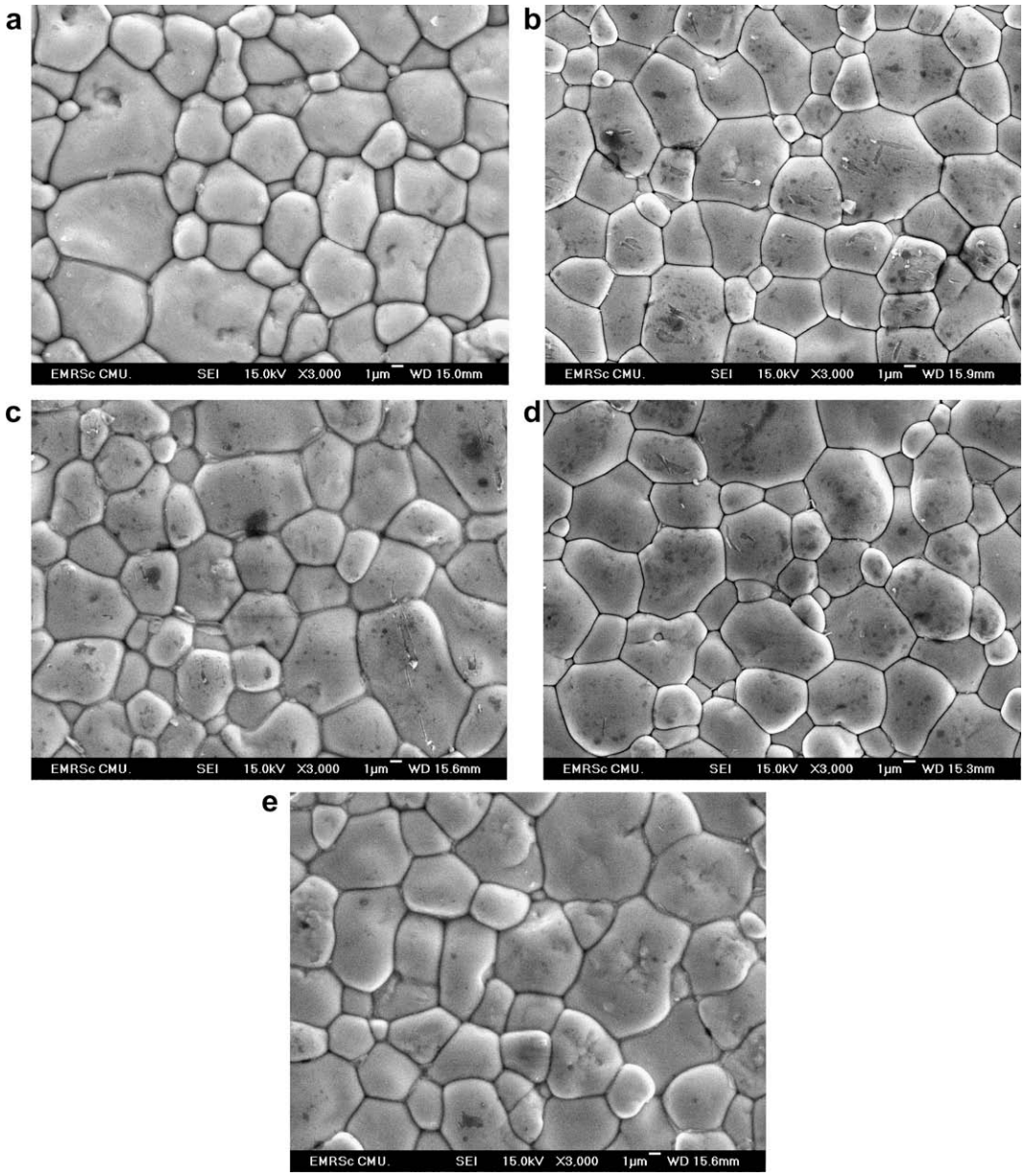

Fig. 2. SEM micrographs of $0.8Pb(Zr_xTi_{1-x})O_3$–$0.2Pb(Co_{1/3}Nb_{2/3})O_3$ with increasing Zr content: (a) $x = 0.46$, (b) $x = 0.48$, (c) $x = 0.50$, (d) $x = 0.52$, and (e) $x = 0.54$.

Table 1
Physical properties of $0.8Pb(Zr_xTi_{1-x})O_3$–$0.2Pb(Co_{1/3}Nb_{2/3})O_3$ ceramics

Zr/Ti ratio	Density (g/cm^3)	Grain size range (μm)	Average grain size (μm)
46/54	7.93 ± 0.05	1.21–10.99	4.34
48/52	7.94 ± 0.05	1.19–10.21	4.36
50/50	7.95 ± 0.05	1.41–11.12	4.54
52/48	7.91 ± 0.05	1.38–11.31	4.66
54/46	7.93 ± 0.05	1.00–9.20	4.72

(RT), with increasing Zr content, the dielectric constant and tan δ tend to increase because the transition temperature of the ceramics shifts towards RT; hence, the value of the dielectric properties measured at RT increases, as listed in Table 2. Many previous works on PZT–PZN, PZT–PNN, and PZT–PMN have reported a similar behavior [4–6]. The maximum dielectric constant (ε_{max}) at 1 kHz is also listed in Table 2. The ε_{max} increases at Zr = 0.46,

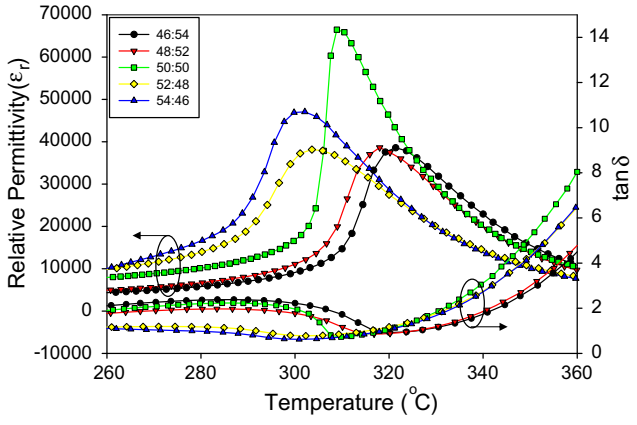

Fig. 3. Temperature dependences of dielectric properties of $0.8Pb(Zr_xTi_{1-x})O_3$–$0.2Pb(Co_{1/3}Nb_{2/3})O_3$ ceramics, where $x = 0.46$, 0.48, 0.50, 0.52, and 0.54.

Table 2
Dielectric properties of $0.8Pb(Zr_xTi_{1-x})O_3$–$0.2Pb(Co_{1/3}Nb_{2/3})O_3$ ceramics

Zr/Ti ratio	Dielectric properties (at 1 kHz)						
	T_{max}	ε_{RT}	$\tan\delta$	ε_{max}	$\tan\delta$	γ	δ
46/54	321	835	0.0437	38,580	0.9232	1.71	15.98
48/52	318	875	0.0467	38,630	0.8548	1.65	15.64
50/50	310	929	0.0484	66,590	0.7797	1.52	15.41
52/48	304	951	0.0547	38,150	0.7302	1.86	16.75
54/46	301	979	0.0657	47,200	0.6215	1.89	16.82

0.48 and 0.50 and then decreases at Zr = 0.52 and 0.54, whereas $\tan\delta$ tends to decrease with increasing Zr content, clearly indicating the maximum dielectric constant at MPB composition of Zr/Ti = 50/50. In addition, a clear transition in T_{max} (defined as the temperature at which ε_r is maximum at 1 kHz) is observed. It is noticed that an increase in Zr mole fraction leads to a decrease in T_{max}, most likely due to crystal structure of the materials was changed from tetragonal to rhombohedral, as shown in XRD patterns in Fig. 1. This result suggests that the transition temperature of 0.8PZT–0.2PCN system can be varied over a range from 301 to 321 °C by controlling the Zr/Ti ratio in the system. Similar behavior is also reported in previous works [13–18].

To further understand the dielectric behavior of the PZT–PCN system, the permittivity of a first-order normal ferroelectric can be described by the Curie–Weiss law and a second-order relaxor ferroelectric can be described by a simple quadratic law [21]. This arises from the fact that the total number of relaxor contributing to the permittivity response in the vicinity of the permittivity peak is temperature dependent, and the temperature distribution of this number is given by a Gaussian function about a mean value T_0 with a standard deviation δ. The relative permittivity can be derived via using the following equation:

$$\frac{\varepsilon_m}{\varepsilon(f,T)} = 1 + \frac{(T - T_m(f))^\gamma}{2\delta^2} \quad (1)$$

where ε_m is the maximum value of the permittivity at $T = T_m(f)$. The value of γ is the expression of the degree of dielectric relaxation, while δ is used to measure the degree of diffuseness of the phase transition. In a material with a "pure" diffuse phase transition, γ is expected to be 2 [10]. As listed in Table 2, the values of γ vary with Zr/Ti ratio between 1.52 and 1.89, which confirms that diffuse phase transition occurs in the PZT–PCN system. It is important to note that in perovskite ferroelectrics it has been established that γ and δ can be affected by Zr/Ti ratio and structure of the materials. The values of γ and δ decrease with increasing Zr from 0.46 to 0.50 mol%, and then increase when Zr content increases further, as tabulated in Table 2. It is interesting to observe that the phase transition is least diffused at MPB, possibly due to a sharp increase of dielectric permittivity at MPB. A similar behavior has also been observed in PZT–PZN systems [16].

The Polarization–Electric field (P–E) hysteresis loops of $0.8Pb(Zr_xTi_{1-x})O_3$–$0.2Pb(Co_{1/3}Nb_{2/3})O_3$ ceramics measured at 15 kV/cm are presented in Fig. 4. To assess effect of Zr/Ti ratio on

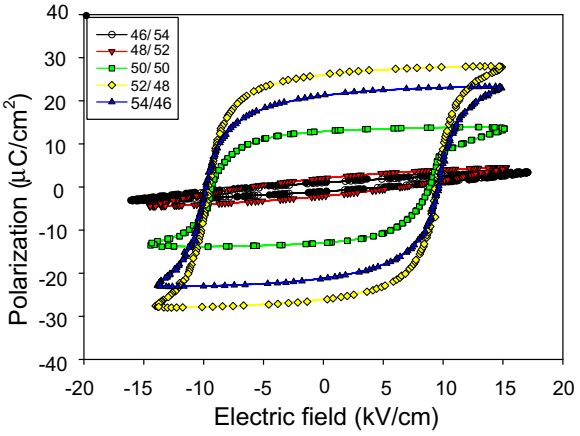

Fig. 4. P–E loops of $0.8Pb(Zr_xTi_{1-x})O_3$–$0.2Pb(Co_{1/3}Nb_{2/3})O_3$ ceramics, where $x = 0.46$, 0.48, 0.50, 0.52, and 0.54.

ferroelectric characteristics of 0.8PZT–0.2PCN ceramics, the ferroelectric parameters have been extracted from the experimental data, as summarized in Table 3. The remnant polarization (P_r) and coercive field (E_c) increase with increasing Zr content. However, the decrease in the remnant polarization at $x = 0.54$ could be caused by Zr-rich rhombohedral phase in this composition [22]. The ferroelectric parameters have been normalized in forms of P_r/P_{max} and E_c/E_{max} values, where P_{max} is the polarization value at the maximum applied field (E_{max}). These normalized values are also listed in Table 3. It can be seen that P_r/P_{max} increases with increasing Zr content and reaches the maximum values at Zr/Ti = 50/50 composition and then decreases, while E_c/E_{max} increases with increasing Zr content. Furthermore, the ferroelectric characteristics can be assessed with the hysteresis loop squareness (R_{sq}) [19], which can be calculated from the empirical expression $R_{sq} = (P_r/P_s) + (P_{1.1E_c}/P_s)$, where P_s is the saturated polarization obtained at some finite field strength below the dielectric breakdown and $P_{1.1E_c}$ is the polarization at the field equal to $1.1E_c$. For the ideal square loop, R_{sq} is equal to 2.00 [23]. As listed in Table 3, the loop squareness parameter R_{sq} increases from 0.90 in Zr/Ti = 54/46 to reach the maximum value of 1.49 in Zr/Ti = 50/50 and then decrease to 1.45 in Zr/Ti = 46/54. As is well known, the values of the dielectric and ferroelectric properties of a solid solution with MPB usually maximize approximately at the MPB composition. It is seen that the highest R_{sq} at Zr/Ti of 50/50 indicates the MPB of this system. This behavior has also been found in previous investigation [14]. This observation could be due to easy polarization rotation in the MPB region with coexistence of the tetragonal and rhombohedral phase [14]. Fig. 5 summarizes the dielectric and ferroelectric properties of $0.8Pb(Zr_xTi_{1-x})O_3$–$0.2Pb(Co_{1/3}Nb_{2/3})O_3$ with various Zr/Ti ratios. Clearly, substantial changes of the electrical properties are observed at Zr/Ti ratio of 50/50, which confirm the MPB of this ceramic system at Zr/Ti = 50/50. An anomaly of electrical properties at the MPB has also been observed in solid solutions of PZT–PNN, PZT–PZN, and PZT–PMN [4–7,24].

Table 3
Ferroelectric properties of $0.8Pb(Zr_xTi_{1-x})O_3$–$0.2Pb(Co_{1/3}Nb_{2/3})O_3$ ceramics

Zr/Ti ratio	Ferroelectric properties					
	P_r (μC/cm²)	P_s (μC/cm²)	E_c (kV/cm)	P_r/P_{max}	E_c/E_{max}	Loop squareness (R_{sq})
46/54	1.00	1.25	5.23	0.33	0.35	0.90
48/52	2.09	2.48	6.78	0.46	0.45	1.00
50/50	12.91	13.71	8.89	0.93	0.60	1.49
52/48	26.16	27.75	9.50	0.93	0.65	1.47
54/46	21.34	22.91	9.65	0.92	0.66	1.45

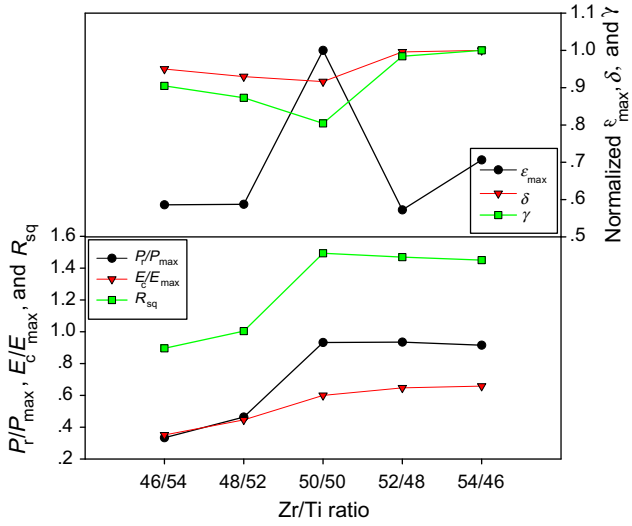

Fig. 5. Relationship of dielectric and ferroelectric parameter P_r/P_{max}, E_c/E_{max}, R_{sq}, and normalized ε_{max}, δ, and γ with various Zr/Ti ratio.

4. Conclusions

In this study, ceramics in the $0.8Pb(Zr_xTi_{1-x})O_3$–$0.2Pb(Co_{1/3}Nb_{2/3})O_3$ system, $x = 0.46$, 0.48, 0.50, 0.52, and 0.54, are successfully prepared by a solid-state mixed-oxide technique. The XRD analysis indicates that the tetragonal and rhombohedral phases coexist around Zr/Ti = 50/50. The surface micrographs show that average grain size slightly increases with increasing Zr content. At 1 kHz, the maximum dielectric constant (ε_{max}) of 65,600 is observed at Zr/Ti = 50/50. However, the diffusivity (γ) and diffuseness parameter (δ) reach minimum at Zr/Ti = 50/50. Moreover, the ferroelectric parameters; remnant polarization (P_r) and coercive field (E_c), increase with increasing Zr content, while the highest loop squareness (R_{sq}) of 1.49 is observed at the MPB composition. Most importantly, a combination of XRD analysis, dielectric and ferroelectric measurements shows that the MPB between the tetragonal and rhombohedral phases exists around Zr/Ti ratio of 50/50. Finally, this study shows that the Zr/Ti ratio could be used to tailor electrical properties in PZT–PCN ceramics.

Acknowledgments

The authors wish to express profound gratitude to Materials Science Groups, Oregon State University for ceramics preparation and measurement. This work was supported by the Commission on Higher Education (CHE), the Thailand Research Fund (TRF), the Faculty of Science, the Graduate School of Chiang Mai University, and Naresuan University Phayao.

References

[1] A.J. Moulson, J.M. Herbert, Electroceramics: Materials, Properties, Applications, Wiley, Chichester, UK, 2003.
[2] L.E. Cross, Mater. Chem. Phys. 43 (1996) 108.
[3] S.-E. Park, T.R. Shrout, IEEE Trans. Ultrason. Ferroelectron. Freq. Control 44 (1997) 1140.
[4] N. Vittayakorn, G. Rujijanagul, X. Tan, M.A. Marquardt, D.P. Cann, J. Appl. Phys. 96 (2004) 5103.
[5] R. Yimnirun, S. Ananta, P. Laoratanakul, J. Eur. Ceram. Soc. 25 (2005) 3235.
[6] H. Fan, G.T. Park, J.J. Choi, J. Ryu, H.E. Kim, J. Mater. Res. 17 (2002) 180.
[7] D. Luff, R. Lane, K.R. Brown, H.J. Marshallsay, Trans. J. Br. Ceram. Soc. 73 (1974) 251.
[8] M. Unruan, N. Vittayakorn, R. Wongmaneeruang, A. Prasatkhetragarn, S. Ananta, R. Yimnirun, J. Alloy Compd. (in press).
[9] T. Hachiga, S. Fujimoto, N. Yasuda, J. Phys. D 20 (1987) 1291.
[10] T. Kudo, T. Yazaki, F. Naito, S. Sugaya, J. Am. Ceram. Soc. 53 (1970) 326.
[11] Z. Brankovic, G. Brankovic, J.A. Varela, J. Mater. Sci. 14 (2003) 37.
[12] R. Guo, L.E. Cross, S.-E. Park, B. Noheda, D.E. Cox, G. Shirane, Phys. Rev. Lett. 84 (2000) 5423.
[13] Y.H. Lee, J.K. Lee, K.S. Hong, J. Korean Phys. Soc. 42 (2003) 1395.
[14] P. Khaenamkaew, S. Muensit, I.K. Bdikin, A.L. Kholkin, Mater. Chem. Phys. 102 (2007) 159.
[15] Z.J. Wang, Y. Aoki, L.J. Yan, H. Kokawa, R. Maeda, J. Crystal Growth 267 (2004) 92.
[16] S.H. Lee, C.B. Yoon, S.M. Lee, H.E. Kim, J. Eur. Ceram. Soc. 26 (2006) 111.
[17] H. Chen, J. Long, Z. Meng, Mater. Sci. Eng. B 99 (2003) 433.
[18] X. Wang, X. Yao, H. Ishiwara, Mater. Sci. Eng. B 137 (2007) 278.
[19] A. Prasatkhetragarn, N. Vittayakorn, S. Ananta, R. Yimnirun, D.P. Cann, Jpn. J. Appl. Phys. 47 (2008) 998.
[20] Q. Zhang, R.W. Whatmore, J. Phys. D: Appl. Phys. 34 (2001) 2296.
[21] A.A. Bokov, Z.G. Ye, Solid State Commun. 116 (2000) 105.
[22] B. Jaffe, W.R. Cook Jr., H. Jaffe, Piezoelectric Ceramics, Academic Press, London, UK, 1971.
[23] G.H. Haertling, W.J. Zimmer, Am. Ceram. Soc. Bull. 45 (1966) 1084.
[24] N. Vittayakorn, G. Rujijanagul, T. Tankasiri, X. Tan, D.P. Cann, Mater. Sci. Eng. B 108 (2004) 258.

J Mater Sci (2009) 44:1868–1872
DOI 10.1007/s10853-008-3235-4

The morphotropic phase boundary and electrical properties of $(1 - x)Pb(Zn_{1/2}W_{1/2})O_3$–$xPb(Zr_{0.5}Ti_{0.5})O_3$ ceramics

O. Khamman · X. Tan · S. Ananta · R. Yimnirun

Received: 20 November 2008 / Accepted: 29 December 2008 / Published online: 3 February 2009

Abstract Ceramics in the solid solution of $(1 - x)Pb(Zn_{1/2}W_{1/2})O_3$–$xPb(Zr_{0.5}Ti_{0.5})O_3$ system, with $x = 0.80$, 0.85, 0.90, and 0.95, were synthesized with the solid-state reaction technique. The perovskite phase formation in the sintered ceramics was analyzed with X-ray diffraction. It shows that the rhombohedral and the tetragonal phases coexist in the ceramic with $x = 0.90$, indicating the morphotropic phase boundary (MPB) within this pseudo-binary system. Dielectric and ferroelectric properties measurements indicate that the transition temperature decreases while the remanent polarization increases with the addition of $Pb(Zn_{1/2}W_{1/2})O_3$. In the composition of $x = 0.85$ which is close to the MPB in the rhombohedral side, a high piezoelectric property with $d_{33} = 222$ pC/N was observed.

Introduction

Lead-containing perovskite ferroelectrics are of great importance to engineering technologies due to their unique dielectric and piezoelectric properties [1]. Lead zirconate titanate, $Pb(Zr_{1-y}Ti_y)O_3$, is the most studied system for piezoelectric applications in transducers and actuators [1–4]. The best piezoelectric properties are found in compositions close to the morphotropic phase boundary (MPB), roughly $Pb(Zr_{0.5}Ti_{0.5})O_3$ [1]. To further enhance their piezoelectric properties, other complex compounds have been incorporated into the $Pb(Zr_{0.5}Ti_{0.5})O_3$, such as $Pb(Ni_{1/3}Nb_{2/3})_3$ [5], $Pb(Zn_{1/3}Nb_{2/3})O_3$ [6], $Pb(Mg_{1/3}Nb_{2/3})O_3$ [7], and $Pb(Mg_{1/2}W_{1/2})O_3$ [8].

Lead zinc tungstate, $Pb(Zn_{1/2}W_{1/2})O_3$, is a complex perovskite compound with Zn^{2+} and W^{6+} ordered on the B-site of the ABO_3 perovskite lattice [9]. When cooling through the Curie temperature of 130 °C, it transforms from the cubic to a tetragonal structure. However, whether the tetragonal phase is ferroelectric or antiferroelectric is still unknown [9]. It should be noted that perovskite $Pb(Zn_{1/2}W_{1/2})O_3$ can only be synthesized under high pressure [10]. The conventional solid-state reaction method invariably leads to the mixture of Pb_2WO_5 and ZnO [11]. To the authors' knowledge, the complex perovskite $Pb(Zn_{1/2}W_{1/2})O_3$ has not been reported in literature to be incorporated into $Pb(Zr_{1-y}Ti_y)O_3$ for solid solutions. In addition to identifying the MPB and investigating the dielectric, piezoelectric, and ferroelectric properties in the $(1 - x)Pb(Zn_{1/2}W_{1/2})O_3$–$xPb(Zr_{0.5}Ti_{0.5})O_3$ solid solution system, the present study aims to determine the solubility limit of $Pb(Zn_{1/2}W_{1/2})O_3$ in $Pb(Zr_{0.5}Ti_{0.5})O_3$ and to explore if long range cation order can be developed in $Pb(Zr_{0.5}Ti_{0.5})O_3$-based solid solutions [8].

Experimental

Ceramics in the $(1 - x)Pb(Zn_{1/2}W_{1/2})O_3$–$xPb(Zr_{0.5}Ti_{0.5})O_3$ pseudo-binary system with $x = 0.80$, 0.85, 0.90, and 0.95 were prepared with a two-step reaction method. First, powders of $ZnWO_4$ and $ZrTiO_4$ were synthesized. The $ZnWO_4$ precursor was formed by reacting ZnO (99.9%) with WO_3 (99.9%) at 1000 °C for 4 h while the $ZrTiO_4$ precursor was formed by reacting ZrO_2 (99%) with TiO_2

O. Khamman · S. Ananta · R. Yimnirun
Department of Physics, Faculty of Science, Chiang Mai University, Chiang Mai 50200, Thailand

X. Tan (✉)
Department of Materials Science and Engineering, Iowa State University, Ames, IA 50011, USA
e-mail: xtan@iastate.edu

(99.9%) at 1400 °C for 4 h. Appropriate amount of $ZnWO_4$ and $ZrTiO_4$ were then mixed with PbO (99.9%, with 2 mol% excess) and milled, dried, and calcined at 900 °C for 4 h. The green compact of ceramics was formed by uniaxially pressing powders containing 2 wt% polyvinyl alcohol binder. Sintering was carried out at temperatures between 1100 and 1175 °C. To prevent PbO loss from the pellets, a PbO atmosphere was provided with a bed of $PbZrO_3$ powder placed in the vicinity of the pellets.

The density of the ceramics was measured by the Archimedes method, and the grain size was examined by scanning electron microscopy (SEM). The X-ray diffraction was used to verify the phase purity and determine the crystal structure. The ceramic pellets were polished and then electroded with gold for dielectric measurements. The samples were heated from room temperature at 2 °C/min for the measurement. For the piezoelectric measurement, samples were poled under 30 kV/cm for 10 min at 120 °C. The piezoelectric coefficient d_{33} was measured using a d_{33} meter 24 h after poling. The polarization hysteresis measurement was carried out with a standardized ferroelectric test system at room temperature with a frequency of about 4 Hz.

Results and discussion

The measured density of the sintered ceramic pellets in the pseudo-binary system $(1-x)Pb(Zn_{1/2}W_{1/2})O_3$–$xPb(Zr_{0.5}Ti_{0.5})O_3$ is listed in Table 1. The relative density for all the pellets was found to be above 90%. The addition of $Pb(Zn_{1/2}W_{1/2})O_3$ seems to enhance the sinterability of the solid solution ceramics. SEM micrographs of the fracture surfaces of the ceramic pellets are shown in Fig. 1. It can be seen that grains are uniform with clear grain boundaries. The average grain size determined from these micrographs is also listed in Table 1. Obviously, incorporating up to 10 mol% of $Pb(Zn_{1/2}W_{1/2})O_3$ into $Pb(Zr_{0.5}Ti_{0.5})O_3$ significantly increases the grain size. However, beyond 10 mol%, it appears to show the opposite effect.

X-ray diffraction patterns of the $(1-x)Pb(Zn_{1/2}W_{1/2})O_3$–$xPb(Zr_{0.5}Ti_{0.5})O_3$ solid solution ceramics are presented in Fig. 2. Within the detection limit of the diffractometer, sintered ceramics are phase pure with the perovskite structure with x down to 0.80. Further increase in $Pb(Zn_{1/2}W_{1/2})O_3$ content invariably leads to the formation of second phases. Therefore, the solubility limit of $Pb(Zn_{1/2}W_{1/2})O_3$ in $Pb(Zr_{0.5}Ti_{0.5})O_3$ is 20 mol%. Furthermore, the X-ray diffraction data in the range of 15–20° for 2θ (not shown in Fig. 2) did not display any diffraction intensity peak, suggesting the absence of long range cation order in these sintered ceramics [8].

Table 1 Characteristics of the sintered $(1-x)Pb(Zn_{1/2}W_{1/2})O_3$–$xPb(Zr_{0.5}Ti_{0.5})O_3$ ceramics

x	Relative density (%)	Grain size (μm)
0.80	95	11.5
0.85	92	28.5
0.90	91	41.8
0.95	90	20.8

Close examination indicates significant changes in the pseudo-cubic $(200)_c$ peak when composition varies, as marked with the dashed box in Fig. 2. For the composition of $x = 0.95$, the X-ray diffraction pattern shows an obvious $(200)_c$ peak splitting which is indicative of the tetragonal symmetry of the perovskite structure. As the $Pb(Zn_{1/2}W_{1/2})O_3$ content increases in the solid solution, the $(200)_c$ peak transforms to a single peak which suggests a rhombohedral distortion of the perovskite structure. The results show that a morphotropic phase boundary (MPB), separating the rhombohedral from the tetragonal phase, exists at $x = 0.90$ in the pseudo-binary $(1-x)Pb(Zn_{1/2}W_{1/2})O_3$–$xPb(Zr_{0.5}Ti_{0.5})O_3$ solid solution system. It is interesting to notice that the phase evolution sequence in the present $Pb(Zn_{1/2}W_{1/2})O_3$–$Pb(Zr_{0.5}Ti_{0.5})O_3$ system is very similar to that in the $Pb(Ni_{1/3}Nb_{2/3})O_3$–$Pb(Zr_{0.5}Ti_{0.5})O_3$ [5] and the $Pb(Zn_{1/3}Nb_{2/3})O_3$–$Pb(Zr_{0.5}Ti_{0.5})O_3$ systems [6].

The temperature dependence of dielectric constant ε_r and loss tangent tan δ measured at 1 kHz for the ceramics are plotted in Fig. 3. It is shown that with increasing $Pb(Zn_{1/2}W_{1/2})O_3$ content in the $(1-x)Pb(Zn_{1/2}W_{1/2})O_3$–$xPb(Zr_{0.5}Ti_{0.5})O_3$ solid solution, the paraelectric–ferroelectric transition temperature T_m decreases continuously. Overall, all the ceramics show very high dielectric permittivity. The dielectric constant at T_m, denoted as ε_m hereafter, shows the highest value of 38410 in the composition of $x = 0.90$. This composition, as revealed by the X-ray diffraction patterns shown in Fig. 2, is the MPB composition. Therefore, the results from the dielectric measurement are in support of the x-ray diffraction data. The values of T_m and ε_m for the ceramic series are listed in Table 2 for clarity.

It is also noticed from Fig. 3 that the paraelectric–ferroelectric transition peak becomes broadened slightly with increasing $Pb(Zn_{1/2}W_{1/2})O_3$ content. In addition, a new dielectric anomaly emerges around 260 °C in the composition of $x = 0.80$. Detailed comparison of the dielectric constant under different measuring frequencies between compositions of $x = 0.80$ and 0.95 is shown in Fig. 4. A weak frequency dependence is seen in the dielectric constant.

The broadened dielectric peak suggests that the dielectric constant ε_r at temperatures above T_m should follow a general expression [5, 12]:

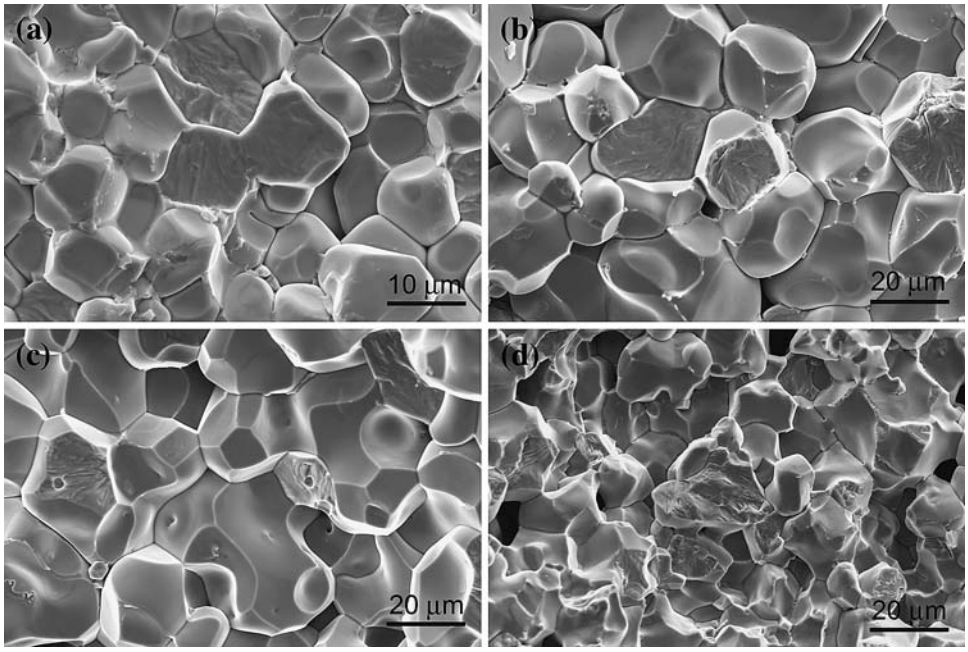

Fig. 1 SEM micrographs revealing the fracture surfaces of $(1 - x)Pb(Zn_{1/2}W_{1/2})O_3$–$xPb(Zr_{0.5}Ti_{0.5})O_3$ ceramics. **a** $x = 0.80$, **b** $x = 0.85$, **c** $x = 0.90$, **d** $x = 0.95$

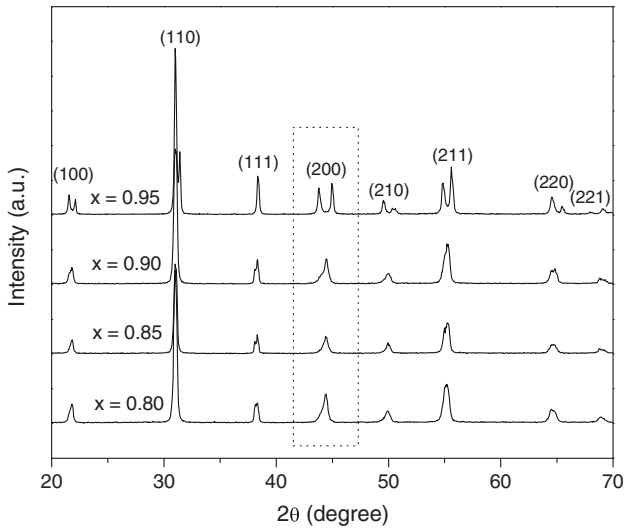

Fig. 2 X-ray diffraction spectra for the sintered $(1 - x)Pb(Zn_{1/2}W_{1/2})O_3$–$xPb(Zr_{0.5}Ti_{0.5})O_3$ ceramics. The intensity peaks are index with the pseudo-cubic perovskite structure. The $(200)_c$ peak in the dashed box reveals the change of distortion

$$\frac{\varepsilon_m}{\varepsilon_r} = 1 + \frac{[T - T_m]^\gamma}{2\delta^2} \quad (1)$$

where γ is a parameter indicating the degree of dielectric relaxation while the parameter δ can be used to evaluate the degree of the diffuseness of the phase transition. When $\gamma = 1$, Eq. 1 becomes the Curie–Weiss law, while for $\gamma = 2$ this equation becomes the quadratic relationship describing the classic relaxor ferroelectric $Pb(Mg_{1/3}Nb_{2/3})O_3$ [13]. According to Eq. 1, the values of ln $[(\varepsilon_m/\varepsilon_r) - 1]$ are plotted against ln $(T - T_m)$ in Fig. 5 for all the sintered

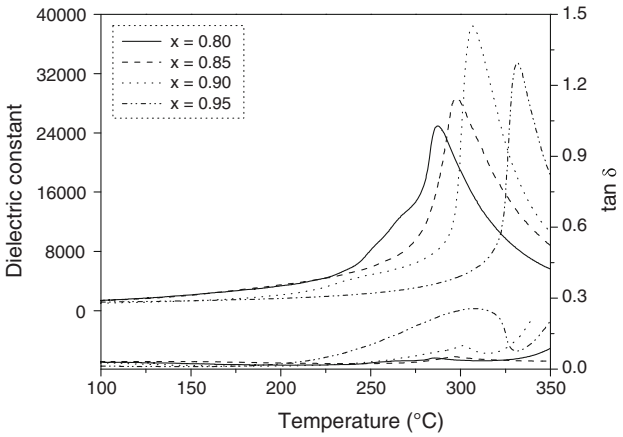

Fig. 3 Dielectric constant ε_r and loss tangent tan δ as a function of temperature measured at 1 kHz during heating in the $(1 - x)Pb(Zn_{1/2}W_{1/2})O_3$–$xPb(Zr_{0.5}Ti_{0.5})O_3$ ceramics

Table 2 Dielectric and piezoelectric properties of the $(1 - x)Pb(Zn_{1/2}W_{1/2})O_3$–$xPb(Zr_{0.5}Ti_{0.5})O_3$ ceramics

x	ε_m	T_m (°C)	γ	δ	d_{33} (pC/N)
0.80	24930	287	1.55	8.07	142
0.85	28730	297	1.55	7.50	222
0.90	38410	306	1.53	7.39	188
0.95	33480	331	1.43	6.13	136

ceramics, using the data obtained at 1 kHz. Remarkably good linearity within the measurement temperature range above T_m is evident. Using the intercept and the slope of the fitted lines in Fig. 5, γ and δ for each composition are determined and listed in Table 2. It is found that with

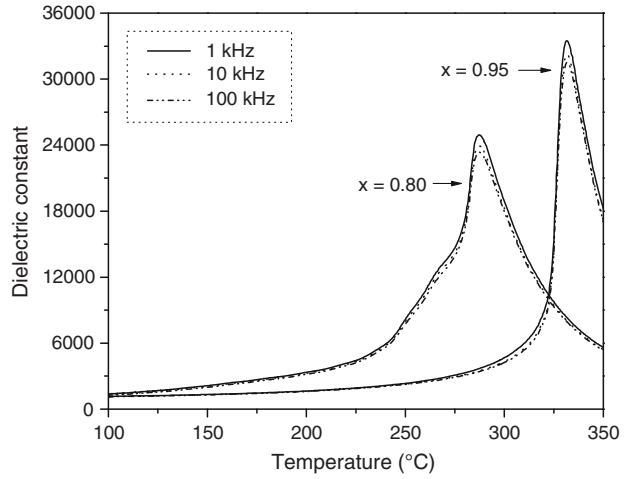

Fig. 4 Dielectric constant ε_r as a function of temperature measured at 1, 10, and 100 kHz during heating in the $0.20Pb(Zn_{1/2}W_{1/2})O_3{-}0.80Pb(Zr_{0.5}Ti_{0.5})O_3$ and the $0.05Pb(Zn_{1/2}W_{1/2})O_3{-}0.95Pb(Zr_{0.5}Ti_{0.5})O_3$ ceramics

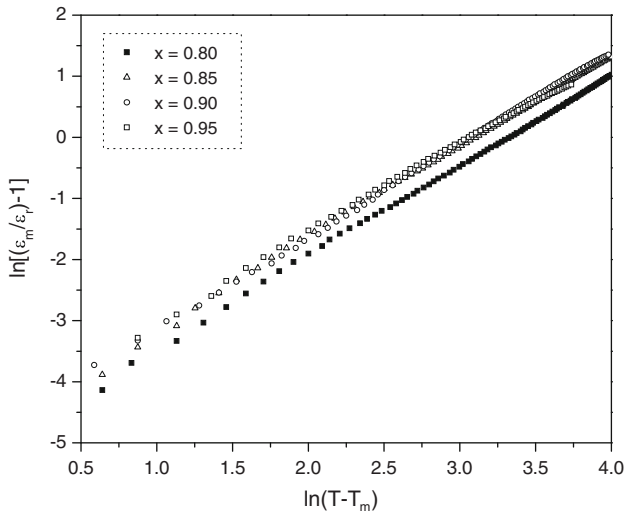

Fig. 5 The ln $[(\varepsilon_m/\varepsilon_r) - 1]$ vs. ln $(T - T_m)$ plot for the $(1 - x)Pb(Zn_{1/2}W_{1/2})O_3$–$xPb(Zr_{0.5}Ti_{0.5})O_3$ ceramics

increasing amount of $Pb(Zn_{1/2}W_{1/2})O_3$ in the $(1 - x)Pb(Zn_{1/2}W_{1/2})O_3$–$xPb(Zr_{0.5}Ti_{0.5})O_3$ solid solution, both the relaxation parameter γ and the diffuseness parameter δ increases. This is indicative of an increasing degree of disorder of the electrical dipole moments in the solid solution ceramics.

The piezoelectric property of the poled ceramics was measured at room temperature with a quasi-static d_{33} meter and is also listed in Table 2. The highest d_{33} value (222 pC/N) is found in the ceramic of $0.15Pb(Zn_{1/2}W_{1/2})O_3$–$0.85Pb(Zr_{0.5}Ti_{0.5})O_3$, a composition close to the MPB in the rhombohedral side. Optimizing processing conditions is expected to further increase the piezoelectric property.

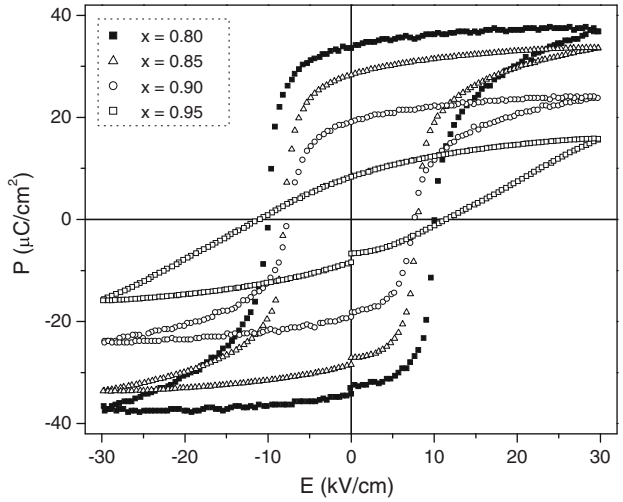

Fig. 6 Polarization versus electric field hysteresis loops measured at room temperature at 4 Hz in the $(1 - x)Pb(Zn_{1/2}W_{1/2})O_3$–$xPb(Zr_{0.5}Ti_{0.5})O_3$ ceramics

Finally, the ferroelectric properties of the sintered ceramics were evaluated with the electrical polarization versus field hysteresis loop measurements. As shown in Fig. 6, all samples exhibit a profound hysteretic behavior. In the ceramic of $0.05Pb(Zn_{1/2}W_{1/2})O_3$–$0.95Pb(Zr_{0.5}Ti_{0.5})O_3$, a non-saturated hysteresis loop is observed at a peak electric field of 30 kV/cm. However, saturated loops are seen in ceramics with a higher content of $Pb(Zn_{1/2}W_{1/2})O_3$. In addition, the remanent polarization P_r is observed to increase dramatically with increasing $Pb(Zn_{1/2}W_{1/2})O_3$ content. In the ceramic with composition of $x = 0.80$, P_r reached 33.6 μC/cm^2. The shape of the ferroelectric hysteresis loop can be quantitatively assessed with the so-called squareness parameter R_{sq}, defined previously in literature [14]:

$$R_{sq} = \left(\frac{P_r}{P_s}\right) + \left(\frac{P_{1.1E_c}}{P_r}\right) \quad (2)$$

where P_s is the saturation polarization, E_c is the coercive field, $P_{1.1E_c}$ is the polarization at the field of $1.1E_c$. For a perfect square loop, R_{sq} is equal to 2.00. With the data presented in Fig. 6, the loop squareness parameter R_{sq} is calculated. The result is listed in Table 3, together with the remanent polarization P_r and the coercive field E_c. Incorporating $Pb(Zn_{1/2}W_{1/2})O_3$ obviously enhances the ferroelectric properties significantly.

Conclusions

Phase pure perovskite ceramics in the $(1 - x)Pb(Zn_{1/2}W_{1/2})O_3$–$xPb(Zr_{0.5}Ti_{0.5})O_3$ system can be prepared with the solid-state reaction method with up to 20 mol% of

Table 3 Ferroelectric properties of the $(1 - x)Pb(Zn_{1/2}W_{1/2})O_3$–$xPb(Zr_{0.5}Ti_{0.5})O_3$ ceramics

x	P_r (μC/cm^2)	E_c (kV/cm)	R_{sq}
0.80	33.6	10.1	1.24
0.85	28.4	8.2	1.36
0.90	19.2	7.8	1.20
0.95	8.4	11.4	0.66

$Pb(Zn_{1/2}W_{1/2})O_3$. In the composition range for a stable perovskite structure, the MPB composition is identified at $x = 0.90$. This MPB separates the tetragonal phase from the rhombohedral phase. At the MPB composition, a remarkably high dielectric constant ε_m of 38410 is observed at the ferroelectric transition temperature T_m. In the ceramic of $0.15Pb(Zn_{1/2}W_{1/2})O_3$–$0.85Pb(Zr_{0.5}Ti_{0.5})O_3$, a composition in the rhombohedral side of MPB, the best piezoelectric property ($d_{33} = 222$ pC/N) is detected. Furthermore, the addition of $Pb(Zn_{1/2}W_{1/2})O_3$ in $Pb(Zr_{0.5}Ti_{0.5})O_3$ dramatically enhances the ferroelectric properties, manifested by the large increase in the remanent polarization and the hysteresis loop squareness parameter. Therefore, the $(1 - x)Pb(Zn_{1/2}W_{1/2})O_3$–$xPb(Zr_{0.5}Ti_{0.5})O_3$ solid solution offers a new material system for various device applications.

Acknowledgements This work was supported by the National Science Foundation through the CAREER grant DMR-0346819 and the Thailand Research Fund (TRF), the Commission on Higher Education (CHE), and the Faculty of Science, Chiang Mai University, Thailand.

References

1. Jaffe B, Cook WR, Jaffe H (1971) Piezoelectric ceramics. Academic Press, London
2. Haertling GH (1999) J Am Ceram Soc 82:797
3. Cross LE (1996) Mater Chem Phys 43:108
4. Uchino K (2000) Ferroelectric devices. Marcel Dekker, Inc, New York
5. Vittayakorn N, Rujijanagul G, Tan X, Marquardt MA, Cann DP (2004) J Appl Phys 96:5103
6. Vittayakorn N, Rujijanagul G, Tan X, He H, Marquardt MA, Cann DP (2006) J Electroceram 16:141
7. Yimnirun R, Ananta S, Laoratanakul P (2005) J Eur Ceram Soc 25:3235
8. White D, Zhao X, Besser MF, Tan X (2008) J Mater Sci 43:5258. doi:10.1007/s10853-008-2772-1
9. Okai B, Yoshimoto J, Fujita T (1974) J Phys Soc Jpn 37:281
10. Fujita T, Fukunaga O, Nakagawa T, Nomura S (1970) Mater Res Bull 5:759
11. Lee WJ, Kim NK (2008) J Mater Sci 43:3608. doi:10.1007/s10853-008-2574-5
12. Uchino K, Nomura S (1982) Ferroelectr Lett 44:55
13. Smolenskii GA (1970) J Phys Soc Jpn 28(Suppl):26
14. Jin B, Kim J, Kim SC (1997) Appl Phys A 65:53

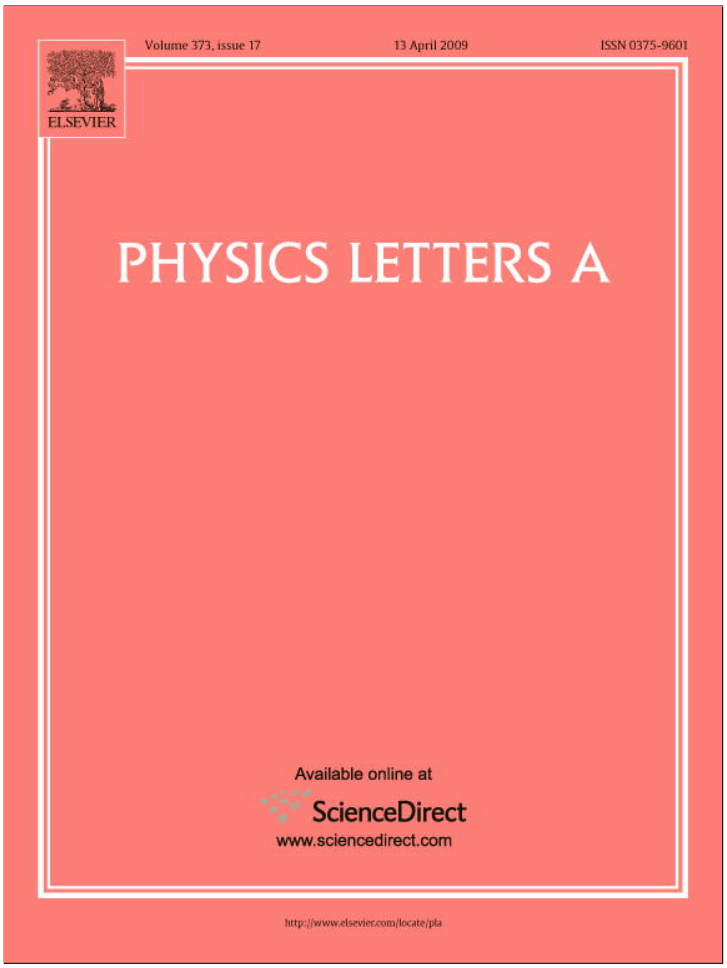

Physics Letters A 373 (2009) 1583–1587

Contents lists available at ScienceDirect

Physics Letters A

www.elsevier.com/locate/pla

Influences of compressive stress and aging on dielectric properties of sodium bismuth titanate ceramics

T. Sareein, M. Unruan, A. Ngamjarurojana, S. Jiansirisomboon, A. Watcharapasorn, R. Yimnirun *

Department of Physics, Faculty of Science, Chiang Mai University, Chiang Mai, 50200, Thailand

ARTICLE INFO

Article history:
Received 15 December 2008
Received in revised form 17 February 2009
Accepted 23 February 2009
Available online 5 March 2009
Communicated by A.R. Bishop

PACS:
77.80.-e
77.80.Fm
77. 84.-s

Keywords:
Dielectric properties
NBT
Compressive stress
Aging

ABSTRACT

The influences of compressive stress and aging on dielectric properties of undoped and Fe-doped sodium bismuth titanate (NBT) ceramics were investigated. The dielectric properties were decreased significantly with the compressive stress applied parallel to the electric field direction, while the changes were reversed with the stress applied perpendicularly. In addition, lower changes of the dielectric properties with stress were observed in Fe-NBT ceramics, likely caused by an enhanced relaxor characteristic with the acceptor doping, which also reduced the aging rate in the ceramics. Finally, the aging behavior of the NBT and Fe-NBT ceramics followed the slightly stretched exponential law, and the aging rate in both ceramics was found to decrease with frequency, a result of the pinning of the polarization components. These observations clearly confirmed the role of the acceptor dopant in enhancing the relaxor ferroelectric characteristics in the NBT-based ceramics.

1. Introduction

Sodium bismuth titanate, $Na_{0.5}Bi_{0.5}TiO_3$ (NBT), and NBT-based ceramics are currently considered as a potential lead-free ferroelectric material to replace the widely used lead-based perovskite materials because of lead-free control atmosphere and lack of lead pollution [1–10]. While several previous investigations have suggested that the NBT exhibits strong ferroelectric properties with a large remnant polarization, $P_r = 38\ \mu C/cm^2$, and a phase transition point from ferroelectric to antiferroelectric should occur above 200 °C, many experiments do not confirm this hypothesis [1,2,4,10]. At present researchers accept that rather coexistence of rhombohedral and tetragonal phases takes place above 200 °C, not antiferroelectric [11]. In addition, this material system has been investigated in terms of variation in their dielectric and piezoelectric properties due to processing conditions, various dopants, and the formation of solid solution with other compounds [2,4–7,9,10].

Piezoelectric and ferroelectric ceramics are widely used in devices such as actuators and transducers. However, when they are used in devices, these ceramics are often subjected to self-induced or under environmental stresses. A prior knowledge of the effects of stresses on the material properties is crucial for proper design of a device and for suitable selection of materials for a specific application. Therefore, it is very important to obtain experimental data, as well as to better understand how these materials behave under stress [12–15]. Recently, the compressive stress dependence of dielectric properties has been studied in lead-based ferroelectric materials [16–23]. Interestingly, there have been many previous reports on the electrical properties of NBT-based ceramics [4–9], but there has been no systematic study on the influence of an applied stress on the dielectric properties of the NBT ceramics. Earlier investigations have already revealed significance of stress-induced ferroelectric phase transition, and domain structure and birefringence in NBT single crystals and NBT-based ceramics [24–31]. In addition to practical implication of stress influence, aging, usually regarded as an unwanted effect [32–35], has also been a subject of interest in lead-free materials, as it has been reported that aging of piezoelectric properties of lead-free materials is dramatic, hence limiting their potential uses in many applications [36–42]. Though aging behavior has been investigated extensively in lead-based materials [33,43–47], the aging behavior of the dielectric properties of NBT-based ceramics has yet to be reported.

Therefore, this study is aimed to examine the dielectric properties of the $Na_{0.5}Bi_{0.5}TiO_3$ ceramics as a function of compressive stress applied parallel and perpendicular to an electric field direction. Aging behavior of the dielectric properties of the ceramics is also investigated. This study is also extended to Fe-doped NBT

* Corresponding author at: School of Physics, Institute of Science, Suranaree University of Technology, Nakhon Ratchasima 30000, Thailand.
E-mail address: rattikornyimnirun@yahoo.com (R. Yimnirun).

0375-9601/$ – see front matter
doi:10.1016/j.physleta.2009.02.065

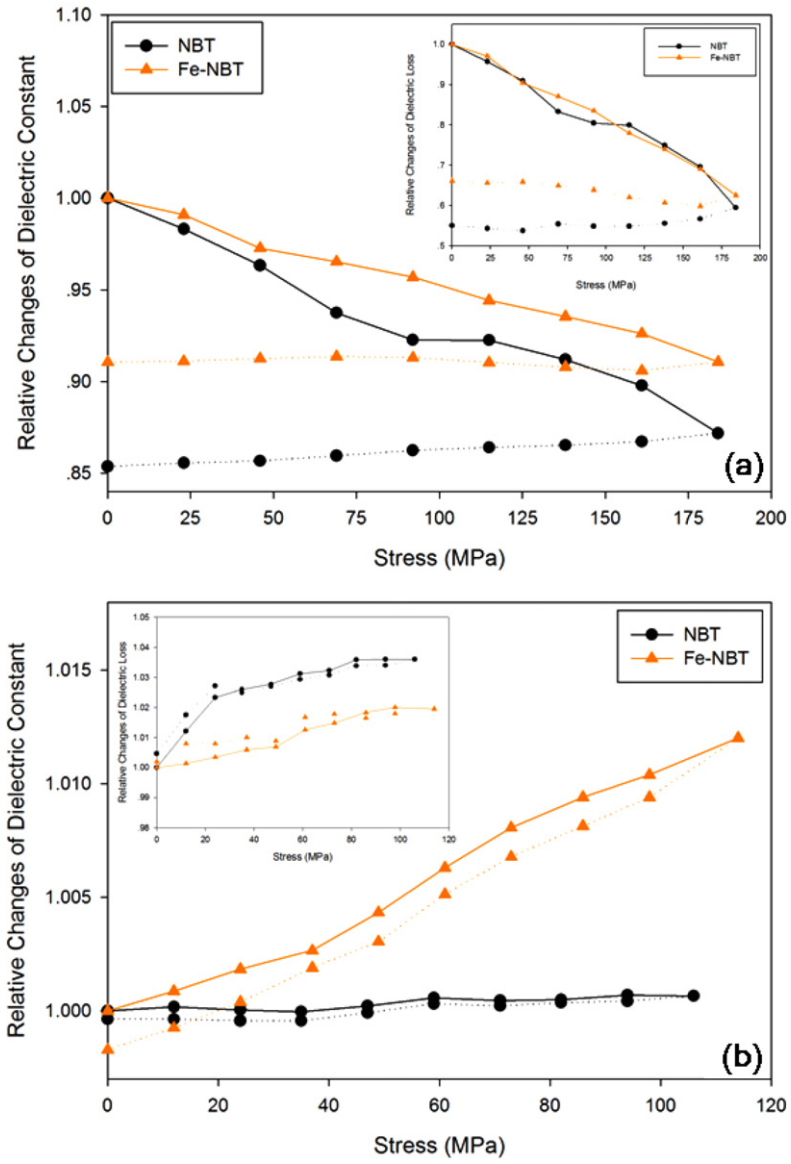

Fig. 1. Relative changes of dielectric constant (ε_r) and relative changes of dielectric loss tangent (tan δ) (inset) for NBT and Fe-NBT ceramics with compressive stress applied parallel (a) and perpendicular (b) to an electric field direction (measured at 25 °C and 10 kHz). Solid lines indicate changes during loading, and dotted lines indicate changes during unloading. Opposite trends are observed in the two stress directions.

ceramics since it is well established that lower-valence doping entails aging and previous investigations already showed significantly different responses to stress in undoped and doped (both lower-valence and higher-valence) lead-based materials [18,19,22,23]. Therefore, it is of very interest to also conduct the same experiments in the Fe-doped NBT ceramics.

2. Experimental

In this study, $Na_{0.5}Bi_{0.5}TiO_3$ (NBT hereafter) and Fe-doped $Na_{0.5}Bi_{0.5}TiO_3$ (Fe-NBT hereafter) powders were prepared from binary oxides and carbonate, i.e. Bi_2O_3 (>98%, Fluka), Na_2CO_3 (99.5%, Carlo Erba), TiO_2 (>99%, Riedel-de Haën) and Fe_2O_3 (99.9%, Fluka) with the nominal composition $Na_{0.5}Bi_{0.5}Ti_{1-x}Fe_xO_{3-0.5x}$, where $x = 0.0$ and 0.015. The powder mixtures were ball milled in ethanol using zirconia milling media for 24 h, calcined at 800 °C for 2 h. The calcined powders were re-ground using agate mortar and pestle, sieved, pressed into pellets and sintered at temperature of 1050 °C for 2 h. Detailed preparation process is given elsewhere [48]. The sintered specimens were then cut as rectangular bars (typical dimensions $6 \times 2 \times 2$ mm^3) and lapped to obtain parallel faces. After coating with silver paint as electrode, the effects of the compressive stress on the dielectric properties of the aged ceramics (the specimens were left at 25 °C for 4 weeks to achieve a fully aged state) were investigated with the compressometer. The compressive stress was applied both parallel and perpendicular to an electric field direction [49,50]. The low-field dielectric properties were measured by LCR-meter (Instrek LCR-821) with applied voltage of 1 V. The room temperature (25 °C) dielectric constant and dielectric loss tangent were determined at frequency 10 kHz. For aging study, the samples were heated to 550 °C and kept for 30 min to remove the aging effect and ensure them to start from unaged states. Then, they were immediately cooled to room temperature. The aging effect was characterized by measuring the changes in the dielectric properties with aging time.

3. Results and discussion

By X-ray diffraction method, both NBT and Fe-NBT ceramics were single phase with a rhombohedral structure. SEM micro-

Table 1
Room temperature stress-free dielectric properties and fitting parameters of Eq. (1) to the data in Fig. 3.

Ceramic	Stress-free (10 kHz)		K_∞			K_1			τ (second)		
	ε_r	$\tan\delta$	1 kHz	10 kHz	100 kHz	1 kHz	10 kHz	100 kHz	1 kHz	10 kHz	100 kHz
NBT	595	0.0269	616.4	576.4	533.5	37.4	29.4	20.2	8530	19062	20762
Fe-NBT	640	0.0224	679.2	635.5	588.9	28.5	26.4	19.6	8817	22890	29469

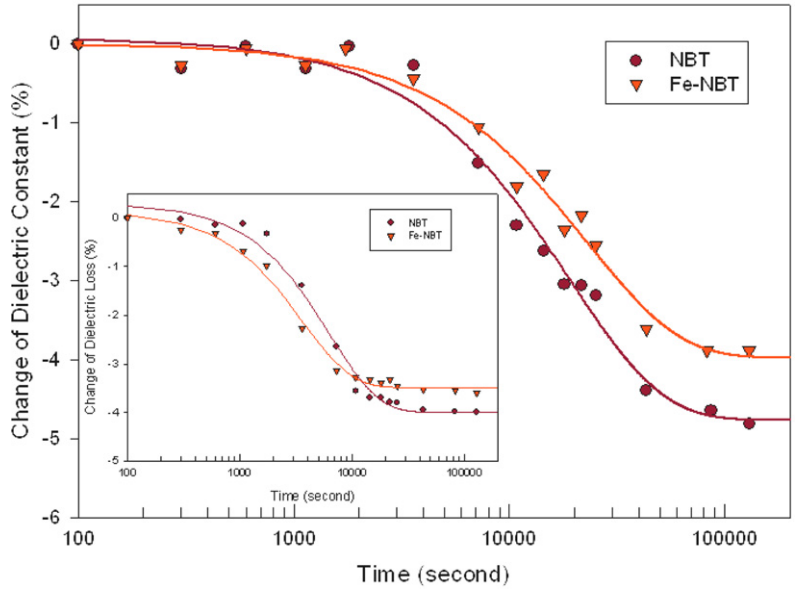

Fig. 2. Dielectric constant and dielectric loss tangent (inset) aging at 25 °C and 10 kHz for NBT and Fe-NBT ceramics. The solid lines are the fitting of the data with Eq. (1). Apparently, dielectric constant of NBT ages more quickly than that of Fe-NBT.

graphs revealed dense and well developed grain morphology with almost no porosity and the measured density of about 92–95% of the theoretical value [48]. For the Fe-doped NBT, the defect equation could be written as the following: $Fe_2O_3 = 2Fe'_{Ti} + 3O_O^x + V_O^{\bullet\bullet}$. It has to be noted that the defect reaction only assumed ionic defect compensation. In addition, it was assumed that Fe ions preferentially substituted Ti sites. The latter assumption was based on the fact that the ionic radius of Fe ion ($r_{Fe}^{3+} = 0.69$ Å) was much closer to the ionic radius of Ti ion ($r_{Ti}^{4+} = 0.61$ Å) than those of Bi ion ($r_{Bi}^{3+} \sim 1.38$ Å) and Na ion ($r_{Na}^{+} = 1.39$ Å). Therefore, one could expect defect complexes $2Fe'_{Ti} - V_O^{\bullet\bullet}$, which should facilitate the aging effect associated with acceptor doping on B site based on the symmetry-conforming principle of point defects, as reported in previous investigations [40,41,51].

The room temperature dielectric properties at 10 kHz of NBT and Fe-NBT ceramics as a function of compressive stress applied parallel and perpendicular to the electric field direction are depicted in Fig. 1(a) and (b), respectively. For better comparison, the dielectric properties of each ceramic under stress are normalized to the stress-free values, which are listed in Table 1. Clearly, there are observable changes of both the dielectric constant and the dielectric loss tangent with stress, in both cases of the compressive stress being applied either parallel or perpendicular to the electric field direction. For the case of stress parallel to the electric field direction, the dielectric constant and dielectric loss of both NBT and Fe-NBT ceramics are seen to significantly decrease with stress (10–15% for dielectric constant and 35-45% for dielectric loss at maximum stress), as displayed in Fig. 1(a). The cause of the decrease in the dielectric properties is likely from the clamping of the domain walls under the compressive stress, which results in a decrease of domain wall mobility and significantly reduced dielectric constant and dielectric loss [16–20]. In addition, a significant decrease in the dielectric properties after a full cycle of stress application is attributed to the stress induced decrease in switchable parts of domains at high stress [18–23]. The results obtained in this study are in parts similar to those for BT, PZT, PMN-PZT, PIN-PT, and PMN-PT systems in earlier investigations [16,17,19,23,49,50]. More interestingly, slightly lower changes of the dielectric properties with stress are observed in Fe-NBT ceramics. The cause for this observation is possibly due to an enhanced relaxor characteristic in Fe-doped NBT ceramics, as previously reported in La-doped and Mn-doped PMN-PT ceramics [44,45], implying that the doping Fe ions (and their associated defect complexes) break the polar regions to smaller size and reduce the crystal anisotropy in these regions, hence lesser contribution from the domains and domain walls [44,45]. This is consistent with other experimental results, i.e. the aging rate is also reduced in Fe-NBT ceramics, which will be discussed later.

For the case of stress applied perpendicular to the electric field direction, as depicted in Fig. 1(b), the changes of the dielectric properties with the stress are significantly different from the parallel stress case. Both the dielectric constant and dielectric loss increase (however, only 0–3%) with the applied stress. Interestingly, the results observed in this current study are in parts similar to earlier studies on commercial PZT ceramics, PIN-PT, and PMN-PT ceramics [19,22,23,49,50]. In this case, a combination of the de-aging and the polarization re-orientation mechanisms is believed to be a reason for the increase of the dielectric properties with stress. During aging process, some of the domain walls become pinned by impurities and structural imperfections. When a large enough stress is applied to the aged samples, it causes structural changes and redistribution of impurities. As a result, the domain walls that were pinned during aging can become active again [19,22,23]. This de-aging can increase the dielectric responses, as seen in Fig. 1(b). The perpendicular stress can also move some of the polarizations towards the electric field direc-

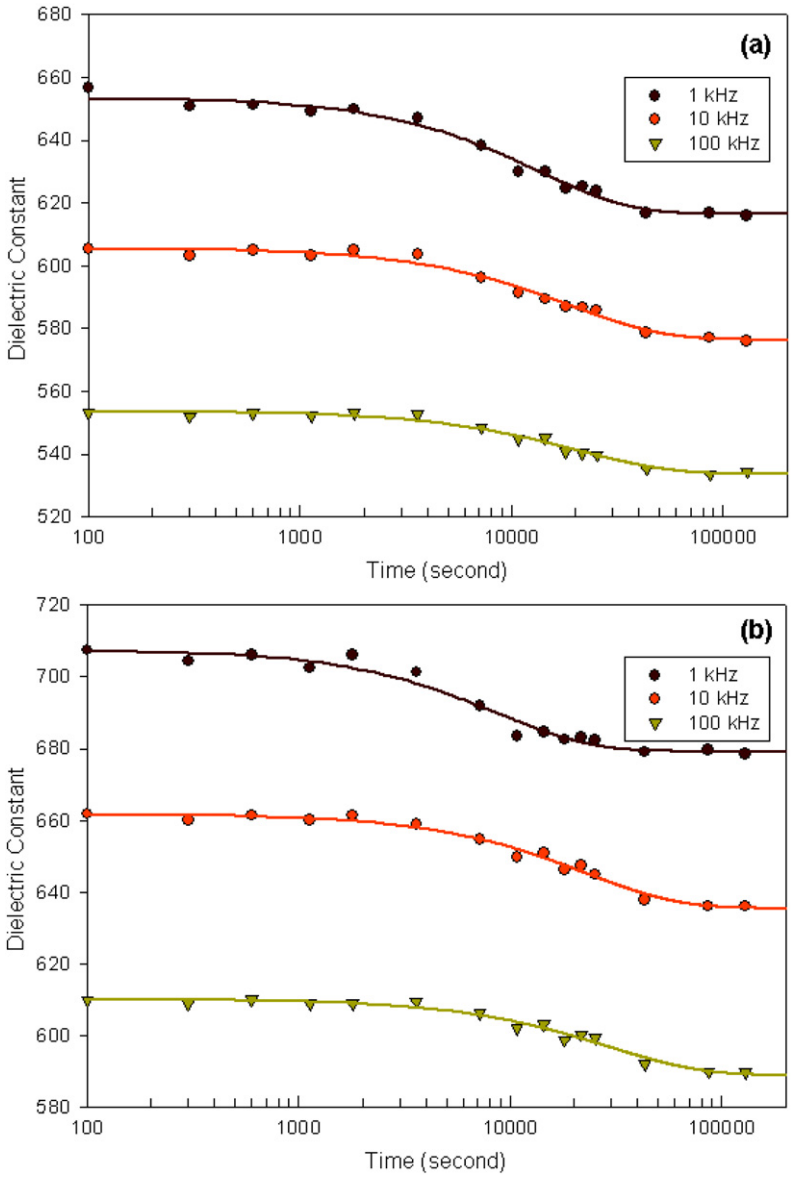

Fig. 3. Frequency dependent dielectric constant aging at 25 °C for (a) NBT and (b) Fe-NBT ceramics. The solid lines are the fitting of the data with Eq. (1). The data show that the relaxation time τ increases with frequency in both ceramics.

tion, hence an increase in the dielectric constant with the applied stress is observed [49,50]. An unexpected larger change of the dielectric constant obtained for Fe-NBT ceramics is believed to be a result of more easily polarization re-orientation process in the ceramics with mobile oxygen vacancies ($V_O^{\bullet\bullet}$) [19,23].

The room temperature aging of the low-field dielectric constant and dielectric loss of NBT and Fe-NBT ceramics is shown in Fig. 2. It is obvious that the aging observed in these ceramics is not linear with logarithmic time. The linear logarithmic time law of the aging successfully applied in normal ferroelectrics is related to the relaxation of the domain structure in the material towards an equilibrium configuration [43–45]. In a relaxor ferroelectric, deviation of the aging behavior from the linear logarithmic time behavior is a result of the lack of the macrodomain structure [44,45]. In this case, the time dependence may follow the stretched exponential law [36,38,39,44,45], which can be expressed, for small signal parameters, as

$$K = K_\infty + K_1 \exp\left[-(t/\tau)^\upsilon\right] \tag{1}$$

where K_∞ represents the part which is not time dependent and the second term on the right-hand side of the equation represent the time dependent part, which becomes zero as $t \to \infty$. The time constant (relaxation time) τ reflects the aging rate. As is evident from the solid curves in Fig. 2, which are fitting to Eq. (1), the stretched exponential function (*however only slightly, as to say not purely exponential*) can describe the experimental data quite well for NBT and FE-NBT ceramics, clearly confirming their relaxor ferroelectric behavior [1,2,4]. It should also be noted that the value of υ fitted from in Eq. (1) varies between 0.97–1.00 in all cases. Previous investigations on PMN-PT ceramics [44,45] also reported a similar value when the aging was determined away from their transition temperatures, which is also the case for this present study. Therefore, for better comparison, the value of υ was fixed at 1.00 to obtain the fitting parameters for the data in Figs. 2 and 3, as listed in Table 1. As shown in Fig. 2, it is noticed that the Fe-NBT ceramics show slightly weaker dielectric properties aging (larger relaxation time τ) than the NBT ceramics. The increased relaxation time τ in Fe-doped NBT ceramics reflects an increase in the activation energy for the motion of the micropolar domains [44,45], which is consistent with the results on the stress-dependent dielectric properties discussed above. This clearly suggests that, as opposed to the aging behavior in normal fer-

roelectrics, acceptor doping does not promote aging in lead-free relaxor ferroelectrics.

Fig. 3 shows the frequency-dependent aging behavior of the NBT and Fe-NBT ceramics. It is observed that in both ceramics the aging rate decreases (relaxation time τ increases) with measuring frequency, as also listed in Table 1. While K_∞ and K_1 decrease with the measuring frequency, K_1/K_∞ does not change very much in the experimental frequency range. To explain the frequency-dependent aging behavior in NBT and Fe-NBT ceramics, it has been previously proposed that the frequency dependent aging could be a result of the pinning of the polarization components which have low relaxation time or high activation energy by the defect field [45,52,53]. In a relaxor ferroelectric, local micropolar domains exist with the size of the domains distributing statistically over a broad range. The energy involved in reorienting a polar microdomain under an internal defect electric bias field E_{def} is proportional to $\nu P E_{\text{def}}$ where P is the polarization and ν is the volume of the micropolar domain. Therefore, the micropolar regions with large ν which have longer relaxation times will be pinned more effectively by E_{def} than the micropolar domains of smaller size, which have shorter relaxation time. Similar observations have been reported in acceptor-doped PMN ceramics, PMN-PT ceramics and BT-based ceramics [36–39, 43–45].

4. Conclusions

The dielectric properties of the NBT and Fe-NBT ceramics responded to the compressive stress applied parallel and perpendicular to the electric field direction in opposite manner. A combination of the clamping of the domain walls, the de-aging, and the polarization re-orientation mechanisms seemed to be the major factors causing the changes observed. In addition, enhanced relaxor behavior as well as reduced aging rate in Fe-NBT samples was likely the main cause of the less dependence on stress of the dielectric properties. Finally, the aging rate in both undoped and acceptor-doped NBT ceramics in this study was found to decrease with frequency, indicating the pinning effect on polarization components. The applied slightly stretched exponential law was also found to explain well this aging behavior. The results of this study suggested that the relaxor ferroelectric characteristics in the NBT-based ceramics could be enhanced by acceptor doping.

Acknowledgements

This work was jointly supported by the Thailand Research Fund (TRF), Commission on Higher Education (CHE), the Thailand Center of Excellence in Physics (through the Research Center in Theoretical and Computational Physics), Royal Golden Jubilee Ph.D. Program, Faculty of Science and Graduate School of Chiang Mai University.

References

[1] G.A. Smolensky, V.A. Isupov, A.I. Agranovskaya, N.N. Ktainik, Sov. Phys. Solid State 2 (1961) 2651.
[2] H. Nagata, T. Takenaka, J. Eur. Ceram. Soc. 21 (2001) 1299.
[3] Y. Saito, H. Takao, T. Tani, T. Nonoyama, K. Takatori, T. Homma, T. Nagaya, M. Nakamura, Nature 432 (2004) 7013.
[4] S.E. Park, K.S. Hong, J. Mater. Res. 12 (1997) 2152.
[5] K. Roleder, I. Franke, A.M. Glazer, P.A. Thomas, S. Miga, J. Suchanicz, J. Phys.: Condens. Matter 14 (2002) 5399.
[6] Y. Lin, S. Zhao, N. Cai, J. Wu, X. Zhou, C.W. Nan, Mater. Sci. Eng. B 99 (2003) 449.
[7] L. Liu, M. Zhu, Y. Hou, H. Yan, R. Liu, J. Mater. Res. 22 (2007) 1188.
[8] T.R. Shrout, S.J. Zhang, J. Electroceram. 19 (2007) 111.
[9] S.H. Lee, C.B. Yoon, S.M. Lee, H.E. Kim, K.W. Lee, J. Mater. Res. 23 (2008) 115.
[10] S.T. Lau, C.H. Cheng, S.H. Choy, D.M. Lin, K.W. Kwok, H.L.W. Chan, J. Appl. Phys. 103 (2008) 104105.
[11] G.O. Jones, P.A. Thomas, Acta Crystallogr. B 58 (2002) 168.
[12] S. Park, T.R. Shrout, J. Appl. Phys. 82 (1997) 1804.
[13] D. Viehland, J. Powers, Appl. Phys. Lett. 78 (2001) 3112.
[14] K. Uchino, Piezoelectric Actuators and Ultrasonic Motors, Kluwer Academic, Boston, 1997.
[15] D. Stansfield, Underwater Electroacoustic Transducers, Bath Univ. Press, Bath, 1991.
[16] G. Yang, S.F. Liu, W. Ren, B.K. Mukherjee, Proc. SPIE Sym. Smart Struct. Mater. 3992 (2000) 103.
[17] R. Yimnirun, S. Ananta, S. Chamunglap, Mater. Chem. Phys. 102 (2007) 165.
[18] D. Zhou, M. Kamlah, D. Munz, J. Eur. Ceram. Soc. 25 (2005) 425.
[19] Q.M. Zhang, J. Zhao, K. Uchino, J. Zheng, J. Mater. Res. 12 (1997) 226.
[20] O. Steiner, A.K. Tagantsev, E.L. Colla, N. Setter, J. Eur. Ceram. Soc. 19 (1999) 1243.
[21] R. Yimnirun, Y. Laosiritaworn, S. Wongsaenmai, J. Phys. D: Appl. Phys. 39 (2006) 759.
[22] J. Zhao, A.E. Glazounov, Q.M. Zhang, Appl. Phys. Lett. 74 (1999) 436.
[23] G. Yang, S.F. Liu, W. Ren, B.K. Mukherjee, Ferroelectrics 262 (2001) 207.
[24] J. Suchanicz, J. Phys. Chem. Solids 62 (2001) 1271.
[25] J. Suchanicz, R. Rosiek, J.P. Mercurio, S. Said, Ferroelectrics 300 (2004) 107.
[26] J. Suchanicz, J.P. Mercurio, S. Said, B. Garbarz-Glos, Phys. Status Solidi A 193 (2002) 179.
[27] V.A. Isupov, T.V. Kruzina, Izv. Akad. Nauk SSSR Ser. Fiz. 47 (1983) 616.
[28] V.A. Isupov, T.V. Kruzina, Izv. Akad. Nauk SSSR Ser. Fiz. 48 (1984) 1178.
[29] T.V. Kruzina, V.M. Duda, J. Suchanicz, Mater. Sci. Eng. B 87 (2001) 48.
[30] J. Suchanicz, T.V. Kruzina, Ferroelectrics 317 (2005) 109.
[31] J. Suchanicz, J.P. Mecurio, P. Marchet, T.V. Kruzina, Phys. Status Solidi B 225 (2001) 459.
[32] K. Carl, K.H. Haerdtl, Ferroelectrics 17 (1978) 473.
[33] W.A. Schulze, K. Ogino, Ferroelectrics 87 (1988) 361.
[34] U. Robels, G. Arlt, J. Appl. Phys. 73 (1993) 3454.
[35] D.C. Lupascu, Y.A. Genenko, N. Balke, J. Am. Ceram. Soc. 89 (2006) 224.
[36] T. Nomura, N. Kawano, J. Yamamatsu, T. Arashi, Y. Nakano, A. Sato, Jpn. J. Appl. Phys. 34 (1995) 5398.
[37] D.A. Hall, M.M. Ben-Omran, J. Phys.: Condens. Matter 10 (1998) 9129.
[38] T. Tsurumi, M. Shono, H. Kakemoto, S. Wada, K. Saito, H. Chazono, Jpn. J. Appl. Phys. Part B 44 (2005) 6989.
[39] J. Portelles, S. Garcia, E. Martinez, O. Raymond, N.S. Almodovar, J.L. Heiras, J.M. Siqueiros, J. Appl. Phys. 97 (2005) 054105.
[40] Z. Feng, X. Ren, Appl. Phys. Lett. 91 (2007) 032904.
[41] H. Bao, L. Zhang, Y. Wang, W.F. Liu, C. Zhou, X. Ren, Appl. Phys. Lett. 91 (2007) 142903.
[42] G.L. Yuan, Y. Yang, S.W. Or, Appl. Phys. Lett. 91 (2007) 122907.
[43] H. Dederichs, G. Arlt, Ferroelectrics 68 (1986) 281.
[44] W.Y. Pan, Q.Y. Jiang, L.E. Cross, Ferroelectrics 82 (1988) 111.
[45] Q.M. Zhang, J. Zhao, L.E. Cross, J. Appl. Phys. 79 (1996) 3181.
[46] D.A. Hall, P.J. Stevenson, Ferroelectrics 187 (1996) 23.
[47] M.I. Toacsan, A. Ioachim, L. Nedelcu, H.V. Alexandru, Prog. Solid State Chem. 35 (2007) 531.
[48] A. Watcharapasorn, S. Jiansirisomboon, T. Tunkasiri, Mater. Lett. 61 (2007) 2986.
[49] M. Unruan, S. Wongsaenmai, Y. Laosiritaworn, S. Ananta, R. Yimnirun, J. Phys. D: Appl. Phys. 41 (2008) 541.
[50] M. Unruan, A. Ngamjarurojana, Y. Laosiritaworn, S. Ananta, R. Yimnirun, J. Appl. Phys. 104 (2008) 034101.
[51] X. Ren, Nature Mater. 3 (2004) 91.
[52] W. Pan, E. Furman, G.O. Dayton, L.E. Cross, J. Mater. Sci. Lett. 5 (1986) 647.
[53] T.B. Wu, M. Shyu, C. Chung, H. Lee, J. Am. Ceram. Soc. 78 (1995) 2168.

Materials Letters 63 (2009) 1281–1284

Contents lists available at ScienceDirect

Materials Letters

journal homepage: www.elsevier.com/locate/matlet

Phase formation, microstructure, and dielectric properties of $(1-x)$PZT–(x)PCN ceramics

A. Prasatkhetragarn [a,*], P. Ketsuwan [b], S. Ananta [c], R. Yimnirun [d], D.P. Cann [e]

[a] Department of Materials Science, School of Science and Technology, Naresuan University at Phayao, Phayao 56000, Thailand
[b] Department of Physics, School of Science and Technology, Naresuan University at Phayao, Phayao 56000, Thailand
[c] Department of Physics, Faculty of Science, Chiang Mai University, Chiang Mai 50200, Thailand
[d] School of Physics, Institute of Science, Suranaree University of Technology, Nakorn Ratchasima 30000, Thailand
[e] Materials Science, School of Mechanical, Industrial and Manufacturing Engineering, Oregon State University, Corvallis, OR 97331, USA

ARTICLE INFO

Article history:
Received 16 October 2008
Accepted 26 February 2009
Available online 11 March 2009

Keywords:
PZT–PCN
MPB
Phase formation
Microstructure
Dielectric properties

ABSTRACT

Ceramics in a PZT–PCN system with the formula $(1-x)Pb(Zr_{1/2}Ti_{1/2})O_3$–$(x)Pb(Co_{1/3}Nb_{2/3})O_3$, where $x=0.0$, 0.1, 0.2, 0.3, 0.4, 0.5, and 1.0, were prepared using a solid-state mixed-oxide technique with columbite—$CoNb_2O_6$ and wolframite—$ZrTiO_4$ precursors. The crystal structure of the specimens studied with X-ray diffraction (XRD) analysis showed a coexistence between tetragonal and pseudo cubic phases at composition $x=0.2$. The SEM micrograph showed that the average grain size significantly decreased with increasing PCN content. A maximum dielectric constant was observed at composition $x=0.2$, while the transition temperature strongly decreased with increasing PCN content. All ceramics also showed diffused phase transition behaviors with a minimum diffusivity at $x=0.2$. The morphotropic phase boundary (MPB) lay at the 0.8PZT–0.2PCN composition.

1. Introduction

Lead zirconate titanate, $PbZr_{1-x}Ti_xO_3$ or PZT ceramics have been investigated from both fundamental and applied viewpoints [1,2]. Most commercial PZT ceramics are designed in the vicinity of the MPB with various doping methods in order to achieve high properties [2–7]. Recently, many piezoelectric ceramic materials have been developed from binary systems containing a combination of relaxor and normal ferroelectric materials [4] that yield high dielectric permittivities (e.g., PZT–PNN [5], and PZT–PMN [6]), excellent piezoelectric coefficients (e.g., PZT–PZN [7]), and high pyroelectric coefficients (e.g., PNN–PT–PZ [8]).

Lead cobalt niobate, $Pb(Co_{1/3}Nb_{2/3})O_3$ or PCN, which exhibits a perovskite structure and a Curie temperature of ≈ -30 °C, is a relaxor ferroelectric material with a high dielectric constant [9,10]. On the basis of the above mentioned approach, solid solutions of PZT and PCN are expected to synergistically combine the properties of both the normal ferroelectric PZT and relaxor ferroelectric PCN, which could exhibit electrical properties that are better than those of the single-phase PZT and PCN [9–12]. Therefore, the overall purpose of this study is to determine the phase formation, microstructure, and dielectric properties of ceramics in a $(1-x)Pb(Zr_{1/2}Ti_{1/2})O_3$–$(x)Pb(Co_{1/3}Nb_{2/3})O_3$ (where $x=0.0$, 0.1, 0.2, 0.3, 0.4, 0.5, and 1.0) system prepared with the columbite–wolframite precursors method via a vibratory-milling technique.

2. Experimental procedure

In the present work, $(1-x)Pb(Zr_{1/2}Ti_{1/2})O_3$–$(x)Pb(Co_{1/3}Nb_{2/3})O_3$ samples with compositions of $x=0.0$, 0.1, 0.2, 0.3, 0.4, 0.5, and 1.0 were prepared from $ZrTiO_4$ [13], $CoNb_2O_6$, and PbO powders. PZT–PCN powders were synthesized using the solid-state reaction of these raw materials and mixed by a vibratory-milling technique in ethanol for 6 h. After drying, the product was calcined in an alumina crucible at a temperature of 900 °C [14]. The calcined powders were uniaxially cold-pressed at 2.5 t into disc-shaped pellets with a diameter of 12.7 mm and a thickness of 1 mm, with 3 wt.% poly (vinyl alcohol) (PVA) added as a binder. Following binder burnout at 500 °C, the pellets were sintered at 1200 °C for 2 h at a heating/cooling rate of 5 °C/min [14].

The phase structure of the powders and ceramics were analyzed via X-ray diffraction (XRD; Bruker-AXS D8). The microstructures of the sintered samples were examined using scanning electron microscopy (SEM; JEOL JSM-840A). The dielectric properties of the samples were measured using an automated measurement system. An Agilent 4284A LCR meter was used to measure the dielectric properties over a wide temperature range using a NorECS ProboStat high temperature measurement cell.

3. Results and discussion

The XRD patterns of $(1-x)$PZT–(x)PCN ceramics with various x values are shown in Fig. 1. The XRD data show a range in symmetry between the tetragonal (JCPDS file no. 70-4057) and pseudo cubic

* Corresponding author. Tel.: +66 54 466666x1716; fax: +66 54 466664.
E-mail address: Prasatkhetragarn@yahoo.com (A. Prasatkhetragarn).

0167-577X/$ – see front matter © 2009 Elsevier B.V. All rights reserved.
doi:10.1016/j.matlet.2009.02.063

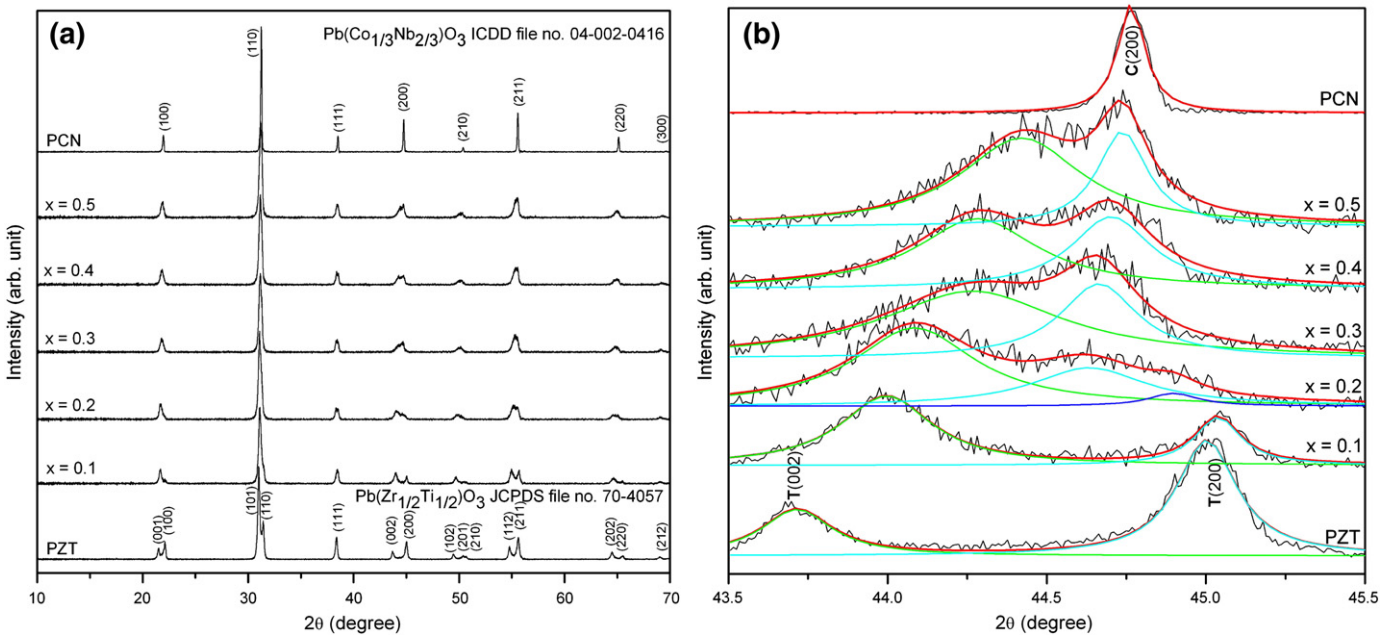

Fig. 1. XRD patterns of (a) $(1-x)$PZT–(x)PCN ceramics (where $x=0$, 0.1, 0.2, 0.3, 0.4, 0.5, and 1) and (b) (002)/(200) peak profile.

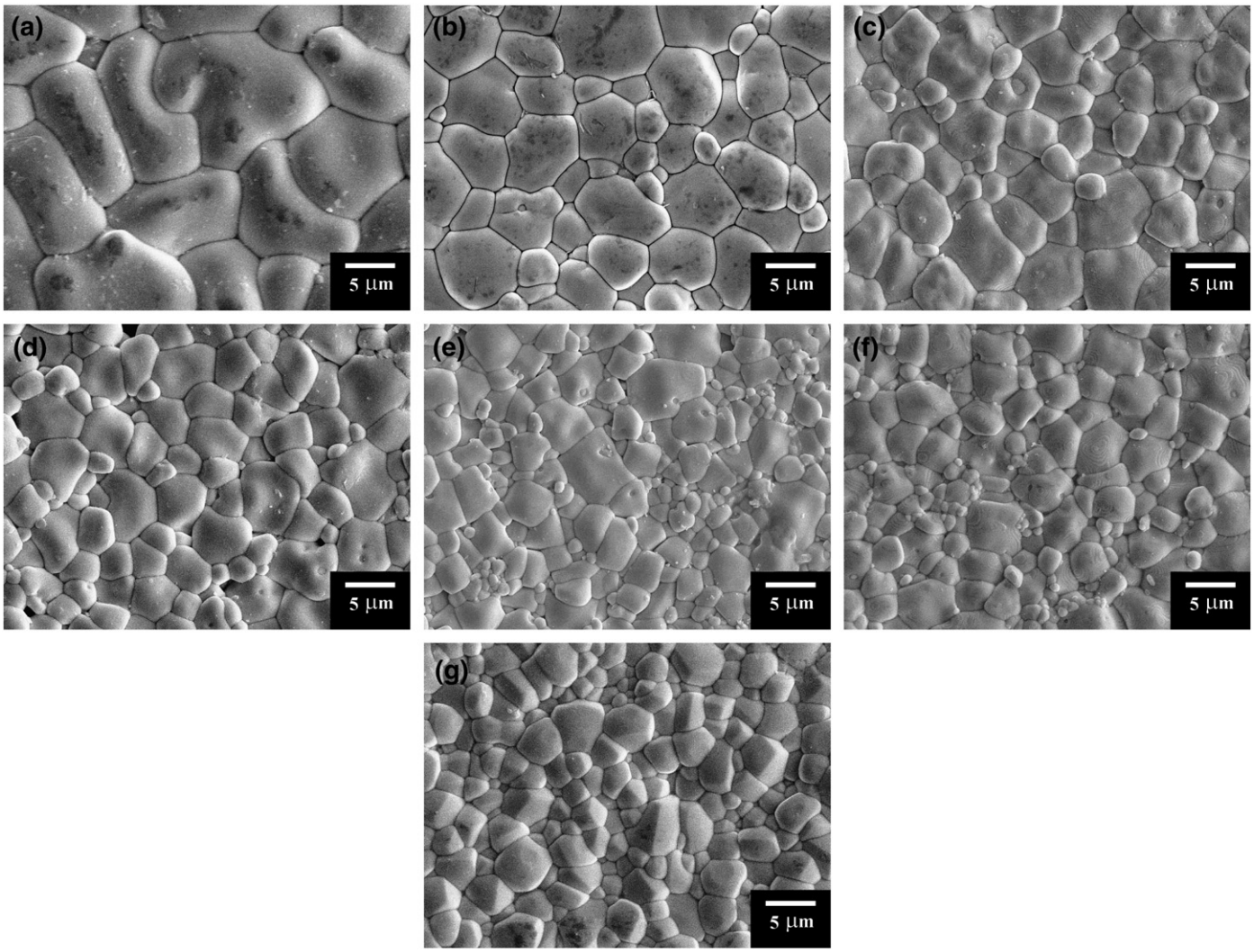

Fig. 2. SEM images of $(1-x)$PZT–(x)PCN ceramics with various compositions: (a) $x=0$, (b) $x=0.1$, (c) $x=0.2$, (d) $x=0.3$, (e) $x=0.4$, (f) $x=0.5$, and (g) $x=1$.

Table 1
Physical properties and dielectric properties of $(1-x)$PZT–(x)PCN ceramics.

x value	Physical properties			Dielectric properties (at 1 kHz)						
	Density (g/cm^3)	Grain size range (μm)	Average grain size (μm)	T_m (°C)	ε_{RT}	tan δ_{RT}	ε_m	tan δ_m	γ	δ
0.0	7.93	3.68–18.55	10.93	392	685	0	26670	1.111	1.57	15.97
0.1	7.93	1.84–14.54	4.14	358	703	0.02	51700	0.864	1.53	15.55
0.2	7.95	1.25–10.94	3.79	310	758	0.05	65700	2.188	1.49	15.28
0.3	7.94	0.75–9.94	3.16	270	785	0.07	47100	1.716	1.65	16.13
0.4	7.92	0.44–9.94	2.48	229	945	0.11	37900	1.653	1.72	16.66
0.5	7.91	0.43–8.77	2.12	175	1508	0.12	27000	0.613	1.79	16.81
1.0	7.94	0.54–6.85	3.08	−25	3905	1.44	3800	0.081	1.95	17.54

(ICDD file no. 04-002-0416) perovskite types [13,15]. It is clear that the structure of the PZT–PCN compositions gradually changes from tetragonal to pseudo cubic with increasing PCN content. However, the 200 peak of pseudo cubic phase is first observed at composition $x=0.2$, while 200 peak of tetragonal phase is also present in this composition, as shown in Fig. 1(b). This observation is obviously associated with the composition showing the coexistence of two symmetries, which in this case are the tetragonal and pseudo cubic phases. To a first approximation, it could be said that the composition with $x=0.2$ is close to the MPB of the $(1-x)$PZT–(x)PCN system.

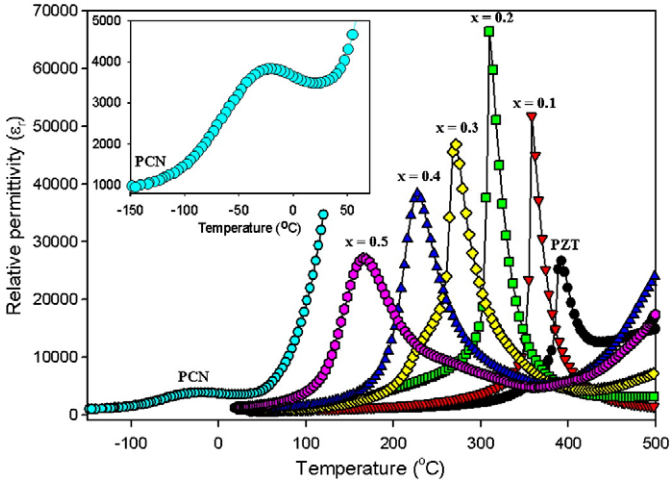

Fig. 3. Relative permittivity (ε_r) of $(1-x)$PZT–(x)PCN ceramics at 1 kHz.

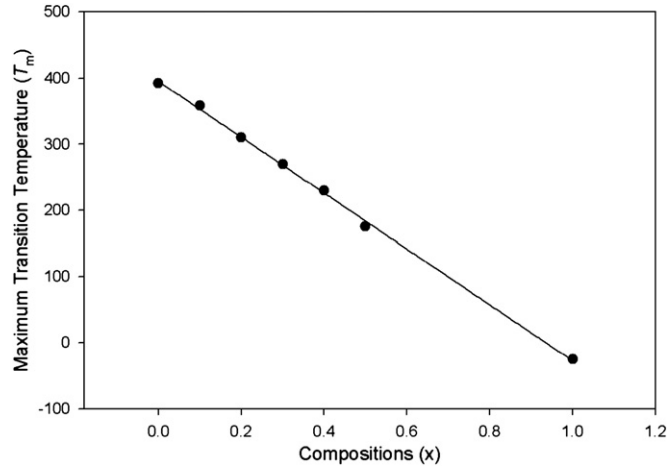

Fig. 4. Relationship of maximum transition temperature (T_m) and composition variation (x).

The SEM images in Fig. 2 reveal that the addition of PCN resulted in significant changes in the microstructure of the ceramics. The images also show that the grain size of the ceramics varied considerably from 0.43 to 18.55 μm (Table 1). However, the average grain size significantly decreased with an increase in the content of PCN. Interestingly, the density results can be correlated to the microstructure because high-density 0.8PZT–0.2PCN ceramics show high degrees of grain close packing, whereas low−density 0.5PZT–0.5PCN ceramics contain many closed pores.

Temperature dependences of the dielectric constant (ε_r) of the $(1-x)$PZT–(x)PCN ceramics with various x values ($x=0$, 0.1, 0.2, 0.3, 0.4, 0.5, and 1) are shown in Fig. 3. The ε_{max} increases from $x=0$ (pure PZT) and shows maximum value at $x=0.2$ and then decreases from $x=0.3$ to 1.0, clearly indicating the maximum dielectric constant at MPB composition of $x=0.2$. In addition, a clear transition in T_m decrease with increasing PCN mole fraction, most likely because the crystal structure of the materials was changed from tetragonal to pseudo cubic, as confirmed with XRD patterns in Fig. 1. This result suggests that the transition temperature of $(1-x)$PZT–(x)PCN system can be varied over a range from −25 to 392 °C by controlling the PCN content in the system, as shown in Fig. 4.

As listed in Table 1, all ceramics also showed diffused phase transition behaviors with a minimum diffusivity (γ) and diffuseness parameter (δ) at $x=0.2$. It is clear that the addition of PCN increases the degree of disorder in $(1-x)$PZT–(x)PCN over the compositional range ($x=0$, 0.1, 0.2, 0.3, 0.4, 0.5, and 1), with the highest degree of diffuseness exhibited in the pure PCN composition. Different dielectric behaviors could also be caused by grain size variation [6,13], as noted in Table 1. A similar behavior has also been observed in PZT–PNN [5], PZT–PMN [6] systems.

4. Conclusions

In this study, ceramics within the $(1-x)Pb(Zr_{1/2}Ti_{1/2})O_3$–$(x)Pb(Co_{1/3}Nb_{2/3})O_3$ solid solution system (where $x=0.0$, 0.1, 0.2, 0.3, 0.4, 0.5, and 1.0) were successfully prepared using a solid-state mixed-oxide technique. The PZT ceramic was identified by XRD analysis as a single-phase tetragonal perovskite, while the addition of PCN resulted in a gradual shift from tetragonal symmetry to pseudo cubic symmetry, with a possible MPB between the two phases located near the 0.8PZT–0.2PCN composition. The SEM micrograph showed that the average grain size significantly decreases with increasing PCN content. At 1 kHz, a maximum dielectric constant was observed at composition of $x=0.2$, while the transition temperature strongly decreased with increasing PCN content. All ceramics also showed diffused phase transition behaviors with a minimum diffusivity at $x=0.2$.

Acknowledgements

The authors wish to express profound gratitude to the Materials Science Groups, Oregon State University for ceramics preparation and measurement. This work was supported by the Commission on Higher

Education (CHE), the Thailand Research Fund (TRF), and Naresuan University at Phayao.

References

[1] Moulson AJ, Herbert JM. Electroceramics: materials, properties, applications. Chichester, U.K.: Wiley; 2003.
[2] Roleder K. Key Eng Mater 1998;155–156:123.
[3] Kuwata J, Uchino K, Nomura S. Ferroelectrics 1981;37:579.
[4] Park S-E, Shrout TR. IEEE Trans Ultrason Ferroelectr Freq Control 1997;44:1140.
[5] Vittayakorn N, Rujijanagul G, Tan X, Marquardt MA, Cann DP. J Appl Phys 2004;96:5103.
[6] Yimnirun R, Ananta S, Laoratanakul P. J Eur Ceram Soc 2005;25:3235.
[7] Fan H, Park GT, Choi JJ, Ryu J, Kim HE. J Mater Res 2002;17:180.
[8] Luff D, Lane R, Brown KR, Marshallsay HJ. Trans J Br Ceram Soc 1974;73:251.
[9] Unruan M, Vittayakorn N, Wongmaneeruang R, Prasatkhetragarn A, Ananta S, Yimnirun R. J Alloy Compd 2008;466:264.
[10] Hachiga T, Fujimoto S, Yasuda N. J Phys D 1987;20:1291.
[11] Kudo T, Yazaki T, Naito F, Sugaya S. J Am Ceram Soc 1970;53:326.
[12] Brankovic Z, Brankovic G, Varela JA. Ferroelectrics 2007;365:203.
[13] Prasatkhetragarn A, Yimnirun R, Ananta S. Ferroelectrics 2007;356:203.
[14] Prasatkhetragarn A, Vittayakorn N, Ananta S, Yimnirun R, Cann DP. Jpn J Appl Phys 2008;47:998.
[15] Vittayakorn N, Wirunchit S, Traisak S, Yimnirun R, Rujijanagul G. Curr Appl Phys 2008;8:128.

Dielectric and ferroelectric properties of lead zirconate titanate-lead nickel niobate ceramics under compressive stress

M. Unruan,[1,a)] A. Prasartketrakarn,[1] A. Ngamjarurojana,[1] Y. Laosiritaworn,[1] S. Ananta,[1] and R. Yimnirun[2]
[1]*Department of Physics and Materials Science, Faculty of Science, Chiang Mai University, Chiang Mai 50200, Thailand*
[2]*School of Physics, Institute of Science, Suranaree University of Technology, Nakhon Ratchasima 30000, Thailand*

(Received 23 December 2008; accepted 21 February 2009; published online 23 April 2009)

Dielectric and ferroelectric properties of complex perovskite lead zirconate titanate-lead nickel niobate ceramic system were investigated under the influence of the compressive stress. The results showed that the dielectric properties, i.e., dielectric constant (ε_r) and dielectric loss (tan δ), and the ferroelectric characteristics, i.e., the area of the ferroelectric hysteresis (P-E) loops, the maximum polarization (P_{max}), and the remanent polarization (P_r) changed significantly with increasing compressive stress. These changes depended greatly on the ceramic compositions. The experimental results on the dielectric properties could be explained by the deaging phenomenon. The stress-induced domain wall motion suppression and non-180° ferroelectric domain switching processes were responsible for the changes observed for the ferroelectric parameters. In addition, a significant decrease in those parameters after a cycle of stress was observed and attributed to the stress-induced decrease in switchable part of spontaneous polarization. This study clearly showed that the applied stress has significant influence on the electrical properties of complex perovskite ceramics. © *2009 American Institute of Physics*. [DOI: 10.1063/1.3106659]

I. INTRODUCTION

There has recently been a great deal of interest in lead zirconate titanate-lead nickel niobate [$Pb(Zr_{1-x}Ti_x)O_3$-$Pb(Ni_{1/3}Nb_{2/3})O_3$ or (PZT-PNN)] ceramics because of their high longitudinal coupling coefficients, as well as good dielectric and excellent piezoelectric properties.[1–3] PZT is a normal ferroelectric material, which has been extensively investigated in the literatures because of its high dielectric properties and high piezoelectric coefficient. The high piezoelectric properties of PZT have been observed for compositions near the morphotropic phase boundary (MPB), i.e., at lead zirconate ($PbZrO_3$ or PZ):lead titanate($PbTiO_3$ or PT)=0.52:0.48.[4–6] PNN is a relaxor ferroelectric material originally reported by Smolenskii and Agranovskaya.[7] It exhibits the excellent dielectric broadening and electrostrictive properties and shows a diffuse phase transition around −120 °C with a peak permittivity of about 4000 at 1 kHz.[8]

Practically, piezoelectric and ferroelectric ceramics are often subjected to mechanical loading either deliberately in the design of the device itself or because the device is used to change shapes as in many smart structure applications or the device is used under environmental stresses.[9–13] A prior knowledge of how the material properties change under different load conditions is crucial for proper design of a device and for suitable selection of materials for a specific application.[12,13] It is therefore important to determine the properties of these materials as a function of applied stress. Previous investigations on the stress-dependence electrical properties of many ceramic systems emphasized the importance of the matter.[11,14–18] Recently, the uniaxial stress dependence of dielectric and ferroelectric properties has been investigated in materials such as barium titanate (BT), lead magnesium niobate (PMN), PMN-PT, PZT-BT, and PMN-PZT.[16–21] The results clearly showed that the effects of stress on the dielectric and ferroelectric properties depended significantly on ceramic compositions and stress levels. Interestingly, there has been no systematic study on the influence of an applied stress on the dielectric and ferroelectric properties of the PZT-PNN ceramics. Therefore, it is the aim of this study to determine the dielectric and ferroelectric properties of the $(1-x)$PZT-(x)PNN ceramics as a function of compressive stress.

II. EXPERIMENTAL

In this study, $(1-x)$PZT-(x)PNN (with $x=0.1-0.5$) ceramics were prepared using the columbite precursor method. The columbite structure ($NiNb_2O_6$) and wolframite structure ($ZrTiO_4$) were synthesized first. The calcined $NiNb_2O_6$ and $ZrTiO_4$ powders were mixed with PbO in a stoichiometric ratio to form the composition $(1-x)$PZT-(x)PNN, with $x=0.1-0.5$. For optimization purpose, the sintering was carried out at temperatures between 1100 and 1250 °C for 4 h. Details of the processing and characterizations were provided elsewhere.[2]

Before studying the electrical properties, the specimens were lapped to obtain parallel faces. After coating with silver paint as electrode at the faces, the specimens were heated at 750 °C for 12 min to ensure the contact between the electrode and surface of ceramic. To study effects of the com-

a)Author to whom correspondence should be addressed. Electronic mail: muangjaiunruan@yahoo.com.

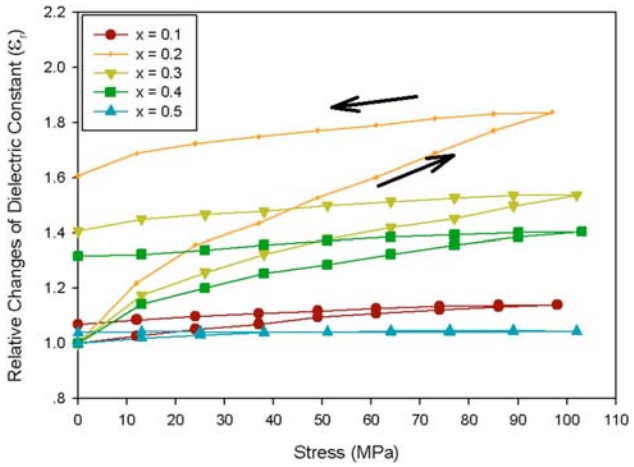

FIG. 1. (Color online) Relative changes in dielectric constant (ε_r) with compressive stress for $(1-x)$PZT-(x)PNN ceramics (measured at 25 °C and 10 kHz; solid arrows indicate loading direction).

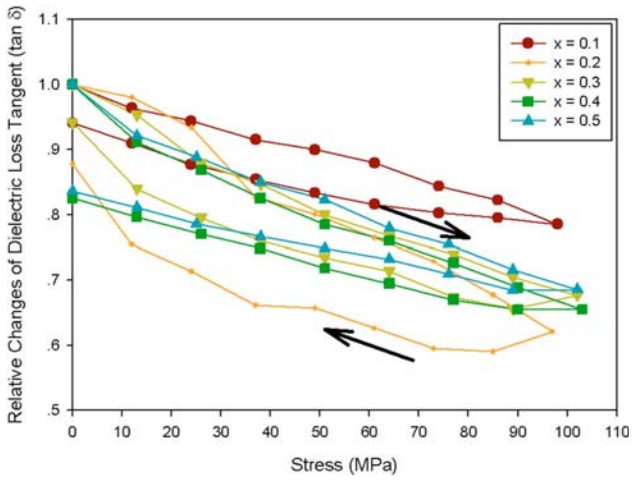

FIG. 2. (Color online) Relative changes in dielectric loss tangent (tan δ) with compressive stress for $(1-x)$PZT-(x)PNN ceramics (measured at 25 °C and 10 kHz; solid arrows indicate loading direction).

pressive stress on the dielectric and ferroelectric properties of the ceramics, the compressometer was constructed.[16–18] The dielectric properties were measured by LCR meter (Instrek LCR-821). The room temperature (25 °C) capacitance and the dielectric loss tangent were obtained at frequency of 10 kHz under compressive stress. The dielectric constant was then calculated from a parallel-plate capacitor equation, e.g., $\varepsilon_r = Cd/\varepsilon_0 A$, where C is the capacitance of the specimens, d and A are respectively the thickness and the area of the electrode, and ε_0 is the dielectric permittivity of vacuum $(8.854 \times 10^{-12}$ F/m).

The ferroelectric hysteresis (P-E) loops were characterized by using a computer controlled modified Sawyer–Tower circuit. The electric field was applied to a sample by a high voltage ac amplifier (Trek, model 610D) with the input sinusoidal signal with a frequency of 50 Hz from a signal generator (Goodwill, model GAG-809). The ferroelectric hysteresis (P-E) loop was recorded at room temperature (25 °C) for both loading and unloading conditions. The parameters obtained from the loops were the maximum polarization (P_{max}), the remanent polarization (P_r), and the coercive field (E_c), which were defined as the points where the loops reach the maximum polarization, cross the zero field, and cross the zero polarization, respectively.

III. RESULTS AND DISCUSSION

A. Dielectric properties under stress

The experimental results of the compressive stress dependence of the dielectric properties during loading and unloading for the ceramics in PZT-PNN system are displayed in Figs. 1 and 2. For better comparison, the dielectric properties of each composition under stress are normalized to the stress-free values. Clearly, there is a considerable change in both the dielectric constant and the dielectric loss tangent with the compressive stress. As depicted in Fig. 1, the dielectric constant is seen to increase with increasing stress in all compositions. The increase in the dielectric constant varies from approximately 4%–14% in the near pseudocubic relaxor ferroelectric 0.5PZT-0.5PNN and tetragonal ferroelectric 0.9PZT-0.1PNN compositions to 40%–54% in the rhombohedral relaxor ferroelectric 0.6PMN-0.4PNN and 0.7PZT-0.3PNN compositions. For the MPB 0.8PZT-0.2PNN composition, the dielectric constant increases drastically with the stress. The dielectric constant increases more than 80% when the stress reaches 100 MPa and returns to 160% of its original value when the stress is removed. On the other hand, the dielectric loss tangent (tan δ) is seen to decrease significantly (20%–40%) with increasing stress, as displayed in Fig. 2. The changing of the dielectric properties with increasing and decreasing stress does not follow the same path. It is also noticed that the changes in the dielectric properties with the compressive stress obtained in this study are in parts similar to those for systems in earlier investigations.[17,19,22]

To understand these experimental results, various effects have to be considered. When a mechanical stress is applied to a ferroelectric material, the domain structure in the material will change to maintain the domain energy at a minimum; during this process some of the domains engulf other domains or change shape irreversibly. Under a compressive stress, the domain structure of ferroelectric ceramics may undergo domain switching, clamping of domain walls, and deaging mechanisms.[14,15,19,23] In this study, the results on the compressive stress dependence of the dielectric properties can easily be explained with the above statements. When the compressive stress is applied in the direction parallel to the polar axis (poling) direction, the stress will move some of the polarization away from the poling direction, resulting in a change in domain structures.[15,19,24,25] This change increases the non-180° domain wall density. Hence the increase in the dielectric constant with the applied stress is observed. The deaging mechanism, which also increases the dielectric constant,[15,18–20] is also expected to play a role here. Therefore, a combination of the domain switching and the deaging mechanisms is believed to be a reason for the increase in the dielectric constant with increasing applied stress in the PZT-PNN system, as shown in Fig. 1. The cause of the stress dependence of the dielectric loss tangent is mainly due to the clamping of the domain walls under compressive stress,

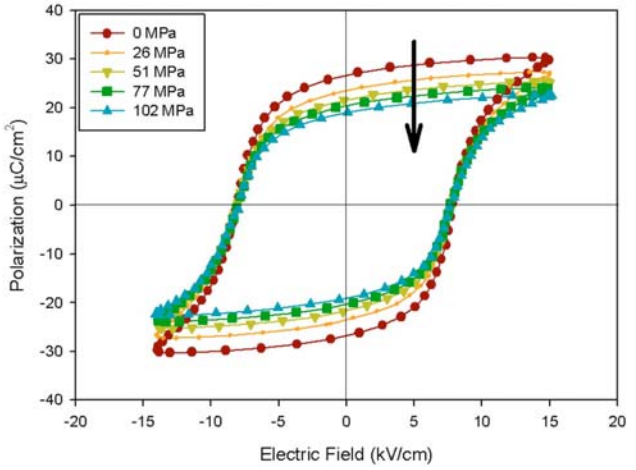

FIG. 3. (Color online) Polarization vs electric field (P-E) hysteresis loops as a function of compressive stress for 0.7PZT-0.3PNN ceramic (loading cycle).

which results in a decrease in domain wall mobility. The deaging mechanism, which also decreases the dielectric loss tangent,[15,22] is also expected to play a role in controlling the change in the dielectric loss tangent with the stress, as observed in Fig. 2.

It should also be noted here that the applied stress could also affect the ferroelectric phase transitions of the ceramics, which consequently change the observed dielectric properties significantly.[15,25] The applied compressive stress has been found to move the Curie temperature (T_C) up to the order of approximately 0.1 °C/MPa in 0.9PMN-0.1PT.[15] In addition, the influence of stress on the properties of ferroelectric materials is strongly dependent on the temperature, especially when the temperature is higher or lower than T_C. In this study, since $(1-x)$PZT-(x)PNN (with $x=0.1-0.5$) ceramics exhibit T_C ranging from 130 °C ($x=0.5$) to 330 °C ($x=0.1$),[2] the change in the dielectric properties with stress in the vicinity of T_C and the stress-induced shift in T_C is rather insignificant because of their high T_C, as compared to the measurement temperature of 25 °C. Therefore, the stress-related ferroelectric phase transition is not expected to have significant effects on the changes in dielectric properties of PZT-PNN ceramics under the applied stress observed in this study.

B. Ferroelectric properties under stress

The polarization versus electric field (P-E) hysteresis loops of the 0.7PZT-0.3PNN ceramic under different compressive stresses are shown in Fig. 3 as a simple representative for the other compositions with similar behavior. It should first be noticed that the area of the P-E loops decreases with increasing compressive stress. The changes follow similar trend for all the ceramics. The P-E loop area indicates the polarization dissipation energy of a ferroelectric material under one full cycle of electric field application. This amount of the energy loss is directly related to the amount of domain participating in the switching process during the application of electric field.[14,17] For a given composition, the decrease in the loop area with increasing the compressive stress is a result of the stress-induced domain wall suppression.[14,26]

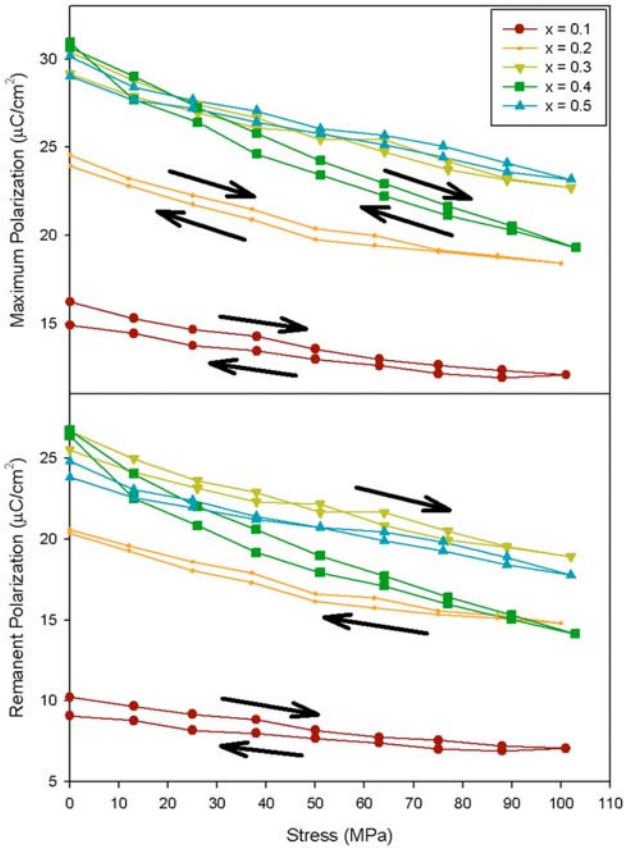

FIG. 4. (Color online) Changes in remanent polarization (P_r) and maximum polarization (P_{max}) with compressive stress for $(1-x)$PZT-xPNN ceramics (loading and unloading).

The changes in the remanent polarization (P_r), maximum polarization (P_{max}), and the coercive field (E_c) with the compressive stresses are plotted in Figs. 4 and 5, respectively. The changes in the maximum polarization (P_{max}) with stress are similar to the P_r. Figure 4 clearly shows that the

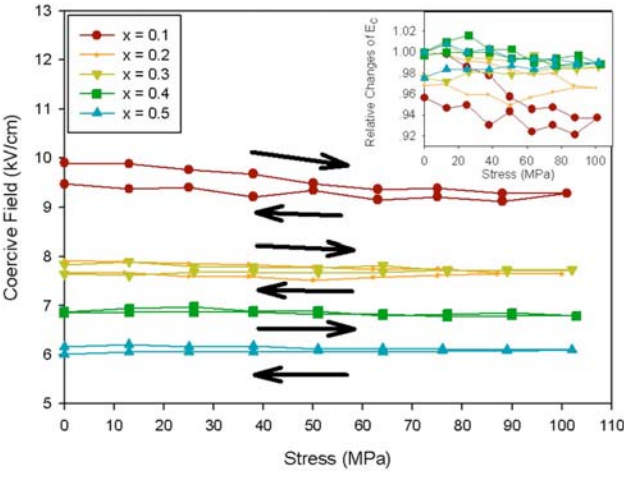

FIG. 5. (Color online) Changes in coercive field (E_c) with compressive stress for $(1-x)$PZT-xPNN ceramics (loading and unloading).

maximum and remanent polarizations decrease as the compressive stress increases. The decrease is generally very similar to the polarization values at 100 MPa, which are approximately 30%–45% of the stress-free values. In addition, noticeable decreases in the polarization values of all the ceramic are also observed after a complete cycle of the mechanical stress. This observation suggests a significant stress-induced depoling in PZT-PNN ceramics, resulting in the observed decrease in the polarization values under high stress levels.[19,27] Since the remanent polarization decreases as the compressive stress increases, it takes lower than usual electric field to force the polarizations to become zero; hence lower coercive field is observed, as demonstrated in Fig. 5.

To understand, at least qualitatively, these experimental results on ferroelectric properties of the PZT-PNN ceramics, one can interpret the changes in terms of domain-reorientation processes. When the compressive stress is applied in the direction parallel to the polar axis (poling) direction, the applied stress tends to keep the ferroelectric domains aligned with their polar axes away from the stress direction through the non-180° ferroelastic domain switching processes.[14,15] Therefore, it takes larger than usual for the applied electric field to reorient the domains along the stress direction, resulting in lower value of the maximum polarization (P_{max}), as shown in Figs. 3 and 4. When the electric field is reduced to zero the domains tend to rotate back away from the applied compressive stress direction, resulting in lower than usual remanent polarization (P_r),[19,28,29] as depicted in Figs. 3 and 4. Furthermore, considering the decrease in the hysteresis loss with increasing compressive stress, it indicates that more and more ferroelectric domains are constrained by the applied stress and cannot be reoriented by the electric field so as to participate in the polarization reversal. Consequently, both the maximum and remanent polarizations become lower with increasing compressive stress.[15] The results of the changes in the hysteresis parameters of the ferroelectric ceramics with increasing compressive stress are in agreement with the previous investigations on many ferroelectric ceramics.[11,14,18,30]

IV. CONCLUSIONS

In this study, effects of compressive stress on the dielectric properties of PZT-PNN ceramics with a formula of $(1-x)$PZT-(x)PNN ($x=0.1-0.5$) have been investigated under compressive stress using a compressometer in conjunction with an automatic LCR meter and a modified Sawyer–Tower circuit. The superimposed compression stress had pronounced effects on both the dielectric constant and the dielectric loss tangent of PZT-PNN ceramics, especially in MPB 0.8PZT-0.2PNN composition. The area of the ferroelectric hysteresis (P-E) loops, the maximum polarization (P_{max}), the remanent polarization (P_r), and the coercive field (E_c) decrease with increasing compressive stresses. The observations were mainly interpreted in terms of domain switching through non-180° domain walls, deaging, and the stress-induced domain wall suppression mechanisms. Furthermore, noticeable decreases in the polarization values of all the ceramic are also observed after a complete cycle of the mechanical stress, indication of a significant stress-induced depoling in PZT-PNN ceramics. Finally, this study undoubtedly shows that the applied compressive stress has significant influences on the dielectric and ferroelectric properties of the PZT-PNN ceramics.

ACKNOWLEDGMENTS

Financial supports from the Thailand Research Fund (TRF), Commission on Higher Education (CHE), Royal Golden Jubilee (RGJ) Ph.D. Program, Thailand Excellent Center in Physics, and Faculty of Science and Graduate School of Chiang Mai University are gratefully acknowledged.

[1] M. Kondo, M. Hida, M. Tsukuda, K. Kurihara, and N. Kamehara, Jpn. J. Appl. Phys., Part 1 **36**, 6043 (1997).
[2] N. Vittayakorn, G. Rujijanagul, X. Tan, M. A. Marquardt, and D. P. Cann, J. Appl. Phys. **96**, 5103 (2004).
[3] D. Luff, R. Lane, K. R. Brown, and H. J. Marshallsay, Trans. J. Br. Ceram. Soc. **73**, 251 (1974).
[4] J. Moulson and J. M. Herbert, *Electroceramics: Materials, Properties, Applications* (Chapman and Hall, New York, 1990).
[5] B. Jaffe, W. R. Cook, and H. Jaffe, *Piezoelectric Ceramic* (RAN, New York, 1971).
[6] Y. H. Xu, *Ferroelectric Materials and Their Applications* (North-Holland, Los Angeles, 1991).
[7] G. A. Smolenskii and A. L. Agranovskaya, Sov. Phys. Tech. Phys. **13**, 80 (1958).
[8] V. A. Bokov and I. E. Mylnikova, Sov. Phys. Solid State **2**, 2428 (1960).
[9] J. Kuwata, K. Uchino, and S. Nomura, Jpn. J. Appl. Phys., Part 1 **21**, 1298 (1982).
[10] S. E. Park and T. R. Shrout, J. Appl. Phys. **82**, 1804 (1997).
[11] D. Viehland and J. Powers, Appl. Phys. Lett. **78**, 3112 (2001).
[12] D. Stansfield, *Underwater Electroacoustic Transducers* (Bath University Press, Bath, UK, 1991).
[13] K. Uchino, *Piezoelectric Actuators and Ultrasonic Motors* (Kluwer, Boston, 1997).
[14] D. Zhou, M. Kamlah, and D. Munz, J. Eur. Ceram. Soc. **25**, 425 (2005).
[15] Q. M. Zhang, J. Zhao, K. Uchino, and J. Zheng, J. Mater. Res. **12**, 226 (1997).
[16] R. Yimnirun, Ferroelectrics **331**, 9 (2006).
[17] R. Yimnirun, S. Ananta, and S. Chamunglap, Mater. Chem. Phys. **102**, 165 (2007).
[18] R. Yimnirun, S. Ananta, A. Ngamjarurojana, and S. Wongsaenmai, Curr. Appl. Phys. **6**, 520 (2006).
[19] G. Yang, S. F. Liu, W. Ren, and B. K. Mukherjee, Proc. SPIE Symposium on Smart Structures and Materials **3992**, 103 (2000).
[20] R. Yimnirun, M. Unruan, Y. Laosiritaworn, and S. Ananta, J. Phys. D **39**, 3097 (2006).
[21] R. Yimnirun, S. Ananta, E. Meechoowas, and S. Wongsaenmai, J. Phys. D **36**, 1615 (2003).
[22] M. Unruan, S. Wongsaenmai, Y. Laosiritaworn, S. Ananta, and R. Yimnirun, J. Phys. D **41**, 541 (2008).
[23] G. Yang, S. F. Liu, W. Ren, and B. K. Mukherjee, Ferroelectrics **262**, 207 (2001).
[24] D. Audigier, Cl. Richard, Cl. Descamps, M. Troccaz, and L. Eyraud, Ferroelectrics **154**, 219 (1994).
[25] I. J. Fritz, J. Appl. Phys. **49**, 4922 (1978).
[26] R. Yimnirun, S. Ananta, A. Ngamjarurojana, and S. Wongsaenmai, Appl. Phys. A: Mater. Sci. Process. **81**, 1227 (2005).
[27] G. Yang, W. Ren, S. F. Liu, A. J. Masys, and B. K. Mukherjee, Proc.-IEEE Ultrason. Symp. **2**, 1005 (2000).
[28] J. Zhao and Q. M. Zhang, Proceedings of the 10th IEEE International Symposium on Applications of Ferroelectrics, Vol. 2, pp. 971–974 (1996).
[29] J. Zhao, A. E. Glazounov, and Q. M. Zhang, Appl. Phys. Lett. **74**, 436 (1999).
[30] C. S. Lynch, Acta Mater. **44**, 4137 (1996).

Dielectric and Ferroelectric Properties of PZT-PNN Ceramics Under Compressive Stress

M. Unruan*, A. Prasartketrakarn, A. Ngamjarurojana, Y. Laosiritaworn, S. Ananta and R. Yimnirun,

Department of Physics, Faculty of Science, Chiang Mai University,

Chiang Mai 50200, Thailand

Abstract

Dielectric and ferroelectric properties of complex perovskite PZT-PNN ceramic system were investigated under the influence of the compressive stress. The results showed that the dielectric properties, i.e. dielectric constant (ε_r) and dielectric loss (tan δ), and the ferroelectric characteristics, i.e. the area of the ferroelectric hysteresis (P-E) loops, the maximum polarization (P_{max}), and the remanent polarization (P_r) changed significantly with increasing compressive stress. These changes depended greatly on the ceramic compositions. The experimental results on the dielectric properties could be explained by the de-aging phenomenon. The stress-induced domain wall motion suppression and non-180º ferroelectric domain switching processes were responsible for the changes observed for the ferroelectric parameters. In addition, a significant decrease in those parameters after a cycle of stress was observed and attributed to the stress induced decrease in switchable part of spontaneous polarization. This study clearly showed that the applied stress has significant influence on the electrical properties of complex perovskite ceramics.

Keywords: Dielectric Properties; Ferroelectric Properties; Stress; Perovskite Ceramics

* Corresponding author: Department of Physics, Faculty of Science, Chiang Mai University, Chiang Mai 50200, Thailand; Fax No. 6653-943-445; E-mail: muangjaiunruan@yahoo.com

1 Introduction

There have recently been a great deal of interest in lead zirconate titanate-lead nickel niobate ($Pb(Zr_{1-x}Ti_x)O_3$-$Pb(Ni_{1/3}Nb_{2/3})O_3$ or (PZT-PNN)) ceramics because of their high longitudinal coupling coefficients, as well as good dielectric and excellent piezoelectric properties [1-3]. Lead zirconate titanate ($Pb(Zr_{1-x}Ti_x)O_3$ or PZT) is a normal ferroelectric material which has been extensively investigated in the literatures because of their high dielectric properties and high piezoelectric coefficient. The high piezoelectric properties of PZT have been observed for compositions near the morphotropic phase boundary (MPB), i.e. at $PbZrO_3$:$PbTiO_3$ = 0.52:0.48 [4-6]. Lead nickel niobate ($Pb(Ni_{1/3}Nb_{2/3})O_3$ or PNN) is a relaxor ferroelectric material originally reported by Smolenskii and Agranovskaya [7]. It exhibits the excellent dielectric broadening and electrostrictive properties and shows a diffuse phase transition around -120 ^{o}C with a peak permittivity of about 4000 at 1 kHz [8].

Practically, piezoelectric and ferroelectric ceramics are often subjected to mechanical loading, either deliberately in the design of the device itself or because the device is used to change shapes as in many smart structure applications or the device is used under environmental stresses [9-13]. A prior knowledge of how the material properties change under different load conditions is crucial for proper design of a device and for suitable selection of materials for a specific application [12,13]. It is therefore important to determine the properties of these materials as a function of applied stress.

Previous investigations on the stress-dependence electrical properties of many ceramic systems have emphasized the importance of the matter [11,14-18]. Recently, the uniaxial stress dependence of dielectric and ferroelectric properties has been investigated in materials such as BT, PZT, PMN, PMN-PT, PZT-BT, and PMN-PZT [16-21]. The results clearly showed that the effects of stress on the dielectric and ferroelectric properties depended significantly on ceramic compositions and stress levels. Interestingly, there has been no systematic study on the influence of an applied stress on the dielectric and ferroelectric properties of the PZT-PNN ceramics. Therefore, it is the aim of this study to determine the dielectric and ferroelectric properties of the (*1-x*)PZT-(*x*)PNN ceramics as a function of compressive stress.

2 Experimental

In this study, (*1-x*)$Pb(Zr_{1/2}Ti_{1/2})O_3$–(*x*)$Pb(Ni_{1/3}Nb_{2/3})O_3$ (with x = 0.1-0.5) ceramics were prepared using the columbite precursor method. The columbite structure ($NiNb_2O_6$) and wolframite structure ($ZrTiO_4$) were synthesized first. The calcined $NiNb_2O_6$ and $ZrTiO_4$ powders were mixed with PbO in a stoichiometric ratio to form the composition (*1-x*)$Pb(Zr_{1/2}Ti_{1/2})O_3$–(*x*)$Pb(Ni_{1/3}Nb_{2/3})O_3$, with x = 0.1-0.5. For optimization purpose, the sintering was carried out at temperatures between 1100 and 1250 °C for 4 h. Details of the processing and characterizations were provided elsewhere [2].

Before studying the electrical properties, the specimens were lapped to obtain parallel faces. After coating with silver paint as electrode at the faces, the specimens were heated at 750°C for 12 min to ensure the contact between the electrode and surface of ceramic. To study effects of the compressive stress on the dielectric and

ferroelectric properties of the ceramics, the compressometer was constructed [16-18]. The dielectric properties were measured by LCR-meter (Instrek LCR-821). The room temperature (25 °C) capacitance and the dielectric loss tangent were obtained at frequency of 10 kHz under compressive stress. The dielectric constant was then calculated from a parallel-plate capacitor equation, e.g. $\varepsilon_r = Cd / \varepsilon_0 A$, where C is the capacitance of the specimens, d and A are, respectively, the thickness and the area of the electrode, and ε_0 is the dielectric permittivity of vacuum (8.854×10^{-12} F/m).

The ferroelectric hysteresis (P-E) loops were characterized by using a computer controlled modified Sawyer-Tower circuit. The electric field was applied to a sample by a high voltage AC amplifier (Trek, model 610D) with the input sinusoidal signal with a frequency of 50 Hz from a signal generator (Goodwill, model GAG-809). The ferroelectric hysteresis (P-E) loop was recorded at room temperature (25 °C) for both loading and unloading conditions. The parameters obtained from the loops were the maximum polarization (P_{max}), the remanent polarization (P_r), and the coercive field (E_c), which were defined as the points where the loops reach the maximum polarization, cross the zero field, and cross the zero polarization, respectively.

3 Results and Discussion

3.1 Dielectric Properties Under Stress

The experimental results of the compressive stress dependence of the dielectric properties during loading and unloading for the ceramics in PZT-PNN system are displayed in Figs. 1 and 2. For better comparison, the dielectric properties of each composition under stress are normalized to the stress-free values. Clearly, there is a

considerable change of both the dielectric constant and the dielectric loss tangent with the compressive stress. As depicted in Fig. 1, the dielectric constant is seen to increase with increasing stress in all compositions. The increase of the dielectric constant varies from approximately 4-14 % in the near pseudo-cubic relaxor ferroelectric 0.5PZT-0.5PNN and tetragonal ferroelectric 0.9PZT-0.1PNN compositions to 40-54% in the rhombohedral relaxor ferroelectric 0.6PMN-0.4PNN and 0.7PZT-0.3PNN compositions. For the morphotropic phase boundary (MPB) 0.8PZT-0.2PNN composition, the dielectric constant increases drastically with the stress. The dielectric constant increases more than 80% when the stress reaches 100 MPa and returns to 160% of its original value when the stress is removed. On the other hand, the dielectric loss tangent (tan δ) is seen to decrease significantly (20-40%) with increasing stress, as displayed in Fig. 2. The changing of the dielectric properties with increasing and decreasing the stress do not follow the same path. It is also noticed that the changes in the dielectric properties with the compressive stress obtained in this study are in parts similar to those for BT, PZT, PMN-PZT, PMN-PT and PIN-PT systems in earlier investigations [17,19,22].

To understand these experimental results, various effects have to be considered. When a mechanical stress is applied to a ferroelectric material, the domain structure in the material will change to maintain the domain energy at a minimum; during this process some of the domains engulf other domains or change shape irreversibly. Under a compressive stress, the domain structure of ferroelectric ceramics may undergo domain switching, clamping of domain walls and de-aging mechanisms [14,15,19,23]. In this study, the results on the compressive stress dependence of the dielectric properties can easily be explained with the above statements. When the compressive stress is applied in the direction parallel to the polar axis (poling) direction, the stress

will move some of the polarization away from the poling direction resulting in a change in domain structures [15,19,24,25]. This change increases the non-180º domain wall density. Hence the increase of the dielectric constant with the applied stress is observed. The de-aging mechanism, which also increases the dielectric constant [15,19,20,26], is also expected to play a role here. Therefore, a combination of the domain switching and the de-aging mechanisms is believed to be a reason for the increase of the dielectric constant with increasing applied stress in the PZT-PNN system, as shown in Fig. 1. The cause of the stress dependence of the dielectric loss tangent, as mainly due to the clamping of the domain walls under compressive stress, which results in a decrease in domain wall mobility. The de-aging mechanism, which also decrease the dielectric loss tangent [15, 22] is also expected to play a role in controlling the change of the dielectric loss tangent with the stress, as observed in Fig. 2.

3.2 Ferroelectric Properties Under Stress

The polarization versus electric field (P-E) hysteresis loops of the 0.7PZT-0.3PNN ceramic under different compressive stresses are shown in Fig. 3 as a simple representative for the other compositions with similar behavior. It should first be noticed that the area of the P-E loops decreases with increasing compressive stress. The changes follow similar trend for all the ceramics. The P-E loop area indicates the polarization dissipation energy of a ferroelectric material under one full cycle of electric field application. This amount of the energy loss is directly related to the amount of domain participating in the switching process during the application of electric field [14,17]. For a given composition, the decrease in the loop area with increasing the

compressive stress is a result of the stress-induced domain wall suppression [14,27].

The changes in the remanent polarization (P_r), maximum polarization (P_{max}) and the coercive field (E_c) with the compressive stresses are plotted in Figs. 4 and 5, respectively. The changes in the maximum polarization (P_{max}) with stress are similar to the P_r. Figure 4 clearly shows that the maximum and remanent polarizations decrease as the compressive stress increases. The decrease is generally very similar with the polarization values at 100 MPa are approximately 30-45% of the stress-free values. In addition, noticeable decreases in the polarization values of all the ceramic are also observed after a complete cycle of the mechanical stress. This observation suggests a significant stress-induced de-poling in PZT-PNN ceramics resulting in the observed decrease of the polarization values under high stress levels [19,28]. Since the remanent polarization decreases as the compressive stress increases, it takes lower than usual electric field to force the polarizations to become zero, hence lower coercive field is observed, as demonstrated in Fig. 5.

To understand, at least qualitatively, these experimental results on ferroelectric properties of the PZT-PNN ceramics, one can interpret the changes in terms of domain-reorientation processes. When the compressive stress is applied in the direction parallel to the polar axis (poling) direction, the applied stress tends to keep the ferroelectric domains aligned with their polar axes away from the stress direction through the non-180º ferroelastic domain switching processes [14,15]. Therefore, it takes larger than usual applied electric field to reorient the domains along the stress direction, resulting in lower value of the maximum polarization (P_{max}), as shown in Fig. 3 and 4. When the electric field is reduced to zero the domains tend to rotate back away from the applied compressive stress direction, resulting in lower than usual remanent polarization (P_r), as

depicted in Figs. 3 and 4 [19,29,30]. Furthermore, considering the decrease of the hysteresis loss with increasing the compressive stress, it indicates that more and more ferroelectric domains are constrained by the applied stress and cannot be re-oriented by the electric field so as to participate in the polarization reversal. Consequently, both the maximum and remanent polarizations become lower with increasing the compressive stress [15]. The results of the changes of the hysteresis parameters of the ferroelectric ceramics with increasing compressive stress are in agreement with the previous investigations on many ferroelectric ceramics [11,14,26,31].

4 Conclusions

In this study, effects of compressive stress on the dielectric properties of PZT-PNN ceramics with a formula $(1\text{-}x)Pb(Zr_{1/2}Ti_{1/2})O_3–(x)Pb(Ni_{1/3}Nb_{2/3})O_3$ or *(1-x)*PZT-*(x)*PNN (x = 0.1-0.5) have been investigated under compressive stress using a compressometer in conjunction with an automatic LCR meter and a modified Sawyer-Tower circuit. The superimposed compression stress had pronounced effects on both the dielectric constant and the dielectric loss tangent of PZT-PNN ceramics, especially in morphotropic phase boundary (MPB) 0.8PZT-0.2PNN composition. The area of the ferroelectric hysteresis (P-E) loops, the maximum polarization (P_{max}) the remanent polarization (P_r) and the coercive field (E_c) decrease with increasing compressive stresses. The observations were mainly interpreted in terms of domain switching through non-180° domain walls, de-aging, and the stress-induced domain wall suppression mechanisms. Furthermore, noticeable decreases in the polarization values of all the ceramic are also observed after a complete cycle of the mechanical stress, indication of a significant stress-induced de-

poling in PZT-PNN ceramics. Finally, this study undoubtedly shows that the applied compressive stress has significant influences on the dielectric and ferroelectric properties of the PZT-PNN ceramics.

5 Acknowledgments

Financial supports from the Thailand Research Fund (TRF), Commission on Higher Education (CHE), Faculty of Science and Graduate School of Chiang Mai University are gratefully acknowledged.

6 References

[1] M. Kondo, M. Hida, M. Tsukuda, K. Kurihara and N. Kamehara, *Jpn. J. Appl. Phys.*, **36** (1997) 6043.

[2] N. Vittayakorn, G. Rujijanagul, X. Tan, M. A. Marquardt and D. P. Cann, *J. Appl. Phys.*, **96 (9)** (2004) 5103.

[3] D. Luff, R. Lane, K. R. Brown and H. J. Marshallsay, *Trans. J. Br. Ceram. Soc.,* **73** (1974) 251.

[4] J. Moulson and J.M. Herbert, *Electroceramics: Materials, Properties, Applications*, Chapman and Hall, New York, 1990.

[5] B. Jaffe, W.R. Cook and H. Jaffe, *Piezoelectric Ceramic*, R.A.N. Publishers, 1971.

[6] Y.H. Xu, *Ferroelectric Materials and Their Applications*, North Holland, Los

Angeles, 1991.

[7] G.A. Smolenskii and A.L. Agranovskaya, *Sov. Phys. Tech. Phys*., **13** (1958) 80.

[8] V. A. Bokov and I. E. Mylnikova, *Sov. Phys. Solid State*, **2**, (1960) 2428.

[9] J. Kuwata, K. Uchino and S. Nomura, *Jpn. J. Appl. Phys*., **21** (1982) 1298.

[10] S.E. Park and T.R. Shrout, *J. Appl. Phys*., **82** (1997) 1804.

[11] D. Viehland and J. Powers, *Appl. Phys. Lett*., **78** (20) (2001) 3112.

[12] D. Stansfield, *Underwater Electroacoustic Transducers*, Bath University Press, Bath, 1991.

[13] K. Uchino, *Piezoelectric Actuators and Ultrasonic Motors*, Kluwer, Boston, 1997.

[14] D. Zhou, M. Kamlah and D. Munz, *J. Euro. Ceram. Soc*., **25** (2005) 425.

[15] Q.M. Zhang, J. Zhao, K. Uchino and J. Zheng, *J. Mater. Res*., **12** (1997) 226.

[16] R. Yimnirun, *Ferroelectrics*, **331** (2006) 9.

[17] R. Yimnirun, S. Ananta and S. Chamunglap, *Mater. Chem. Phys*., **102** (2007) 165.

[18] R. Yimnirun, S. Ananta, A. Ngamjarurojana and S. Wongsaenmai*, Curr. Appl. Phys*., **6** (2006) 520.

[19] G. Yang, S.F. Liu, W. Ren and B.K. Mukherjee, *Proc. SPIE Sym. Smart Struct. Mater*., **3992** (2000) 103.

[20] R. Yimnirun, M. Unruan, Y. Laosiritaworn and S. Ananta, *J. Phys. D: Appl. Phys*.,

39 (2006) 3097.

[21] R. Yimnirun, *Inter. J. Mod. Phys. B* (2007) *in press*.

[22] M. Unruan, S. Wongsaenmai, Y. Laosiritaworn, S. Ananta and R. Yimnirun, *J. Phys. D: Appl. Phys*., **41** (2008) in press.

[23] G. Yang, S.F. Liu, W. Ren and B.K. Mukherjee, *Ferroelectrics*, **262** (2001) 207.

[24] D. Audigier, Cl. Richard, Cl. Descamps, M. Troccaz and L. Eyraud, *Ferroelectrics*, **154** (1994) 219.

[25] I.J. Fritz, *J. Appl. Phys*., **49** (1978) 4922.

[26] R. Yimnirun, S. Ananta, A. Ngamjarurojana and S. Wongsaenmai, 2006 *Curr. Appl. Phys*, **6** (2006) 52.

[27] R. Yimnirun, S. Ananta, A. Ngamjarurojana and S. Wongsaenmai, *Appl. Phys. A*, **81(6)** (2005) 1227.

[28] G. Yang, W. Ren, S.F. Liu, A.J. Masys and B.K. Mukherjee, *Proc. of the IEEE Ultrasonic Symposium*, (2000) 1005.

[29] J. Zhao and Q.M. Zhang, *Proc. of the IEEE International Symposium on Applications of Ferroelectrics*, (1996) 971.

[30] J. Zhao, A.E. Glazounov and Q.M. Zhang, *Appl. Phys. Lett*., **74**, (1999) 436.

[32] C.S. Lynch, *Acta Mater*., **44**, (1996) 4137.

Caption of Figures

Figure 1. Relative changes of dielectric constant (ε_r) with compressive stress for (1-*x*)PZT-(*x*)PNN ceramics (measured at 25 ºC and 10 kHz; solid arrows indicate loading direction).

Figure 2. Relative changes of dielectric loss tangent (tan δ) with compressive stress for (1-*x*)PZT-(*x*)PNN ceramics (measured at 25 ºC and 10 kHz; solid arrows indicate loading direction).

Figure 3. Polarization vs. electric field (P-E) hysteresis loops as a function of compressive stress for 0.7PZT-0.3PNN ceramic (loading cycle).

Figure 4. Changes in remanent polarization (P_r) and maximum polarization (P_{max}) with compressive stress for (*1-x*)PZT-*x*PNN ceramics (loading and unloading).

Figure 5. Changes in coercive field (E_c) with compressive stress for (*1-x*)PZT-*x*PNN ceramics (loading and unloading).

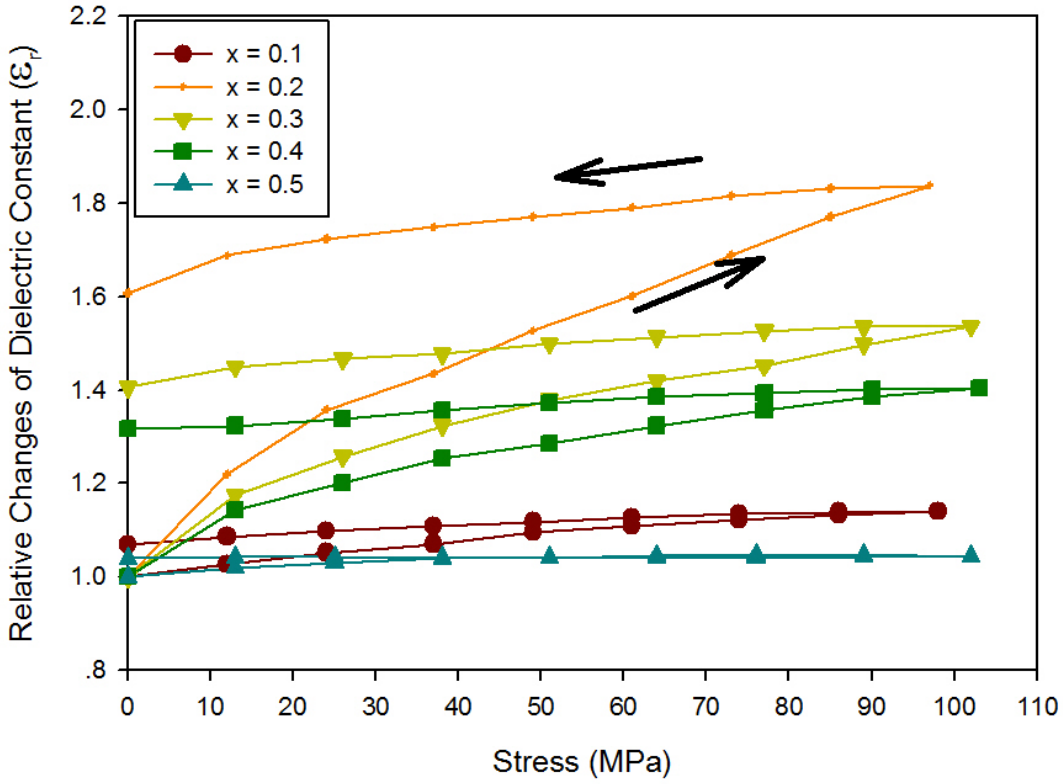
x = 0.1
x = 0.2
x = 0.3
x = 0.4
x = 0.5
Relative Changes of Dielectric Constant (ε_r)
Stress (MPa)
2.2
2.0
1.8
1.6
1.4
1.2
1.0
.8
0
10
20
30
40
50
60
70
80
90
100
110

Fig. 1

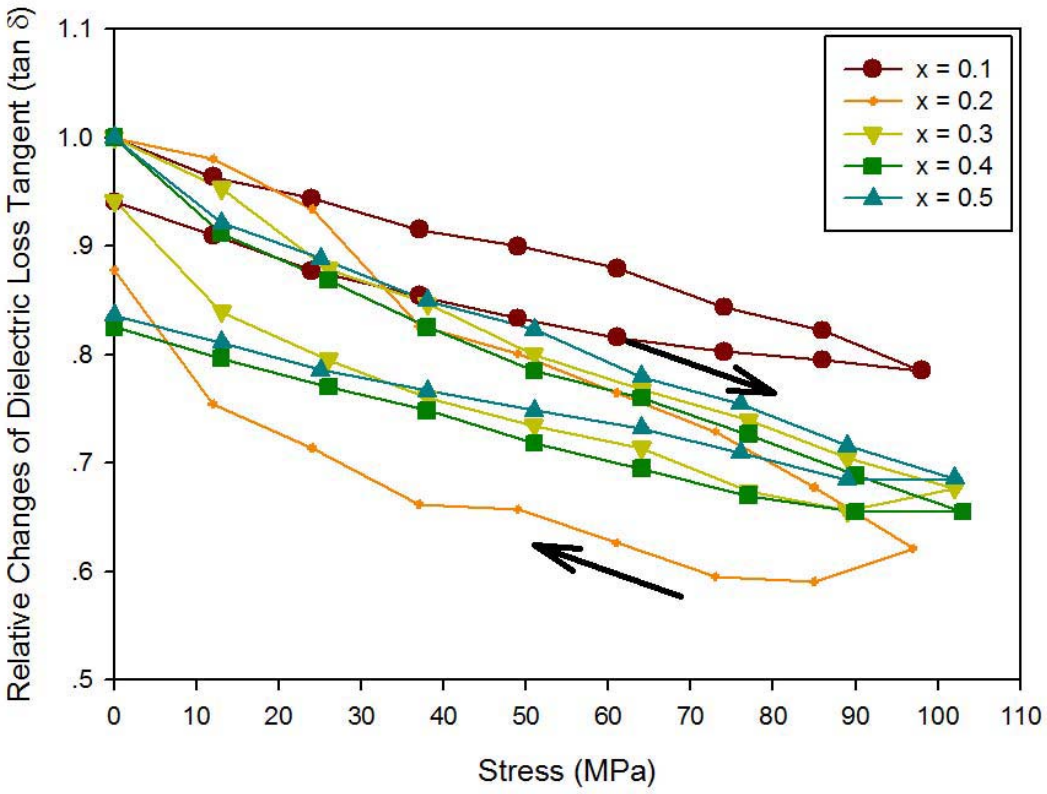
Relative Changes of Dielectric Loss Tangent (tan δ)
1.1
1.0
.9
.8
.7
.6
.5
0
10
20
30
40
50
60
70
80
90
100
110
Stress (MPa)
x = 0.1
x = 0.2
x = 0.3
x = 0.4
x = 0.5

Fig. 2

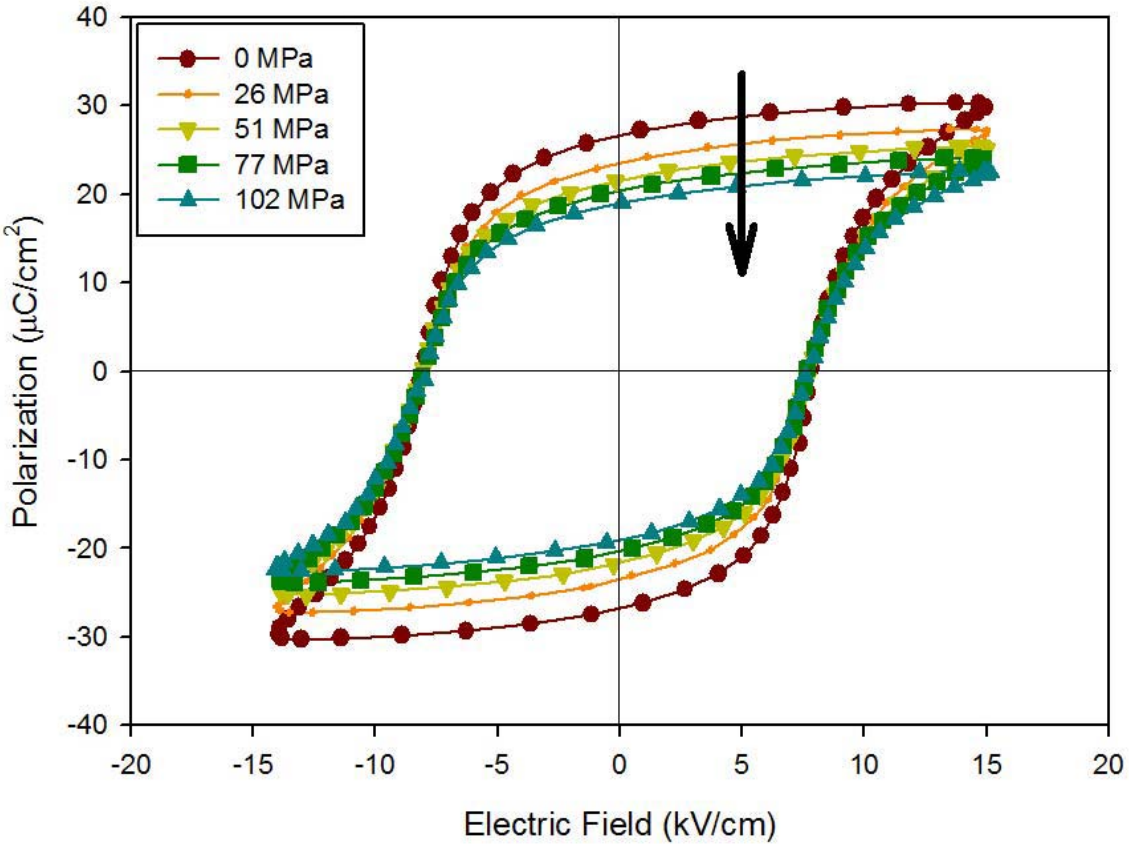
0 MPa
26 MPa
51 MPa
77 MPa
102 MPa
Polarization (μC/cm²)
Electric Field (kV/cm)
40
30
20
10
0
-10
-20
-30
-40
-20
-15
-10
-5
0
5
10
15
20

Fig. 3

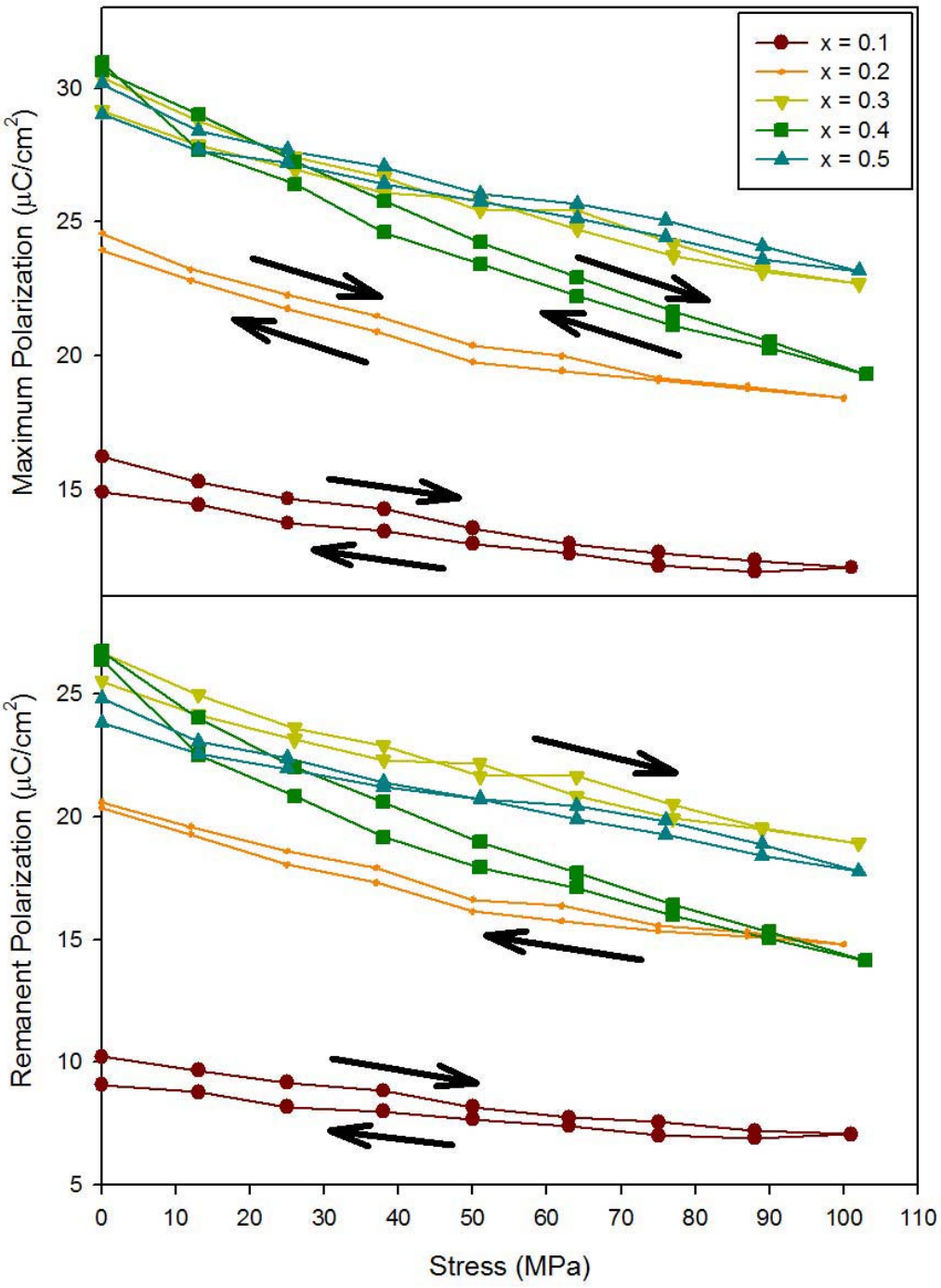
x = 0.1
x = 0.2
x = 0.3
x = 0.4
x = 0.5
Maximum Polarization (μC/cm²)
Remanent Polarization (μC/cm²)
Stress (MPa)
30
25
20
15
10
5
0
10
20
30
40
50
60
70
80
90
100
110

Fig. 4

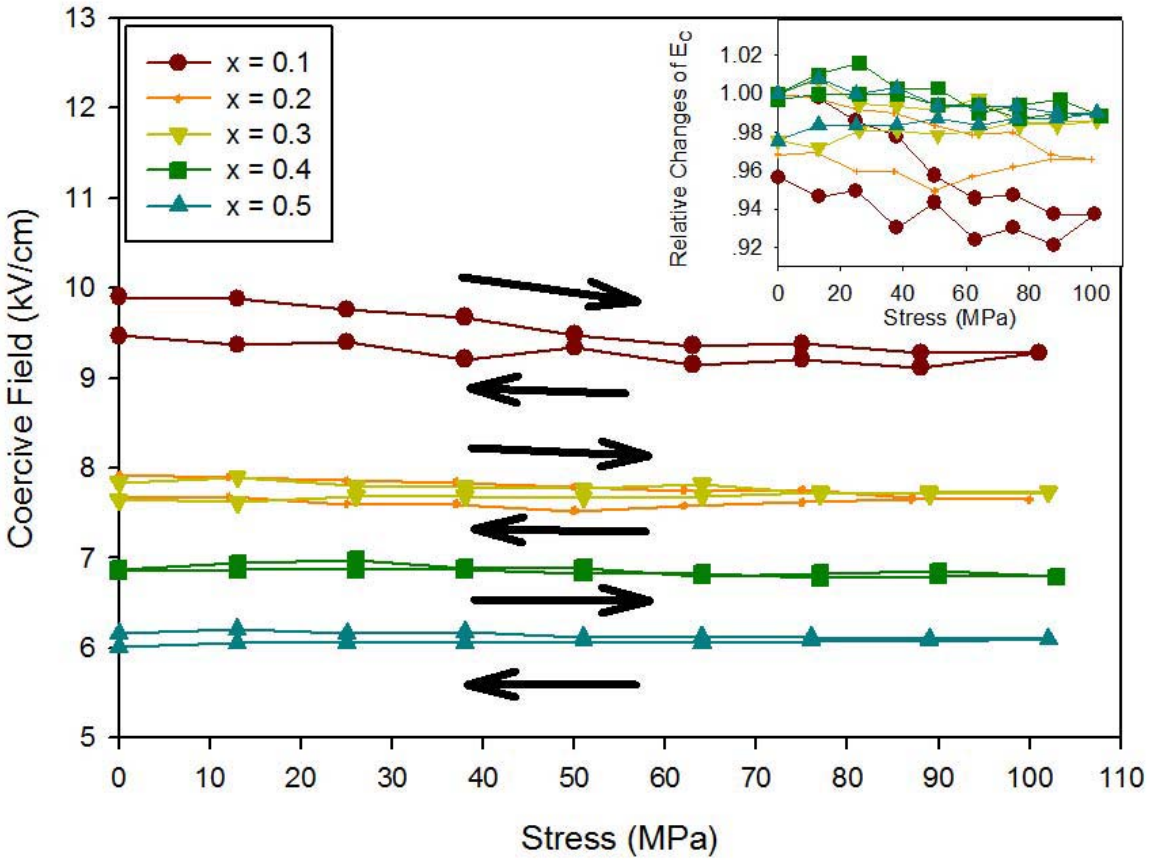
x = 0.1
x = 0.2
x = 0.3
x = 0.4
x = 0.5
Coercive Field (kV/cm)
Stress (MPa)
Relative Changes of Ec
Stress (MPa)

Fig. 5

Dielectric and ferroelectric properties of lead zirconate titanate-lead nickel niobate ceramics under compressive stress

M. Unruan,[1,a)] A. Prasartketrakarn,[1] A. Ngamjarurojana,[1] Y. Laosiritaworn,[1] S. Ananta,[1] and R. Yimnirun[2]
[1]*Department of Physics and Materials Science, Faculty of Science, Chiang Mai University, Chiang Mai 50200, Thailand*
[2]*School of Physics, Institute of Science, Suranaree University of Technology, Nakhon Ratchasima 30000, Thailand*

(Received 23 December 2008; accepted 21 February 2009; published online 23 April 2009)

Dielectric and ferroelectric properties of complex perovskite lead zirconate titanate-lead nickel niobate ceramic system were investigated under the influence of the compressive stress. The results showed that the dielectric properties, i.e., dielectric constant (ε_r) and dielectric loss (tan δ), and the ferroelectric characteristics, i.e., the area of the ferroelectric hysteresis (P-E) loops, the maximum polarization (P_{max}), and the remanent polarization (P_r) changed significantly with increasing compressive stress. These changes depended greatly on the ceramic compositions. The experimental results on the dielectric properties could be explained by the deaging phenomenon. The stress-induced domain wall motion suppression and non-180° ferroelectric domain switching processes were responsible for the changes observed for the ferroelectric parameters. In addition, a significant decrease in those parameters after a cycle of stress was observed and attributed to the stress-induced decrease in switchable part of spontaneous polarization. This study clearly showed that the applied stress has significant influence on the electrical properties of complex perovskite ceramics. © *2009 American Institute of Physics*. [DOI: 10.1063/1.3106659]

I. INTRODUCTION

There has recently been a great deal of interest in lead zirconate titanate-lead nickel niobate [$Pb(Zr_{1-x}Ti_x)O_3$-$Pb(Ni_{1/3}Nb_{2/3})O_3$ or (PZT-PNN)] ceramics because of their high longitudinal coupling coefficients, as well as good dielectric and excellent piezoelectric properties.[1–3] PZT is a normal ferroelectric material, which has been extensively investigated in the literatures because of its high dielectric properties and high piezoelectric coefficient. The high piezoelectric properties of PZT have been observed for compositions near the morphotropic phase boundary (MPB), i.e., at lead zirconate ($PbZrO_3$ or PZ):lead titanate($PbTiO_3$ or PT)=0.52:0.48.[4–6] PNN is a relaxor ferroelectric material originally reported by Smolenskii and Agranovskaya.[7] It exhibits the excellent dielectric broadening and electrostrictive properties and shows a diffuse phase transition around −120 °C with a peak permittivity of about 4000 at 1 kHz.[8]

Practically, piezoelectric and ferroelectric ceramics are often subjected to mechanical loading either deliberately in the design of the device itself or because the device is used to change shapes as in many smart structure applications or the device is used under environmental stresses.[9–13] A prior knowledge of how the material properties change under different load conditions is crucial for proper design of a device and for suitable selection of materials for a specific application.[12,13] It is therefore important to determine the properties of these materials as a function of applied stress. Previous investigations on the stress-dependence electrical properties of many ceramic systems emphasized the importance of the matter.[11,14–18] Recently, the uniaxial stress dependence of dielectric and ferroelectric properties has been investigated in materials such as barium titanate (BT), lead magnesium niobate (PMN), PMN-PT, PZT-BT, and PMN-PZT.[16–21] The results clearly showed that the effects of stress on the dielectric and ferroelectric properties depended significantly on ceramic compositions and stress levels. Interestingly, there has been no systematic study on the influence of an applied stress on the dielectric and ferroelectric properties of the PZT-PNN ceramics. Therefore, it is the aim of this study to determine the dielectric and ferroelectric properties of the $(1-x)$PZT-(x)PNN ceramics as a function of compressive stress.

II. EXPERIMENTAL

In this study, $(1-x)$PZT-(x)PNN (with $x=0.1-0.5$) ceramics were prepared using the columbite precursor method. The columbite structure ($NiNb_2O_6$) and wolframite structure ($ZrTiO_4$) were synthesized first. The calcined $NiNb_2O_6$ and $ZrTiO_4$ powders were mixed with PbO in a stoichiometric ratio to form the composition $(1-x)$PZT-(x)PNN, with $x=0.1-0.5$. For optimization purpose, the sintering was carried out at temperatures between 1100 and 1250 °C for 4 h. Details of the processing and characterizations were provided elsewhere.[2]

Before studying the electrical properties, the specimens were lapped to obtain parallel faces. After coating with silver paint as electrode at the faces, the specimens were heated at 750 °C for 12 min to ensure the contact between the electrode and surface of ceramic. To study effects of the com-

a)Author to whom correspondence should be addressed. Electronic mail: muangjaiunruan@yahoo.com.

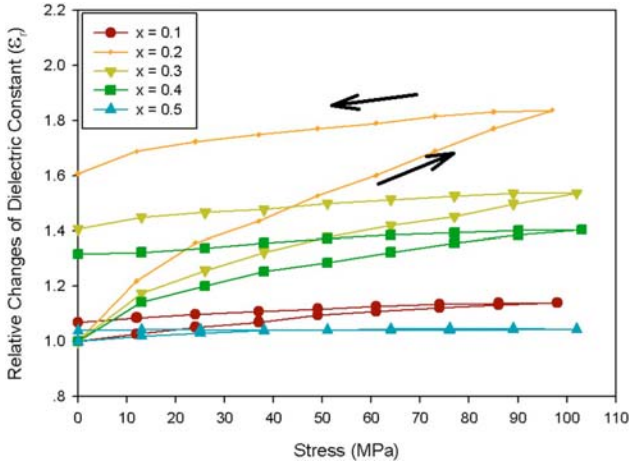

FIG. 1. (Color online) Relative changes in dielectric constant (ε_r) with compressive stress for $(1-x)$PZT-(x)PNN ceramics (measured at 25 °C and 10 kHz; solid arrows indicate loading direction).

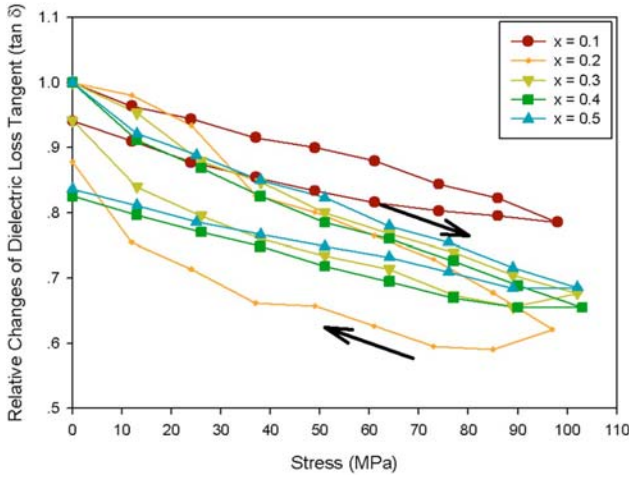

FIG. 2. (Color online) Relative changes in dielectric loss tangent (tan δ) with compressive stress for $(1-x)$PZT-(x)PNN ceramics (measured at 25 °C and 10 kHz; solid arrows indicate loading direction).

pressive stress on the dielectric and ferroelectric properties of the ceramics, the compressometer was constructed.[16–18] The dielectric properties were measured by LCR meter (Instrek LCR-821). The room temperature (25 °C) capacitance and the dielectric loss tangent were obtained at frequency of 10 kHz under compressive stress. The dielectric constant was then calculated from a parallel-plate capacitor equation, e.g., $\varepsilon_r = Cd/\varepsilon_0 A$, where C is the capacitance of the specimens, d and A are respectively the thickness and the area of the electrode, and ε_0 is the dielectric permittivity of vacuum $(8.854 \times 10^{-12}$ F/m).

The ferroelectric hysteresis (P-E) loops were characterized by using a computer controlled modified Sawyer–Tower circuit. The electric field was applied to a sample by a high voltage ac amplifier (Trek, model 610D) with the input sinusoidal signal with a frequency of 50 Hz from a signal generator (Goodwill, model GAG-809). The ferroelectric hysteresis (P-E) loop was recorded at room temperature (25 °C) for both loading and unloading conditions. The parameters obtained from the loops were the maximum polarization (P_{max}), the remanent polarization (P_r), and the coercive field (E_c), which were defined as the points where the loops reach the maximum polarization, cross the zero field, and cross the zero polarization, respectively.

III. RESULTS AND DISCUSSION

A. Dielectric properties under stress

The experimental results of the compressive stress dependence of the dielectric properties during loading and unloading for the ceramics in PZT-PNN system are displayed in Figs. 1 and 2. For better comparison, the dielectric properties of each composition under stress are normalized to the stress-free values. Clearly, there is a considerable change in both the dielectric constant and the dielectric loss tangent with the compressive stress. As depicted in Fig. 1, the dielectric constant is seen to increase with increasing stress in all compositions. The increase in the dielectric constant varies from approximately 4%–14% in the near pseudocubic relaxor ferroelectric 0.5PZT-0.5PNN and tetragonal ferroelectric 0.9PZT-0.1PNN compositions to 40%–54% in the rhombohedral relaxor ferroelectric 0.6PMN-0.4PNN and 0.7PZT-0.3PNN compositions. For the MPB 0.8PZT-0.2PNN composition, the dielectric constant increases drastically with the stress. The dielectric constant increases more than 80% when the stress reaches 100 MPa and returns to 160% of its original value when the stress is removed. On the other hand, the dielectric loss tangent (tan δ) is seen to decrease significantly (20%–40%) with increasing stress, as displayed in Fig. 2. The changing of the dielectric properties with increasing and decreasing stress does not follow the same path. It is also noticed that the changes in the dielectric properties with the compressive stress obtained in this study are in parts similar to those for systems in earlier investigations.[17,19,22]

To understand these experimental results, various effects have to be considered. When a mechanical stress is applied to a ferroelectric material, the domain structure in the material will change to maintain the domain energy at a minimum; during this process some of the domains engulf other domains or change shape irreversibly. Under a compressive stress, the domain structure of ferroelectric ceramics may undergo domain switching, clamping of domain walls, and deaging mechanisms.[14,15,19,23] In this study, the results on the compressive stress dependence of the dielectric properties can easily be explained with the above statements. When the compressive stress is applied in the direction parallel to the polar axis (poling) direction, the stress will move some of the polarization away from the poling direction, resulting in a change in domain structures.[15,19,24,25] This change increases the non-180° domain wall density. Hence the increase in the dielectric constant with the applied stress is observed. The deaging mechanism, which also increases the dielectric constant,[15,18–20] is also expected to play a role here. Therefore, a combination of the domain switching and the deaging mechanisms is believed to be a reason for the increase in the dielectric constant with increasing applied stress in the PZT-PNN system, as shown in Fig. 1. The cause of the stress dependence of the dielectric loss tangent is mainly due to the clamping of the domain walls under compressive stress,

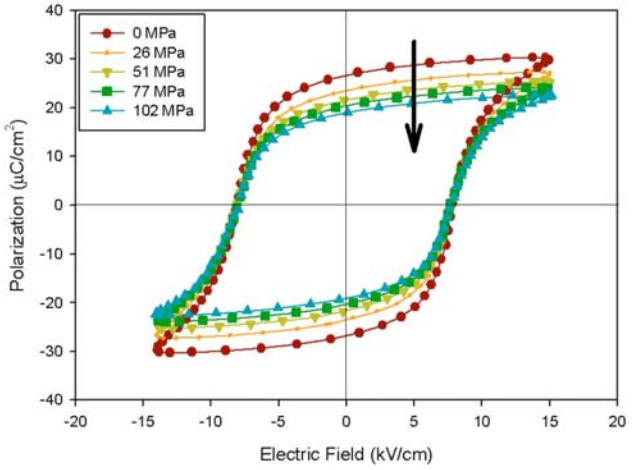

FIG. 3. (Color online) Polarization vs electric field (P-E) hysteresis loops as a function of compressive stress for 0.7PZT-0.3PNN ceramic (loading cycle).

which results in a decrease in domain wall mobility. The deaging mechanism, which also decreases the dielectric loss tangent,[15,22] is also expected to play a role in controlling the change in the dielectric loss tangent with the stress, as observed in Fig. 2.

It should also be noted here that the applied stress could also affect the ferroelectric phase transitions of the ceramics, which consequently change the observed dielectric properties significantly.[15,25] The applied compressive stress has been found to move the Curie temperature (T_C) up to the order of approximately 0.1 °C/MPa in 0.9PMN-0.1PT.[15] In addition, the influence of stress on the properties of ferroelectric materials is strongly dependent on the temperature, especially when the temperature is higher or lower than T_C. In this study, since $(1-x)$PZT-(x)PNN (with $x=0.1-0.5$) ceramics exhibit T_C ranging from 130 °C ($x=0.5$) to 330 °C ($x=0.1$),[2] the change in the dielectric properties with stress in the vicinity of T_C and the stress-induced shift in T_C is rather insignificant because of their high T_C, as compared to the measurement temperature of 25 °C. Therefore, the stress-related ferroelectric phase transition is not expected to have significant effects on the changes in dielectric properties of PZT-PNN ceramics under the applied stress observed in this study.

B. Ferroelectric properties under stress

The polarization versus electric field (P-E) hysteresis loops of the 0.7PZT-0.3PNN ceramic under different compressive stresses are shown in Fig. 3 as a simple representative for the other compositions with similar behavior. It should first be noticed that the area of the P-E loops decreases with increasing compressive stress. The changes follow similar trend for all the ceramics. The P-E loop area indicates the polarization dissipation energy of a ferroelectric material under one full cycle of electric field application. This amount of the energy loss is directly related to the amount of domain participating in the switching process during the application of electric field.[14,17] For a given composition, the decrease in the loop area with increasing the compressive stress is a result of the stress-induced domain wall suppression.[14,26]

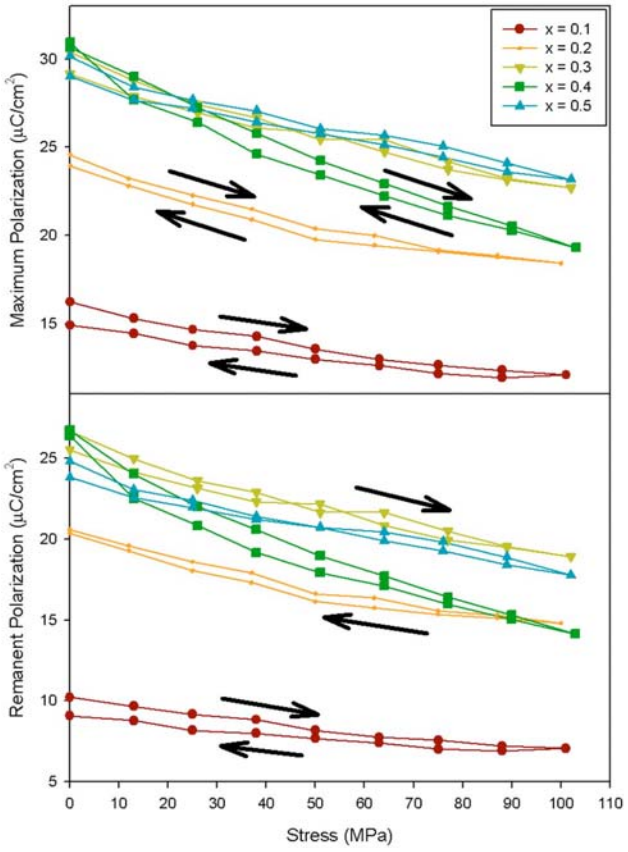

FIG. 4. (Color online) Changes in remanent polarization (P_r) and maximum polarization (P_{max}) with compressive stress for $(1-x)$PZT-xPNN ceramics (loading and unloading).

The changes in the remanent polarization (P_r), maximum polarization (P_{max}), and the coercive field (E_c) with the compressive stresses are plotted in Figs. 4 and 5, respectively. The changes in the maximum polarization (P_{max}) with stress are similar to the P_r. Figure 4 clearly shows that the

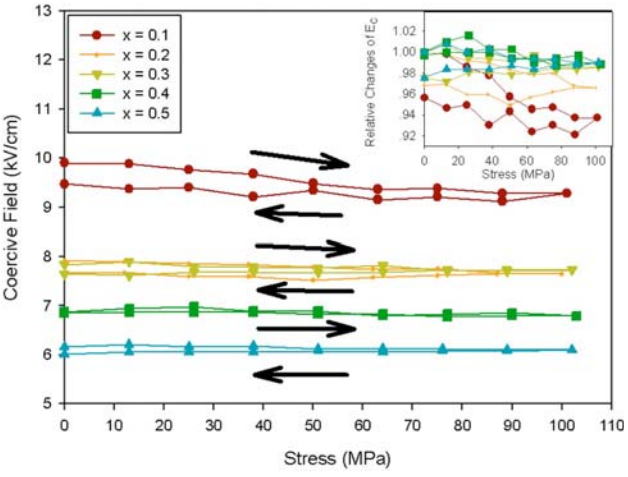

FIG. 5. (Color online) Changes in coercive field (E_c) with compressive stress for $(1-x)$PZT-xPNN ceramics (loading and unloading).

maximum and remanent polarizations decrease as the compressive stress increases. The decrease is generally very similar to the polarization values at 100 MPa, which are approximately 30%–45% of the stress-free values. In addition, noticeable decreases in the polarization values of all the ceramic are also observed after a complete cycle of the mechanical stress. This observation suggests a significant stress-induced depoling in PZT-PNN ceramics, resulting in the observed decrease in the polarization values under high stress levels.[19,27] Since the remanent polarization decreases as the compressive stress increases, it takes lower than usual electric field to force the polarizations to become zero; hence lower coercive field is observed, as demonstrated in Fig. 5.

To understand, at least qualitatively, these experimental results on ferroelectric properties of the PZT-PNN ceramics, one can interpret the changes in terms of domain-reorientation processes. When the compressive stress is applied in the direction parallel to the polar axis (poling) direction, the applied stress tends to keep the ferroelectric domains aligned with their polar axes away from the stress direction through the non-180° ferroelastic domain switching processes.[14,15] Therefore, it takes larger than usual for the applied electric field to reorient the domains along the stress direction, resulting in lower value of the maximum polarization (P_{max}), as shown in Figs. 3 and 4. When the electric field is reduced to zero the domains tend to rotate back away from the applied compressive stress direction, resulting in lower than usual remanent polarization (P_r),[19,28,29] as depicted in Figs. 3 and 4. Furthermore, considering the decrease in the hysteresis loss with increasing compressive stress, it indicates that more and more ferroelectric domains are constrained by the applied stress and cannot be reoriented by the electric field so as to participate in the polarization reversal. Consequently, both the maximum and remanent polarizations become lower with increasing compressive stress.[15] The results of the changes in the hysteresis parameters of the ferroelectric ceramics with increasing compressive stress are in agreement with the previous investigations on many ferroelectric ceramics.[11,14,18,30]

IV. CONCLUSIONS

In this study, effects of compressive stress on the dielectric properties of PZT-PNN ceramics with a formula of $(1-x)$PZT-(x)PNN ($x=0.1-0.5$) have been investigated under compressive stress using a compressometer in conjunction with an automatic LCR meter and a modified Sawyer–Tower circuit. The superimposed compression stress had pronounced effects on both the dielectric constant and the dielectric loss tangent of PZT-PNN ceramics, especially in MPB 0.8PZT-0.2PNN composition. The area of the ferroelectric hysteresis (P-E) loops, the maximum polarization (P_{max}), the remanent polarization (P_r), and the coercive field (E_c) decrease with increasing compressive stresses. The observations were mainly interpreted in terms of domain switching through non-180° domain walls, deaging, and the stress-induced domain wall suppression mechanisms. Furthermore, noticeable decreases in the polarization values of all the ceramic are also observed after a complete cycle of the mechanical stress, indication of a significant stress-induced depoling in PZT-PNN ceramics. Finally, this study undoubtedly shows that the applied compressive stress has significant influences on the dielectric and ferroelectric properties of the PZT-PNN ceramics.

ACKNOWLEDGMENTS

Financial supports from the Thailand Research Fund (TRF), Commission on Higher Education (CHE), Royal Golden Jubilee (RGJ) Ph.D. Program, Thailand Excellent Center in Physics, and Faculty of Science and Graduate School of Chiang Mai University are gratefully acknowledged.

[1] M. Kondo, M. Hida, M. Tsukuda, K. Kurihara, and N. Kamehara, Jpn. J. Appl. Phys., Part 1 **36**, 6043 (1997).
[2] N. Vittayakorn, G. Rujijanagul, X. Tan, M. A. Marquardt, and D. P. Cann, J. Appl. Phys. **96**, 5103 (2004).
[3] D. Luff, R. Lane, K. R. Brown, and H. J. Marshallsay, Trans. J. Br. Ceram. Soc. **73**, 251 (1974).
[4] J. Moulson and J. M. Herbert, *Electroceramics: Materials, Properties, Applications* (Chapman and Hall, New York, 1990).
[5] B. Jaffe, W. R. Cook, and H. Jaffe, *Piezoelectric Ceramic* (RAN, New York, 1971).
[6] Y. H. Xu, *Ferroelectric Materials and Their Applications* (North-Holland, Los Angeles, 1991).
[7] G. A. Smolenskii and A. L. Agranovskaya, Sov. Phys. Tech. Phys. **13**, 80 (1958).
[8] V. A. Bokov and I. E. Mylnikova, Sov. Phys. Solid State **2**, 2428 (1960).
[9] J. Kuwata, K. Uchino, and S. Nomura, Jpn. J. Appl. Phys., Part 1 **21**, 1298 (1982).
[10] S. E. Park and T. R. Shrout, J. Appl. Phys. **82**, 1804 (1997).
[11] D. Viehland and J. Powers, Appl. Phys. Lett. **78**, 3112 (2001).
[12] D. Stansfield, *Underwater Electroacoustic Transducers* (Bath University Press, Bath, UK, 1991).
[13] K. Uchino, *Piezoelectric Actuators and Ultrasonic Motors* (Kluwer, Boston, 1997).
[14] D. Zhou, M. Kamlah, and D. Munz, J. Eur. Ceram. Soc. **25**, 425 (2005).
[15] Q. M. Zhang, J. Zhao, K. Uchino, and J. Zheng, J. Mater. Res. **12**, 226 (1997).
[16] R. Yimnirun, Ferroelectrics **331**, 9 (2006).
[17] R. Yimnirun, S. Ananta, and S. Chamunglap, Mater. Chem. Phys. **102**, 165 (2007).
[18] R. Yimnirun, S. Ananta, A. Ngamjarurojana, and S. Wongsaenmai, Curr. Appl. Phys. **6**, 520 (2006).
[19] G. Yang, S. F. Liu, W. Ren, and B. K. Mukherjee, Proc. SPIE Symposium on Smart Structures and Materials **3992**, 103 (2000).
[20] R. Yimnirun, M. Unruan, Y. Laosiritaworn, and S. Ananta, J. Phys. D **39**, 3097 (2006).
[21] R. Yimnirun, S. Ananta, E. Meechoowas, and S. Wongsaenmai, J. Phys. D **36**, 1615 (2003).
[22] M. Unruan, S. Wongsaenmai, Y. Laosiritaworn, S. Ananta, and R. Yimnirun, J. Phys. D **41**, 541 (2008).
[23] G. Yang, S. F. Liu, W. Ren, and B. K. Mukherjee, Ferroelectrics **262**, 207 (2001).
[24] D. Audigier, Cl. Richard, Cl. Descamps, M. Troccaz, and L. Eyraud, Ferroelectrics **154**, 219 (1994).
[25] I. J. Fritz, J. Appl. Phys. **49**, 4922 (1978).
[26] R. Yimnirun, S. Ananta, A. Ngamjarurojana, and S. Wongsaenmai, Appl. Phys. A: Mater. Sci. Process. **81**, 1227 (2005).
[27] G. Yang, W. Ren, S. F. Liu, A. J. Masys, and B. K. Mukherjee, Proc.-IEEE Ultrason. Symp. **2**, 1005 (2000).
[28] J. Zhao and Q. M. Zhang, Proceedings of the 10th IEEE International Symposium on Applications of Ferroelectrics, Vol. 2, pp. 971–974 (1996).
[29] J. Zhao, A. E. Glazounov, and Q. M. Zhang, Appl. Phys. Lett. **74**, 436 (1999).
[30] C. S. Lynch, Acta Mater. **44**, 4137 (1996).

Journal of Alloys and Compounds xxx (2008) xxx–xxx

Contents lists available at ScienceDirect

Journal of Alloys and Compounds

journal homepage: www.elsevier.com/locate/jallcom

Effect of magnesium niobate precursors on phase formation, microstructure and dielectric properties of perovskite lead magnesium niobate ceramics

R. Wongmaneerung[a,*], R. Yimnirun[b], S. Ananta[b]

[a] Department of Physics, Faculty of Science, Maejo University, Chiang Mai 50290, Thailand
[b] Department of Physics, Faculty of Science, Chiang Mai University, Chiang Mai 50200, Thailand

ARTICLE INFO

Article history:
Received 2 January 2008
Received in revised form 28 October 2008
Accepted 30 October 2008
Available online xxx

Keywords:
Lead magnesium niobate
Perovskite
Relaxor
B-site precursor

ABSTRACT

Lead magnesium niobate, $Pb(Mg_{1/3}Nb_{2/3})O_3$ or PMN, ceramics were fabricated by using *B*-site precursor method where both $MgNb_2O_6$ and $Mg_4Nb_2O_9$ were employed as magnesium niobate precursors. It has been found that under suitable sintering condition highly dense and pure $Pb(Mg_{1/3}Nb_{2/3})O_3$ ceramics can be successfully achieved in both processing routes. In addition, pure perovskite $Pb(Mg_{1/3}Nb_{2/3})O_3$ ceramic with slightly higher dielectric constant can be produced at lower sintering temperature by using a corundum-route.

1. Introduction

Lead magnesium niobate, $Pb(Mg_{1/3}Nb_{2/3})O_3$ or PMN, is one of the most widely investigated perovskite relaxor ferroelectric materials, which has been extensively studied because of its high dielectric constant and electrostrictive coefficient [1–4]. The excellent properties make it a promising material for capacitor, actuator and transducer applications [5–7]. As is well-known, in the preparation of PMN via the conventional solid-state reaction using PbO, MgO and Nb_2O_5 [8,9], significant amount of the pyrochlore-type phases with relatively low dielectric constant are inevitably formed with PMN and these phases significantly degrade the overall electrical properties of the products. In order to avoid the formation of pyrochlores, several methods have been introduced [10–13]. So far, the columbite method [12,13], in which prefabricated $MgNb_2O_6$ is reacted with an appropriate proportion of PbO, has been widely accepted as one of the promising methods for the preparation of phase-pure PMN-based materials. To date, only a few work [10,11] on the preparation of PMN powders by using a corundum $Mg_4Nb_2O_9$ precursor have been reported. Moreover, effects of $Mg_4Nb_2O_9$ precursor on phase formation, microstructure and dielectric properties of PMN ceramics has not been adequately characterized. Thus, in the present study, the PMN ceramics were fabricated by using both $MgNb_2O_6$ and $Mg_4Nb_2O_9$ as precursor. Their dielectric properties with respect to temperature and frequency were examined, compared and explained on the basis of their final composition, densification, and microstructural development.

2. Experimental

PMN powders were synthesized by employing two different *B*-site precursors (i.e. columbite-route versus corundum-route) mixed oxide synthetic route, as reported earlier [12,13]. Starting precursors were as follows: PbO (JCPDS file no. 77-1971), MgO (periclase: JCPDS file no. 71-1176) and Nb_2O_5 (JCPDS file no. 80-2493) (Aldrich, 99% purity). These three oxide powders exhibited an average particle size in the range of 3.0–5.0 μm. First, two intermediate phases of magnesium niobate: $MgNb_2O_6$ and $Mg_4Nb_2O_9$ were separately prepared by the solid-state reaction method previously reported [14–16]. The appropriate amount of PbO was then added to the $MgNb_2O_6$ and $Mg_4Nb_2O_9$, and vibro-milled in isopropanol alcohol for 1 h. Columbite- and corundum-route mixtures were then calcined at 900 and 950 °C, respectively, for 1 h with heating/cooling rates of 30 °C/min [15].

Green pellets were pressed into disks and sintered at various temperatures between 1100 and 1290 °C. Densities of the sintered pellets were determined by using the Archimedes principles. Room temperature X-ray diffraction (XRD; Philips PW 1729 diffractometer) was used to identify the phases formed and optimum sintering condition. The relative amounts of perovskite and pyrochlore phases were determined from XRD patterns of the samples by measuring the major peak intensities for the perovskite and pyrochlore phases. The following qualitative equation [12] was used.

$$\%\text{Perovskite} = 100 \times \frac{I_{per}}{I_{per} + I_{pyr}} \quad (1)$$

Here, I_{per} refers to the intensity of the perovskite (1 1 0) peak and I_{pyr} refers to the intensity of the pyrochlore (2 2 2) peak.

The microstructural development was examined by scanning electron microscopy (SEM; JEOL JSM-840A). Average grain size of the sintered ceramics was

* Corresponding author. Tel.: +66 81 8554973.
E-mail address: re_nok@yahoo.com (R. Wongmaneerung).

0925-8388/$ – see front matter © 2008 Elsevier B.V. All rights reserved.
doi:10.1016/j.jallcom.2008.10.152

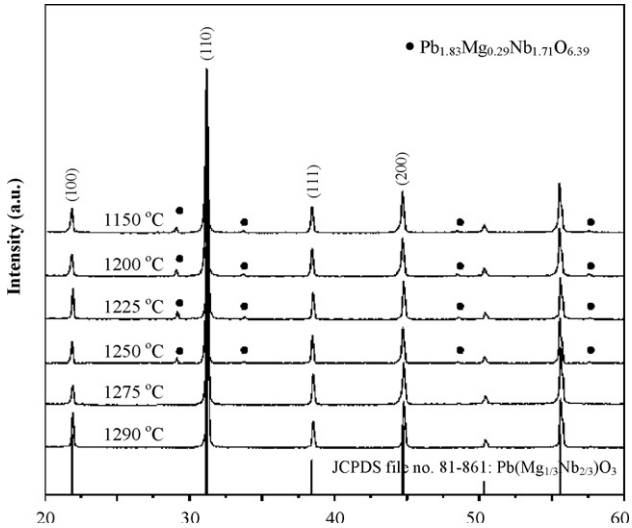

Fig. 1. XRD patterns of the columbite-route PMN ceramics sintered at various temperatures.

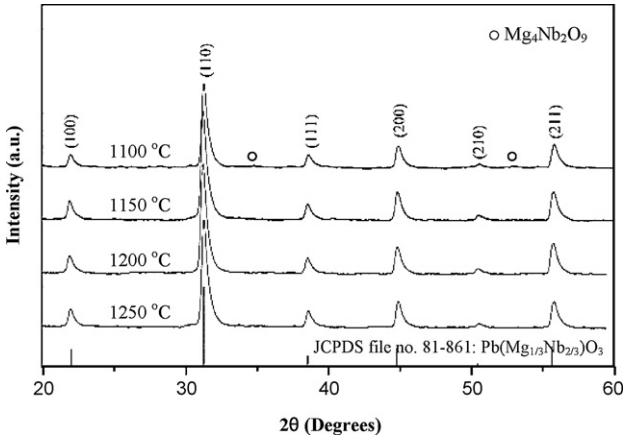

Fig. 2. XRD patterns of the corundum-route PMN ceramics sintered at various temperatures.

estimated by using a linear intercept method [17], in which the linear intercept length is determined by laying a series of uniformly distributed test lines on the planar section and counting the number of times the grain boundaries are intercepted. In this work, five samples from each processing condition were used in determining the average grain size and the standard deviation of the grain size was estimated as ±0.05 μm. For the dielectric measurement, ceramic surfaces were parallel polished and sputtered with gold. Dielectric characterization was performed with a LCR meter (HP-4284A, Hewlett-Packard) in conjunction with an environmental chamber (9023, Delta Design). A heating rate of 3 °C/min was used during the measurement.

3. Results and discussion

The X-ray diffraction patterns of columbite- and corundum-route PMN ceramics sintered at various temperatures are given in Figs. 1 and 2, respectively. As shown in Fig. 1, the strongest reflections in the majority of the XRD patterns indicate the formation of PMN phase, which could be matched with JCPDS file no. 81-861 [18], in agreement with other works [16,19]. To a first approximation, this phase has a pseudo-cubic perovskite-type structure with cell parameter $a = 404.41$ pm in space group *Pm3m* (no. 221). However, some additional reflections (marked by ●), which correlate with a pyrochlore phase of composition $Pb_{1.83}Mg_{0.29}Nb_{1.71}O_{6.39}$ (JCPDS file no. 33-769 [20]) are found in XRD patterns of columbite-route PMN samples sintered at low sintering temperatures (1150–1250 °C). This phase has orthorhombic structure with cell parameter $a = 105.9$ pm in space group *Fd3m* (no. 227) [21]. As shown in Fig. 2, XRD patterns of corundum-route PMN ceramics which sintered above 1100 °C show 100% perovskite phase and could be matched with JCPDS file no. 81-861 [18], similar to PMN phase occurs in columbite-route. It should be noted that no evidence of pyrochlore phases such as $Pb_2Nb_2O_7$, $Pb_3Nb_2O_8$ and $Pb_5Nb_4O_{15}$ has been found here whereas these phases were found in other works [22,23]. However, some additional reflections (marked by ○), which correlate with $Mg_4Nb_2O_9$ phase are found in XRD patterns of PMN sample sintered at 1100 °C. This observation indicates that $Mg_4Nb_2O_9$ was formed at this low temperature at which the complete reaction between PbO and $Mg_4Nb_2O_9$ could not occur. This is likely due to the poor reactivity of the solid-state reaction method commonly found in the mixed oxide perovskite compounds.

For the purpose of estimating the concentration of pyrochlore phase present, Eq. (1) has been applied to the obtained diffraction patterns, as given in Table 1. It can be noticed that pure PMN ceramics can be produced at the lower optimized sintering temperature by using corundum precursor. Moreover, the dense PMN ceramics can be formed by using both *B*-site precursors. Based on the XRD data obtained here, it may be concluded that the optimal sintering temperature for the production of columbite- and corundum-route PMN ceramic is 1275 °C for 4 h with heating/cooling rates of 10 °C/min, and 1250 °C for 2 h with heating/cooling rates of 10 °C/min, respectively.

The densification data of all samples are shown in Table 1. It is observed that the density of about 93–95% and 89–92% of the theoretical value can be achieved for columbite- and corundum-route PMN ceramics, respectively. Density increases as sintering temperature increases. Further, increase in the sintering temperature up to 1300 °C caused to the decrease in density values. This may be attributed to the loss of lead oxide at high sintering temperatures,

Table 1
Phase and densification characteristics of columbite- and corundum-route PMN ceramics from various sintering conditions.

Preparation route	Sintering temperature (°C)	Perovskite phase[a] (%)	Pyrochlore phase[a] (%)	Relative density[b] (%)
Columbite	1150	96.76	3.24	96.48
	1200	96.72	3.28	96.85
	1225	96.10	3.90	96.11
	1250	97.37	2.63	95.24
	1275	100.00	0.00	95.37
	1290	100.00	0.00	93.64
Corundum	1100	100.00	0.00	89.32
	1150	100.00	0.00	90.83
	1200	100.00	0.00	91.76
	1250	100.00	0.00	92.14

[a] The estimated precision of the perovskite and pyrichlorephase is ±0.1%.
[b] The estimated precision of the density is ±0.1%.

Please cite this article in press as: R. Wongmaneerung, et al., J. Alloys Compd. (2008), doi:10.1016/j.jallcom.2008.10.152

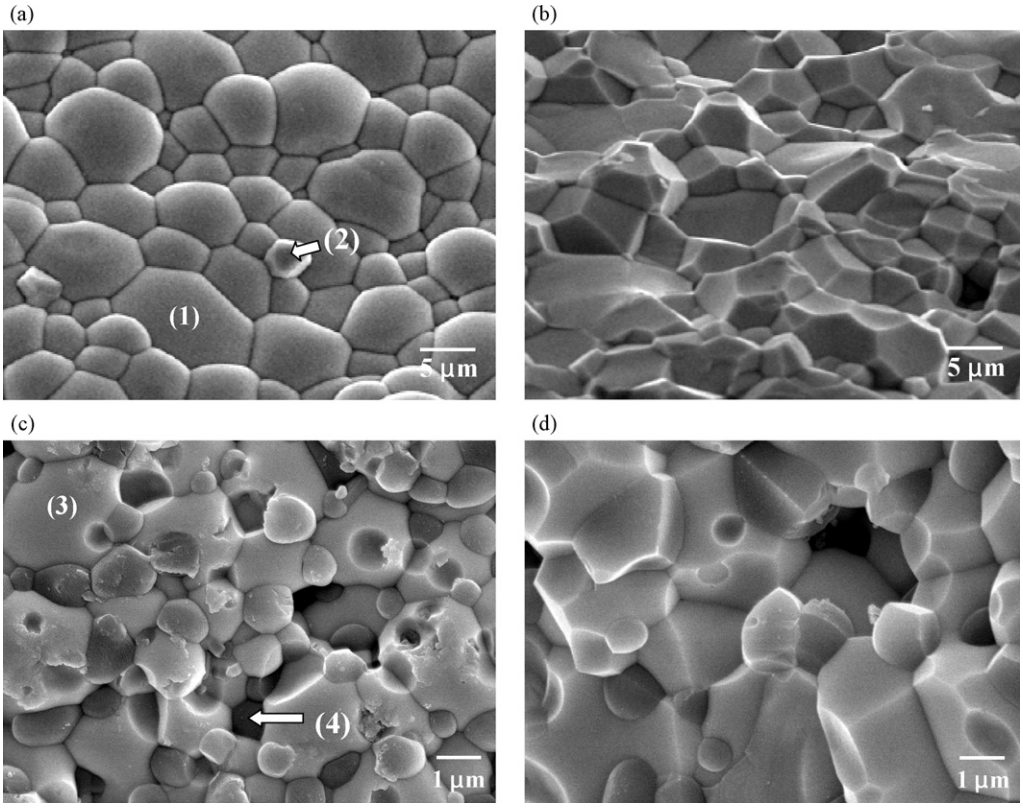

Fig. 3. SEM micrographs of (a) as-sintered and (b) fracture surfaces for columbite-route PMN ceramics, (c) as-sintered and (d) fracture surfaces for corundum-route PMN ceramics with maximum bulk density.

which is similar to the results found in other Pb-based perovskite systems [24,25].

Microstructural development was investigated by scanning electron microscopy. Free and fracture surface micrographs of columbite- and corundum-route PMN ceramics with maximum bulk density are compared in Fig. 3. In general, typical PMN microstructure consisting of highly dense grain-packing and round microstructural is observed in both samples and in good agreement with previous works [26,27]. Moreover, the grain sizes are in the range of 2–12 μm and 0.8–2.3 μm for columbite- and corundum-route PMN ceramics, respectively. In columbite-route sample, it is seen that a few facet grain is observed on the surface. By employing the combination of SEM/EDX techniques, more information is obtained as shown in Table 2 and Fig. 4 (a). EDX analysis of the facet grains (marked as "(2)") indicated the chemical composition of $Pb_6(MgNb_{10})O_{32}$ or $Pb_{1.83}(Mg_{0.37}Nb_{3.06})O_{10}$, although the concentration is too low for XRD detection, consistent with earlier work [28]. It is, therefore, intriguing to note the advantage of a combination between SEM and EDX techniques, which lies in its ability to reveal microstructural features often missed by the XRD diffraction method which requires at least 5 wt% of the component [29]. It should be noted that in this sample, no unreacted MgO and PbO liquid phase has been found on the grain boundary [22,26,30]. This phase is mainly observed between perovskite grains (marked as "(1)"). It should be noted here that EDX is now the most commonly used elemental analysis available within the SEM technique. This

Table 2
Chemical compositions of both PMN ceramics from EDX analyzer.

EDX positions	Composition (at%)			Possible phase
	Mg (K)	Nb (L)	Pb (M)	
(1)	16.13	33.34	50.52	Pb3(MgNb2)O9
(2)	7.17	58.41	34.76	$Pb_6(MgNb_{10})O_{32}$
(3)	17.06	28.33	54.62	Pb3(MgNb2)O9
(4)	100.00	–	–	MgO

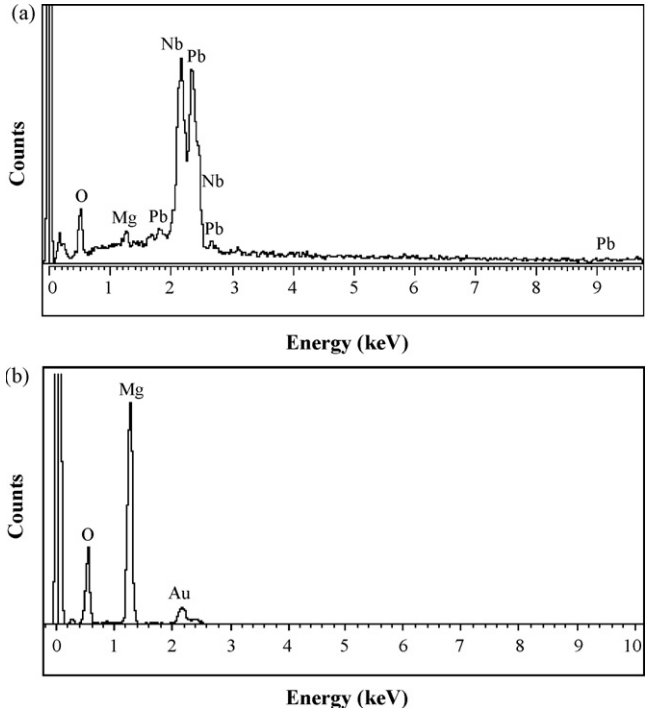

Fig. 4. EDX analysis of (a) the pyrochlore phase and (b) the MgO phase from both PMN ceramics (some spectra indexed as Au come from coated electrode).

Please cite this article in press as: R. Wongmaneerung, et al., J. Alloys Compd. (2008), doi:10.1016/j.jallcom.2008.10.152

Table 3
Comparison of $\varepsilon_{r,max}$ and grain size of PMN ceramics obtained by various methods.

Sample from	Lejeune and Boilot [8]	Liou et al. [45]	Han and Kim [46]	This work	This work
Processing	Mixed oxide with $MgCO_3$	Simplified columbite	Mixed oxide with $Mg(NO_3)_2$	Columbite	Corundum
Calcination temperature/time	800/2 h	1100/3 h	950/2 h	900/1 h	950/1 h
Sintering temperature/time	900/2 h	1250/2 h	900/2 h	1275/4 h	1250/2 h
Relative density	96.0%	93.6%	95.6%	95.4%	92.1%
$\varepsilon_{r,max}$	15400	17060	n.a.	12984	16566
Grain size (μm)	n.a.	7.1	2–4	2–12	0.8–2.3

technique offers a means of rapidly evaluating the elemental constituents of a sample; major constituents (10 wt% or more) can be indicated in 10 s and a 100-s accumulation is often sufficient for identification of minor elements (on the order of 1 wt%). In addition to rapid qualitative analysis, accurate quantitative analysis can also be achieved with EDX technique. However, there are techniques for microanalysis of inorganic materials. One of these techniques is electron probe microanalyzer (EPMA). The EPMA's usefulness is compositional information, using characteristic X-ray lines, with a spatial resolution on the order of 1 μm can be obtained from a sample. The EPMA technique will be used for analysis of the PMN samples and the results will be presented in the future. Nonetheless, for the purpose of comparison, the EDX results obtained in this study are used for preliminary analysis.

For corundum-route PMN sample, the as-sintered ceramic (Fig. 3 (c)) shows few apparent open pores at grain boundaries and triple points; but cracks and microcracks are not observed. These could be caused by MgO inclusions (the dark area) present at triple points. It seems that the grain boundary movement is depressed by the MgO phase; hence the open pores were formed. Furthermore, the dark areas are determined by SEM/EDX to be MgO inclusions (marked as "(4)" in the microstructure in Fig. 4 (b)) neighbouring the parent PMN phase (marked as "(3)") as shown in Table 2, similar to the inclusions observed in a series of non-stoichiometric PMN compositions as reported earlier [31]. Furthermore, there were the MgO inclusions previously observed by Goo et al. [32] in a stoichiometric PMN doped with excess MgO. It is believed to be another cause for the lower density values in corundum-route PMN ceramic compared to columbite-route. Similar finding was also reported in SiC reinforced PZT ceramics [33]. Moreover, the microstructure in Fig. 3 (c) displays few small grains. EDX analysis indicated the chemical composition of $Pb(Mg_{1/3}Nb_{2/3})O_3$. It is evident that the coarsening of big grains over small grains is through a process coherent with a solid-state sintering mechanism. Micrographs of fracture surface (Fig. 3 (b) and (d)) show highly dense microstructures consisting of equiaxed grains in agreement with other researchers [26,27,34]. The PMN ceramics also have an intergranular fracture mechanism, indicating that the grain boundaries are mechanically weaker than the grains [35].

In order to evaluate the dielectric properties, both columbite- and corundum-route PMN ceramics with the maximum bulk density were measured at frequencies between 1 and 100 kHz in the

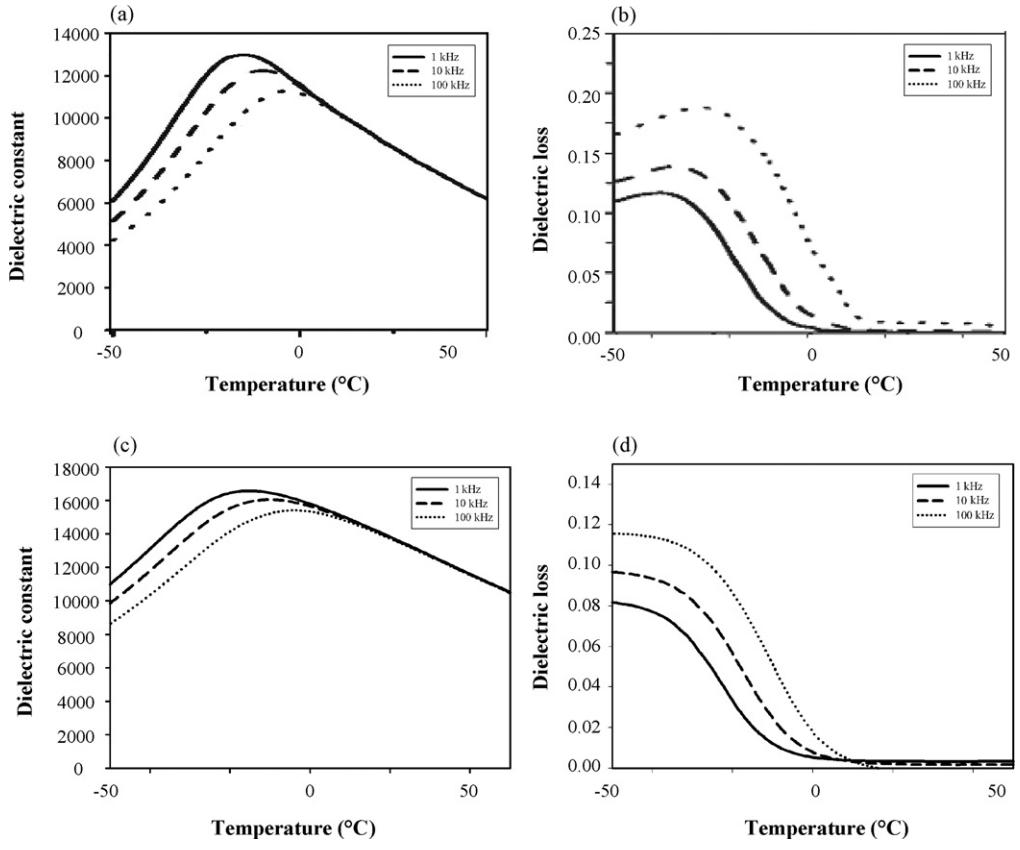

Fig. 5. Temperature dependence of (a) dielectric constant (ε_r) and (b) dielectric loss ($\tan\delta$) for the columbite-route PMN ceramic, (c) dielectric constant (ε_r) and (d) dielectric loss ($\tan\delta$) for the corundum-route PMN ceramic.

Please cite this article in press as: R. Wongmaneerung, et al., J. Alloys Compd. (2008), doi:10.1016/j.jallcom.2008.10.152

Table 4
Dielectric properties of PMN ceramics.

Preparation route	Frequency (kHz)	T_{max} (°C)	ΔT_{max} (°C) (1–100 kHz)	$\varepsilon_{r,max}$	$\tan\delta_{max}$	Diffusivity (γ)	Diffuseness parameter (δ)
Columbite	1	−10.6	13.05	12960.7	0.12	1.98	42.03
	10	−5.2		12458.9	0.14	1.97	39.58
	100	2.5		11855.7	0.19	1.92	37.28
Corundum	1	−15.6	11.45	16566.5	0.07	1.79	35.64
	10	−10.0		16042.0	0.08	1.76	35.28
	100	−4.1		15406.5	0.11	1.73	32.73

temperature range from −50 to +50 °C as shown in Fig. 5. In general, the typical relaxor behavior [36,37] with the characteristic dispersive frequency dependence of the dielectric maxima has been observed in both PMN samples. The dielectric constant (ε_r) and dielectric loss ($\tan\delta$) are compared in Fig. 5. The maximum dielectric constant reached 12984 and 16566 at 1 kHz, the temperatures for $\varepsilon_{r,max}$ are −10 °C and −15 °C for columbite- and corundum-route samples, respectively, which are close to previously published values [26,38,39]. It can be noticed that the presence of MgO phase may slightly shift the temperature of $\varepsilon_{r,max}$. Characteristics of various PMN obtained by different methods in this work and those reported in other works are compared in Table 3. By comparison to columbite-route PMN ceramic, $\varepsilon_{r,max}$ of corundum-route ceramic is slightly higher. It should be noted that the presence of MgO resulted in an enhancement of the dielectric constant of PMN ceramics. This was originally attributed to the elimination of the pyrochlore phase [39], in agreement with the XRD results. Moreover, it should be noted that an increase of dielectric constant could be a combination of various effects; i.e. (i) phase present, (ii) density/porosity of the sample and (iii) grain size. Here it is observed that smaller grain size leads to an enhanced the dielectric constant. There are two other interesting features in this study. Firstly, the sample containing a small amount of MgO phase shows a high dielectric constant with similar results reported by Wang and Schulze [38]. The second feature is seen in Table 1, e.g. while the density of corundum-route PMN sample is low compared to columbite-route sample, the sample still exhibits all the characteristics of a relaxor materials.

Unlike the normal ferroelectrics, the dielectric behavior of PMN ceramics cannot be described by the Curie-Weiss law equation. Their behaviors tally well with the law $1/\varepsilon \propto (T - T_m)^2$. The dielectric constant can be written in the form [40]:

$$\frac{1}{\varepsilon} = \frac{1}{\varepsilon_m} + \frac{(T - T_m)^2}{2\varepsilon_m \delta^2} \quad (2)$$

Here γ is the expression of the degree of dielectric relaxation in the relaxor ferroelectric materials and δ is diffuseness parameter and gives an estimation of the relaxor characteristic of the transition.

Fig. 6 shows dependencies of the $(\varepsilon_m/\varepsilon) - 1$ versus $(T - T_m)^2$, with determined values of the two diffuseness parameters (γ and δ). The diffuseness exponent for columbite-route sintered PMN ceramic is $\gamma = 1.98$ (Table 4), which is higher than reported value of 1.64 [41] but is very close to 2.0 [42]. Moreover, the diffuseness exponent tends to decrease while the frequency increases. By comparison, the diffuseness exponent for corundum-route sintered PMN ceramic is much smaller than those observed in columbite-route sample. It may be caused by the presence of MgO. The MgO inclusions might affect the low-frequency contributions to the dielectric constant. This interaction would be modeled by δ in Eq. (2) as shown in Table 4 and would suggest that the MgO phase could slightly decrease the diffuseness of the phase transition, in agreement with previous report [38]. Furthermore, for a perovskite ferroelectric, it can be established that the diffuseness could be caused by grain size dependence [43,44]. Therefore, this effect can partly be the cause of the increase of diffuseness exponent

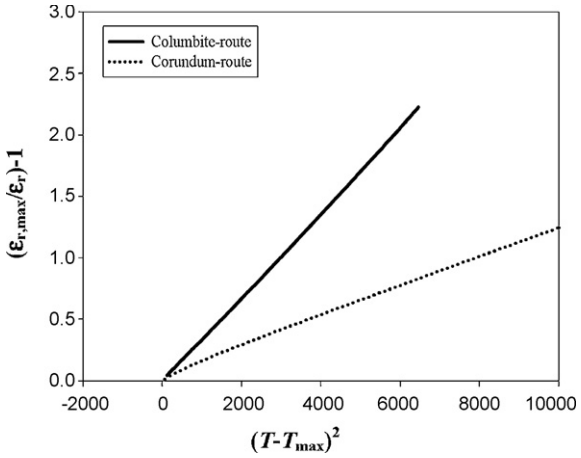

Fig. 6. Dependence of $(\varepsilon_{r,max}/\varepsilon_r) - 1$ with $(T - T_{max})^2$ for (a) columbite- and (b) corundum-route PMN ceramics.

in columbite-route PMN ceramic. Finally, it should be noted that the dielectric constant is increased with decreasing grain size. The factor leading to this result is probably the variation in the stress to which the grains are subjected as they cool through the Curie point. Moreover, the columbite-route PMN ceramic containing a small amount of pyrochlore phase ($Pb_{1.83}Mg_{0.29}Nb_{1.71}O_{6.39}$) shows a low dielectric constant. This observation is clearly a result of the paraelectric pyrochlore phase with a low dielectric constant at room temperature of 130; hence reducing the dielectric properties of the columbite-route PMN ceramic sample.

4. Conclusion

Results indicate that using different magnesium niobate precursors to produce PMN ceramics greatly influences phase formation, microstructure and dielectric properties of the resulting products. It has been concluded that the single-phase perovskite PMN ceramics can be successfully formed by employing either columbite- or corundum-route precursor method under optimized sintering temperatures. Between the two *B*-site precursor methods, it is seen that lower optimized sintering temperature for the production of pure PMN ceramics can be obtained by using corundum-route, whereas the large obtainable grain size was found in the columbite-route PMN ceramics. Moreover, the presence of MgO phase in the microstructures of corundum-route PMN ceramics may lead to the pyrochlore elimination and results in enhancement of the dielectric properties.

Acknowledgements

This work was supported by the Thailand Research Fund (TRF) and the Commission on Higher Education (CHE).

Please cite this article in press as: R. Wongmaneerung, et al., J. Alloys Compd. (2008), doi:10.1016/j.jallcom.2008.10.152

References

[1] G.A. Smolenskii, A.I. Agranovskaya, Sov. Phys. Tech. Phys. (Engl. Transl.) 3 (7) (1958) 1380.
[2] V.V. Kirillov, V.A. Isupov, Ferroelectrics 5 (1973) 3.
[3] E.P. Smirnova, O.V. Rubinshtein, B.A. Isupov, Ferroelectrics 143 (1993) 263.
[4] L.E. Cross, S.J. Jang, R.E. Newnham, K. Uchino, Ferroelectrics 23 (1980) 187.
[5] A.J. Moulson, J.M. Herbert, Electroceramics, 2nd ed., John Wiley & Sons, Chichester, 2003.
[6] G.H. Haertling, J. Am. Ceram. Soc. 82 (1999) 797.
[7] S.J. Jang, K. Uchino, S. Nomura, L.E. Cross, Ferroelectrics 27 (1980) 31.
[8] M. Lejeune, J.P. Boilot, Mater. Res. Bull. 20 (1985) 493.
[9] J.P. Guha, J. Mater. Sci. 36 (2001) 5219.
[10] P.A. Joy, K. Sreedhar, J. Am. Ceram. Soc. 80 (1997) 770.
[11] C.H. Lu, H.S. Yang, Mater. Sci. Eng. B 84 (2001) 159.
[12] S.L. Swartz, T.R. Shrout, Mater. Res. Bull. 17 (1982) 1245.
[13] Y.-C. Liou, J.-H. Chen, Ceram. Int. 30 (2004) 17.
[14] S. Ananta, Mater. Lett. 58 (2004) 2781.
[15] R. Wongmaneerung, T. Sarakonsri, R. Yimnirun, S. Ananta, Mater. Sci. Eng. B 132 (2006) 292.
[16] S. Ananta, N.W. Thomas, J. Eur. Ceram. Soc. 19 (1999) 155.
[17] W.E. Lee, W.M. Rainforth, Ceramic Microstructures Property Control by Processing, Chapman & Hall, London, 1994.
[18] Powder Diffraction File No. 81-861, International Centre for Diffraction Data, Newton Square, PA, 2000.
[19] S. Ananta, N.W. Thomas, J. Eur. Ceram. Soc. 19 (1999) 629.
[20] Powder Diffraction File No. 33-769, International Centre for Diffraction Data, Newton Square, PA, 2000.
[21] A. Mergen, W.E. Lee, J. Eur. Ceram. Soc. 17 (1997) 1033.
[22] J. Wang, X. Junmin, W. Dongmei, N. Weibeng, Solid State Ionics 124 (1999) 271.
[23] P. Lucas, W.T. Petuskey, J. Am. Ceram. Soc. 84 (9) (2001) 2150.
[24] E.R. Nielsen, E. Ringgaard, M. Kosec, J. Eur. Ceram. Soc. 22 (2002) 1847.
[25] A. Boutarfaia, Ceram. Int. 26 (2000) 583.
[26] A.L. Costa, C. Galassi, G. Fabbri, E. Roncari, C. Capiani, J. Eur. Ceram. Soc. 21 (2001) 1165.
[27] J.P. Guha, H.U. Anderson, J. Am. Ceram. Soc. 69 (1986) C-287.
[28] S. Ananta, Mater. Lett. 58 (2004) 2530.
[29] H. Klug, L. Alexander, X-Ray Diffraction Procedures for Polycrystalline and Amorphous Materials, 2nd ed., John Wiley & Sons Ltd., New York, 1974.
[30] L.B. Kong, J. Ma, W. Zhu, O.K. Tan, J. Mater. Sci. Lett. 20 (2001) 1241.
[31] M.F. Yan, H.C. Ling, W.W. Rhodes, J. Mater. Res. 4 (4) (1989) 930.
[32] E. Goo, T. Yamamoto, K. Okazaki, J. Am. Ceram. Soc. 68 (8) (1986) C-188.
[33] T. Yamamoto, H. Igarashi, K. Okazaki, Ferroelectrics 63 (1985) 281.
[34] S. Ananta, N.W. Thomas, J. Eur. Ceram. Soc. 19 (1999) 2917.
[35] O. Guillon, F. Thiebaud, D. Perreux, C. Courtoris, P. Champagne, A. Leriche, J. Crampon, J. Eur. Ceram. Soc. 25 (2005) 2421.
[36] L.E. Cross, Ferroelectrics 76 (1987) 241.
[37] L.E. Cross, Ferroelectrics 151 (1994) 305.
[38] H.-C. Wang, W.A. Schulze, J. Am. Ceram. Soc. 73 (4) (1990) 825.
[39] S.L. Swartz, T.R. Shrout, W.A. Schulze, L.E. Cross, J. Am. Ceram. Soc. 67 (5) (1984) 311.
[40] Z. Li, L. Zhang, X. Yao, J. Mater. Res. 16 (2001) 834.
[41] K. Uchino, S. Nomura, Ferroelectr. Lett. 44 (3) (1982) 55.
[42] M. Kuwabara, S. Takahashi, K. Goda, K. Oshima, K. Watanabe, Jpn. J. Appl. Phys. 31 (9B) (1992) 3241.
[43] V. Koval, C. Alemany, J. Briančin, H. Bruncková, J. Electroceram. 10 (2003) 19.
[44] R. Yimnirun, S. Ananta, P. Laoratanakul, J. Eur. Ceram. Soc. 25 (2005) 3235.
[45] Y.-C. Liou, L. Wu, S.S. Liou, Jpn. J. Appl. Phys. 33 (9B) (1994) L1320.
[46] K.R. Han, S. Kim, J. Mater. Sci. 35 (2000) 2055.

Please cite this article in press as: R. Wongmaneerung, et al., J. Alloys Compd. (2008), doi:10.1016/j.jallcom.2008.10.152